1961

An investigation into the performance of grain augers

A W. Roberts
University of Wollongong

AN INVESTIGATION INTO THE PERFORMANCE OF GRAIN AUGERS

BY

A. W. ROBERTS, B.E., A.S.T.C., A.M.I.E.(Aust.),
A.M.I. Mech. E.

THESIS SUBMITTED FOR THE DEGREE OF
DOCTOR OF PHILOSOPHY

School of Mechanical Engineering,
The University of New South Wales,
January, 1961.

SYNOPSIS.

With the growing increase in the bulk handling of grain, the grain auger type elevator is now being widely used. While some theoretical analyses of the grain auger have been made and performance data for particular size augers have been obtained, little information is available for general design purposes. This work, which is based on an experimental approach, is aimed at producing such information. The investigation has been carried out using a small scale model auger which allowed a comprehensive range of tests to be conducted on a more manageable basis.

In the first part of the investigation, a study is made of the auger performance characteristics with the aim of determining the conditions for most efficient operation. An examination is made of output and volumetric efficiency in relation to speed, angle of elevation and choke length (the length of exposed screw projecting from the lower end of the casing). The effect of casing clearance on auger output is also partially examined. In addition, the variation of auger horsepower and overall efficiency with speed and angle of elevation is observed.

In the second part of the investigation, equations are developed and design charts given which enable the performance of augers to be predicted. The equations and charts are based on the application of dimensional analysis and dynamic similarity and apply to augers of the same geometrical proportions as those of the model. The data apply mainly to granular materials of similar shape and properties to wheat. A comparison is made between the predicted performance with the actual performance of a 6 inch auger, good agreement being obtained.

The third part of the investigation is devoted to the study of the grain vortex motion in augers. This is an important facet of the grain motion having a significant bearing on the ratio of the core diameter to the outside diameter of the screw.

The investigation shows that many combinations of auger size, speed and angle of elevation may be adopted for a particular conveying application and general recommendations are given regarding the choice of these variables for efficient operation.

ACKNOWLEDGMENTS

The writer wishes to express his sincere thanks to Professor A. H. Willis, Dean of the Faculty of Engineering, for his continued interest in this investigation and for his advice and guidance throughout all stages of the work.

Thanks are due also to the staff of the School of Mechanical Engineering at the Wollongong Division of the University of New South Wales where the latter part of the work was completed; Mr. S. E. Bonamy, Senior Lecturer, rendered invaluable assistance in the preparation of this report, while Messrs. R.W. Upfold and P. Van der Werf, Lecturers, gave assistance in other aspects of the work.

Grateful acknowledgment is made of the assistance given by the workshop staffs of Sydney and Wollongong in the preparation of the apparatus.

LIST OF SYMBOLS

While the various symbols adopted in the investigation are introduced at the appropriate places in the text, for convenience, they are also listed here in alphabetical order.

A Slope of lines in C_Q versus C_S graphs.

a Constant in grain speed and critical speed equations.

B Constant in output, volumetric efficiency and overall efficiency equations.

b Constant in grain speed and critical speed equations.

C Radial casing clearance, ft.

C_1 Constant in vortex equations.

C_2 Constant in vortex equations.

C_Q Discharge coefficient.

C_P Power coefficient.

C_S Speed coefficient.

C_{VT} Tangential velocity coefficient

D Outside diameter of screw, ft.

D_c Core diameter of screw, ft.

D_m Diameter of model, ft.

D_p Diameter of prototype, ft.

d Average particle size, ft.

E Constant in output, volumetric efficiency and overall efficiency equations.

F Efficiency factor.

G Constant in output, volumetric efficiency and overall efficiency equations.

g Acceleration due to gravity, 32.2 ft/sec.^{2}

H Height of lift, ft.

J Constant in choke length correction factor equation.

K_c Choke length correction factor.

k Factor relating radial and vertical pressures in vortex motion of grain.

L Length of auger, ft.

l_c Choke length, ft.

M Constant in choke length correction factor equation.

m Index of choke length correction factor equation.

N Rotational speed of auger, r.p.m.

N_C Critical auger speed, r.p.m.

N_{max} Maximum economical speed, r.p.m.

N_m Speed of model, r.p.m.

N_p Speed of prototype, r.p.m.

N_T Rotational speed of grain r.p.m.

N_T' Rotational speed of grain at outer screw periphery r.p.m.

N_T'' Rotational speed of grain at core, r.p.m.

n Index in vortex velocity distribution equations.

O Origin of co-ordinate system.

P Auger horsepower.

P_t Theoretical horsepower.

p Screw pitch, ft.

p_o Constant in vortex pressure distribution equation.

p_r Radial pressure due to vortex motion, lb/sq.ft.

p_x Horizontal pressure in mass of grain, lb/sq.ft.

p_z Vertical pressure in mass of grain, lb/sq.ft.

p_σ Pressure parallel to surface of mass of grain in which surface is inclined at angle σ, lb/sq.ft.

Q Auger output, cub.ft/min.

Q_t Theoretical output, cub.ft/min.

R Constant in choke length correction factor equation.

r Radius, ft.

r' Radius of outer screw periphery, ft.

S Slope of lines in C_P versus C_S graphs

T Constant in horsepower equation.

t Thickness of auger flight, ft.

U Constant in horsepower equation.

V_A Absolute velocity of grain, ft/sec.

V_A' Absolute velocity of grain at outer periphery, ft/sec.

V_L Lifting velocity of grain, ft/sec.

V_L' Lifting velocity of grain at outer periphery, ft/sec.

V_{Lo} Optimum lifting velocity of grain, ft/sec.

V_{Lt} Theoretical maximum lifting velocity of grain, ft/sec.

V_{Lt}' Theoretical lifting velocity at outer periphery, ft/sec.

V_R Relative velocity of grain ft/sec.

V_R' Relative velocity of grain at outer periphery, ft/sec.

V_S Peripheral velocity of screw, ft/sec.

V_S' Peripheral velocity of screw at outer periphery, ft/sec.

V_T Peripheral velocity of grain ft/sec.

V_T' Peripheral velocity of grain at outer periphery ft/sec.

w Specific weight, lb/cub.ft.

X Constant in horsepower and overall efficiency equations.

x Index in experimentally obtained vortex equations. Also co-ordinate of point.

Y Constant in horsepower and overall efficiency equations.

y Co-ordinate of point.

Z Constant in choke length correction factor equations.

z Height ordinate for vortex profile, ft.

z'' Ordinate used to establish vortex equation from experimental results, ft.

z_o Constant in fluid vortex profile equation.

z_o' Constant in grain vortex profile equation.

α Angle of elevation of auger, degrees.

ε Angle absolute grain velocity vector makes with normal to screw surface, degrees.

γ Constant dependent on the geometry of an auger.

ϵ Constant in horsepower and overall efficiency equations.

η_v Volumetric efficiency.

η_o Overall efficiency.

θ Helix angle of screw, degrees.

θ' Helix angle of screw at outer periphery, degrees.

θ'' Helix angle of screw at core, degrees.

λ Helix angle of grain path, degrees.

μ Coefficient of internal grain friction.

μ_c Coefficient of friction between grain and casing.

μ_s Coefficient of friction between grain and screw surface.

π 3.1416

ρ Bulk density, slugs/cub.ft.

σ Angle of inclination of a mass of grain, degrees.

ϕ Angle of repose of grain, degrees.

ϕ_c Friction angle for grain on casing, degrees.

ϕ_s Friction angle for grain on screw surface, degrees.

ψ Constant in output, volumetric efficiency and overall efficiency equations.

C O N T E N T S

SECTION 1

INTRODUCTION AND CONSIDERATION OF VARIABLES

1.1 INTRODUCTION

In recent years, the modern mechanization of farming methods in Australia has led to a considerable increase in the bulk handling of grain both on individual farms and at Government grain terminals. Mechanical handling equipment plays an important role in the bulk handling process and in this respect the grain auger type elevator is widely used.

Grain augers may be arranged for operation at all angles of elevation up to the vertical. They consist essentially of a power-driven spiral or helical flight which revolves in a stationary tubular casing; practical limitations require a liberal clearance between the flight and the casing and this has been shown to be beneficial rather than detrimental to performance. The auger flight projects beyond the casing at the lower or intake end, this projection being referred to as the "choke". Grain is discharged through a chute at the top end of the casing.

Grain augers are an adaptation of the screw type conveyor which has been long established for the handling of materials in industry. However, the industrial type screw conveyors usually have a U-shaped open trough casing and are generally used in the horizontal or slightly inclined positions. They function primarily by positive displacement and operate at much lower speeds than augers, the speed depending largely on the size of the conveyor and nature of the material conveyed.

The principle of the screw and auger type conveyors originates from the Archimedean Screw which was first used more than 2,000 years ago for the pumping of water. However, the Archimedean screw differs in that the casing is attached to the flight, both rotating together. For this

reason, it is essentially a positive displacement conveyor, particularly at low speeds, and depends on the free flow of the material conveyed. Its use is limited therefore to low angles of elevation, and mainly to the conveying of fluids.

Despite the widespread application of augers, little work has been done to investigate their performance characteristics with a view to improving efficiency of operation and obtaining data for design purposes. Because of this, auger manufacturers have had to rely on established practice and subjective judgment for the design of their augers. Most manufacturers have conducted tests on their products and produced tabulated data of output and power requirements for selection purposes.

Experiments have been conducted to investigate the performance of Archimedean screws handling fluids (1) (2) * and data are available for the design of open-trough type screw conveyors handling various materials mainly in the horizontal and slightly inclined positions (3 to 9 incl.). However, these data cannot be applied directly to augers and therefore serve only as a guide. Fundamental investigations have been carried out on viscous liquid extruders of the helical screw type (10 to 18 incl.), but again this information serves only as a guide.

Some experimental work has been carried out recently in the United States of America and the findings of this work have been published (19 to 23 incl.). This work illustrates some performance characteristics of particular size augers but does not present data for general design purposes.

---

* Numbers in parenthesis refer to bibliography.

Some attempts have been made to give a theoretical analysis of the auger type conveyor. In 1956, Morin (24) developed theoretical expressions for the performance of the horizontal auger as used in combine harvesters; this followed previous work by the same author in 1954 (25) and also the work of Drozdov (26) in 1948 and Anakin (27) in 1954. Further work on the combine harvester auger has since been done by Zaika (28) in 1958. In 1956, Gutyar (29) carried out a comprehensive analysis of the vertical auger with extensions of the theory to cover augers in the inclined positions. The vertical auger has also been analysed by Thüsing (30) in 1958 and more recently by Baks and Schmid (31) in 1960.

Because of the complex dynamical behaviour of the granular materials in passing through an auger, an accurate account of the true conveying action is very difficult and the theoretical analyses carried out so far have, generally speaking, been based on somewhat simplified concepts. For instance, the vertical auger analyses have been built up on a study of a single grain particle in contact with both the surface of the screw at the outer periphery and the casing. This assumes that the grain behaves as a homogeneous mass and neglects the interaction between the grain particles under the influence of the various screw helix angles between the outside of the screw and the core. In addition, no attempt has been made to study the feeding action of the grain in the choke, which is shown to be an important factor governing auger output; all analyses carried out so far have been confined to a section of the screw within the casing. While these theoretical analyses have brought to light some interesting findings, the equations derived do not, in

general, give a true indication of auger performance. The need for more experimental work to be carried out, therefore, is emphasised.

Based on an experimental approach, the present investigation has been conducted on a model auger constructed to a quarter scale of a commercial unit; this permitted a comprehensive range of experiments to be conducted on a more manageable basis. The performance characteristics of the model auger have been studied and with the aid of dimensional analysis and dynamic similarity, equations have been developed and charts prepared to enable the performance of geometrically similar augers to be predicted.

The work on the model auger was first commenced in 1954 by Cady (32) as an undergraduate thesis; Cady developed the initial apparatus and studied some of its performance characteristics. The investigation was continued in 1955 by Roberts (33), also as an undergraduate thesis. This work was concentrated on improving the original apparatus which principally involved the construction of a new variable speed drive unit and dynamometer motor mounting for power measurement; some performance characteristics of the modified apparatus were studied. The present investigation is a continuation of this work.

Concurrently with the present work on the model auger, other undergraduate theses have been carried out at The University of New South Wales on a full scale auger.

In 1958 Cumming (34) designed a full scale auger test apparatus and conducted tests on a 6 in. auger. This work was continued in 1959 by Tong (35) who obtained further performance characteristics for the 6 in. auger. These data have been used as a check against the predicted data from the model auger investigation.

FIG. 1.

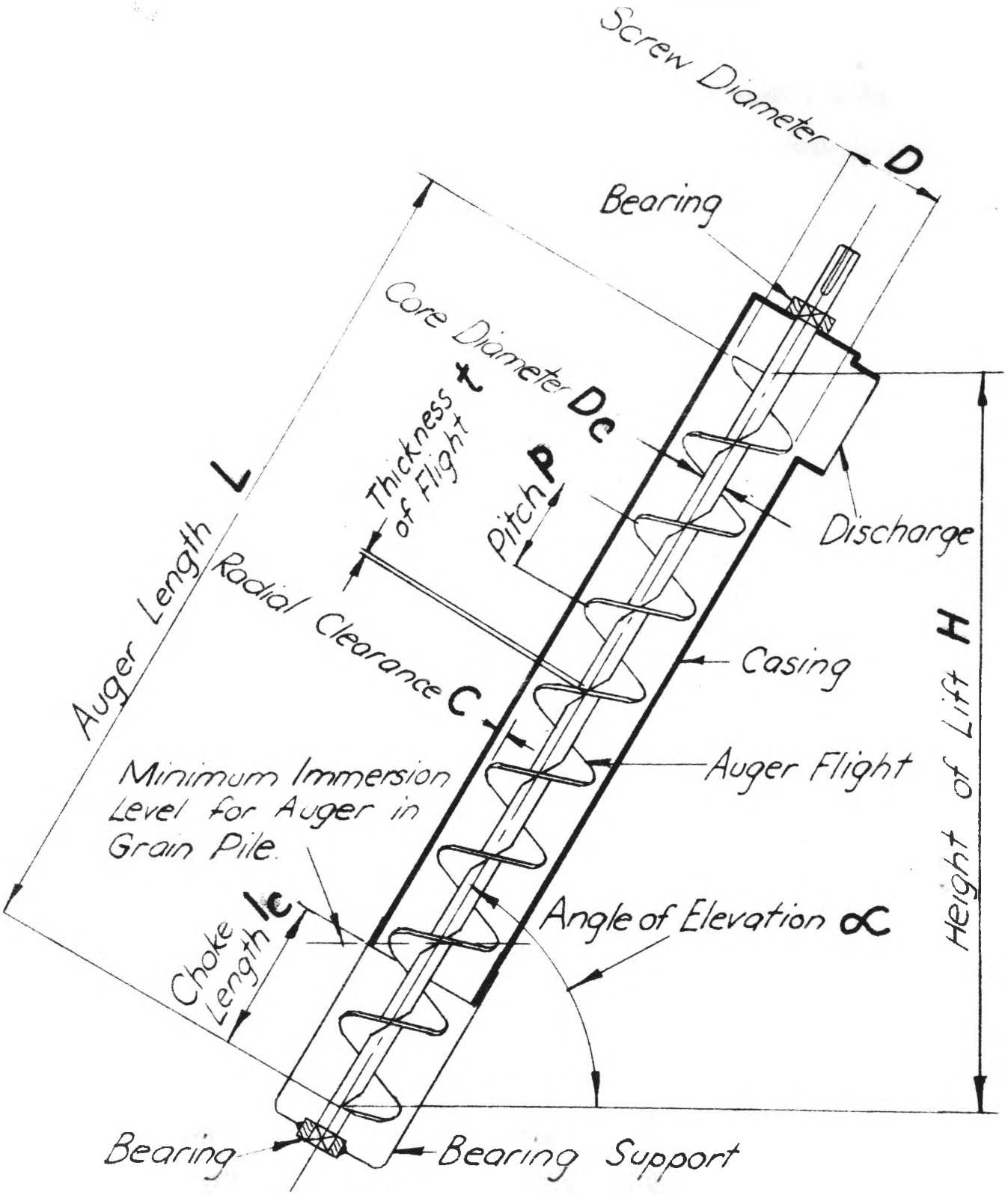

FIG. 1. AUGER VARIABLES

1.2 CONSIDERATION OF VARIABLES

In planning the investigation consideration was given to the variables influencing the auger performance. These variables, listed below, have been divided into two groups, those for the auger and those for the material conveyed:-

Auger Variables (Refer to Fig. 1)

Pitch	p	ft.
Outside diameter	D	ft.
Core diameter	Dc	ft.
Angle of elevation	α	degrees
Speed of rotation	N	r.p.m.
Auger length	L	ft.
Radial clearance between screw and casing	C	ft.
Choke length	l_c	ft.

Variables for materials conveyed

Average particle size	d	ft.
Bulk density	ρ	slugs/ft.^{3}
Acceleration due to gravity	g	ft/sec.^{2}
Co-efficient of internal grain friction	μ	where μ = tan ϕ, ϕ being the angle of repose

Coefficient of friction between grain and screw surfaces μ_s

where $\mu_s = \tan \phi_s$, ϕ_s being the friction angle

Coefficient of friction between grain and casing surface μ_c

where $\mu_c = \tan \phi_c$, ϕ_c being the friction angle

For a study of auger performance from the viewpoint of efficiency, the grain variables may be assumed constant; the results would be comparable for similar granular materials. However, consideration must be given to the grain variables in the data obtained for auger design purposes.

In studying the performance characteristics, the main aim is to examine the effects of varying speeds and angles of elevation on auger output, volumetric efficiency, power and overall efficiency for different auger proportions. For the work on the model auger, a one-to-one screw pitch to screw diameter ratio has been adopted, this being the most common ratio used in practice. Various choke lengths and two radial clearances have been tested. Although the model auger tests have been restricted to a core diameter one third of the outside screw diameter, a separate study of grain vortex motion in augers has given some indication of the effect of other core diameter to screw diameter ratios in relation to performance.

The principal material used in the model tests was Japanese millet seed, chosen for its small size to suit the model scale and its similarity in shape to that of wheat; the average grain size * of this millet is $d = 0{\cdot}075$ in. To examine the effect of other grain sizes, two output tests were conducted using wheat for which $d = 0{\cdot}18$ in., while in some preliminary experiments, clover seed, $d = 0{\cdot}03$ in., and polished millet seed were used. The effect of differing coefficients of friction have not been examined, although for many granular materials, there is no appreciable difference between the respective coefficients of friction μ , μ_s and μ_c; the design data presented in this work apply mainly to granular materials having similar properties to that of wheat.

---

* The grain size d is taken to be the mean of the three principal dimensions (length, breadth and thickness) of a granular particle. Such measurements were made for granular particles in a small sub-sample of the grain, the average size being accepted. This method of grain size determination is satisfactory for comparing grain particles of different size but of similar shape.

SECTION 2

APPARATUS AND METHOD OF CONDUCTING MEASUREMENTS

FIG. 2.

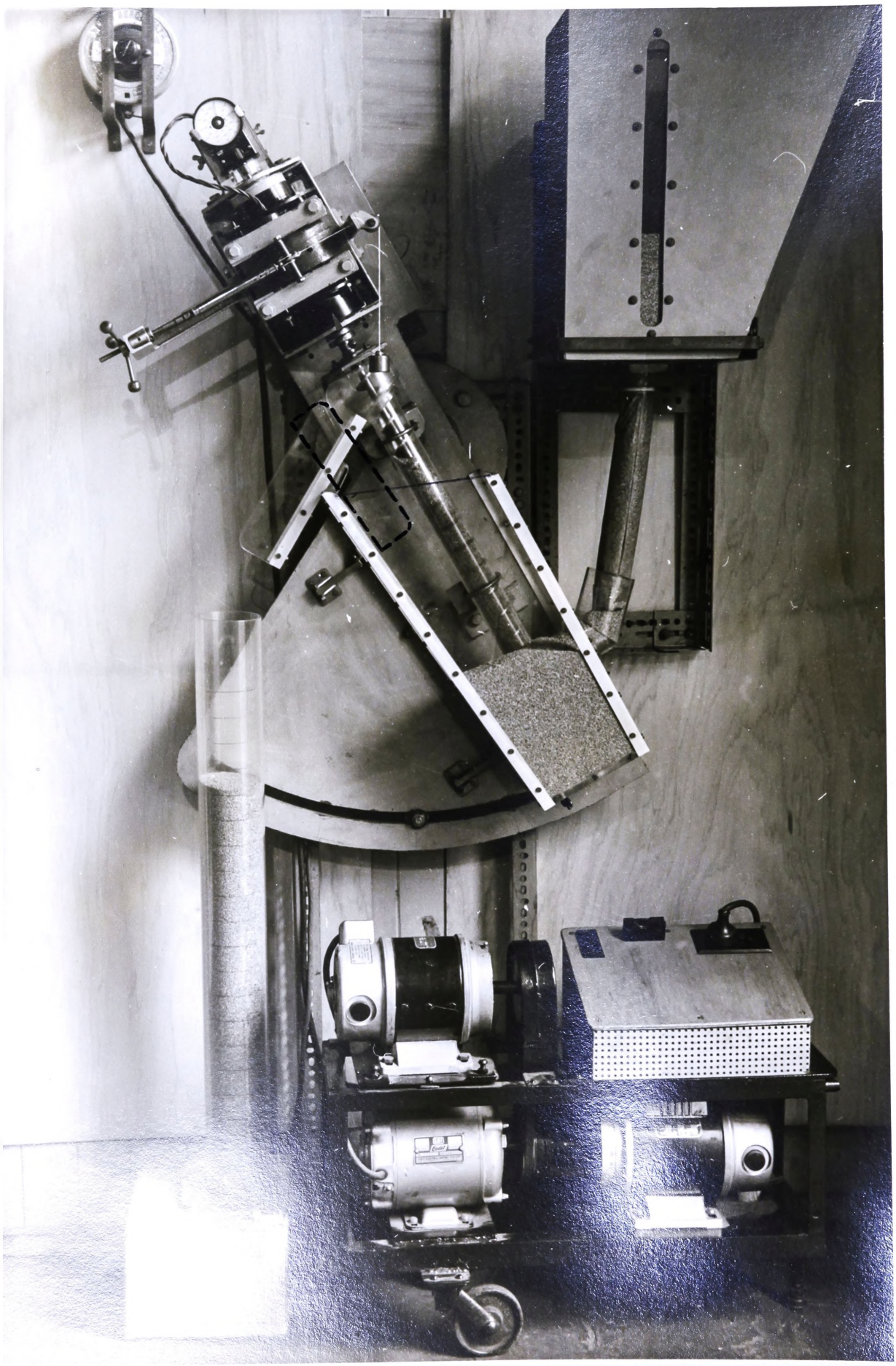

FIG. 2.
APPARATUS

2.1 DESCRIPTION OF APPARATUS

In this section a general description of the model auger apparatus as used in the main work of the investigation is given; an arrangement of this apparatus is shown in Fig. 2.

(a) Model Auger.

The auger screw has a pitch and diameter each of 1-1/2 inches, a core of 1/2 inch and a length of 24 inches, and was machined from a solid brass bar. The thickness of the screw is 1/8 inch; although large by proportion this thickness was considered to be the minimum for strength during the machining operation. The screw is mounted in two self-aligning, sealed, ballrace bearings which are attached to a pivoting base plate; this base plate allows operation at all angles of elevation varying from 0° to 90°.

Tests have been conducted with two auger casings having radial clearances of 1/8 inch and 1/64 inch respectively. These casings are of clear plastic allowing visual observation of the grain motion through the auger. The casings are shorter than the screw with extension pieces of different lengths which are clamped to the lower end of the casings to give any desired choke length; the lower end of one casing is featured in Fig. 3. As shown in Fig. 4, the auger is fitted with a special radial discharge chute. Preliminary tests (33) using a conventional type discharge chute leading off perpendicularly to the casing revealed that grain compaction occurred in the top of the casing at the higher angles of elevation, particularly at high speed; this resulted in an excessive power consumption. By using the radial discharge chute the compaction was eliminated and the power substantially

FIGS. 3 & 4.

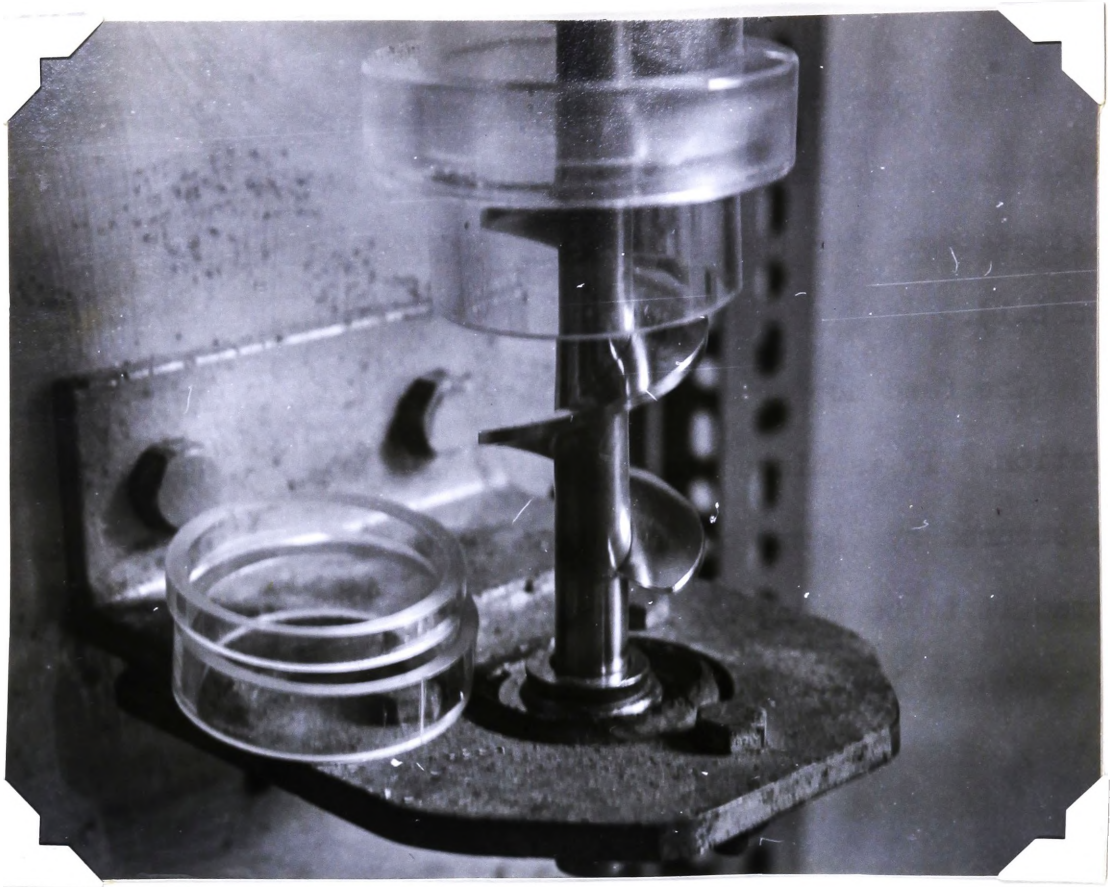

FIG. 3. DETAILS OF CHOKE AND EXTENSION PIECES

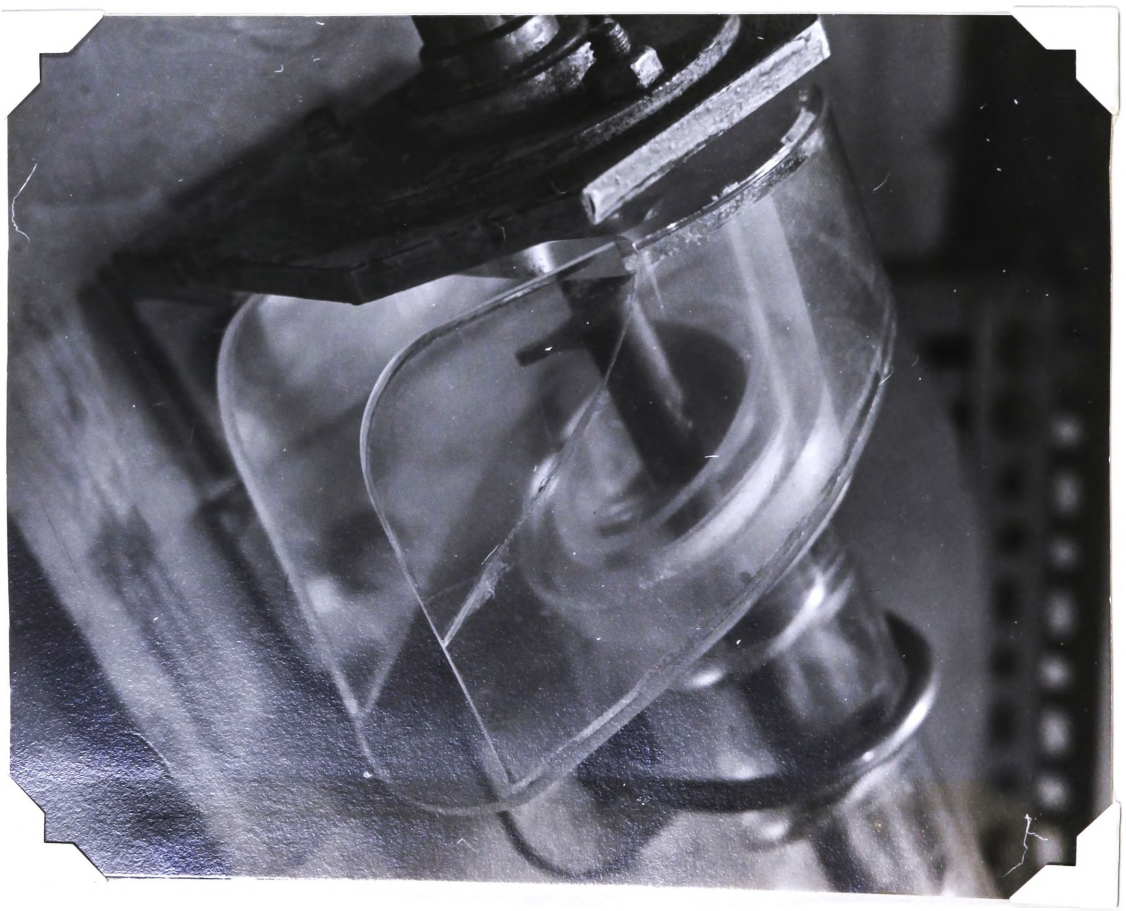

FIG. 4. RADIAL DISCHARGE CHUTE.

reduced; the power reduction ranged from approximately 35 per cent at 200 r.p.m. to approximately 66 per cent at 800 r.p.m. (Details of the comparative tests for the two types of discharge chute are given in Section 6.1).

The feed hopper is also of clear plastic to allow visual observation. It is hinged to the auger base plate on the left hand side and is secured by clamps on the right hand side; this arrangement permitted it to be swung clear with relative ease when it was desired to alter the choke length of the auger. A swinging flap is incorporated in the bottom of the hopper for emptying purposes while a filling pipe is mounted on the right hand side. The hopper covers more than two thirds the length of the auger, reducing grain spillage to a minimum.

As shown in Fig. 2, a pivoting outlet chute is fitted to the top of the feed hopper. This serves the purpose of directing the grain either into the measuring cylinder, as shown, or back into the bottom of the case hopper for recirculation; for the latter case, the pivoting chute is arranged in the position indicated by dotted lines in Fig. 2. Owing to the limited grain capacity, recirculating the grain was found to be very convenient when it was desired to study the grain flow through the auger, although this could only be employed at the higher angles of elevation; at low angles of elevation the grain would not flow back to the bottom of the hopper at a rate fast enough to meet the demand.

A supply hopper, mounted above the feed hopper as shown in Fig. 2, maintains a reasonably constant level of grain at intake. This hopper is fitted with a sliding valve in the bottom to control the flow

of the grain; a flexible plastic tube connects the outlet of this hopper to the filling pipe of the feed hopper.

(b) Variable Speed Control Unit

Speed variation for the model auger is obtained by using a direct current driving motor in conjunction with a variable speed control unit which is based on the Ward Leonard system. The motor-generator set and control rheostat are shown in Fig. 2, while an enlarged view of the motor-generator set is given in Fig. 5. The circuit diagram for the control unit is given in Fig. 6.

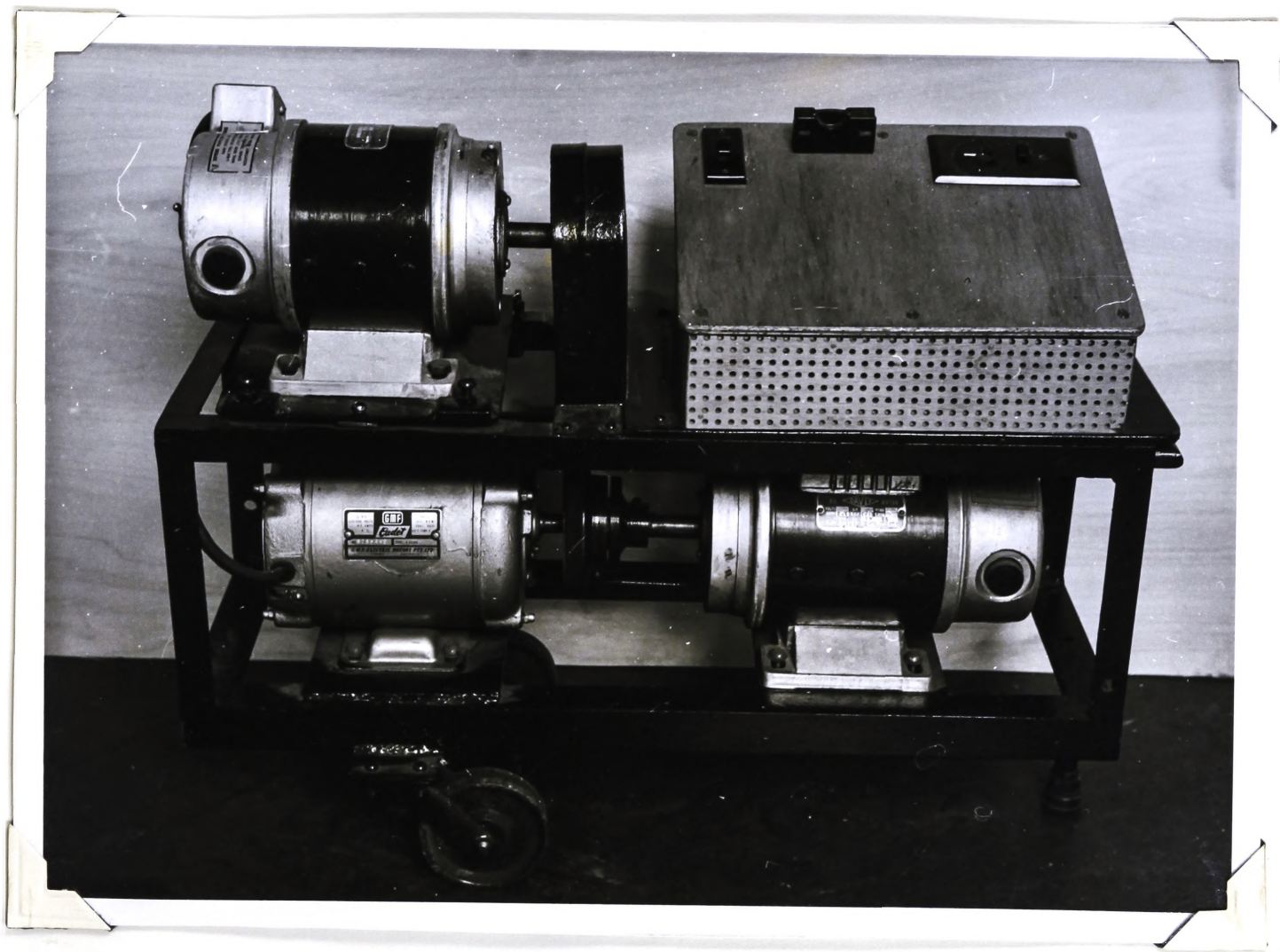

FIG.5. MOTOR - GENERATOR SET

FIG. 6.

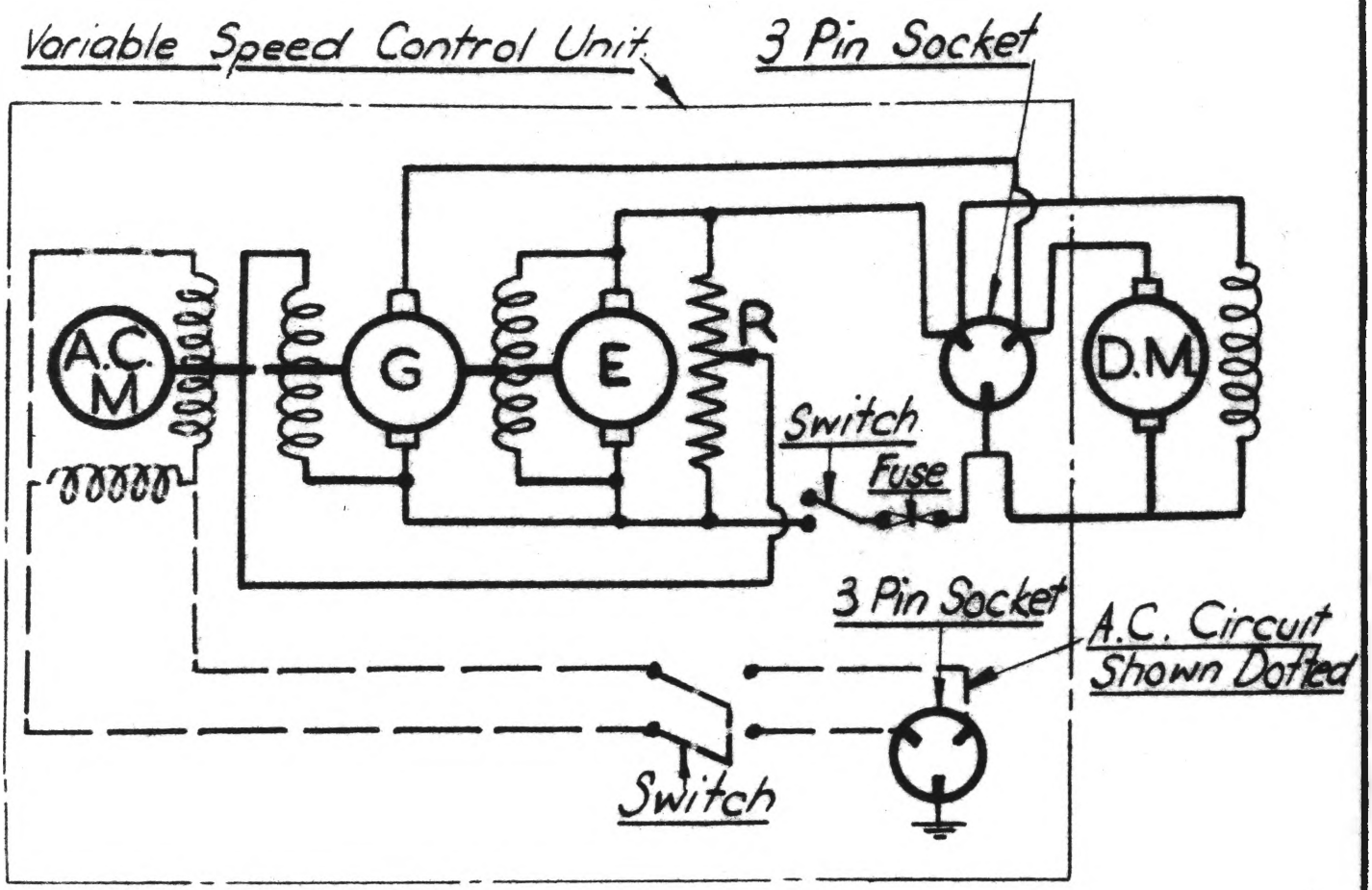

A.C.M. — A.C. Driving Motor ~ $\frac{1}{2}$ H.P., 1425 R.P.M., 240 Volt, Single Phase.

G. — D.C. Shunt Generator ~ $\frac{1}{2}$ H.P., 1440 R.P.M., 240 Volt.

E — D.C. Shunt Exciter ~ $\frac{1}{4}$ H.P., 1440 R.P.M. 240 Volt

D.M. — D.C. Shunt Driving Motor ~ $\frac{1}{4}$ H.P.

R — 200 Ohm, 300 Watt, Toroidal Type Rheostat, 1·22 amp Current Carrying Capacity.

FIG. 6. CIRCUIT DIAGRAM FOR VARIABLE SPEED CONTROL UNIT.

The 1/2 horsepower A.C. motor drives the 1/2 horsepower D.C. shunt generator through a flexible coupling and the 1/4 horsepower D.C. exciter, which is mounted above the driving motor, through a V-belt drive. The driving motor, generator and exciter each operate at a speed of approximately 1425 r.p.m.

As shown in the circuit diagram, a 200 ohm rheostat is connected as a variable resistance in series with the field of the generator and also as a fixed resistance in parallel with the armature and field of the exciter. This rheostat is of the toroidal type with a power rating of 300 watts and a current carrying capacity of 1.22 amps. The D.C. exciter supplies constant voltage excitation to the field of the 1/4 horsepower shunt wound driving motor and also variable voltage excitation to the field of the generator. This provides means of controlling the voltage applied to the armature of the driving motor permitting speed variation.

Satisfactory speed control of the driving motor with adequate torque could be obtained over the range 200 to 3000 r.p.m.

(c) Dynamometer Motor.

An enlarged view of the variable speed dynamometer driving motor is shown in Fig. 7, while an arrangement drawing is given in Fig. 8. The dynamometer was developed (33) by constructing a special pivoting cradle to suit the 1/4 horsepower, direct current driving motor.

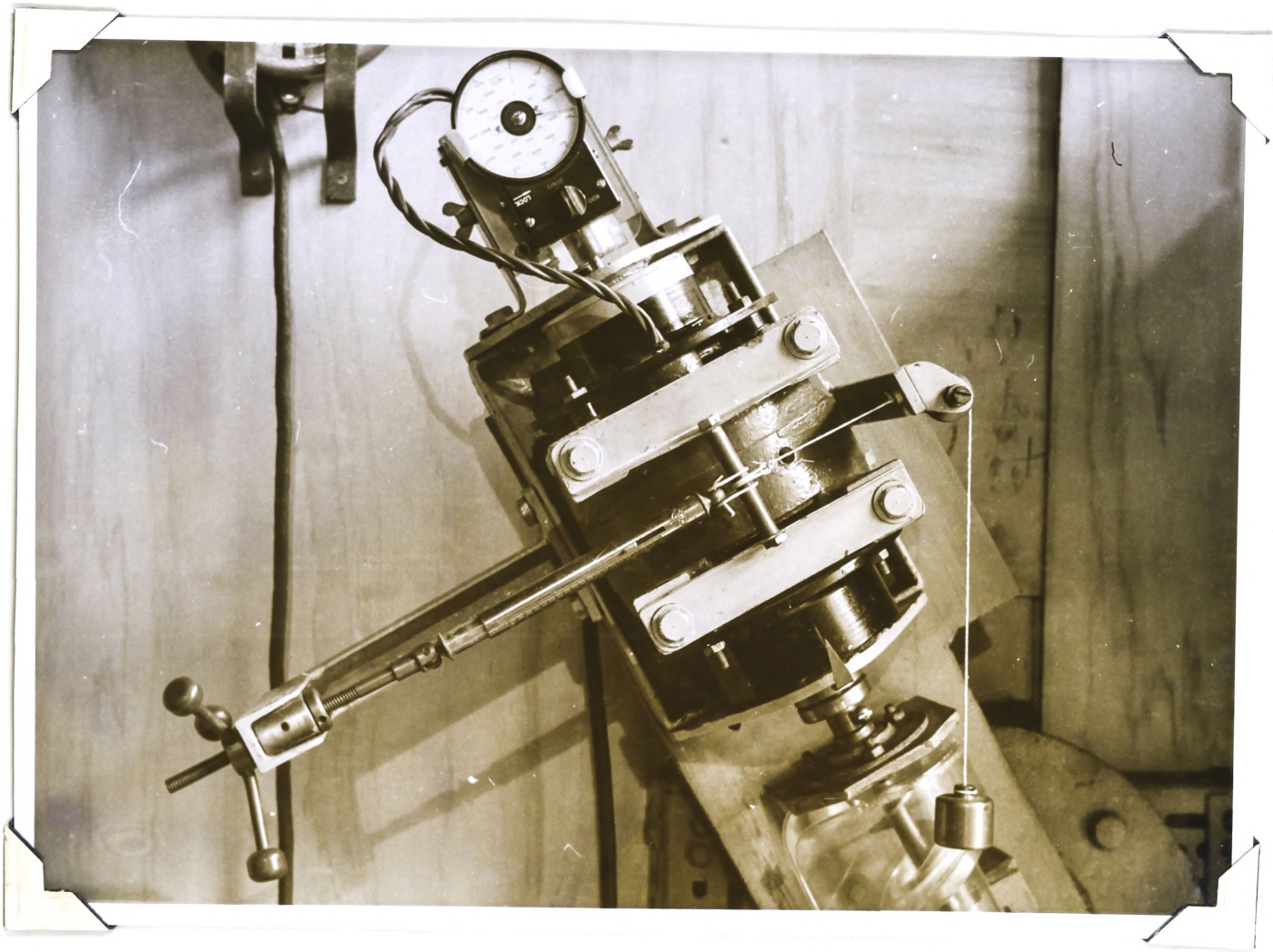

FIG. 7. DYNAMOMETER MOTOR

FIG. 8.

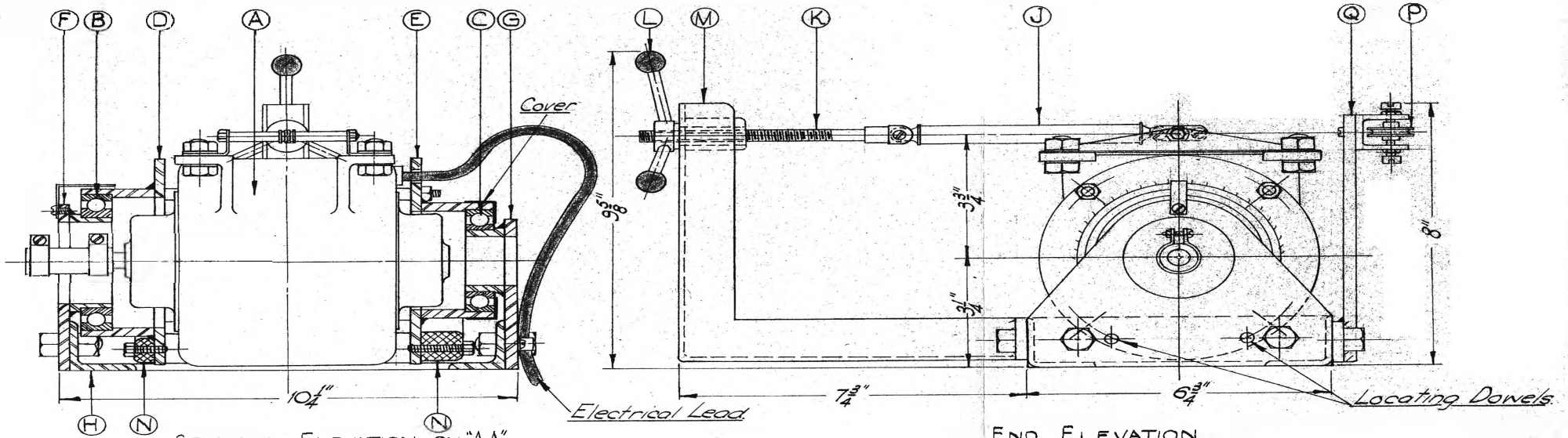

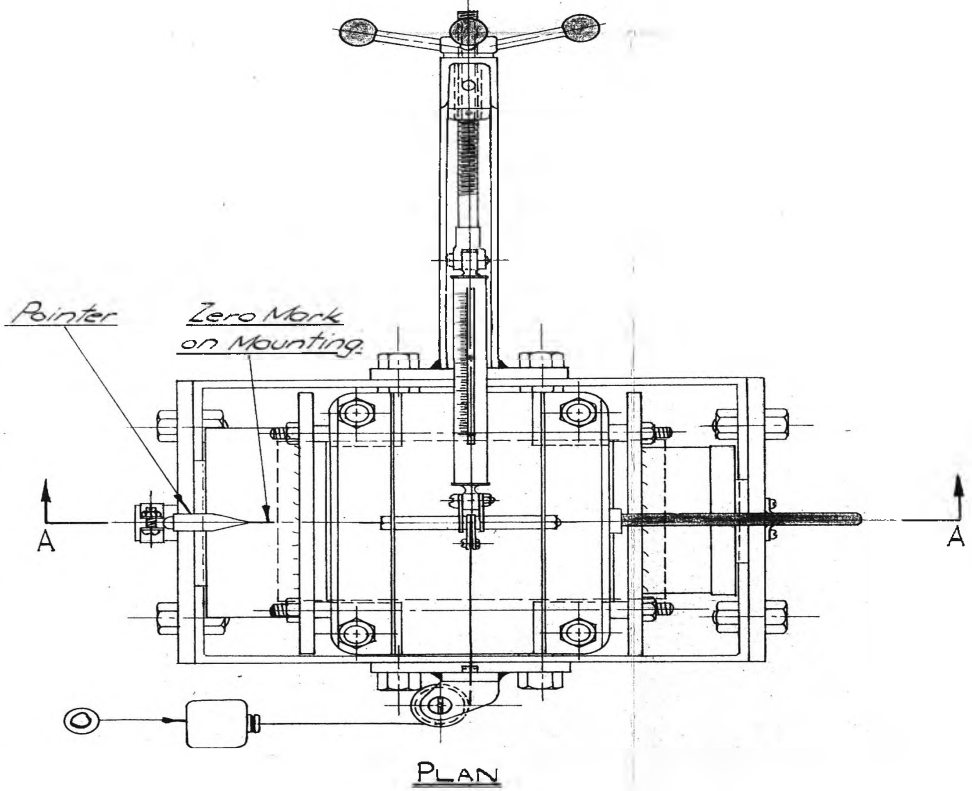

— LIST OF ITEMS —

ITEM	DESCRIPTION
Q	Arm for Pulley "P"
P	Pulley
O	Counterweight
N	Lead Balance Weights
M	Arm
L	Adjusting Nut
K	Adjusting Screw
J	1000 gm. Spring Balance
H	Base Frame
G	Supporting Bracket
F	Supporting Bracket
E	End Plate
D	End Plate
C	Ball Race Bearing XLS 1 7/8"
B	Ball Race Bearing XLS 2 3/4"
A	1/4 H.P., D.C. Driving Motor

FIG. 8.

N.S.W. UNIVERSITY OF TECHNOLOGY
SCHOOL OF MECHANICAL ENGINEERING.

GENERAL ARRANGEMENT OF DYNAMOMETER MOTOR FOR EXPL GRAIN AUGER

SCALE: 6"=1'-0"

DRAWN: A.W.R. 13-2-56

Referring to Fig. 8, it can be seen that the motor "A" is mounted on ballrace bearings "B" and "C" which are of the extra light, deep groove type. The end plates "D" and "E" are each fitted with four locating pegs; these pegs were machined on the inside concentric with the bearing housings and are used for the purpose of locating the plates on the end covers of the motor; the end covers of the motor were appropriately machined for this purpose. The plates are secured by the four bolts fastening the motor framework. The supporting brackets "F" and "G" are bolted to the base frame "H", the bracket "F" being located in position by means of dowels.

For the reaction load measurement, the 1000 gram tubular type spring balance "J" is used. This is fixed to the motor frame at one end at a radius of 3-3/4 in; the other end is secured to the adjusting screw "K" attached by means of the adjusting nut "L" to the arm "M". The adjusting screw is used for centering the motor for the load measurement.

Since the dynamometer is required for use at all angles of elevation, the motor was balanced by means of lead weights "N". In addition, the counterweight "O" attached to the motor frame by means of a string passing over the pulley "P" on arm "Q" gives the spring balance an initial zero reading. This serves the purpose of overcoming the tendency for the balance to stick when measuring light loads; also, it allows correct readings to be obtained when the balance is used in positions other than the vertical.

A tachometer is used for the measurement of the motor speed. As shown in Fig. 7, this is held in an adjustable bracket permitting it to be locked in position against the motor shaft when speed measurement is required.

2.2 METHOD OF CONDUCTING MEASUREMENTS

The tests on the model auger have been carried out over the speed range 200 to 2000 r.p.m. for various angles of elevation and choke lengths. In this section a brief description of the method of conducting the output, "fullness" of running, and power measurements is given. (The various test results are tabulated in the Appendices).

(a) Measurement of Output.

The output was determined volumetrically by timing the flow of grain into a 0.20 cubic feet capacity measuring cylinder. Because volumetric measurement is subject to error, since the volume of a given mass of grain changes with different degrees of compaction, to avoid such error, all output measurements were based on approximately the same condition of grain compaction; the actual volume of grain as delivered by the auger was measured. The somewhat loosely packed state of the grain in the measuring cylinder would correspond approximately to the state of grain elevated by a full scale auger into a storage bin.

The effect of compaction was observed by allowing different quantities of grain delivered by the model auger into the measuring cylinder to be compacted; this was done by jolting the measuring cylinder a given number of times in each case. It was found that the percentage reduction in volume was approximately constant for all quantities examined, the average reduction being 10 per cent.

Also to avoid error, the head of grain over the choke was kept as near constant as possible during each test. However, small changes in head were shown to produce no noticeable change in output. The

critical factor as far as output is concerned is for the auger to be immersed in the grain pile at least to the level of the lower end of the casing, otherwise the auger will not elevate the grain.

(b) Measurement of "Fullness" of Running.

To estimate the "fullness" of running of the auger under various operating conditions, approximate measurements of the mean axial height of grain on each pitch of the auger flight have been obtained. These measurements were confined to the tests using the auger casing having the smaller radial clearance. The approximate mean grain heights were measured with the auger stationary following each output test; the small casing clearance and full immersion of the choke which prevented the grain from slipping back allowed these measurements to be taken.

(c) Measurement of Power.

To eliminate the effect of varying drive losses, the net power to convey grain has been determined; full-load and no-load tests were carried out for this purpose. The no-load power measurements were obtained with the auger running empty; each no-load test was conducted either immediately before or immediately after the corresponding full-load test in order to eliminate, as far as possible, errors due to changes in operating conditions.

Because of the very small power requirements of the model auger, it was difficult to obtain accurate power measurements. While the dynamometer proved to be quite responsive to changes in load, its sensitivity was somewhat impaired by friction in the moving parts. For this reason, two spring balance readings were taken for each power

measurement, one reading for increasing load and one reading for decreasing load; the mean of the two readings was accepted in each case. The method of obtaining the final power figures from the experimental results is described in Appendix IX.

SECTION 3

PERFORMANCE CHARACTERISTICS

FIG.9.

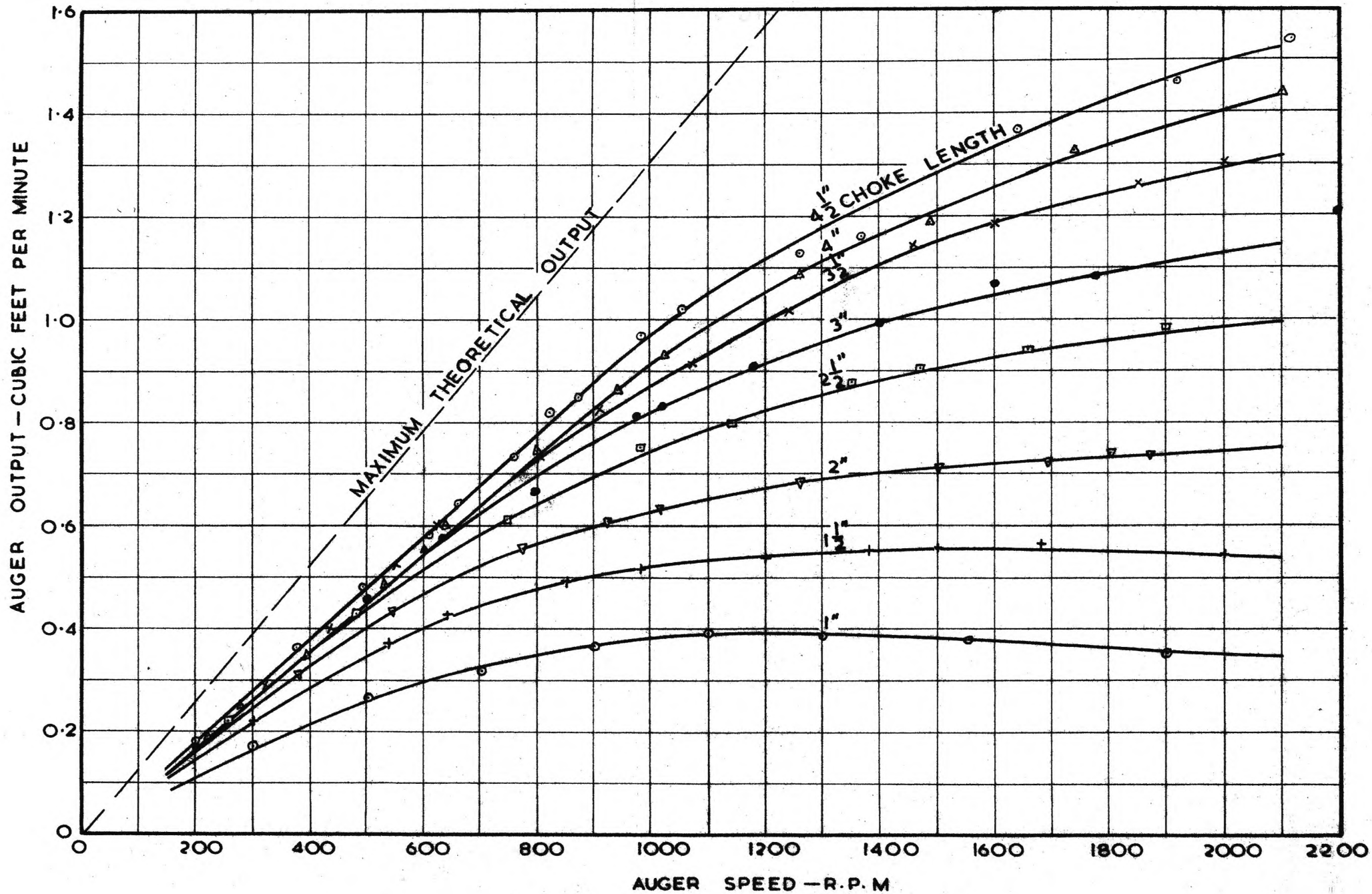

FIG. 9. OUTPUT VERSUS SPEED FOR VARIOUS CHOKE LENGTHS

Angle of Elevation: 30° Radial Clearance: $\frac{1}{64}$ inches Material Conveyed: Millet

FIG. 10.

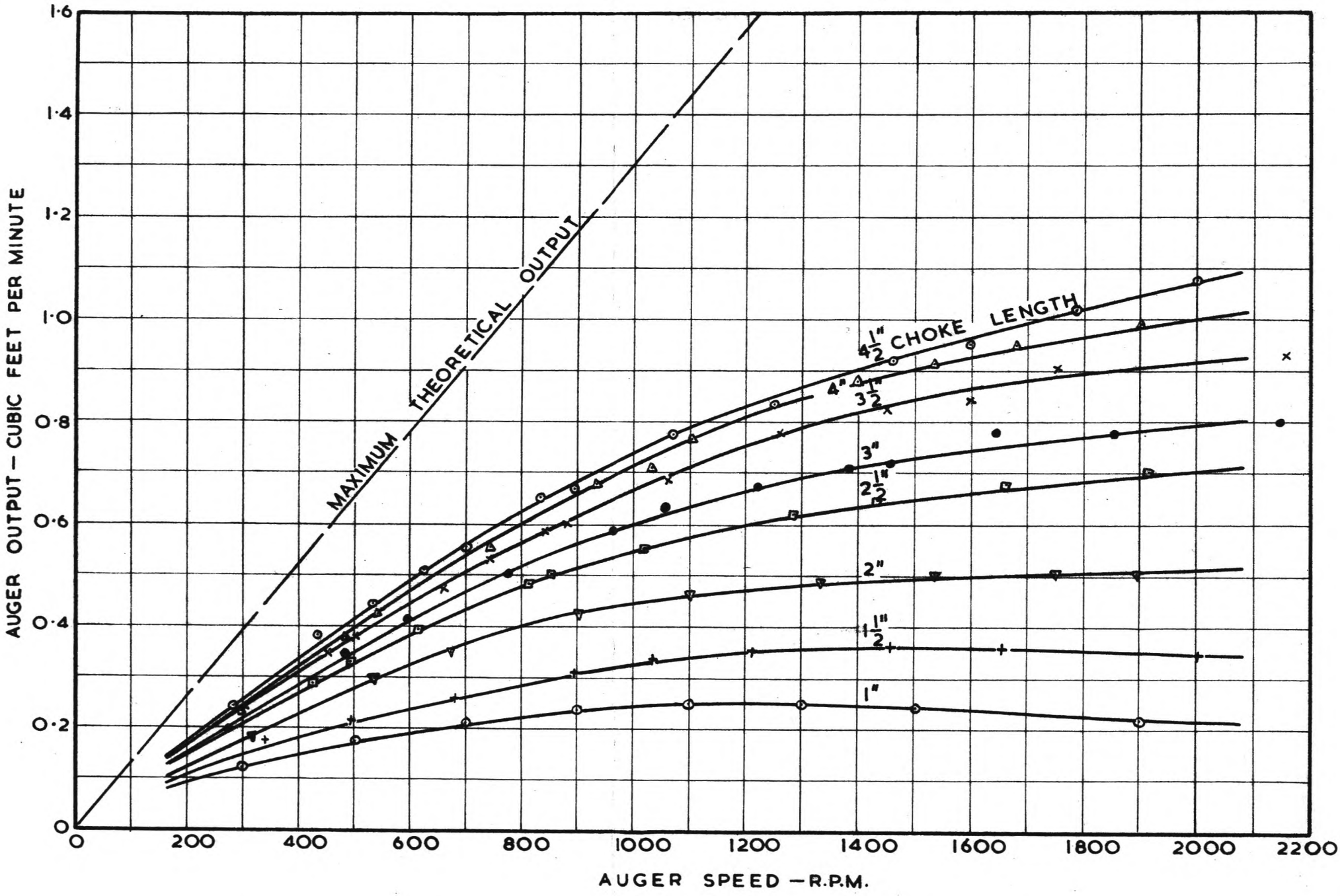

FIG. 10. OUTPUT VERSUS SPEED FOR VARIOUS CHOKE LENGTHS
Angle of Elevation: 60° Radial Clearance: $\frac{1}{64}$ inches Material Conveyed: Millet

FIG. 11

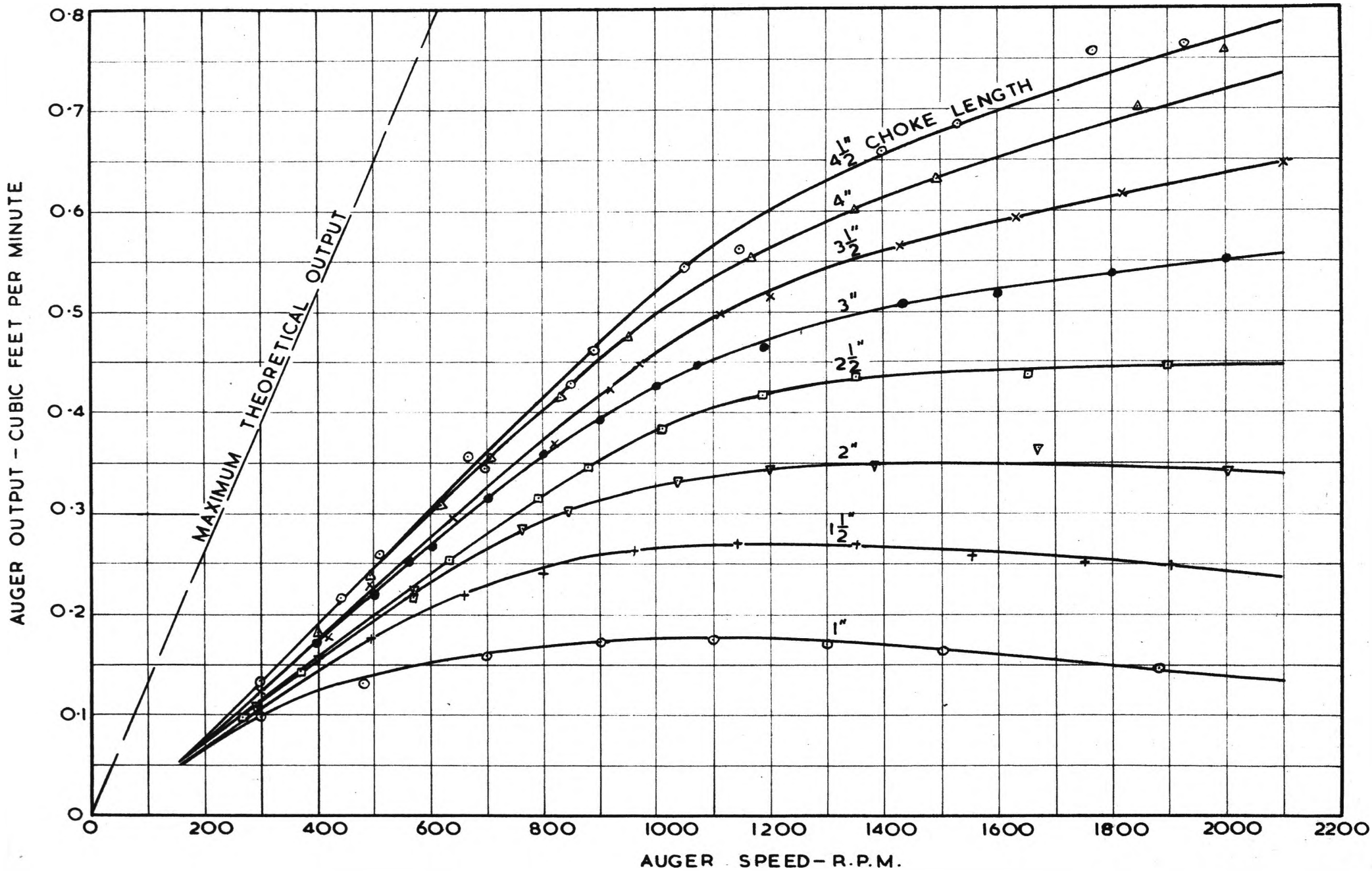

FIG. 11. OUTPUT VERSUS SPEED FOR VARIOUS CHOKE LENGTHS
Angle of Elevation: 90° Radial Clearance: $\frac{1}{64}$ inches Material Conveyed: Millet

FIG. 12.

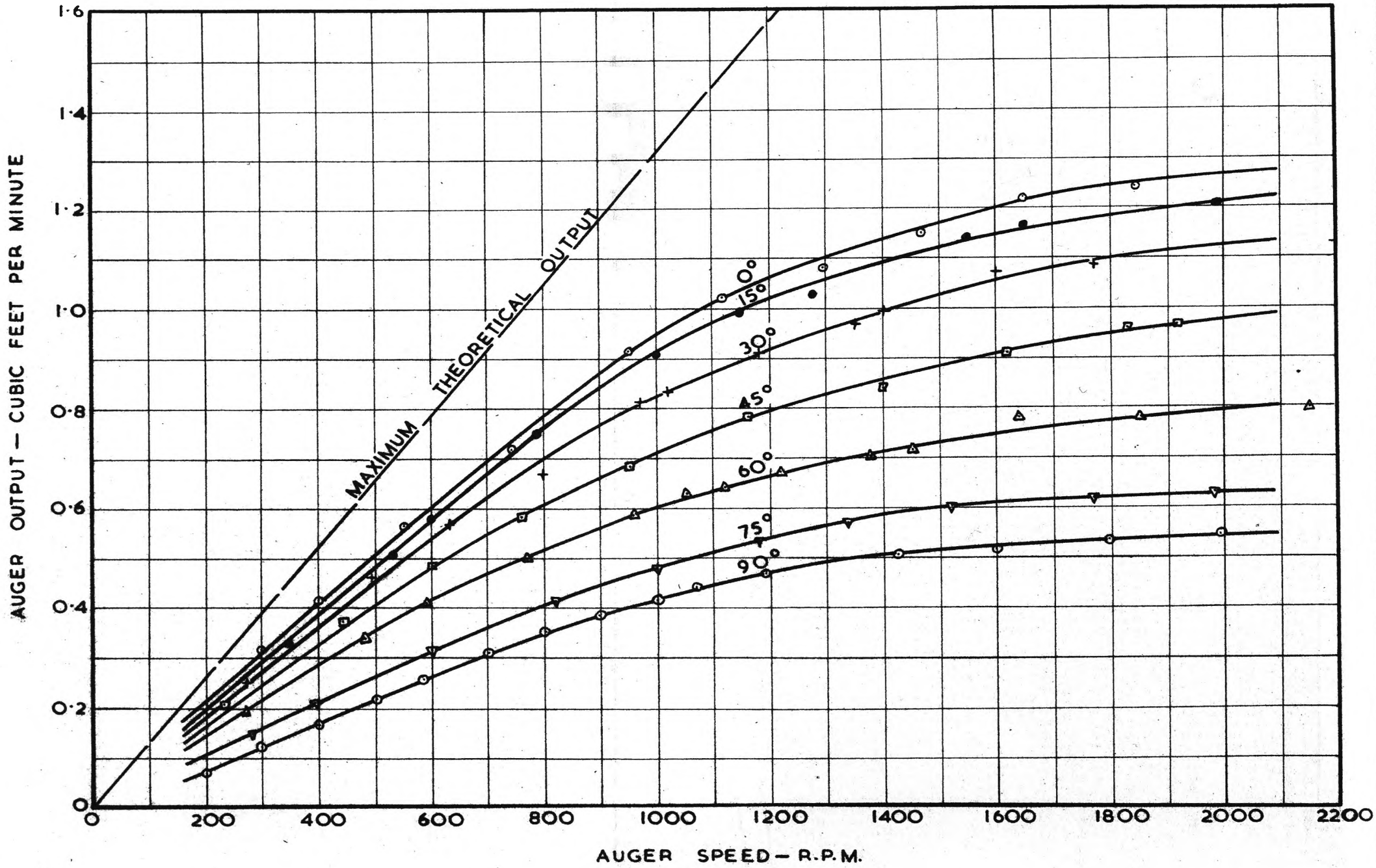

FIG. 12. OUTPUT VERSUS SPEED FOR VARIOUS ANGLES OF ELEVATION
Choke Length: 3 inches Radial Clearance: $\frac{1}{64}$ inches Material Conveyed: Millet

FIG. 13.

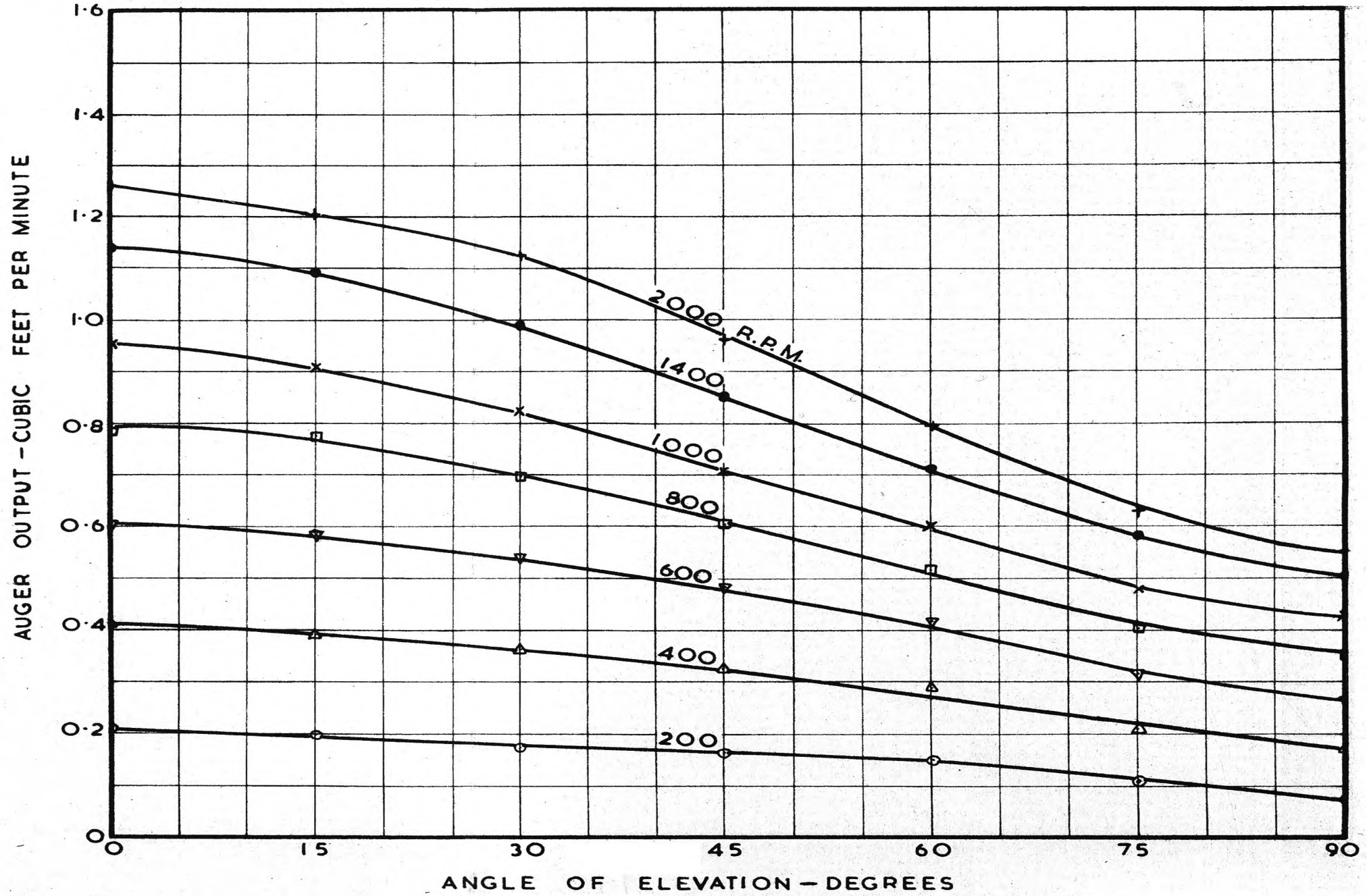

FIG. 13. OUTPUT VERSUS ANGLE OF ELEVATION FOR VARIOUS SPEEDS
Choke Length: 3 inches Radial Clearance: $\frac{1}{64}$ inches Material Conveyed: Millet

FIG. 14.

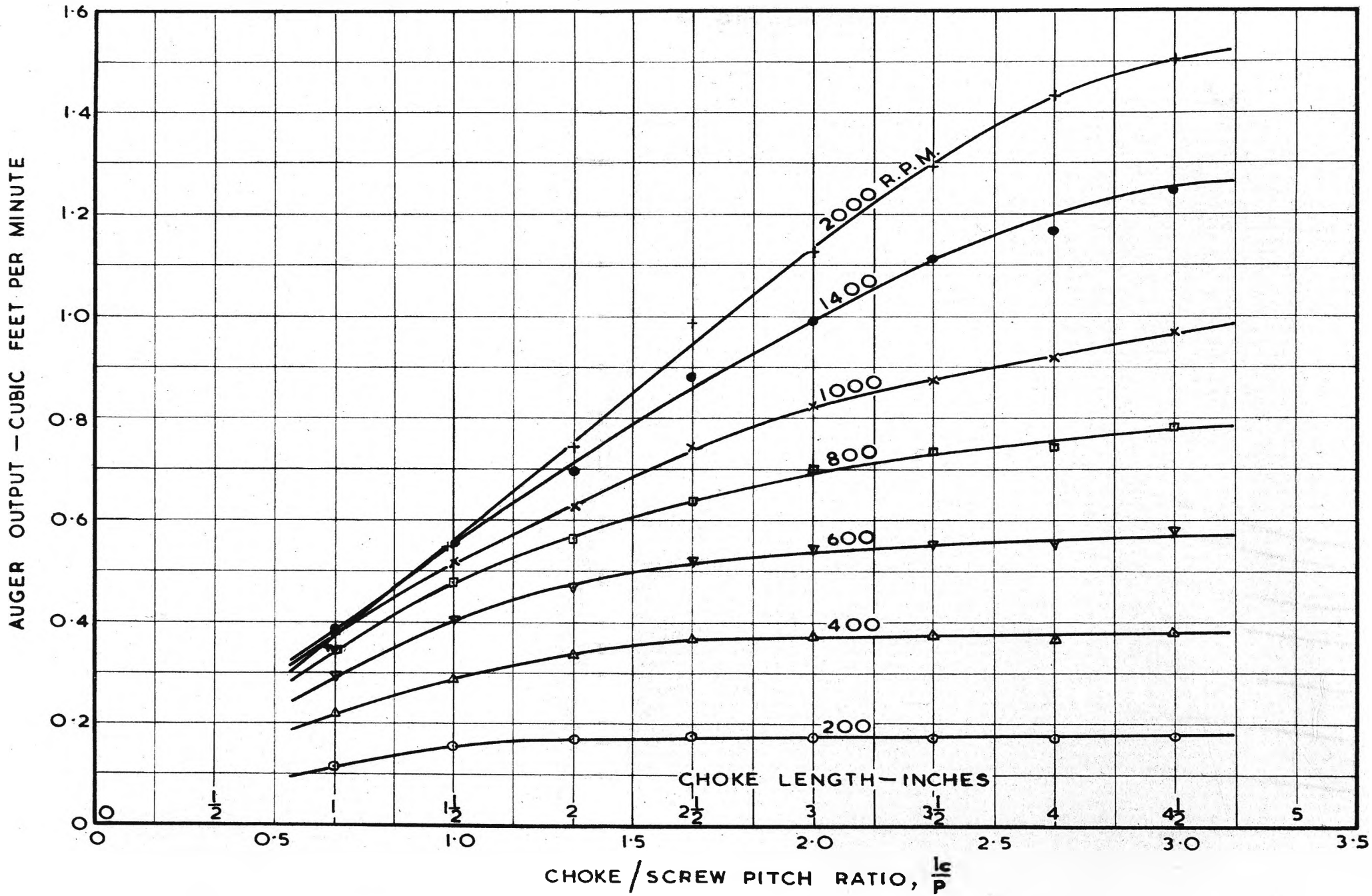

FIG. 14. OUTPUT VERSUS CHOKE LENGTH FOR VARIOUS SPEEDS

Angle of Elevation: 30° Radial Clearance: $\frac{1}{64}$ inches: Material Conveyed: Millet

FIG. 15.

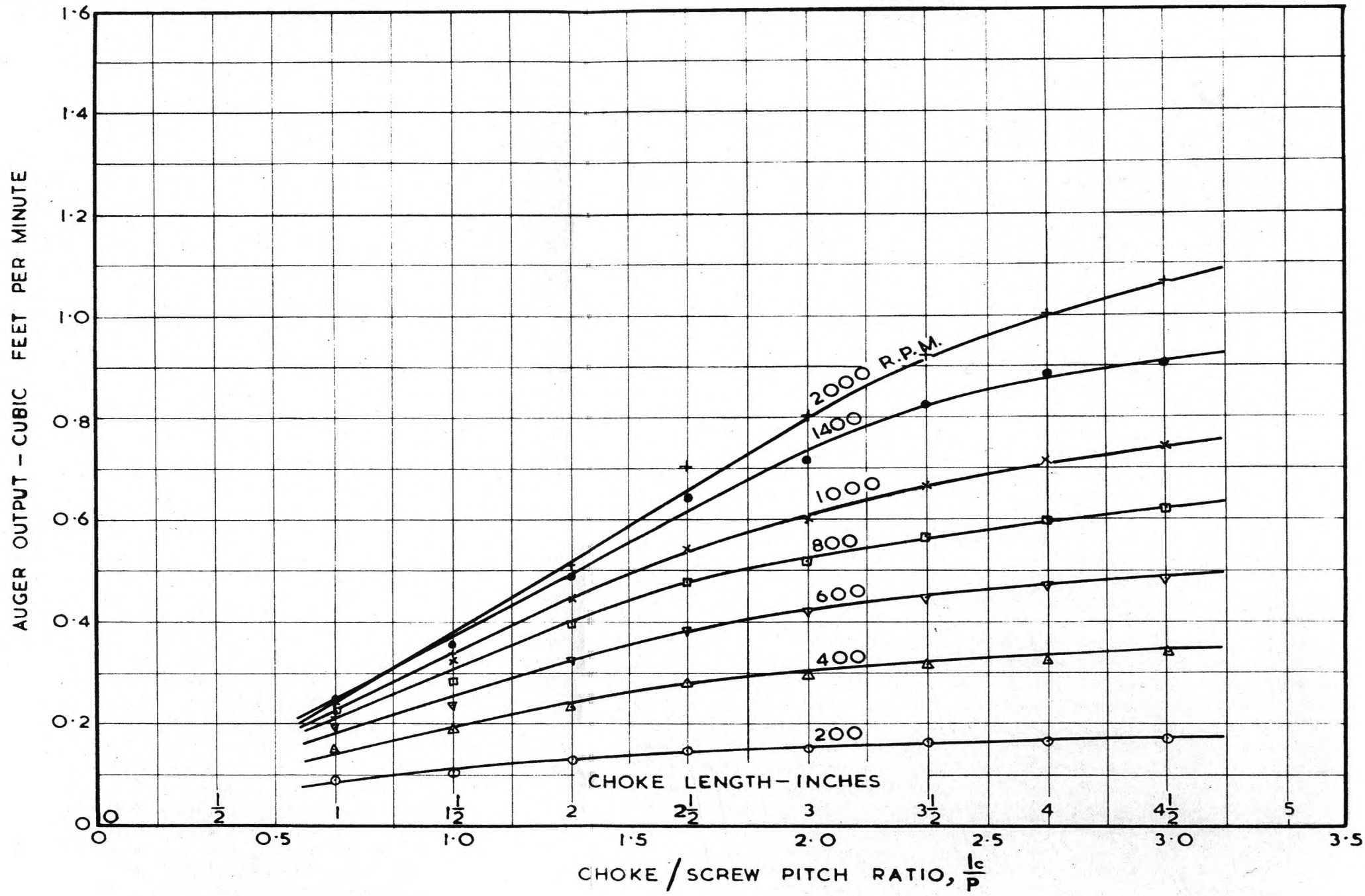

FIG.15. OUTPUT VERSUS CHOKE LENGTH FOR VARIOUS SPEEDS
Angle of Elevation: 60° Radial Clearance: 1/64 inches Material Conveyed: Millet

FIG. 16.

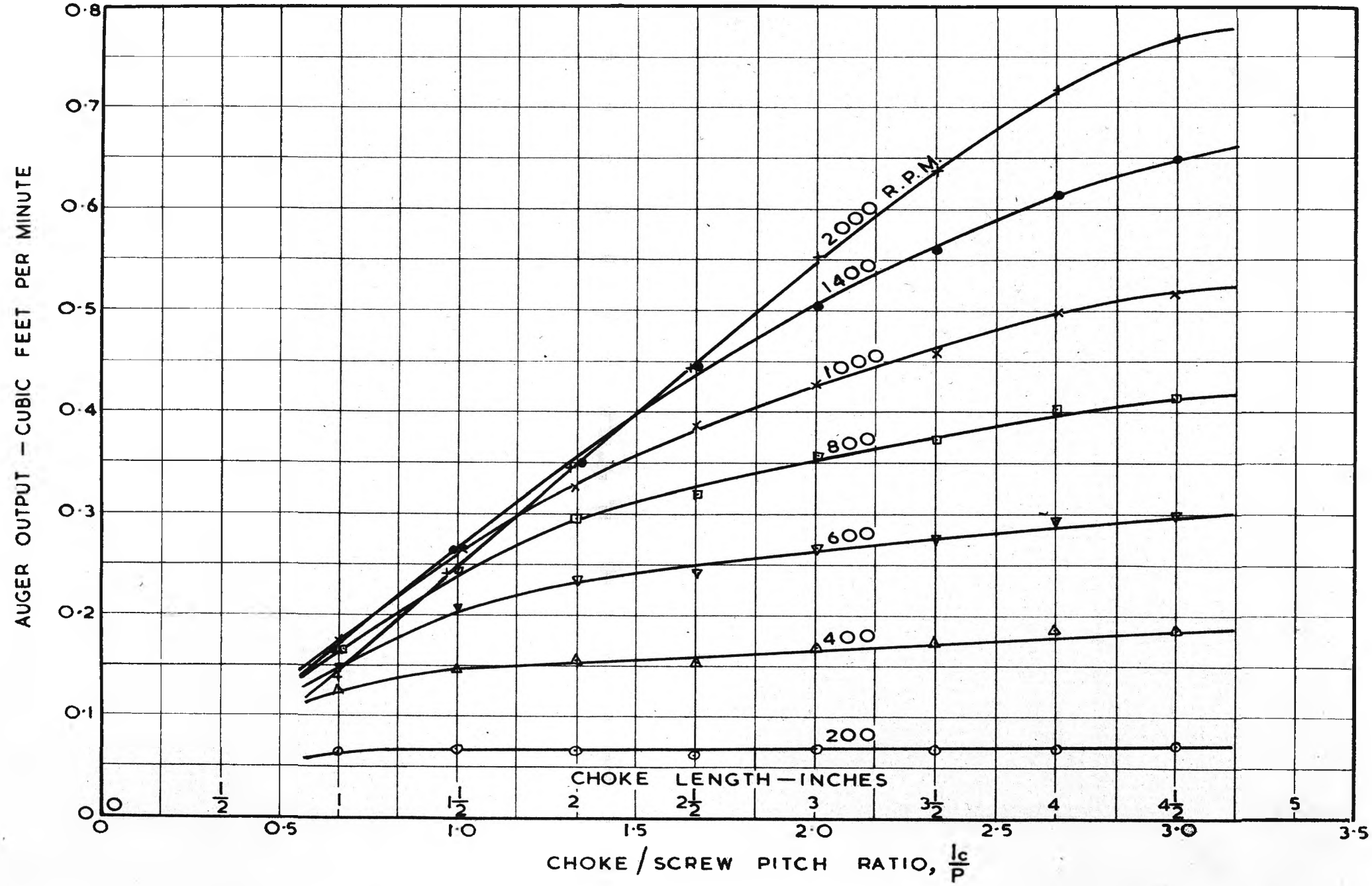

FIG. 16. OUTPUT VERSUS CHOKE LENGTH FOR VARIOUS SPEEDS
Angle of Elevation: 90° Radial Clearance: $\frac{1}{64}$ inches Material Conveyed: Millet

3.1 AUGER OUTPUT

An examination has been made of the model auger output primarily in relation to speed, angle of elevation, and choke length. Typical output graphs are shown in Figs. 9 to 16, the results plotted being for a radial casing clearance of 1/64 inch (C/D = 0.0104).

Figs. 9, 10 and 11 show how the output varies with speed and choke length for the respective angles of elevation 30°, 60°, and 90°, while Fig. 12 summarises the output versus speed graphs for several angles of elevation for the 3 inch choke length ($^{1}c/p = 2$). In the low speed range the output increases uniformly with speed but the rate of increase lessens as the speed becomes higher; at the smaller choke lengths the output is shown to reach a maximum and then to remain constant or to decrease slightly, particularly at the higher angles of elevation. Fig. 13 shows how the output decreases with increase in angle of elevation, the rate of decrease being higher at the higher speeds than at the lower.

The experiments have shown that choke length has a marked influence on auger output, this being best illustrated in Figs. 14, 15 and 16. At very slow speeds, under near static conditions, a minimum choke length of one screw pitch is sufficient to trap the maximum amount of grain. However, as the speed increases, the vortex formed limits the amount of grain that can be trapped; also the centrifugal grain pressure impairs the inward flow of grain in the choke, particularly at the higher angles of elevation. To compensate for this, larger choke lengths are necessary at higher speeds.

Choke lengths up to three pitches have been tested and it can be observed that the optimum output is obtained in this range only at the lower speeds; greater choke lengths would be required at the higher speeds to attain maximum output. The high rate at which the output increases with choke length at the higher speeds is clearly shown. For instance, at 2,000 r.p.m. and angle of elevation 90°, (Fig. 16) the output increases from 0.25 cub.ft. per min. for $^{1}c/p = 1$ to 0.77 cub.ft. per min. for $^{1}c/p = 3$, an increase of over 200 per cent.

The choice of a choke length for a particular auger may be a matter of compromise between practical limitations and the desirability for optimum performance. However, in general, choke lengths less than two pitches should be avoided.

3.2 VOLUMETRIC EFFICIENCY

Comparisons of the volumetric efficiencies under various operating conditions provide important information in the study of auger performance. The volumetric efficiency is based on the optimum output and is defined as follows:-

$$\eta_V = \frac{\text{Actual volume of grain delivered}}{\text{Maximum theoretical output}}$$

The theoretical output is independent of auger length and angle of elevation and is given by

$$Q_t = \frac{\pi}{4}\left[(D + 2C)^2 - D_c^2\right]\left[p - t\right] N \qquad \text{--------(3 - 1)}$$

Considering all geometrical proportions of the auger to be in fixed ratios to the auger diameter D, the above equation may be reduced to

$$Q_t = \gamma N D^3 \qquad \text{----------(3 - 2)}$$

where γ is a constant dependent on the geometry of the auger. For the model auger $\gamma = 0.67$ when fitted with the casing having the small clearance ratio, $\frac{C}{D} = 0.0104$ (Q_t will be in cubic feet per minute for D expressed in feet.)

The auger output and volumetric efficiency are controlled by two factors; firstly the amount of grain that can be trapped in the choke and conveyed into the casing; secondly, the amount of rotational motion given to the grain as it passes through the auger. As a means for

FIG. 17.

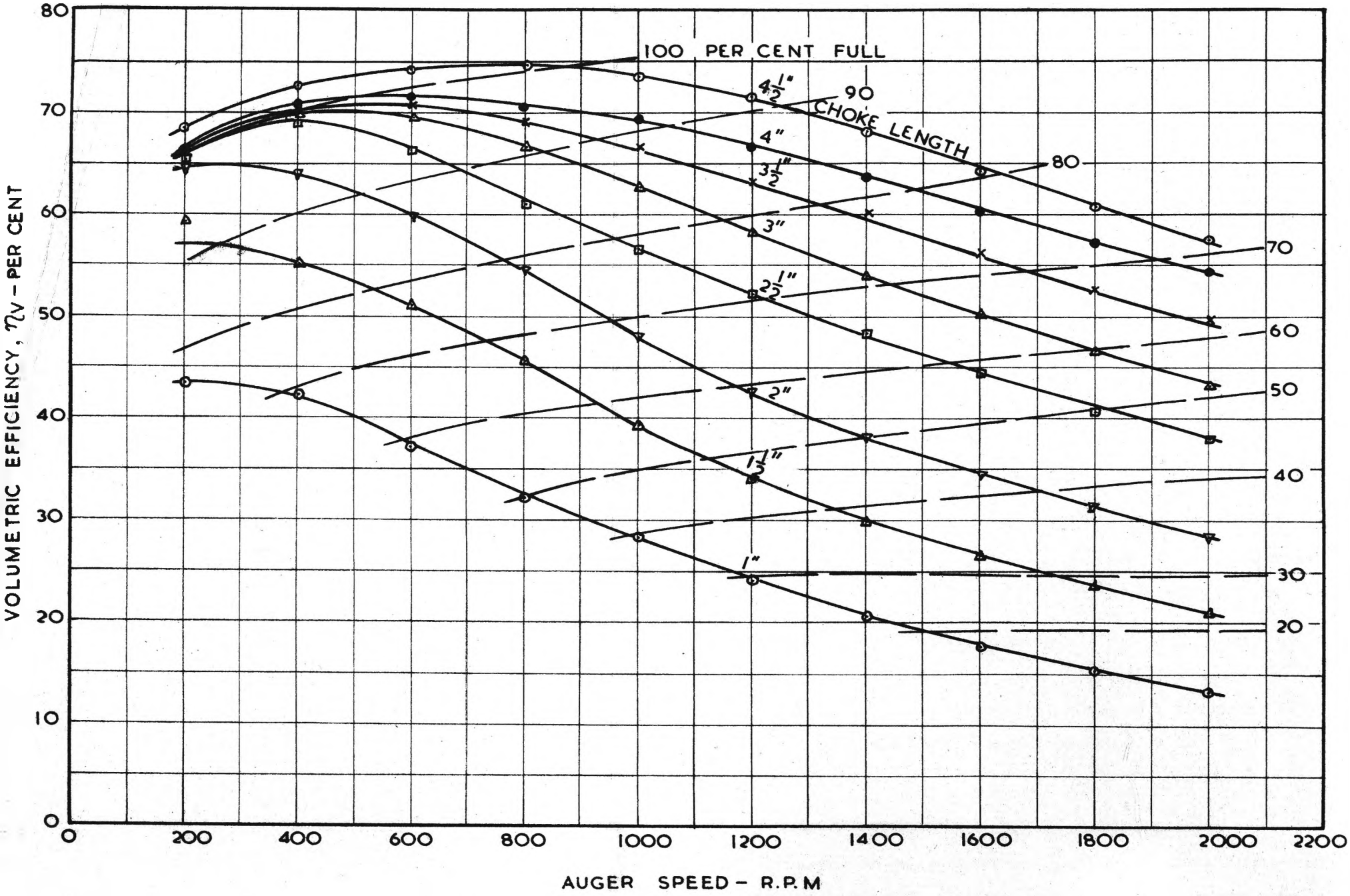

FIG. 17. VOLUMETRIC EFFICIENCY VERSUS SPEED FOR VARIOUS CHOKE LENGTHS
Angle of Elevation: 30° Radial Clearance: 1/64 inches Material Conveyed: Millet

FIG. 18.

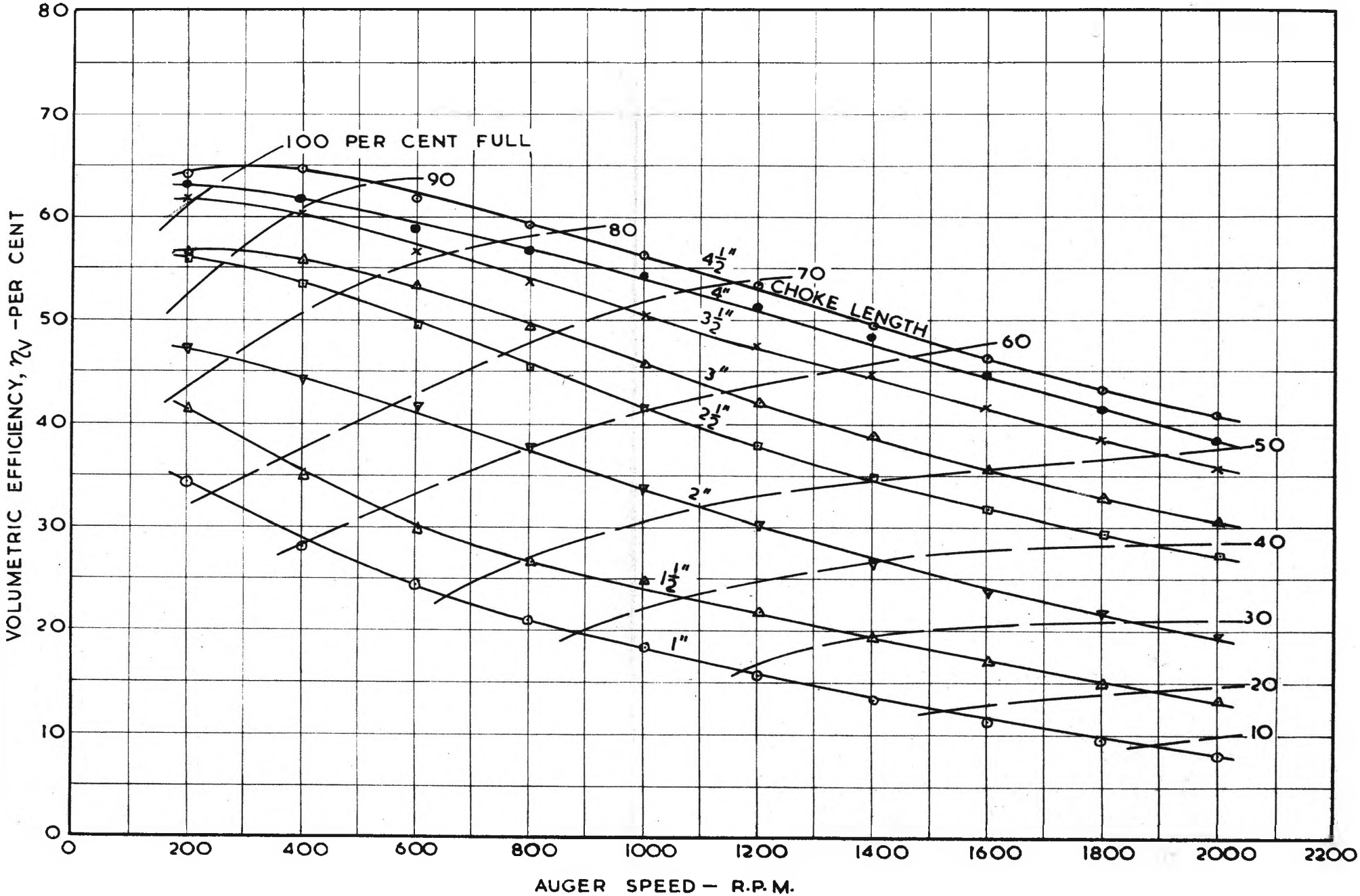

FIG. 18. VOLUMETRIC EFFICIENCY VERSUS SPEED FOR VARIOUS CHOKE LENGTHS
Angle of Elevation: 60° Radial Clearance: $\frac{1}{64}$ inches Material Conveyed: Millet

FIG. 19.

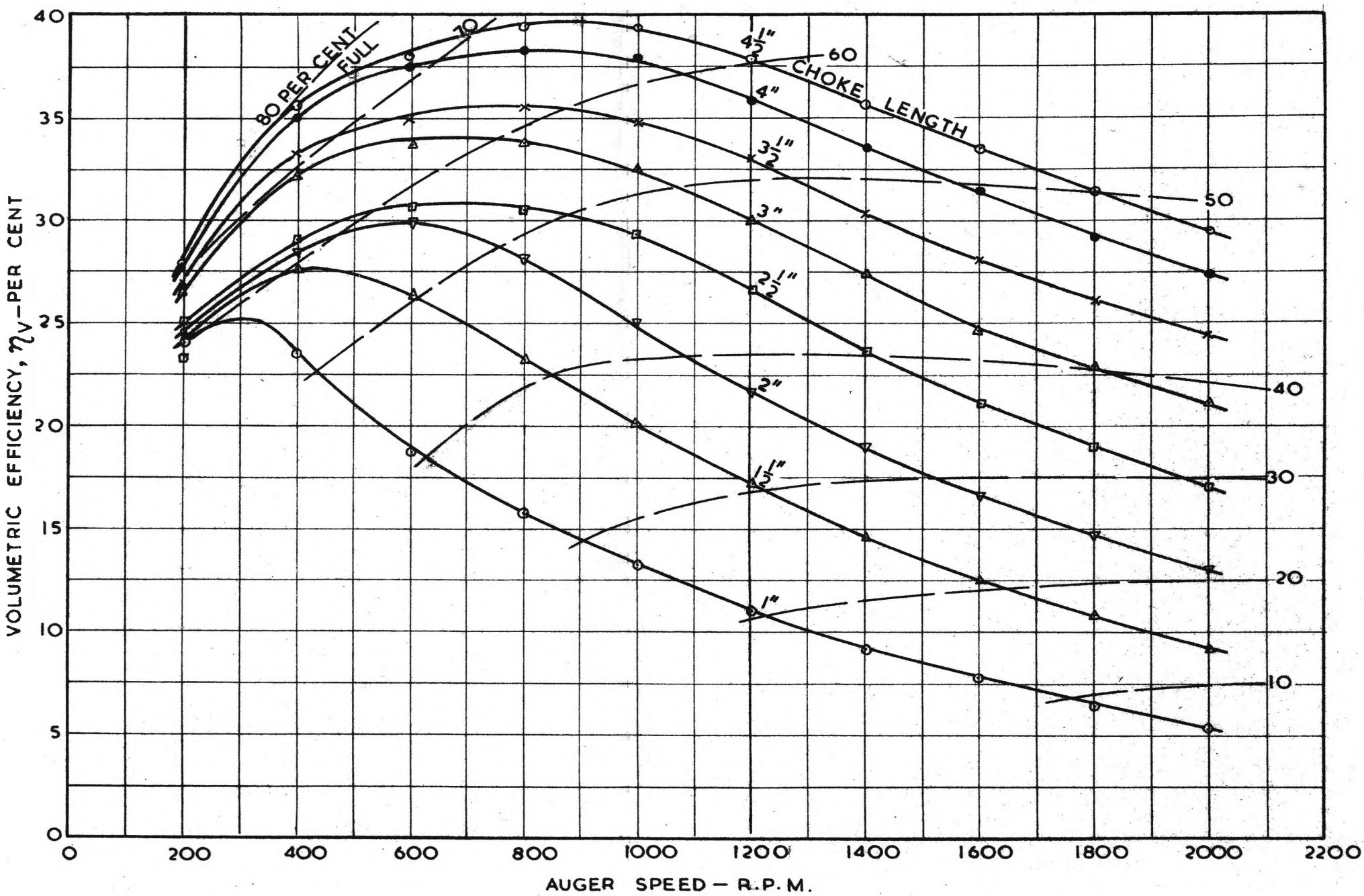

FIG. 19. VOLUMETRIC EFFICIENCY VERSUS SPEED FOR VARIOUS CHOKE LENGTHS

Angle of Elevation: 90° Radial Clearance: $\frac{1}{64}$ inches Material Conveyed: Millet

FIG. 20.

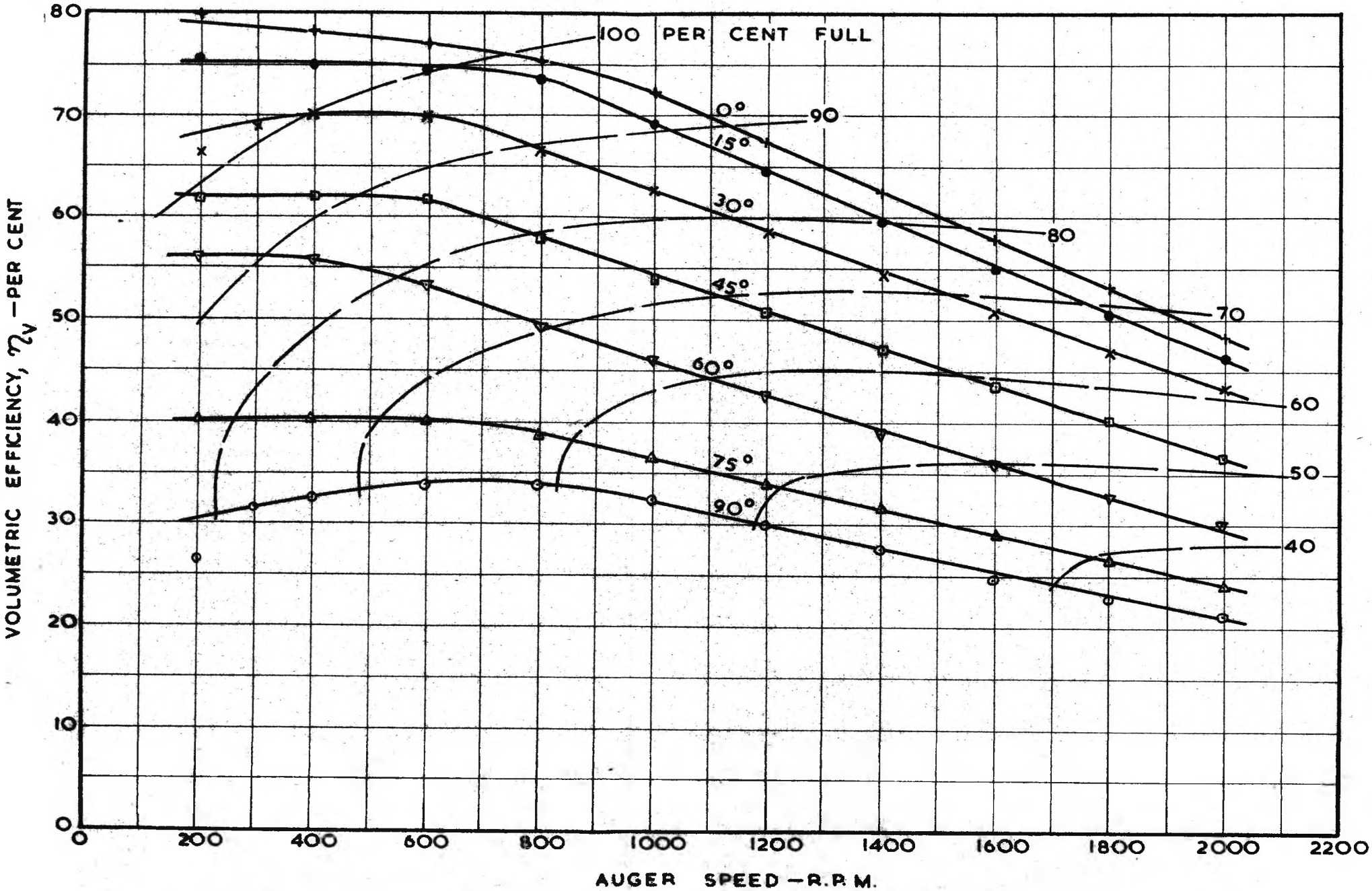

FIG. 20. VOLUMETRIC EFFICIENCY VERSUS SPEED FOR VARIOUS ANGLES OF ELEVATION

Choke Length: 3 inches Radial Clearance: $\frac{1}{64}$ inches Material Conveyed: Millet

determining the approximate amount of rotational motion, measurements of the "fullness" of the grain in the auger have been taken. As previously described, these measurements are based on the estimated mean axial height of grain on each pitch of the auger flight. Typical graphs showing the variation of the volumetric efficiency with speed, angle of elevation and choke length are shown in Figs. 17 to 20. The percentage "fullness" graphs have been superimposed to give an indirect indication of rotational motion.

Figs. 17, 18 and 19 show the variation of volumetric efficiency with speed at different choke lengths for the respective angles of elevation 30°, 60° and 90°, while the volumetric efficiency graphs for the 3 inch choke are summarised in Fig. 20. The maximum volumetric efficiencies are obtained at the lower speeds, decreasing at an almost uniform rate with increase in speed; for each angle of elevation the rate of decrease is approximately constant for all choke lengths but the decrease gradually lessens as the angle of elevation is raised.

The volumetric efficiency at the higher angles of elevation is generally quite low, and this is due largely to the high rotational motion of the grain occurring in the steeper positions. It is interesting to observe, for example, that at 90° and 400 r.p.m. (Fig.19) the auger runs approximately 80 per cent full when the choke length equals $4\frac{1}{2}$ inches ($^{1}c/p = 3$) and approximately 60 per cent full when the choke length equals $1\frac{1}{2}$ inches, but the corresponding volumetric efficiencies are only 37 and 27 per cent respectively; the respective

FIG.21.

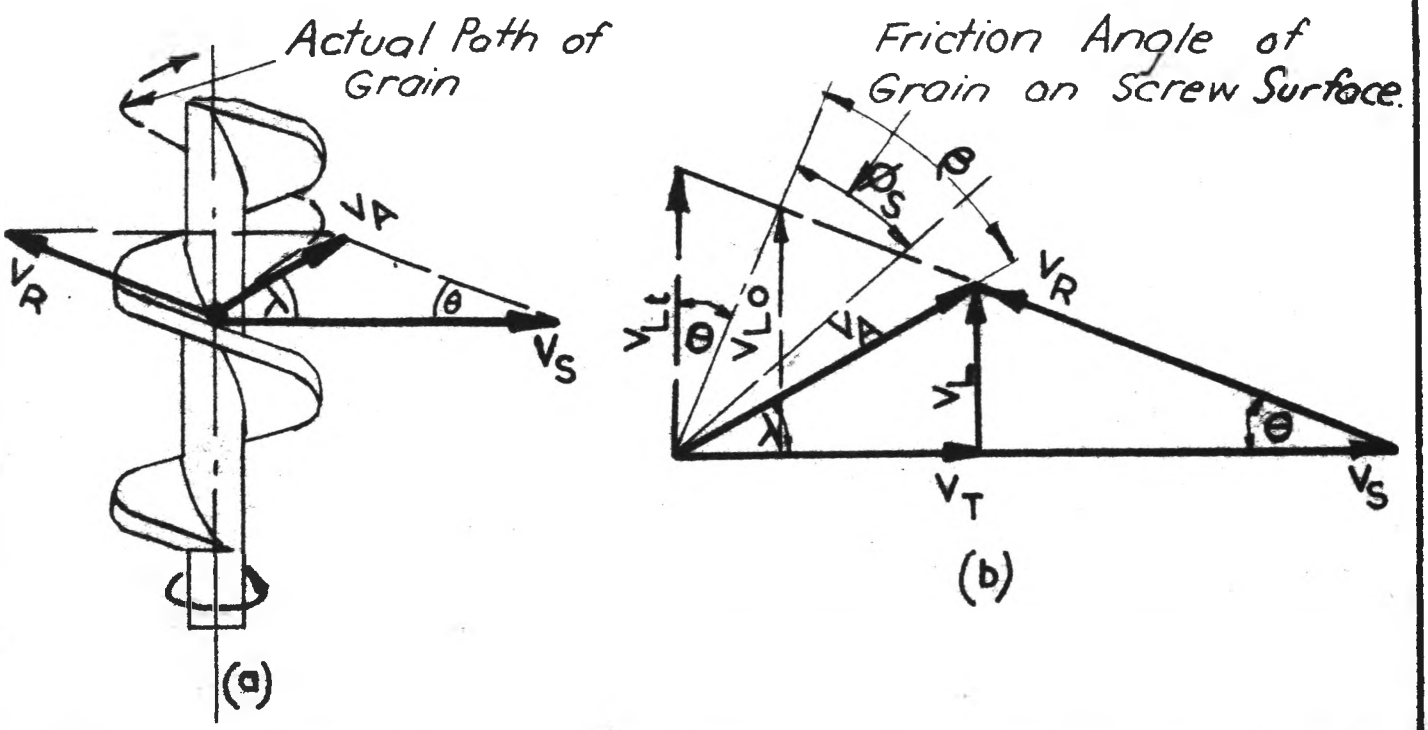

FIG.21. VELOCITY DIAGRAM FOR GRAIN PARTICLE

losses in output due to rotational motion are therefore 43 and 33 per cent. On the other hand, at 30° and 400 r.p.m. (Fig. 17) the auger runs 100 per cent full with a choke length of 4½ inches and approximately 85 per cent full with a choke length of 1½ inches, the corresponding volumetric efficiencies being 73 and 55 per cent respectively; the respective rotational effects in this case amount to only 15 and 18 per cent. The rotational motion is shown to decrease with increase in speed.

In its passage through an auger, the grain describes a helical path of the opposite hand to that of the screw. The velocity diagrams used by Gutyar (29) and Baks and Schmid (31) in their vertical auger analyses provide a useful means for studying the grain flow. Consider a particle of grain on the screw surface as shown in Fig.21 (a). V_S is the peripheral velocity of the screw at the radius considered and V_R is the relative velocity of the grain on the screw surface. The absolute velocity V_A of the grain is then the vector sum of the screw velocity and the relative velocity. V_A is inclined at an angle λ to the screw velocity; θ is the helix angle of the screw at the radius considered. V_A can be resolved into two components, the useful lifting velocity V_L and the undesirable grain peripheral velocity V_T. The optimum lifting velocity V_{Lo} occurs when λ equals $(90° - \theta)$, Fig. 21 (b), which could only be approached when the frictional resistance of the screw surface is zero. The theoretical maximum lifting velocity V_{Lt} upon which the theoretical output in the volumetric efficiency calculations is based occurs when λ equals $90°$.

FIG. 22.

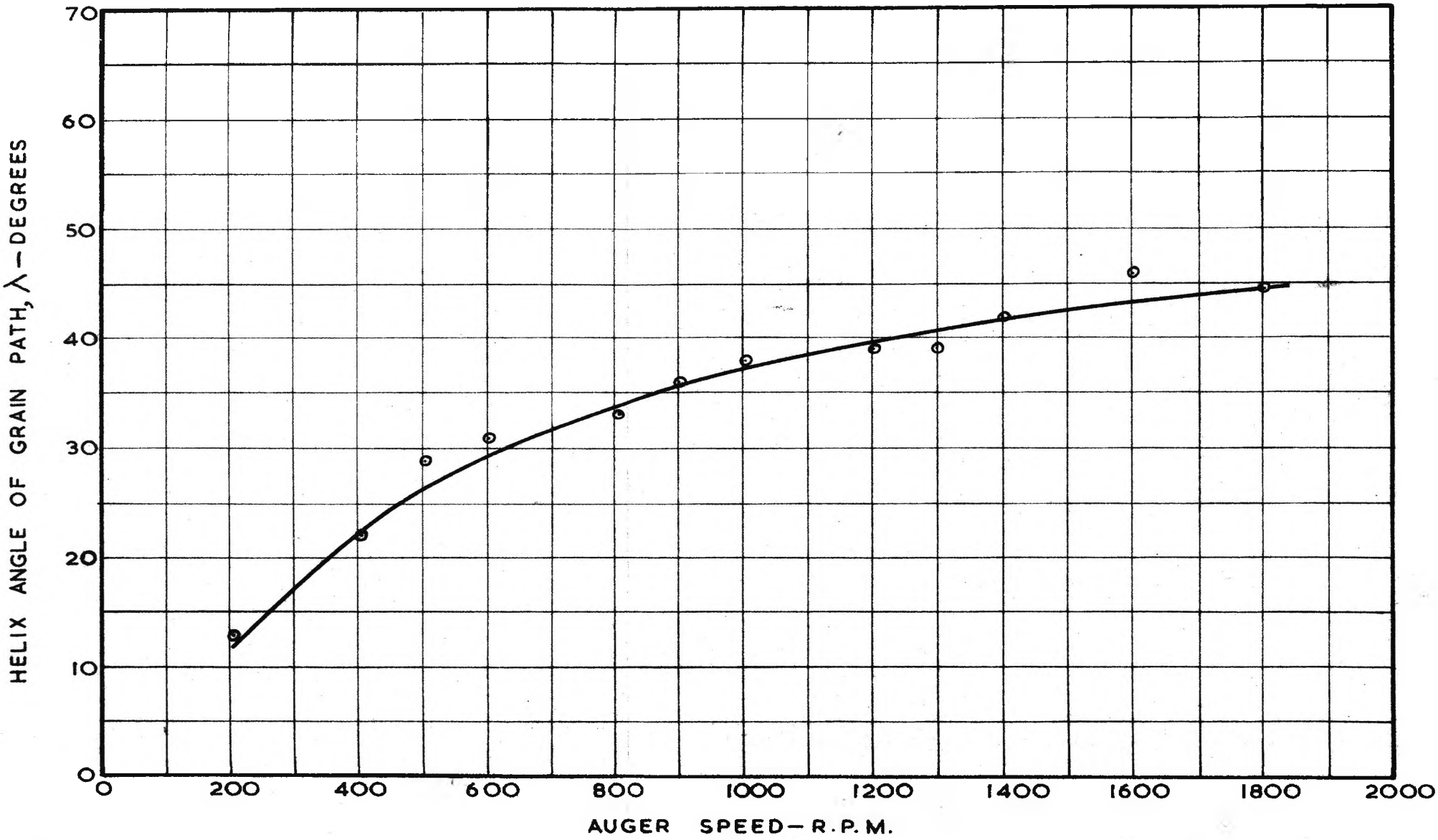

FIG. 22. HELIX ANGLE OF GRAIN PATH AT OUTER SCREW PERIPHERY AGAINST CASING.
Angle of Elevation: 90° (Choke Length: 3 inches)

FIG. 23.

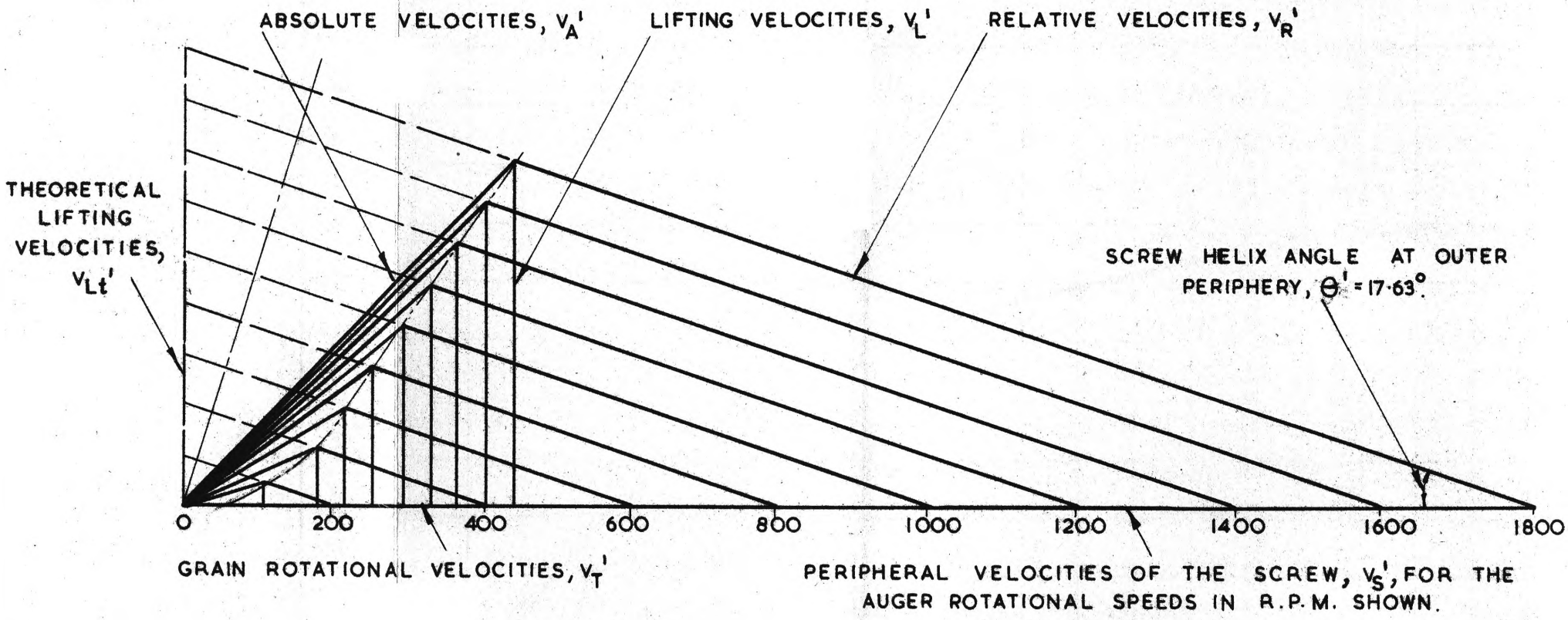

FIG. 23. VELOCITY DIAGRAMS FOR OUTER SCREW PERIPHERY.

Angle of Elevation: 90° (Choke Length: 3 inches)

The magnitude of the relative velocity depends primarily on the frictional resistive force of the casing impairing the grain rotation; this force depends on the casing friction coefficient and the normal force on the inner casing surface as imposed by the centrifugal force of the rotating grain and, to a lesser extent, by the lateral or Rankine pressure of the grain mass on the auger flight. Tests on the model auger operating as an Archimedean screw with the casing rotating with the auger flight showed that the auger would only convey grain for angles of elevation up to 20° ; above this angle the auger would not function. In this case there was no arresting of the grain rotary motion by the casing.

As a means for determining the grain lifting and rotational velocities at the outer periphery, measurements were taken of the grain helix angle λ at different auger speeds for the 90° angle of elevation. (These measurements were made possible by the transparent auger casing, the direction of the grain path being clearly visible.) The angle was found to increase at a diminishing rate from about 12° at 200 r.p.m. to about 45° at 2,000 r.p.m. as shown in Fig. 22. Baks and Schmid have pointed out that the maximum value of λ occurs at infinitely high speed when the angle β becomes equal to the friction angle ϕ_S. A series of velocity diagrams for a range of auger speeds are shown in Fig. 23, while the various grain velocities are shown plotted against auger speed in Fig. 24. In order that the grain and screw velocities occurring at the outer periphery may be distinguished from those at any radius, they will be denoted by V_L', V_T', V_{Lt}', and V_S'.

FIG. 24.

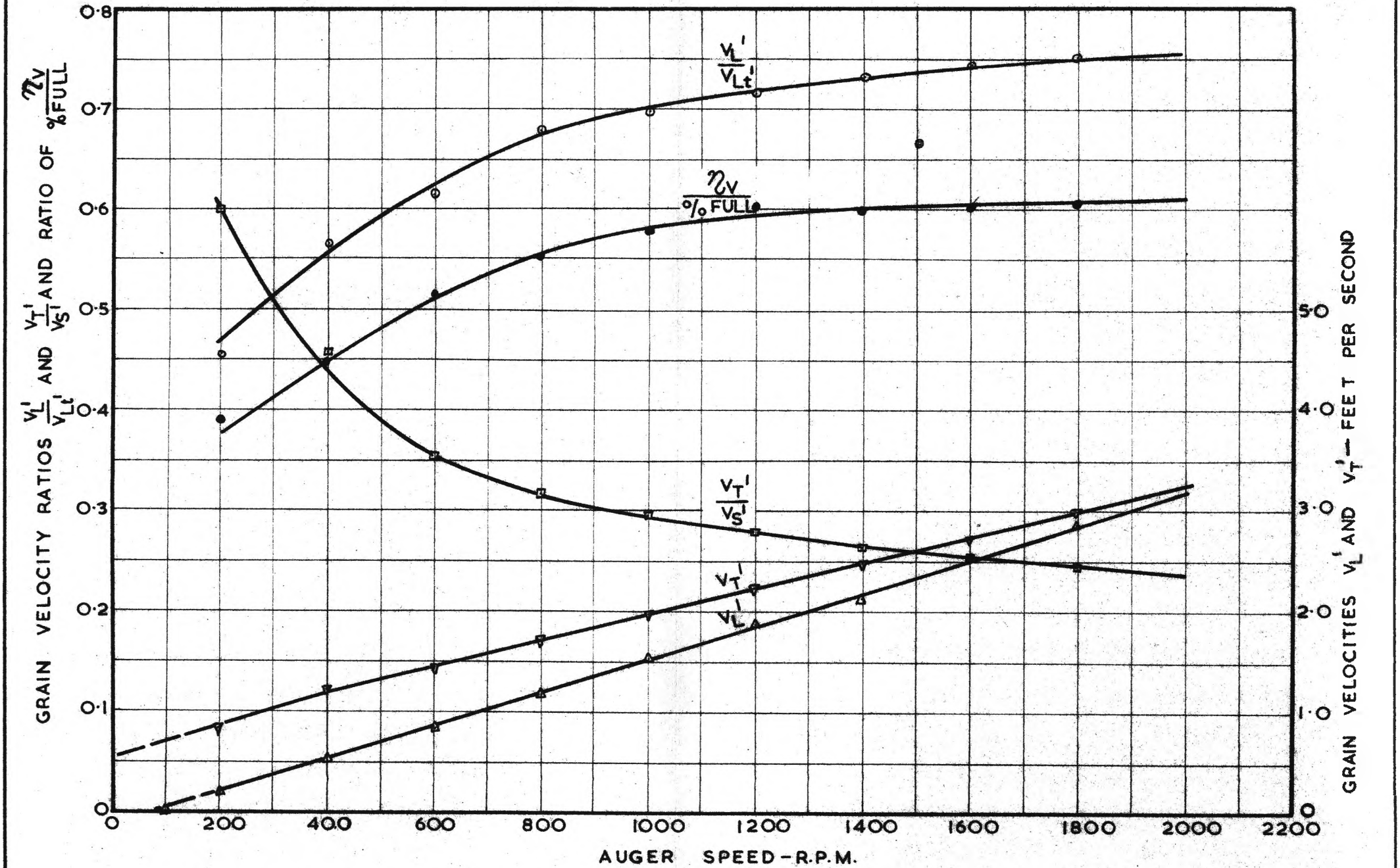

FIG. 24. VARIATION OF GRAIN VELOCITIES AND VELOCITY RATIOS WITH AUGER SPEED.
Velocities shown are for outer screw periphery. Angle of elevation of auger = 90°
(Choke Length = 3 inches)

Above 200 r.p.m. the lifting velocity V_L' and rotational velocity V_T' both increase uniformly with speed. The lifting velocity passes through zero at about 75 r.p.m.; below this speed, V_L' is negative and there is no discharge. The greater slope of the V_L' graph indicates that the ratio of the two velocities V_L'/V_T' increases with increase in speed and this is accompanied by a reduction in the ratio of the grain peripheral velocity to the auger peripheral velocity, V_T'/V_S', as shown. Comparing the actual lifting velocity V_L' with the theoretical lifting velocity V_{Lt}', the increase in the ratio V_L'/V_{Lt}' with speed indicates that, for a given quantity of grain conveyed, the volumetric efficiency would improve with speed. In practice, the volumetric efficiency falls off slightly with speed, this being due to a decrease in the volume of grain trapped in the choke. There is a further factor; at high speed, the increased turbulence of the grain particles causes a reduction in the bulk density of the grain passing through the auger.

The grain velocities plotted in Fig. 24, being for the outer periphery, correspond to the minimum helix angle of the screw. Since the helix angle increases towards the centre of the screw, the rotational grain velocity also increases in this direction with an accompanying reduction in lifting velocity. Also plotted in Fig. 24 is the ratio of the actual volumetric efficiency to the percentage fullness, η_V / % full. This graph has the same characteristics as the V_L'/V_{Lt}' graph and may be regarded as representing the mean ratio of the actual lifting velocity to the theoretical lifting velocity for the whole of the screw surface.

Although the η_V / % full graph of Fig. 24 is for a 3 inch choke length, examination of the performance results in Appendix VI shows that this ratio remains substantially constant for a wide range of grain loadings produced by varying choke lengths.

In the study of grain vortex motion described in detail in Section 5, tests were conducted using a special apparatus designed to simulate, as near as possible, the rotary motion of grain on an auger flight. Essentially this apparatus consisted of a rotating impeller which imparted vortex motion to a column of grain held inside a stationary tubular casing. The impeller had four blades of pitch equal to that of the screw and, under test conditions, was just fully immersed in the grain.

It was found that the rotational speed of the grain increased towards the axis of rotation and that the grain surface profile approximated that of a free vortex. For this motion the tangential velocity is inversely proportional to the radius which is the same relationship as followed by the tangent of the helix angle.

While these findings may only be true for a vertical or steeply inclined auger running partially full when the grain vortex is unrestricted, the results have shown that, at the lower auger speeds, the spiral motion will cause grain to flow back in the region of the screw nearest the core where the helix angles are highest. Although such regions may only represent a small percentage of the total cross-sectional area of the screw space, nevertheless there will be a small loss in output. This accounts largely for the "curving down" of the volumetric efficiency graphs for the vertical auger in the low

speed range as shown in Fig. 19.

For the reasons stated, it follows that the ratio of the core diameter to the screw diameter, D_c/D, for a given screw pitch has a significant bearing on auger performance. The vortex investigation has shown that, for a given vortex velocity distribution, the critical speed at which grain slip just ceases decreases both with increase in auger diameter D and increase in the D_c/D ratio. The results indicate that D_c/D ratios less than about 0.4 are undesirable, although further experimental evidence is necessary to support this. It is probable that the use of high D_c/D ratios would allow more efficient feeding of the grain into the choke leading to an improvement in output. Partial examination of grain leakage in the central region of the screw is given also in the theoretical work of Gutyar, while Zaika (28) has investigated the core diameter in relation to the output of the horizontal combine auger.

With a view to reducing the grain rotational motion, tests were conducted using a casing with four, equally spaced, longitudinal vanes which projected into the clearance space between the screw and the casing. No improvement was achieved; the vanes arrested the rotation of the outer grain particles, but this was offset by a greater leakage back in the clearance space. (The details of this test are given in Section 6.2). The best results that may be achieved in practice is when the casing friction is equal to or greater than the grain-on-grain friction and when the screw friction is as low as possible.

The grain lifting and rotational velocities, as well as depending on the auger speed, also depend on the screw helix angles.

Consideration must be given, therefore, to the screw pitch. Referring to Fig. 21 (b), the following expressions for the lifting and rotational velocities of the vertical auger may be obtained:

$$V_L = \frac{V_S \sin \theta \cos (\theta + \beta)}{\cos \beta} \qquad \text{----------(3 - 3)}$$

and

$$V_T = \frac{V_S \sin \theta \sin (\theta + \beta)}{\cos \beta} \qquad \text{----------(3 - 4)}$$

Because the angle β diminishes with increase in V_S, an approximate guide to the optimum screw pitch may be obtained by considering the high speed operation of an auger. Under these conditions, β approaches a constant value becoming approximately equal to the friction angle ϕ_S. On this basis, the helix angles for maximum lifting and rotational velocities are:

$$\text{for max. } V_L \qquad \theta = 45^\circ - \frac{\phi_S}{2} \qquad \text{----------(3 - 5)}$$

$$\text{for max. } V_T \qquad \theta = 90^\circ - \frac{\phi_S}{2} \qquad \text{----------(3 - 6)}$$

Helix angles approaching that given by equation (3 - 6) should be avoided.

Assuming ϕ_S to be 30°, the helix angle for the maximum lifting velocity also equals 30°. Applying this helix angle to the mean diameter of the model auger yields the following pitch expressed in terms of the outside diameter of the screw:

$$p = 1.2\ D$$

Although this pitch applies to high speed operation, it indicates that the one-to-one screw pitch to screw diameter ratio as adopted in the model is near the optimum as far as the lifting velocity of the vertical auger is concerned. However, since volumetric efficiency also depends on the rotational velocity and the amount of grain trapped in the choke, there is no indication of whether this is the optimum screw pitch for best output.

Zaika has shown that the one-to-one screw pitch to screw diameter ratio gives the highest outputs in the horizontal combine auger and experimental evidence as given by Rehkugler (23) shows that this ratio also gives the maximum output of an auger working at an angle of elevation of 30°. However, further experimental investigation is required to establish whether or not this is the optimum ratio for the steeper angles of elevation.

FIG. 25.

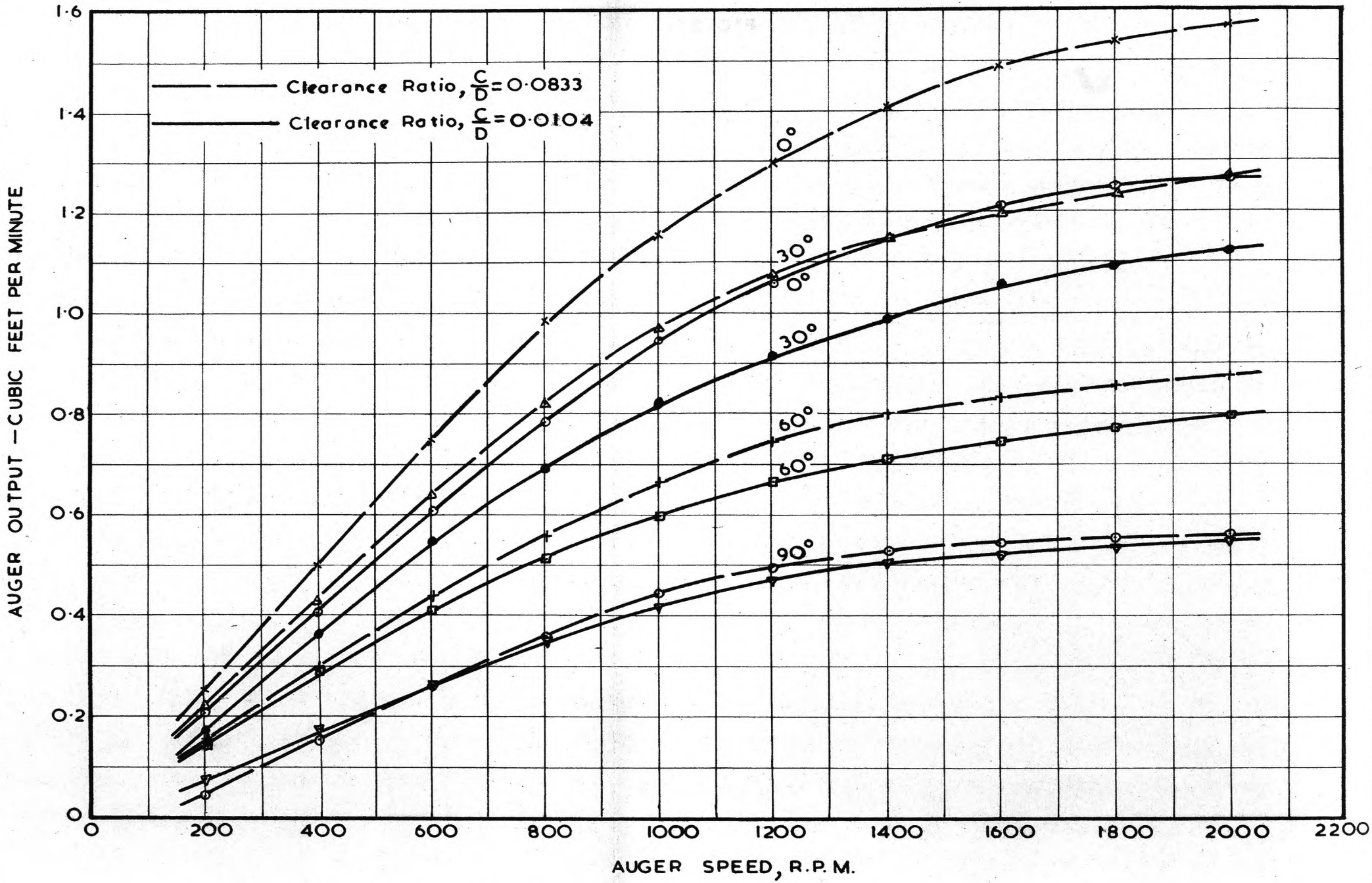

FIG. 25. EFFECT OF CASING CLEARANCE ON AUGER OUTPUT AT VARIOUS SPEEDS AND ANGLES OF ELEVATION

Choke Length: 3 inches Material Conveyed: Millet

3.3 EFFECT OF CLEARANCE

The effect of variation in radial casing clearance on auger output has been partially examined and typical results are shown graphically in Fig. 25. These results compare radial casing clearances of 1/64 inch ($\frac{C}{D}$ = 0.0104) and 1/8 inch ($\frac{C}{D}$ = 0.0833) for a choke length of two pitches. The geometrical constant γ of equation (3 - 2) for the auger with the larger casing is 0.90. The potential capacity of this auger is 34 per cent greater than the auger with the smaller casing.

For the lower speeds and for the higher angles of elevation there is little difference in the outputs; the larger size casing with the greater clearance allows a greater volume of grain to be elevated, but this is offset by leakage back through the clearance space. However, decrease in angle of elevation shows that a substantial increase in output is obtained with the larger casing, particularly at high speeds; the actual increases range from approximately zero at 90° to about 24 per cent at 0° and 2000 r.p.m.

The experiments on the model have shown that when clearances approximately equal to the grain size are used, grain particles are apt to wedge in the clearance space. This results in an excessive power consumption as well as grain damage. Clearances of this magnitude should therefore be avoided.

FIG. 26

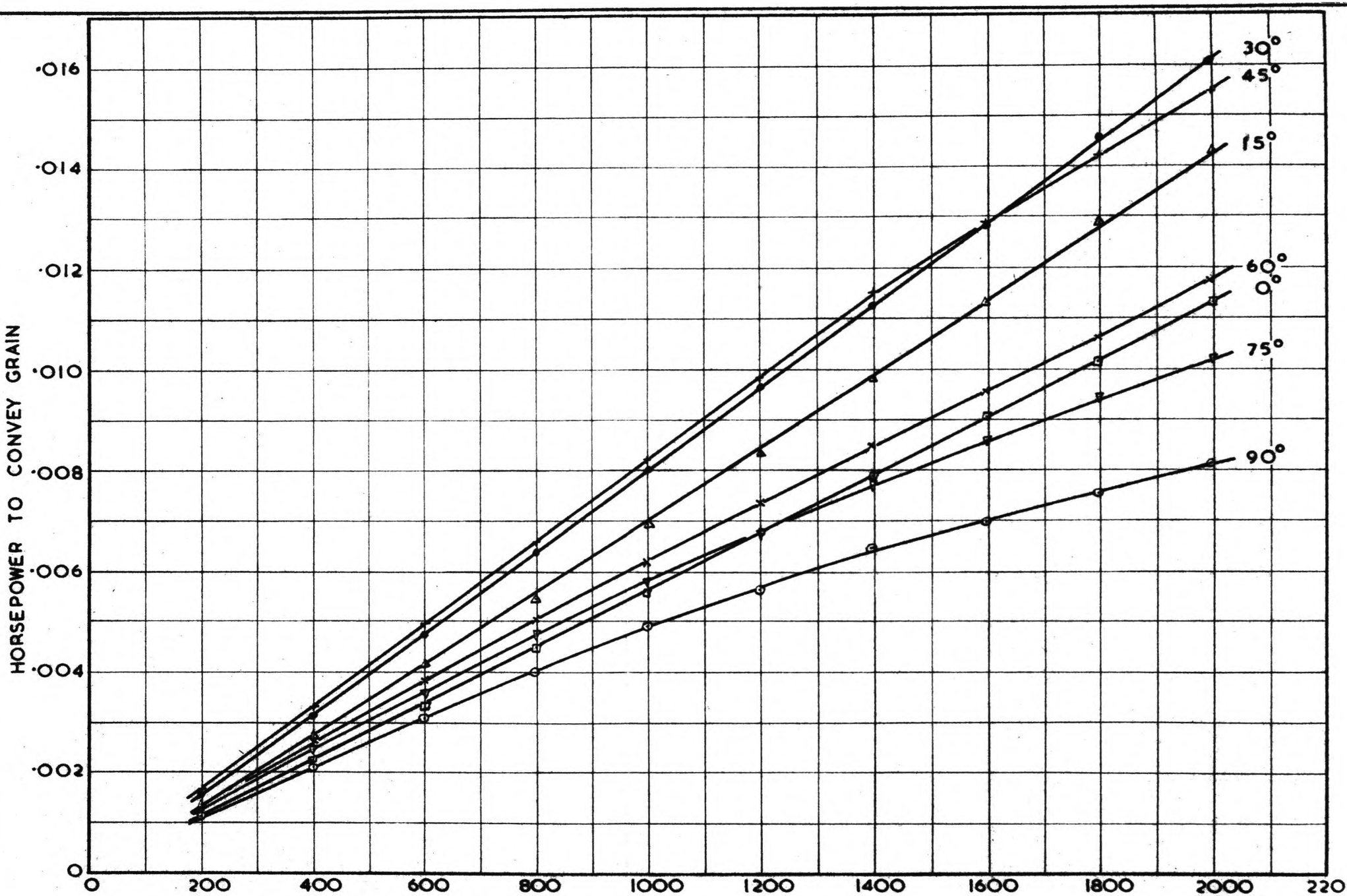

FIG. 26. HORSEPOWER VERSUS SPEED FOR VARIOUS ANGLES OF ELEVATION
Choke Length: 3 inches Radial Clearance: $\frac{1}{8}$ inches Material Conveyed: Millet

FIG .27.

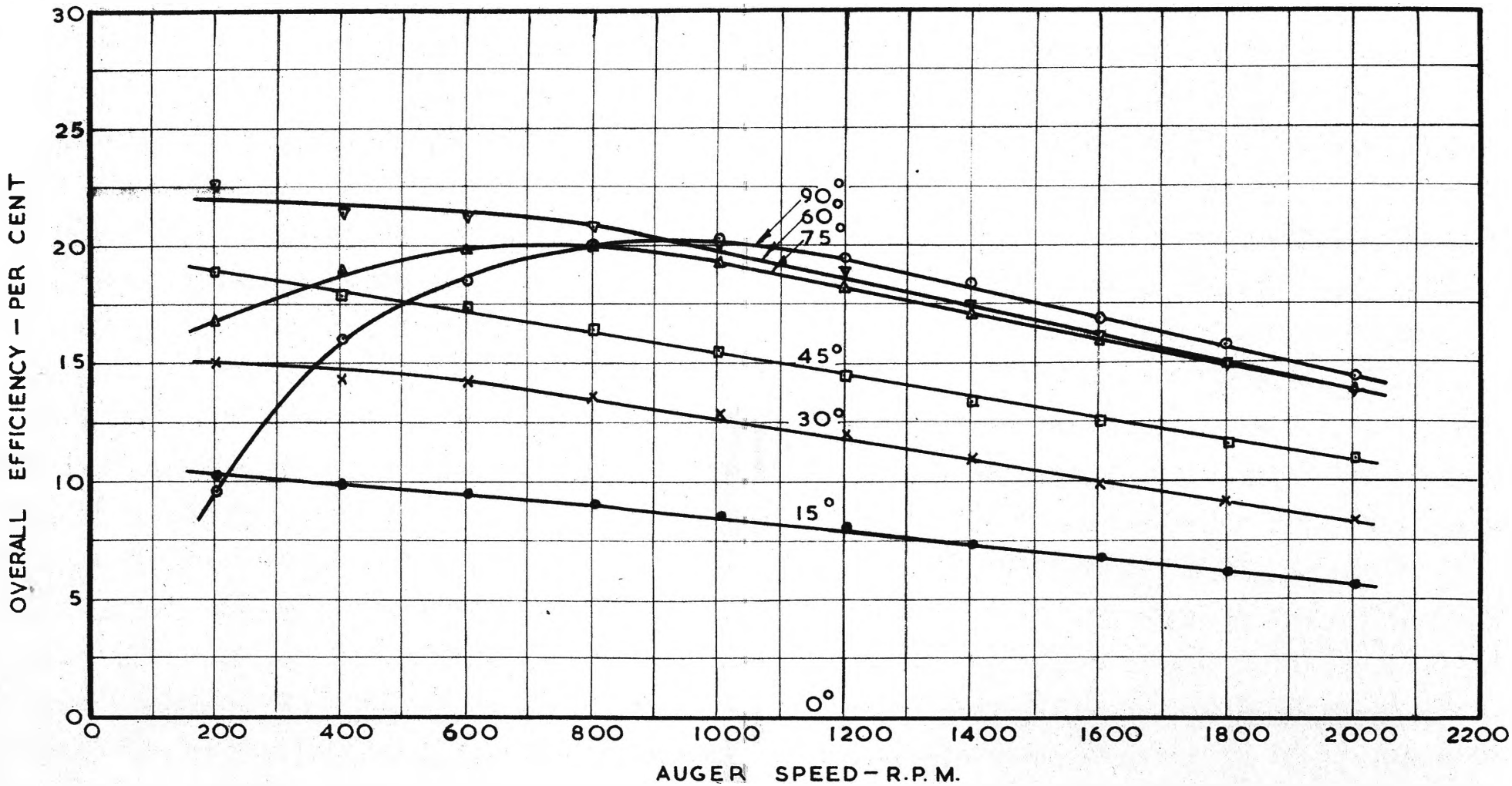

FIG. 27. OVERALL EFFICIENCY VERSUS SPEED FOR VARIOUS ANGLES OF ELEVATION.

Choke Length : 3 inches Radial Clearance: $\frac{1}{8}$ inch Material Conveyed: Millet

3.4 AUGER HORSEPOWER AND OVERALL EFFICIENCY

An examination has been made of the model auger power consumption in relation to speed and angle of elevation for a choke length of two pitches and a radial clearance of 1/8 inch. (It was not possible to obtain accurate power readings for the auger when fitted with the smaller casing owing to the screw periodically rubbing against the casing.) The results shown plotted in Fig. 26 are the horsepowers necessary to convey grain only; they are the differences between the no-load and full-load powers. For each angle of elevation the horsepower is shown to increase at an almost uniform rate with speed. For each speed, the horsepower is shown to increase with angle of elevation from 0° to a maximum at 30° to 45° and then to decrease again.

The variation in overall efficiency, η_o, with speed and angle of elevation is shown in Fig. 27. The overall efficiency is defined as follows:-

$$\eta_o = \frac{\text{Theoretical Power}}{\text{Actual Power}}$$

The theoretical power is the power required to give the required output at the required height in the absence of friction and is given by

$$P_t = \frac{Q\,w\,H}{33.000} \qquad \text{----------(3 - 7)}$$

where Q = output in cub. ft/min.

w = Specific weight of grain in lbs/cub.ft.

H = $L \sin \alpha$ = height of lift in ft.

The overall efficiencies are generally quite low, the maximum values occurring at the higher angles of elevation where the auger

lengths for a given height are a minimum. The "curving down" of the 90° and 75° graphs in the low speed range is mainly due to leakage back in the clearance space, and in the central region of the screw.

The auger power losses may be divided into three groups:-

(i) Power lost in overcoming friction as the grain moves axially along the conveyor. This is an inevitable loss; it includes the grain-on-casing and grain-on-screw surface friction losses.

(ii) Power lost in rotating the grain.

(iii) Power lost in the choke.

Examination of screw pitch in relation to output for steeply inclined augers would be also of interest in the study of overall efficiency. Also of importance is the relationship of the core diameter to the outside screw diameter with regard to the critical speed for reverse motion or leakage in the central region of the screw. Because grain leakage occurs at auger speeds below the critical speed resulting in a loss in output, such action will also result in a wastage of power. This suggests that an improvement in the overall efficiency of a steeply inclined auger, particularly in the low speed range, could be achieved by lowering the critical speed. For a given screw pitch, this may be done by increasing the core diameter in relation to the outside screw diameter, that is, by increasing the D_c/D ratio. However, it is desirable that this be verified with further evidence obtained by investigating the effect of varying D_c/D ratios on auger performance over a wide range of operating conditions.

SECTION 4

DESIGN PARAMETERS AND PREDICTED PERFORMANCE

4.1 DIMENSIONAL ANALYSIS

In order to use the performance data from the model tests to predict the performance of the full scale prototype, the appropriate dimensionless parameters for dynamic similarity need to be derived. By means of dimensional analysis, these parameters may be obtained as follows:-

$$f(Q, P, D, g, N, \alpha, d, \varrho, \mu, \mu_s, \mu_c) = 0 \qquad \text{--------(4 - 1)}$$

Here Q is the auger output in cub.ft/min. and P is the horsepower to convey the grain (excluding the power lost in bearing friction etc.). Note that D, the auger diameter, is the characteristic dimension for the auger; the other auger dimensions, that is, pitch, choke length, radial clearance, and auger length are in fixed ratios with D for geometrically similar augers.

Choosing the prime quantities D, ϱ and N, it follows that

$$\phi\left(\frac{Q}{ND^3}, \frac{P}{\varrho D^5 N^3}, \frac{g}{N^2 D}, \alpha, \frac{d}{D}, \mu, \mu_s, \mu_c\right) = 0 \qquad \text{--------(4 - 2)}$$

(Both f and ϕ are used in (4 - 1) and (4 - 2) to denote functions.)

The discharge parameter, $\frac{Q}{N D^3}$ will be referred to as the discharge coefficient and denoted by C_Q

i.e. $$C_Q = \frac{Q}{N D^3} \qquad \text{----------(4 - 3)}$$

The power parameter $\frac{P}{\rho D^5 N^3}$ will be referred to as the power coefficient and denoted by C_P

$$\text{i.e.} \quad C_P = \frac{P}{\rho D^5 N^3} \qquad \text{----------(4 - 4)}$$

The acceleration parameter $\frac{g}{N^2 D}$ takes into account the centripetal acceleration of the grain and provides a means for comparing the speeds of geometrically similar augers. Although the actual rotational speed of the grain is less than that of the auger, it is proportional to the auger speed; hence the centripetal acceleration of the grain is proportional to $N^2 D$. Since the auger output is controlled largely by the centrifugal inertia effect of the grain both in the choke and in the casing, it is apparent that augers of large diameter would attain their maximum output at lower speeds than augers of smaller diameter.

Because g in the acceleration parameter is constant, it will be taken as being unity.* Also, for convenience, the parameter will be inverted. It will be referred to as the speed coefficient and denoted by C_S .

$$\text{i.e.} \quad C_S = N^2 D \qquad \text{----------(4 - 5)}$$

It is assumed that, for a given value of C_S , the discharge coefficient and power coefficient respectively are theoretically the same for all geometrically similar augers, the other parameters being constant. Then the corresponding speeds for the model and prototype for

* This is equivalent to multiplying the acceleration parameter by a constant g.

similarity may be obtained by considering the equality of the speed coefficients:

For a given set of conditions

$$C_{Sp} = C_{Sm}$$

$$N_p^{\,2} D_p = N_m^{\,2} D_m$$

$$N_p = N_m \sqrt{\frac{D_m}{D_p}} \qquad \text{----------(4 - 6)}$$

(Suffix m refers to the model and p to the prototype.)

Equation (4 - 6) expressed in words :

Prototype speed = model speed $\sqrt{\frac{1}{\text{scale factor}}}$

The principal data required for design purposes are the relationships of both C_Q and C_P with C_S for various angles of elevation α. Consideration must be given, also, to the choke length to screw pitch ratio, $\frac{l_c}{p}$, and to the auger length to screw diameter ratio, $\frac{L}{D}$. Since the output of an auger is governed by the amount of grain that can be trapped in the choke, the actual elevating action through the casing being identical for every pitch of the screw, it is expected that, for a given set of conditions, the output will be independent of variation in auger length. The auger power requirements depend on the total mass of grain that is held in the conveyor at any one instant and this is dependent on auger length. This suggests that the power would be directly proportional to auger length.

Available data on grain properties show that for many granular materials, there is no appreciable difference between the respective friction coefficients for grain-on-grain and grain-on-metal. Therefore it will be initially assumed that μ , μ_s and μ_c are constant. Quite large variations occur in the particle size of different granular materials so that some investigation of different $\frac{d}{D}$ ratios is required. Only partial examination of this effect has been made in the present investigation.

FIG·28·

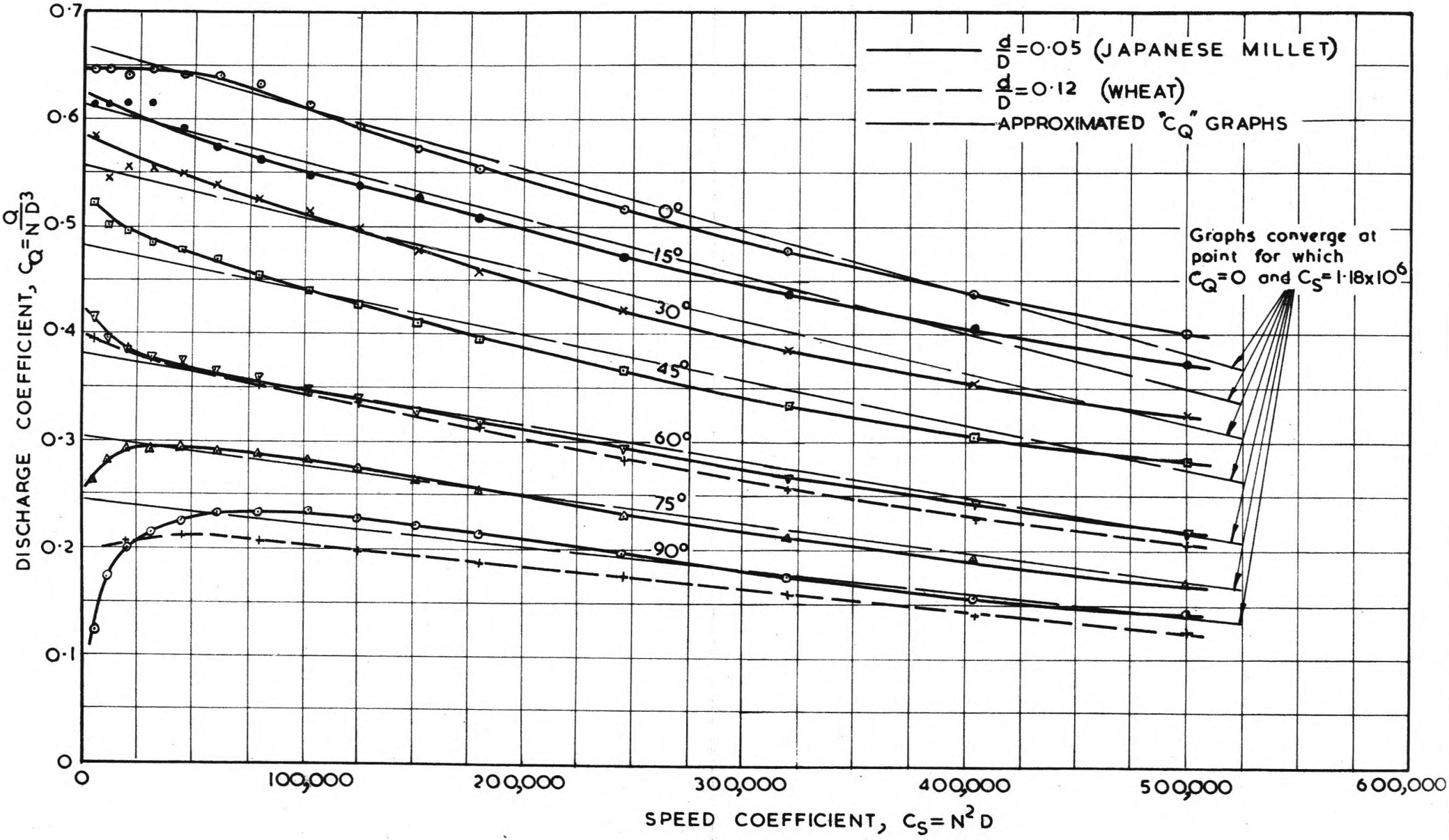

FIG. 28. DISCHARGE COEFFICIENT VERSUS SPEED COEFFICIENT FOR VARIOUS ANGLES OF ELEVATION

Auger Geometrical Proportions: P=D; $\frac{lc}{P}$=2·0; $\frac{Dc}{D}$=0·333; $\frac{C}{D}$=0·0833; $\frac{L}{D}$=16

4.2 PREDICTED AUGER OUTPUT

The plot of discharge coefficient C_Q versus speed coefficient C_S for various angles of elevation is shown in Fig. 28. For these results, a choke length to screw pitch ratio, $\frac{l_c}{p}$, of two to one has been adopted, which, by compromise, is considered to be a reasonable ratio for most practical purposes. The results are also based on radial clearance ratio, $\frac{C}{D}$, of 0.0833. For the model auger, the length to diameter ratio, $\frac{L}{D}$, is sixteen to one.

Since the tests on the model auger have been conducted primarily using Japanese millet seed as the material conveyed, the corresponding C_Q values, plotted as full lines in Fig. 28, are for a grain size to auger diameter ratio $\frac{d}{D}$ of 0.05. However, to observe the effect of a larger grain size, discharge tests were carried out on the model auger using wheat as the material conveyed, for which the $\frac{d}{D}$ ratio is 0.12. Only two angles of elevation, 90° and 60° were tested and the corresponding C_Q values are plotted as "dotted" lines in Fig. 28. There is shown to be little departure from the respective graphs for the Japanese millet seed. (In the preliminary work on the model auger, a comparison was made between polished millet seed and clover seed, which is approximately one third the size of the millet. The comparative results for this work are given in Section 6.1).

The output of any geometrically similar auger may be now found. For the required speed N and diameter D, the speed coefficient is determined from equation (4 - 5) and the corresponding

discharge coefficient C_Q for the required angle of elevation α is read from Fig. 28. The output is then calculated from equation (4 - 3).

It can be observed that the various C_Q versus C_S graphs appear to be almost linear over most of the range. The actual "curving down" of the 90° and 75° graphs at the lower C_S values is largely due to leakage in the clearance space. A reasonably accurate equation for determining the output may be obtained by assuming that the relationship is linear; the approximated straight line graphs are shown as broken lines in Fig. 28. By extending these lines, it is found that they all converge at a point on the C_S axis for which C_Q is zero. The form of the equation is:

$$C_Q = A (B - C_s) \qquad \text{----------(4 - 7)}$$

which gives

$$Q = N D^3 A (B - N^2 D) \qquad \text{----------(4 - 8)}$$

B is the point of convergence of the various graphs.

A represents the slope of each line. A plot of A versus angle of elevation α reveals a cosine curve which, as shown in Appendix I, can be fitted by the following equation:

$$A = \left[E + G \cos (\alpha + \psi) \right] \qquad \text{----------(4 - 9)}$$

The final equation for output now becomes:-

$$Q = N D^3 \left[E + G \cos (\alpha + \psi) \right] \left[B - N^2 D \right] \text{------(4 - 10)}$$

FIG. 29.

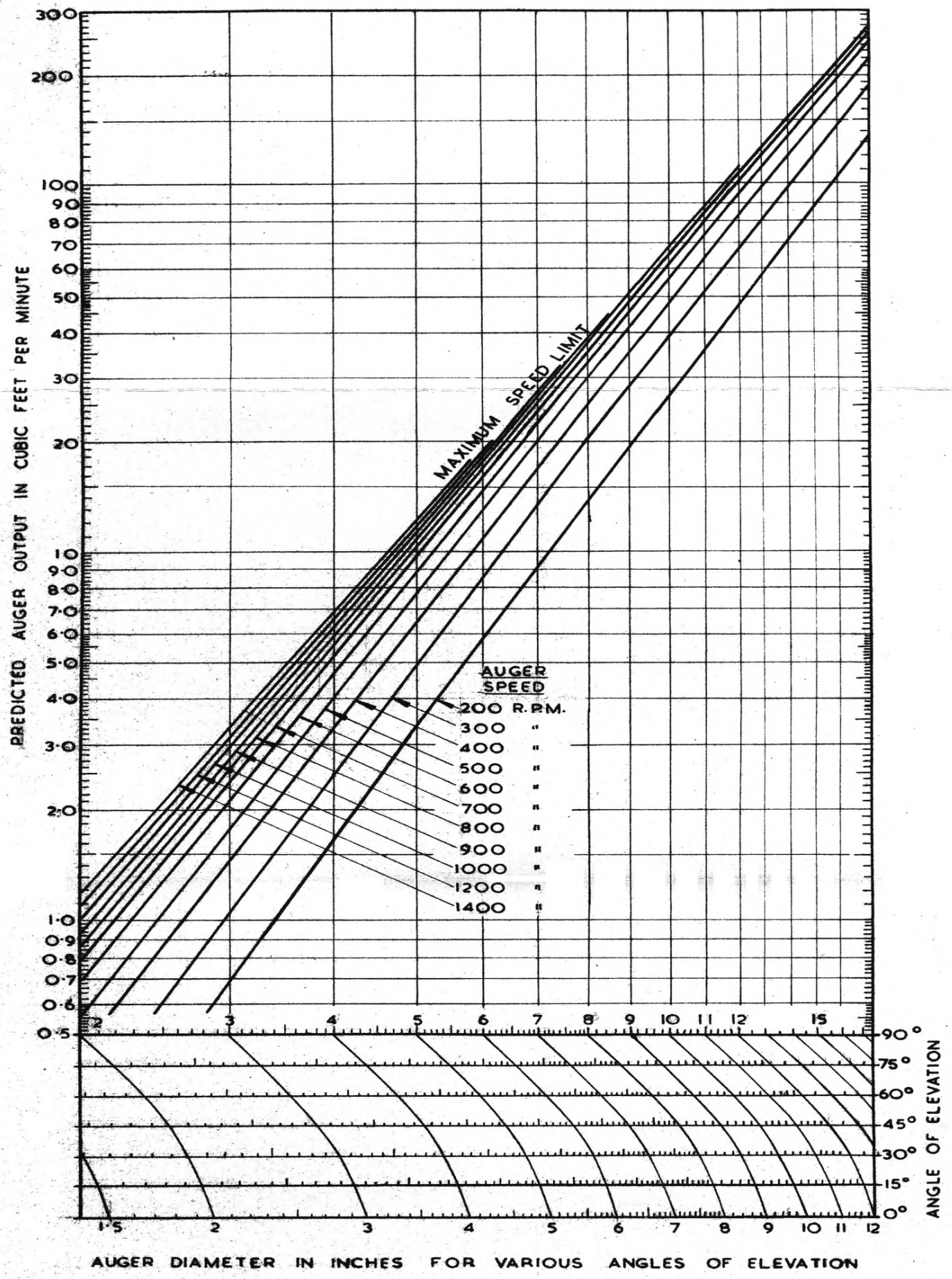

FIG. 29. PREDICTED OUTPUT OF DIFFERENT SIZE AUGERS AT VARIOUS SPEEDS AND ANGLES OF ELEVATION.

Auger Geometrical Proportions: $P = D$; $\frac{l_c}{P} = 2{\cdot}0$; $\frac{D_c}{D} = 0{\cdot}333$; $\frac{C}{D} = 0{\cdot}0833$; $\frac{d}{D} = 0{\cdot}05$.

It may be noted that equation (4 - 10) is of the form - theoretical output times volumetric efficiency, and, therefore, can be written as:

$$Q = \gamma \; N \; D^3 \quad \eta_V \qquad \text{---------(4 - 11)}$$

where the volumetric efficiency is given by

$$\eta_V = \frac{[E + G \cos (\alpha + \psi)][B - N^2 D]}{\gamma} \qquad \text{---(4 - 12)}$$

The values of the various constants obtained from the experimental data and which apply to augers of the same geometrical proportions as that of the model are

$$B = 1.18 \times 10^6$$

$$E = 3.9 \times 10^{-7}$$

$$G = 2.57 \times 10^{-7}$$

$$\psi = 45^\circ$$

$$\gamma = 0.90 \quad (\text{ for casing with clearance ratio } \frac{C}{D} = 0.0833)$$

A graph of output versus auger diameter for different speeds and angles of elevation is shown in Fig. 29. This is drawn up using the actual C_Q values of Fig. 28 (Appendix XI); check calculations using equation (4 - 10) produced figures in close agreement (Appendix XII). Fig. 29 permits the various combinations of speed, diameter and angle of elevation to produce a desired output to

FIG. 30.

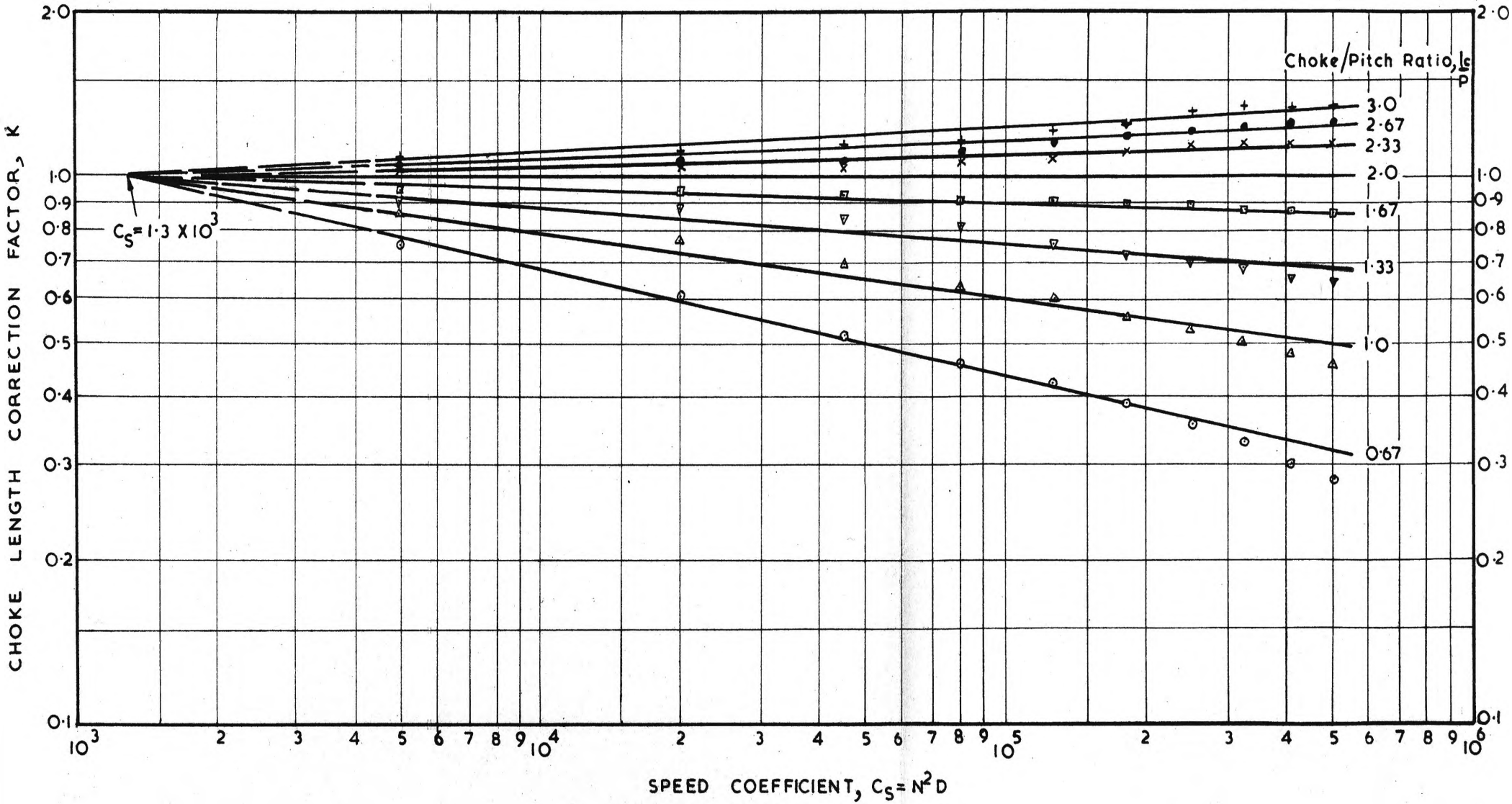

FIG. 30. AVERAGE CHOKE LENGTH CORRECTION FACTORS FOR ANGLES OF ELEVATION 30° TO 90°

Auger Geometrical Proportions : $P = D$; $\frac{D_c}{D} = 0·333$; $\frac{C}{D} = 0·0103$; $\frac{L}{D} = 16$; $\frac{d}{D} = 0·05$

be readily obtained. For example, an output of 10 cub.ft/min. may be obtained at speeds ranging from 200 to 1,400 r.p.m., the corresponding ranges in diameter varying from 7.2 inches to 4.7 inches at $\alpha = 90^{\circ}$ down to 5 inches to 3.3 inches at $\alpha = 0^{\circ}$. The final combination chosen would depend largely on the height of lift and length of auger available.

The usefulness of Fig. 29 is limited by its restriction to the case when $\frac{l_c}{p} = 2.0$ but the application of a choke length correction factor allows the output to be estimated when other choke lengths are used. Suitable correction factors may be obtained from the data on the choke length investigation. Although the choke length investigation was confined to only three angles of elevation, namely 30°, 60° and 90°, examination of the computed correction factors shows little variation (Appendix XIII). Therefore, for most practical purposes, it may be assumed that the correction factors are constant for variation in angle of elevation, at least for the range 30° to 90°; whether this is true for the lower angles of elevation requires verification.

The final correction factors, denoted by K_c, are the mean values for the 90°, 60° and 30° angles of elevation. They are plotted non-dimensionally against the speed coefficient C_S for various choke length to screw pitch ratios in Fig. 30. In this case a logarithmic plot is used since the various graphs may be approximated by straight lines. The extensions of these lines converge at a point on the line for which $K_c = 1.0$ corresponding to $\frac{l_c}{p} = 2.0$. Therefore, an approximate equation for the determination of K_c over the range of

FIG. 31.

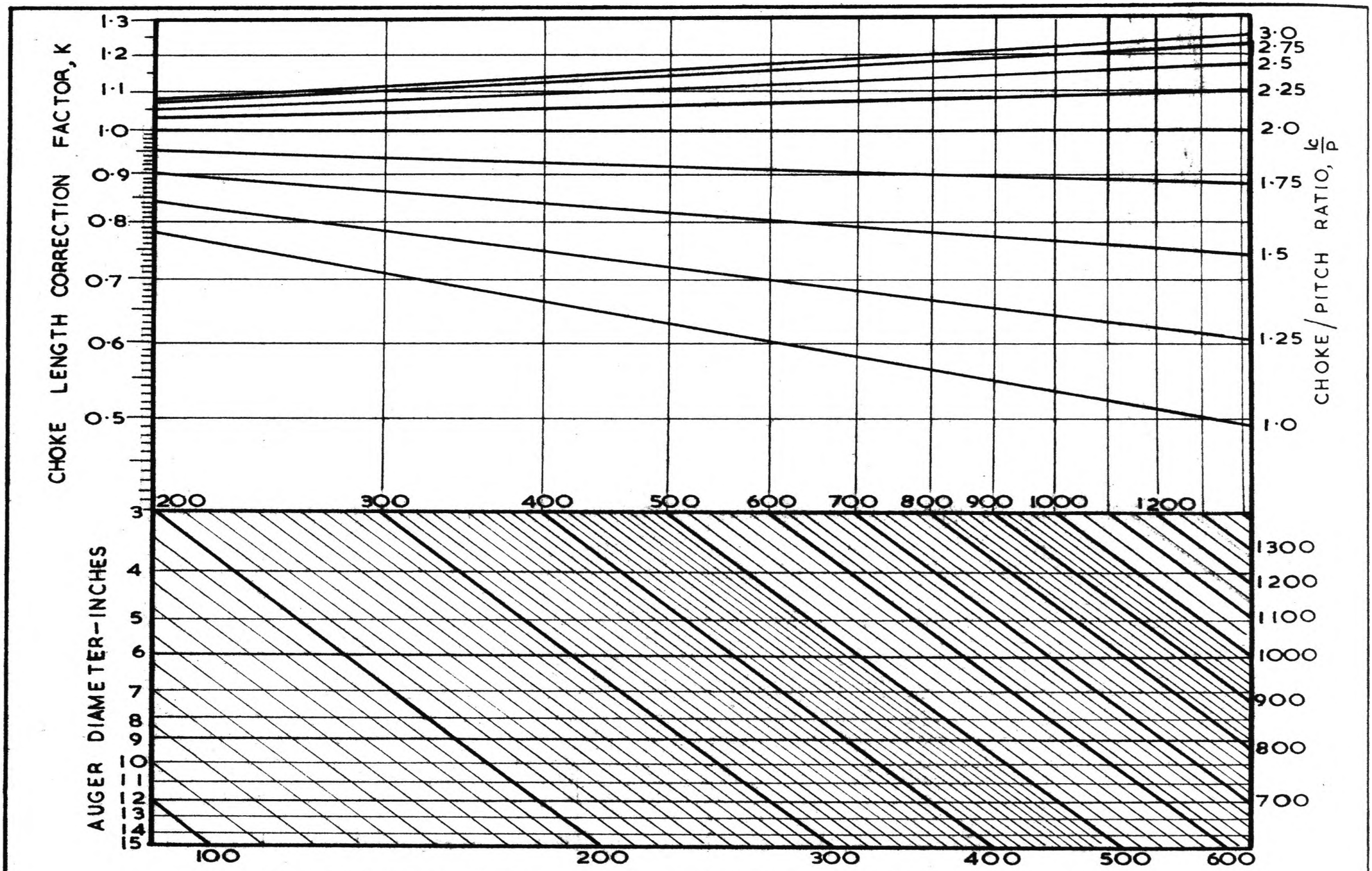

FIG. 31. AVERAGE CHOKE LENGTH CORRECTION FACTORS FOR ANGLES OF ELEVATION 30° TO 90°

C_S values tested is of the form

$$K_c = \left[\frac{C_S}{Z}\right]^m \qquad \text{----------(4 - 13)}$$

$$\text{i.e. } K_c = \left[\frac{N^2 D}{Z}\right]^m \qquad \text{----------(4 - 14)}$$

Z is the point of convergence of the various lines on the line $K_c = 1$. A plot of the index m versus $\frac{l_c}{p}$ reveals a cubic curve which, as shown in Appendix II, can be fitted by the following equation

$$m = \frac{J - \left(M - \frac{l_c}{p}\right)^3}{R} \qquad \text{----------(4 - 15)}$$

The final equation for K_c becomes

$$K_c = \left[\frac{N^2 D}{Z}\right]^{\frac{J - \left(M - \frac{l_c}{p}\right)^3}{R}} \qquad \text{----------(4 - 16)}$$

The values of the constants obtained experimentally are:-

$Z = 1300$

$J = 0.042$

$M = 3.67$

$R = 112$

Values of K_c may be either obtained from equation (4 - 17) or they may be read direct from Fig. 31 which is based on this equation.

It should be noted that the correction factors have been determined from the experimental data for the smaller clearance ratio, $\frac{C}{D} = 0.0104$. However, it is reasonable to assume that they are applicable also to other clearance ratios.

The factor K_c may now be included in equations (4 - 10) and (4 - 12) to give expressions for the output and volumetric efficiencies respectively for a range of choke lengths.

$$Q = N D^3 \left[E + G \cos (\alpha + \psi) \right] \left[B - N^2 D \right] K_c \qquad \text{------(4 - 18)}$$

and $$\eta_V = \frac{\left[E + G \cos (\alpha + \psi) \right] \left[B - N^2 D \right] K_c}{\gamma} \qquad \text{------(4 - 19)}$$

FIG.32.

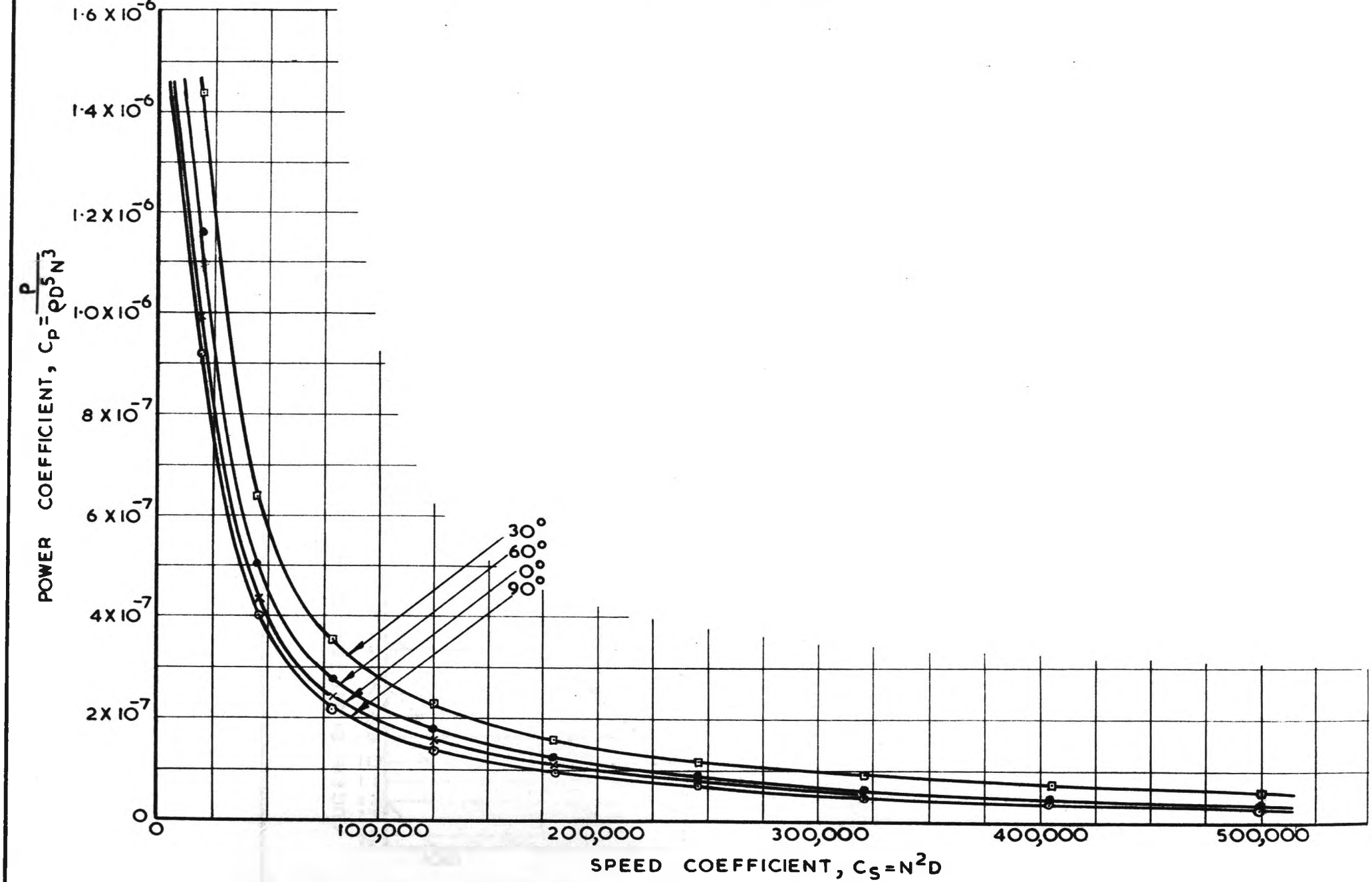

FIG. 32. POWER COEFFICIENT VERSUS SPEED COEFFICIENT FOR VARIOUS ANGLES OF ELEVATION

Auger Geometrical Proportions: P=D; $\frac{l_e}{P}$=2·0; $\frac{D_c}{D}$=0·333; $\frac{C}{D}$=0·0833; $\frac{L}{D}$=16; $\frac{d}{D}$ 0·05

FIG. 33.

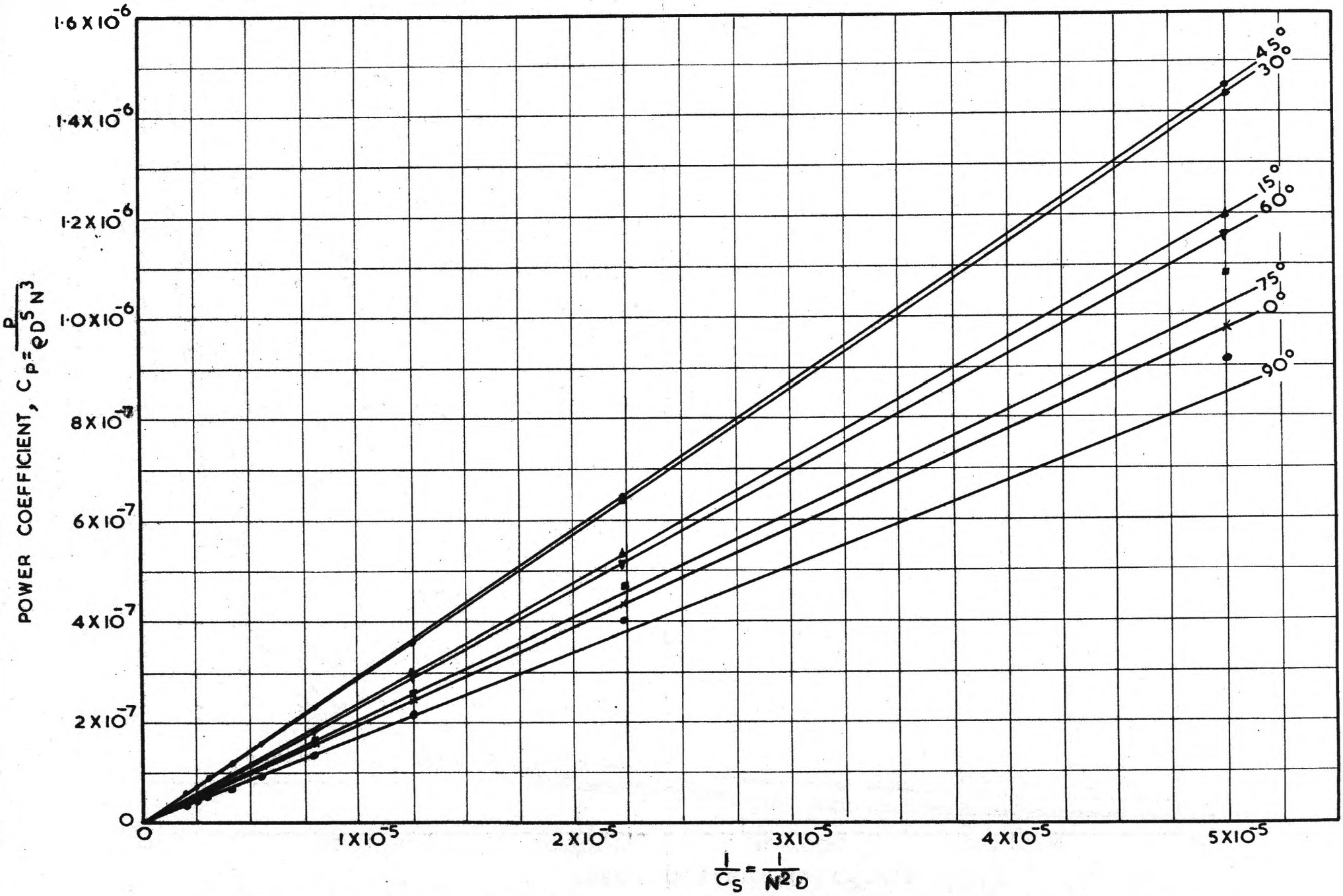

FIG. 33. POWER COEFFICIENT VERSUS RECIPROCAL OF SPEED COEFFICIENT FOR VARIOUS ANGLES OF ELEVATION

4.3 PREDICTED AUGER HORSEPOWER.

From the model auger power results, the power coefficients C_P have been calculated and are shown plotted against the speed coefficient C_S for various angles of elevation in Fig. 32. The horsepower for any geometrically similar auger may now be found by reading off the C_P value for the required C_S value and computing the horsepower from equation (4 - 4).

When C_P is plotted against C_S on logarithmic axes, (Appendix III), a series of parallel straight lines for the various angles of elevation are obtained. These lines have a negative slope of magnitude unity. This shows that the curves plotted in Fig. 32 are hyperbolic in form and that the power coefficient is inversely proportional to the speed coefficient. This is also verified by the straight line graphs obtained in Fig. 33 where C_P is plotted against $\frac{1}{C_S}$. An equation for determining auger horsepower is readily obtainable, the form of the equation being:-

$$C_P = \frac{S}{C_S} \qquad \text{----------(4 - 20)}$$

which gives $$P = S \rho D^4 N \qquad \text{----------(4 - 21)}$$

S represents the slope of each line. A plot of S versus angle of elevation α reveals a sine curve which, as shown in Appendix III, can be approximated by the following equation:-

$$S = \left[T + U \sin (2\alpha + \epsilon)\right] \qquad \text{-------(4 - 22)}$$

The horsepower equation becomes

$$P = \left[T + U \sin (2\alpha + \epsilon)\right] \rho D^4 N \qquad \text{-----(4 - 23)}$$

where the experimentally obtained constants are:-

$$T = 1.7 \times 10^{-2}$$

$$U = 1.03 \times 10^{-2}$$

$$\epsilon = 15^{\circ}$$

This gives the horsepower for a length to diameter ratio, $\frac{L}{D}$, of sixteen to one. Assuming the power to be directly proportional to auger length, that is to the $\frac{L}{D}$ ratio, an equation giving horsepower in terms of auger length may be obtained by dividing the right hand side of equation (4 - 23) by $\frac{L}{16D}$. Also, $\frac{w}{g}$ may be written in place of the bulk density ρ, w being the bulk specific weight in lb./cub.ft. Since the above equation gives the horsepower to convey grain only, it is necessary to include an efficiency factor F to cover all losses in the bearings and drive in order to determine the motor horsepower required. The final equation for the total required horsepower becomes:-

$$P = \left[X + Y \sin (2\alpha + \epsilon) \right] w N D^3 L F \qquad \text{---------(4 - 24)}$$

where the constants obtained experimentally are

$$X = 3.3 \times 10^{-5}$$

and $$Y = 2.0 \times 10^{-5}$$

The efficiency factor is dependent on the auger construction, type of bearings, type of drive, type of motor and starting conditions, etc. For average conditions, a conservative value of F of about 1.5 would be satisfactory; comparison of the power obtained from equation (4 - 24) with the power requirements of some commercial augers shows

FIG. 34.

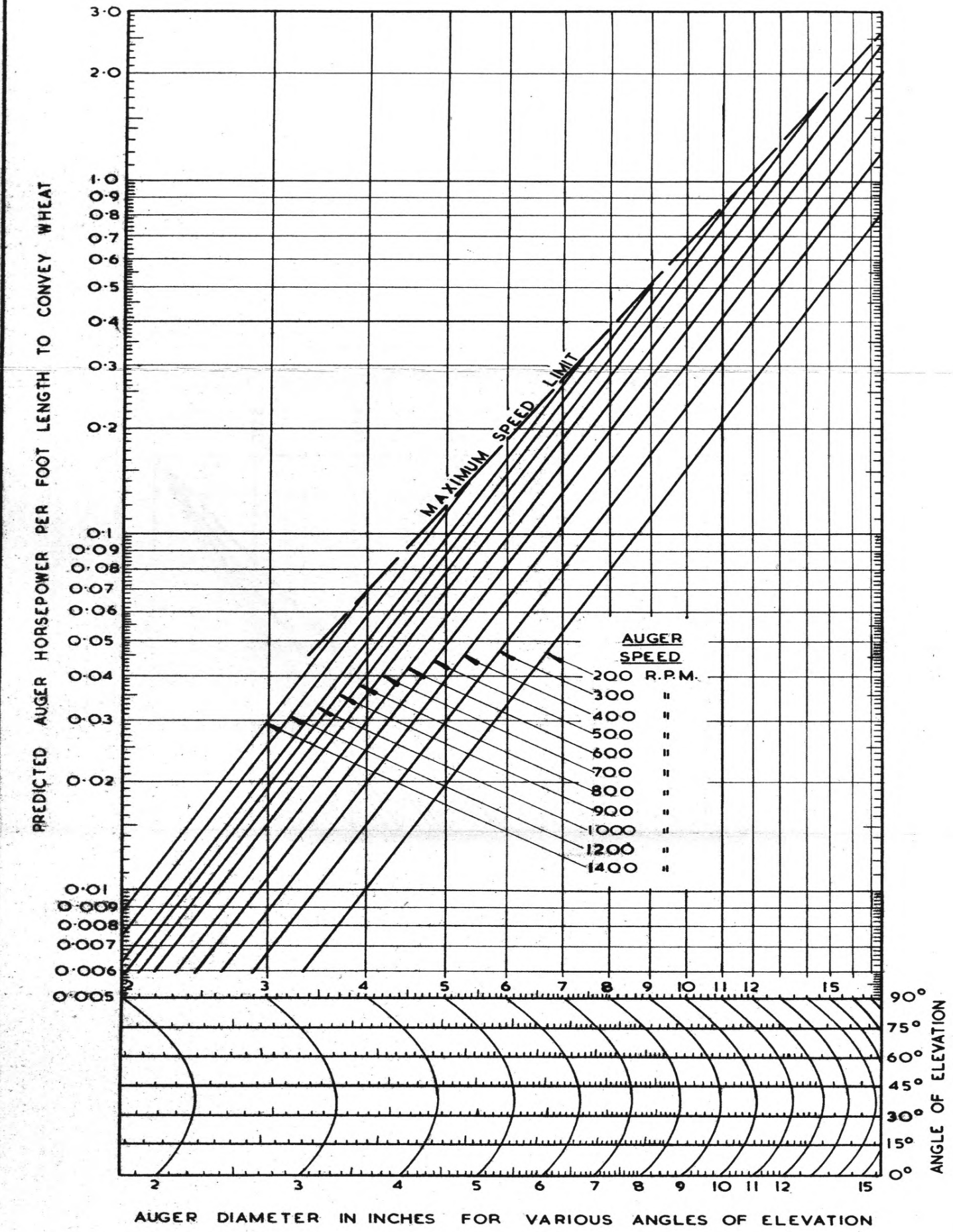

FIG. 34. PREDICTED HORSEPOWER PER FOOT LENGTH OF DIFFERENT SIZE AUGERS AT VARIOUS SPEEDS AND ANGLES OF ELEVATION TO CONVEY WHEAT. (BULK WEIGHT = 48 LB PER CUBIC FOOT)

Auger Geometrical Proportions: $P = D$; $\frac{l_c}{p}$ 2·0; $\frac{D_c}{D} = 0{\cdot}333$; $\frac{C}{D} = 0{\cdot}0833$

this to be a reasonable figure. A lower value of F of say 1.2 to 1.3 may be used when an efficient drive is employed.

The above horsepower equation only applies to a choke length to screw pitch ratio of two to one. Owing to the difficulty in obtaining accurate power readings in the model tests, such measurements were omitted in the choke length investigation. It is probable that power correction factors covering a range of choke lengths would be related to the factor K_c previously determined. However, the relatively high magnitude of the drive losses would somewhat overshadow the variations in the power for conveying purposes for different choke lengths. The estimation of total horsepower for such cases may be made by using equation (4 - 24) but choosing the factor F with discretion.

Fig. 34 gives a horsepower per foot run for different diameters, speeds and angles of elevation for conveying wheat and enables the power for various combinations to be readily obtained. The total power is found by multiplying the observed values by the auger length L and efficiency factor F. In using Fig. 34 it is assumed that the decrease in the grain size ratio, $\frac{d}{D}$, with increase in auger diameter has negligible effect on the predicted horsepower. (Equation (4 - 24) on which Fig. 34 is based, assumes that the $\frac{d}{D}$ ratio remains constant).

An equation for the overall efficiency can be now obtained:-

$$\eta_o = \frac{Q\, w\, L \sin\alpha}{33{,}000\, P} \qquad \text{----------(4 - 25)}$$

Substituting for Q from equation (4 - 10) and P from

equation (4 - 24) it follows that

$$\eta_o = \frac{\left[E + G \cos (\alpha + \psi) \right] \left[B - N^2 D \right] \sin\alpha}{\left[X + Y \sin (2\alpha + \varepsilon) \right] 33{,}000} \text{ -------(4 - 26)}$$

Equation (4 - 26) is for a choke to screw pitch ratio, $\frac{l_c}{p}$ of two to one. The drive losses have been neglected, that is, F has been made equal to unity.

FIG. 35.

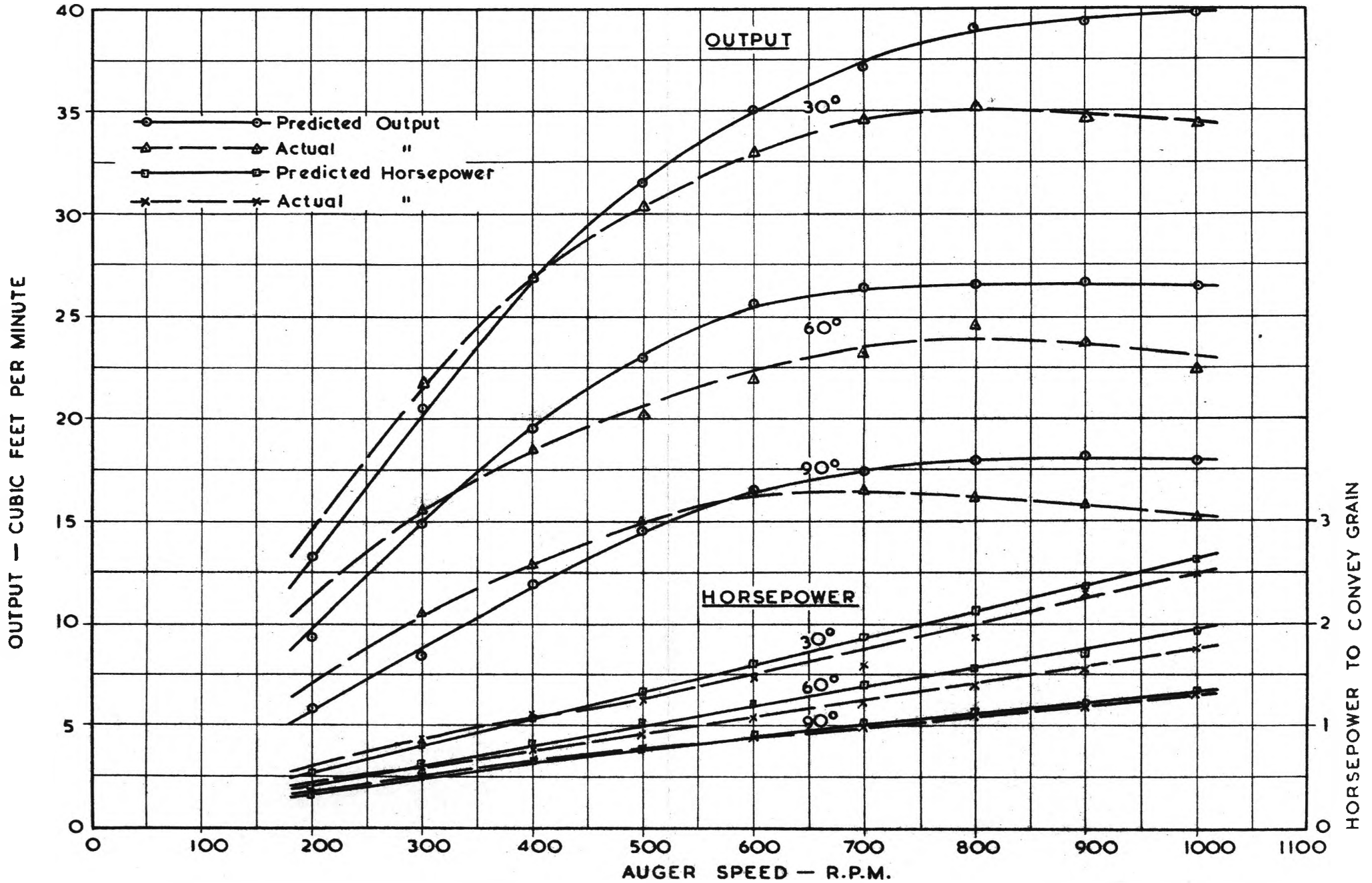

FIG. 35. COMPARISON OF PREDICTED PERFORMANCE WITH ACTUAL PERFORMANCE OF 6 INCH DIAMETER AUGER.

4.4 COMPARISON OF PREDICTED PERFORMANCE WITH ACTUAL PERFORMANCE

In order to test the validity of the design parameters obtained from the model, Fig. 35 shows a comparison of the predicted outputs and horsepowers with the actual output and horsepowers obtained from a test on a full scale 6 inch diameter auger conveying wheat (35). The full scale auger had a clearance ratio of 0.0625, slightly less than that of the model which is 0.0833. However, all other geometrical proportions are identical to that of the model.

The actual performance graphs appear as broken lines while the predicted performance graphs are shown as full lines. It can be seen that good agreement is obtained; the differences that occur may be due largely to the different clearance ratios, since the predicted performance graphs are based on an auger with a potential capacity of 8.2 per cent greater than that of the actual auger. Differences may be also due to spurious effects such as variation in head of grain over the choke, different grain sizes and accuracy of measurements.

The predicted performance figures from the model tests have also been compared with performance figures obtained from commercially manufactured augers, and again good agreement has been obtained. However, it is desirable to conduct more tests on prototype augers to obtain further confirmation of the design parameters. Although it would appear that variation of grain size to auger diameter ratio causes little variation in the design parameters, further tests on the model auger, using different size grains, are required. Also the effect of grains of different internal friction should be studied. Appropriate correction

factors could then be included in the design equations allowing their application to a wide range of granular materials.

FIG. 36.

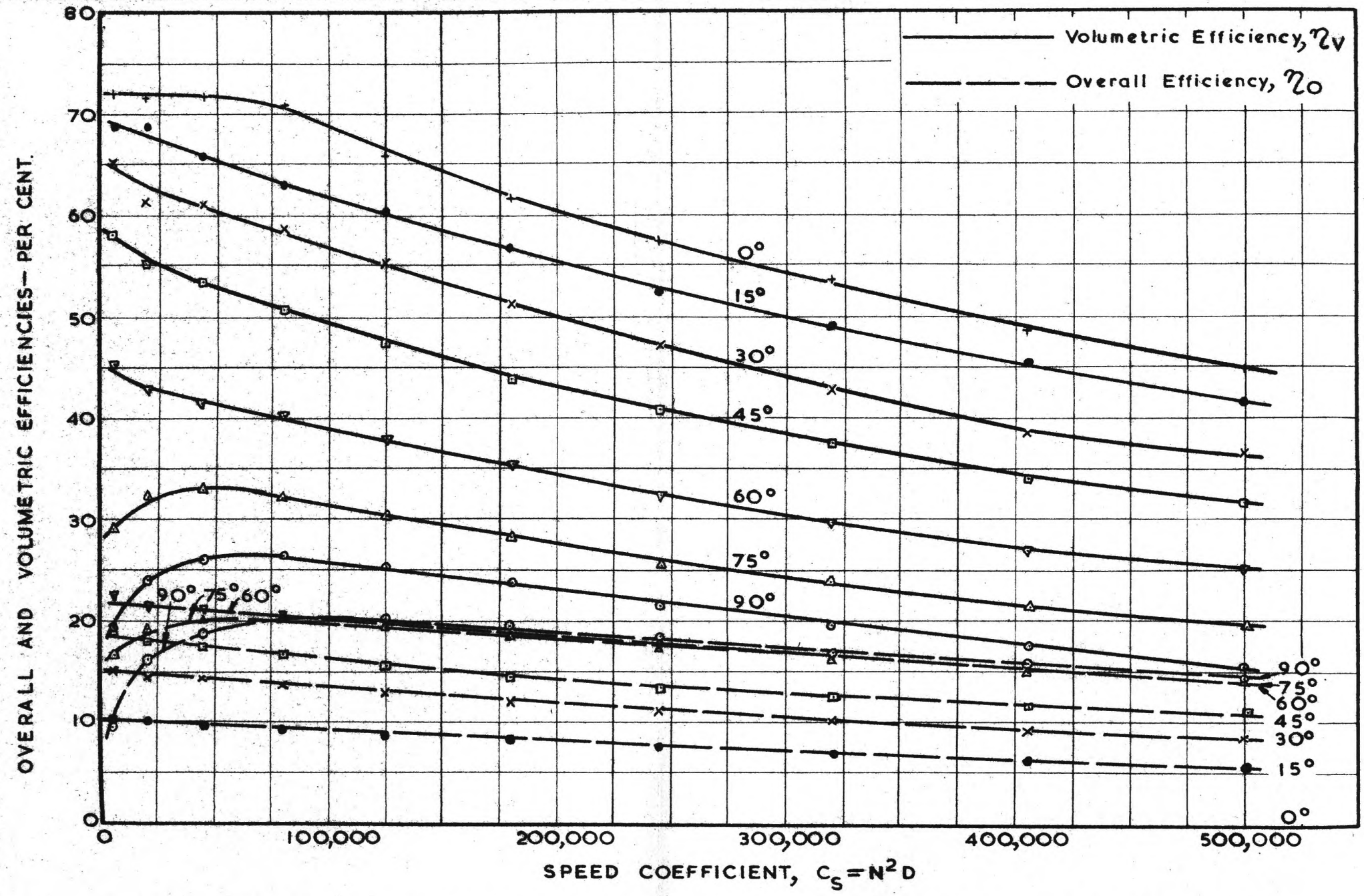

FIG. 36. OVERALL AND VOLUMETRIC EFFICIENCIES VERSUS SPEED COEFFICIENT FOR VARIOUS ANGLES OF ELEVATION

Auger Geometrical Proportions: $p = D$; $\frac{l_c}{p} = 2{\cdot}0$; $\frac{D_c}{D} = 0{\cdot}333$; $\frac{C}{D} = 0{\cdot}0833$; $\frac{L}{D} = 16$; $\frac{d}{D} = 0{\cdot}05$

4.5 AUGER EFFICIENCY AND CHOICE OF OPERATING CONDITIONS

The volumetric and overall efficiencies as given approximately by equations (4 - 12) and (4 - 26) respectively are shown plotted non-dimensionally against the speed coefficient C_S in Fig.36. For these graphs $\frac{l_c}{p} = 2.0$ and $\frac{C}{D} = 0.0833$. The best volumetric efficiencies are obtained at the lower angles of elevation and are an important consideration as far as output is concerned. In contrast, the best overall efficiencies are obtained at the higher angles of elevation, indicating the conditions for most economical operation.

It is interesting to compare augers of equal diameter giving equal outputs at the same height of lift but working at different angles of elevation. For example, compare two 6-inch diameter augers conveying wheat, one working at an angle of elevation of 90° and the other at 30°. Reference to Fig. 29 shows that the 90° auger has an output of 18 cub.ft. per min. at a speed of 1,000 r.p.m. The same output is obtained with the 30° auger running at approximately 260 r.p.m.; the corresponding horsepowers for the 90° and 30° augers per foot of lift are each approximately 0.24 (an efficiency factor of 1.5 has been applied in the horsepower determinations). Thus it is necessary for the 30° auger to be twice the length of the 90° auger to give the same height of lift. However, the slower speed of the 30° auger may be a practical advantage giving smoother operation and less wear. Comparing efficiencies, the volumetric efficiencies of the 90° and 30° augers are respectively 16 and 61 per cent while the overall efficiencies are both approximately 15 per cent.

In determining the operating conditions for a particular auger, consideration must be given to the maximum economical speed; speeds higher than this will not yield any gain in output and in some cases may cause a reduction in output. The maximum speeds are indicated both in Figs. 29 and 34. An expression for the maximum speed may be obtained from equation (4 - 6). For the model auger the maximum speed is approximately 2,000 r.p.m.; on this basis the maximum speed for any geometrically similar auger would be -

$$N_{max} = \frac{700}{\sqrt{D}} \quad \text{r.p.m.} \qquad \text{----------(4 - 27)}$$

(D is the auger diameter expressed in feet.)

SECTION 5

EXAMINATION OF GRAIN VORTEX MOTION IN RELATION TO AUGER PERFORMANCE

FIG. 37

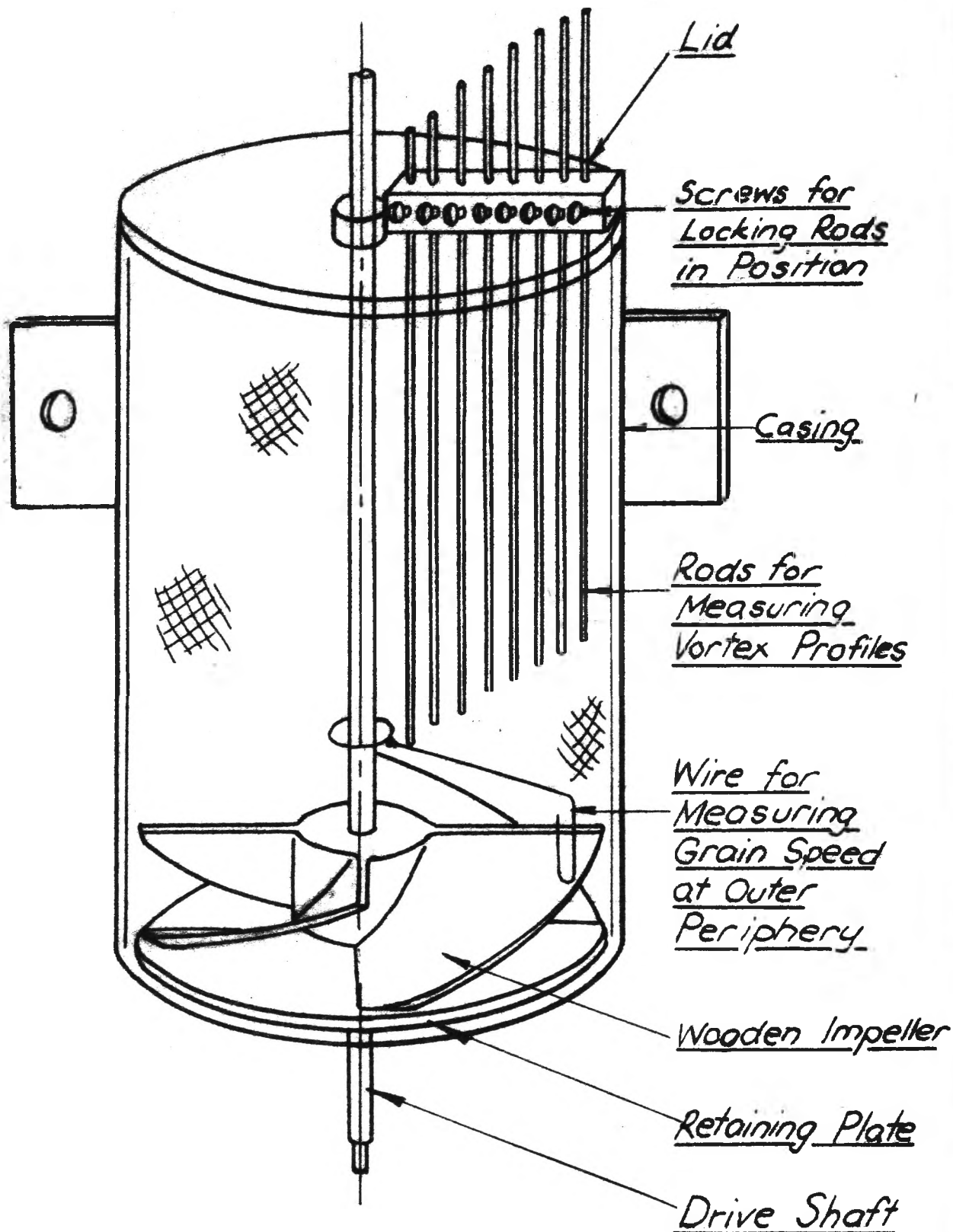

FIG. 37. APPARATUS FOR GRAIN VORTEX MOTION INVESTIGATION

5.1 INVESTIGATION OF GRAIN VORTEX MOTION

An important facet of the performance of augers, particularly in the steeply inclined or vertical position, is the vortex motion imparted to the grain being conveyed. In order to study the characteristics of this vortex motion, an investigation was conducted using a special apparatus designed to simulate, as near as possible, the rotary motion of grain on an auger flight. While the findings of this investigation may be restricted to augers running partially full, some interesting results have been obtained which are shown to have a significant bearing on the ratio of the core diameter to the screw diameter in relation to auger performance.

(a) Description of Apparatus and Tests Conducted

The apparatus used for this investigation is shown diagrammatically in Fig. 37 and was constructed to represent an auger approximately four times the scale of the model auger. The apparatus was designed so that it could be mounted on the model auger base plate to enable the variable speed drive motor to be employed.

The rotating four-bladed impeller, constructed from wood for ease of manufacture, represents one pitch of a 6-inch auger cut into four parts and telescoped together as shown. The pitch of the blades is 6-inches, the outside diameter 5-3/8 inches, the core diameter 1-1/2 inches and the height 1-1/2 inches. The stationary casing is of clear plastic tubing of 1/8 inch wall thickness and having an inside diameter of 5-3/4 inches; the length of the casing is 9 inches. The casing is fitted with a lid which carries nine 1/8 inch diameter brass rods each 10 inches long.

These rods are arranged along a radial line and slide in holes drilled through the lid; they are used to measure the vortex profile of the rotating grain, being locked in position against the grain surface by means of set screws. A flat circular retaining plate attached to the drive shaft beneath the impeller prevents grain from leaking out of the casing.

Two tests were conducted for the vertical position of the apparatus, one using Japanese millet seed and the other using wheat. In each case the casing was filled with grain to a height of two inches measured above the circular retaining plate, this being considered to be the maximum height for the grain to be under the full action of the rotating impeller. The tests were conducted over the speed range 400 to 1000 r.p.m.; for each speed the grain vortex profile was obtained by adjusting each measuring rod to just touch the grain surface. Measurements of the rotational speed of the grain at the outer periphery near the casing were also taken. This was accomplished by using a piece of light gauge wire looped loosely around the drive shaft at the centre and extending out radially with the extremity bent down to enter the grain pile as shown in Fig. 37. The wire was carried around with the grain and the grain speed determined by counting the number of revolutions in a given period of time. Attempts to measure the grain speed near the centre of the vortex by this method were unsuccessful, since the spiral motion of the grain buried the wire beneath the surface.

(b) Theoretical Considerations

Before discussing the results of this investigation, it is necessary to consider some of the theoretical aspects of vortex motion.

While the vortex equations for fluids may be readily established, the vortex equations for grain are less simple to derive. An approximate analysis is given based on the vortex equations for fluids:-

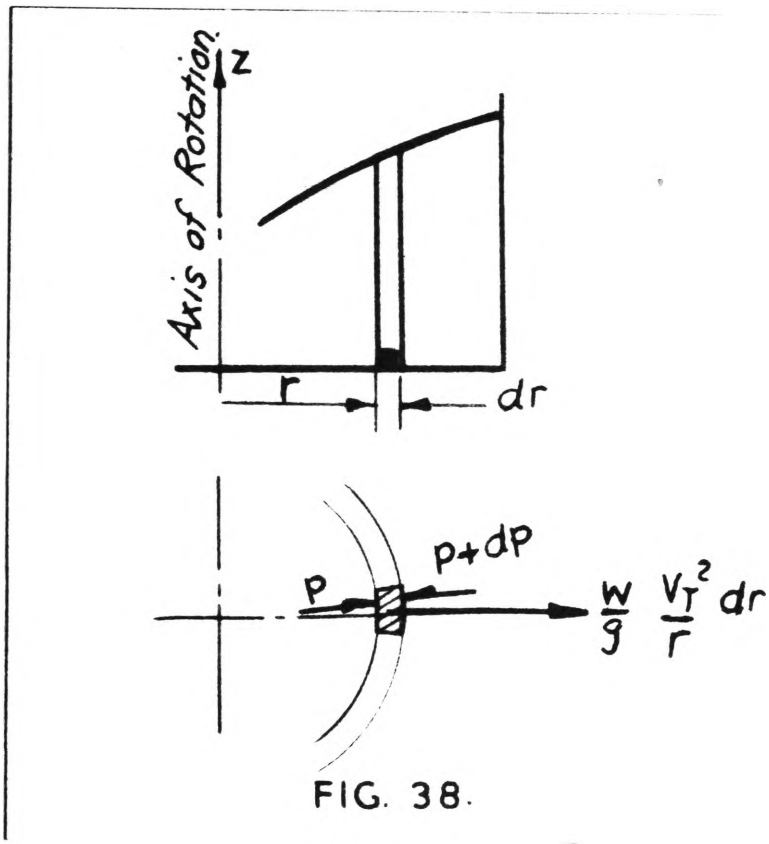

FIG. 38.

Fig. 38 shows a substance of specific weight w having vortex motion. Consider an elemental ring of the substance of radius r. Let the rotational speed of this ring at the radius considered be N_T r.p.m. and the corresponding peripheral velocity be V_T ft per sec.; also let p_r be the radial pressure acting on this ring. For equilibrium the radial pressure must balance the centrifugal pressure.

$$p_r + \frac{w}{g}\frac{V_T^2}{r}dr = p_r + dp_r$$

$$\therefore \quad \frac{dp_r}{dr} = \frac{w}{g}\frac{V_T^2}{r} \qquad \text{----------(5 - 1)}$$

The general equation for the velocity distribution in a fluid vortex is

$$V_T \; r^n = C_1 \qquad \text{----------(5 - 2)}$$

or $$N_T \; r^{n+1} = C_2 \qquad \text{----------(5 - 3)}$$

where C_1 and C_2 are constants $\left(C_2 = \frac{30}{\pi} C_1\right)$

It will be assumed that the velocity distribution in a grain vortex is given by the same general equations.

Vortices in which the index n of equations (5 - 2) and (5 - 3) is greater than -1 have the characteristic of a higher angular velocity nearer the axis of rotation than at the outer periphery; for values of n less than -1 the angular velocity is higher at the outer periphery than near the centre.

Combining (5 - 1) and (5 - 2)

$$\frac{dp_r}{dr} = \frac{w \, C_1^{\,2}}{g \, r^{2n+1}} \qquad \text{----------(5 - 4)}$$

The integration of (5 - 4) gives the relationship for radial pressure distribution

$$p_r = - \frac{w \, C_1^{\,2}}{2 \, n \, g \, r^{2n}} + p_o \qquad \text{----------(5 - 5)}$$

where p_o is a constant of integration.

For a fluid, the equation of the vortex surface is obtained quite readily since the pressure p_r will equal the hydrostatic pressure

wz, z being the head or height of fluid at the radius considered. The equation for a fluid vortex then becomes

$$z = - \frac{C_1^2}{2ngr^{2n}} + z_o \qquad \text{----------(5 - 6)}$$

where $z_o = p_{o/w}$

In order to establish a relationship for a grain vortex it is first necessary to write down the basic equations for granular materials loaded under their own weight. Under static conditions, the vertical pressure p_z at a depth z for a pile of grain in which the surface is inclined at an angle σ (Fig. 39 (a)) is

$$p_z = wz \cos \sigma \qquad \text{----------(5 - 7)}$$

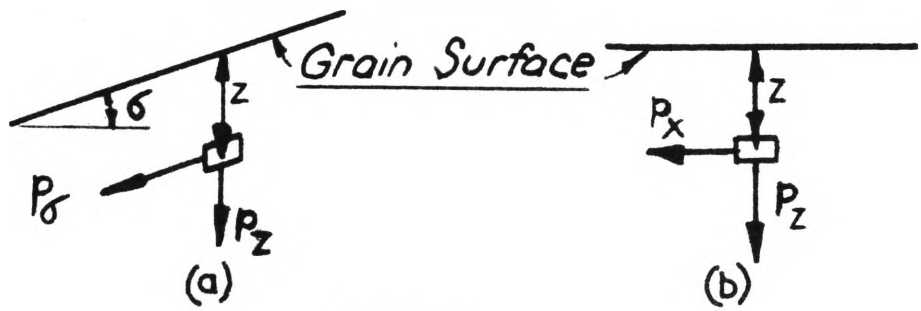

FIG. 39.

Rankine showed that the conjugate stress or pressure p_σ acts parallel to the surface and is given by

$$p_\sigma = p_z \frac{\cos \sigma - \sqrt{\cos^2 \sigma - \cos^2 \phi}}{\cos \sigma + \sqrt{\cos^2 \sigma - \cos^2 \phi}} \qquad \text{-----(5 - 8)}$$

where ϕ = angle of repose.

Equation (5 - 8) shows that because of friction between the granular particles, p_σ is less than p_z.

For the special case of a horizontal surface (Fig. 39 (b)), equations (5 - 7) and (5 - 8) are simplified.

For $\phi = 0$ $\quad p_z = w\,z$ ----------(5 - 9)

and $\quad p_x = p_z \dfrac{1 - \sin \phi}{1 + \sin \phi}$ ----------(5 - 10)

In this case p_x is horizontal.

While grain at rest is loaded by its own weight in the vertical plane, in contrast, grain having vortex motion about a vertical axis is loaded by centrifugal forces in the horizontal plane. Therefore an approximate theory for grain vortex motion may be established by applying the basic equations for grain statics in the reverse way as described:-

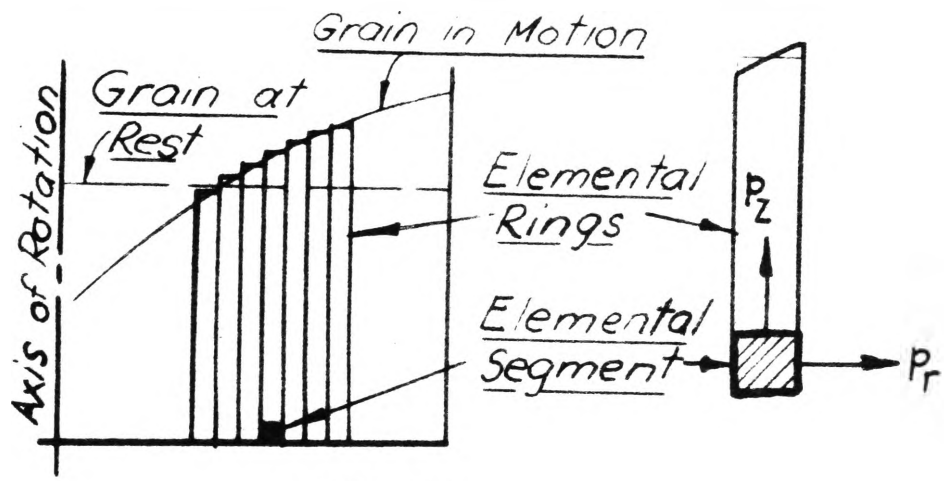

FIG. 40.

Consider a mass of grain at rest with the surface horizontal inside a cylindrical chamber. The vertical and horizontal pressures at

a depth z from the surface will be respectively constant throughout. Now suppose the chamber is made to rotate; because of friction between the walls of the chamber and the grain, the grain will also rotate. Owing to varying centrifugal forces the horizontal or radial pressure will be no longer constant but will vary with the radius as indicated in equation (5 - 5). To maintain equilibrium, the vertical pressure must also vary in the same way; hence the surface of the grain must assume a shape characteristic of the particular vortex motion.

Assuming the rotating grain mass to consist of a large number of concentric rings of elemental thickness as shown in Fig. 40 (a). Then an elemental segment of each ring may be considered to have pressures p_r and p_z acting on perpendicular faces as shown in Fig. 40 (b). Because adjacent grain cylinders tend to slide relative to one another in the vertical or z direction as the grain surface takes up the equilibrium position, this sliding will be resisted by frictional forces. Therefore, the vertical pressure p_z required to maintain equilibrium will be less than the radial pressure p_r. For convenience p_z may be expressed as follows:

$$p_z = k\, p_r \qquad \text{----------(5 - 11)}$$

where k is a factor dependent on the angle of repose and the slope of the surface.

To simplify the analysis, the effect of the varying slope of the grain surface will be neglected making k solely dependent on the

angle of repose. This simplification assumes that each elemental cylinder is part of a large mass of grain with a horizontal surface.

since $p_z = w\,z$

then $p_r = \frac{w\,z}{k}$ ----------(5 - 12)

From equation (5 - 10) for perpendicular conjugate stresses, k will be given by

$$k = \frac{1 - \sin \phi}{1 + \sin \phi} \qquad \text{----------(5 - 13)}$$

Substituting for p_r from equation (5 - 12) into equation (5 - 5) the general equation for a grain vortex becomes

$$z = -\frac{k\,C_1^2}{2\,n\,g\,r^{2n}} + z_o' \qquad \text{----------(5 - 14)}$$

where $z_o' = \frac{p_o}{k\,w} = \frac{z_o}{k}$, z_o being the equivalent constant in equation (5 - 6) for a fluid vortex.

For grain k will be always less than one and will be constant for a particular granular material. Comparing equations (5 - 14) and (5 - 6) it follows that, for a given speed of rotation, the height of a grain vortex will be less than the corresponding height of a fluid vortex. It may be noted that for a fluid $\phi = 0$, therefore, $k = 1$; in this case the radial pressure equals the vertical pressure as previously discussed.

FIG. 41.

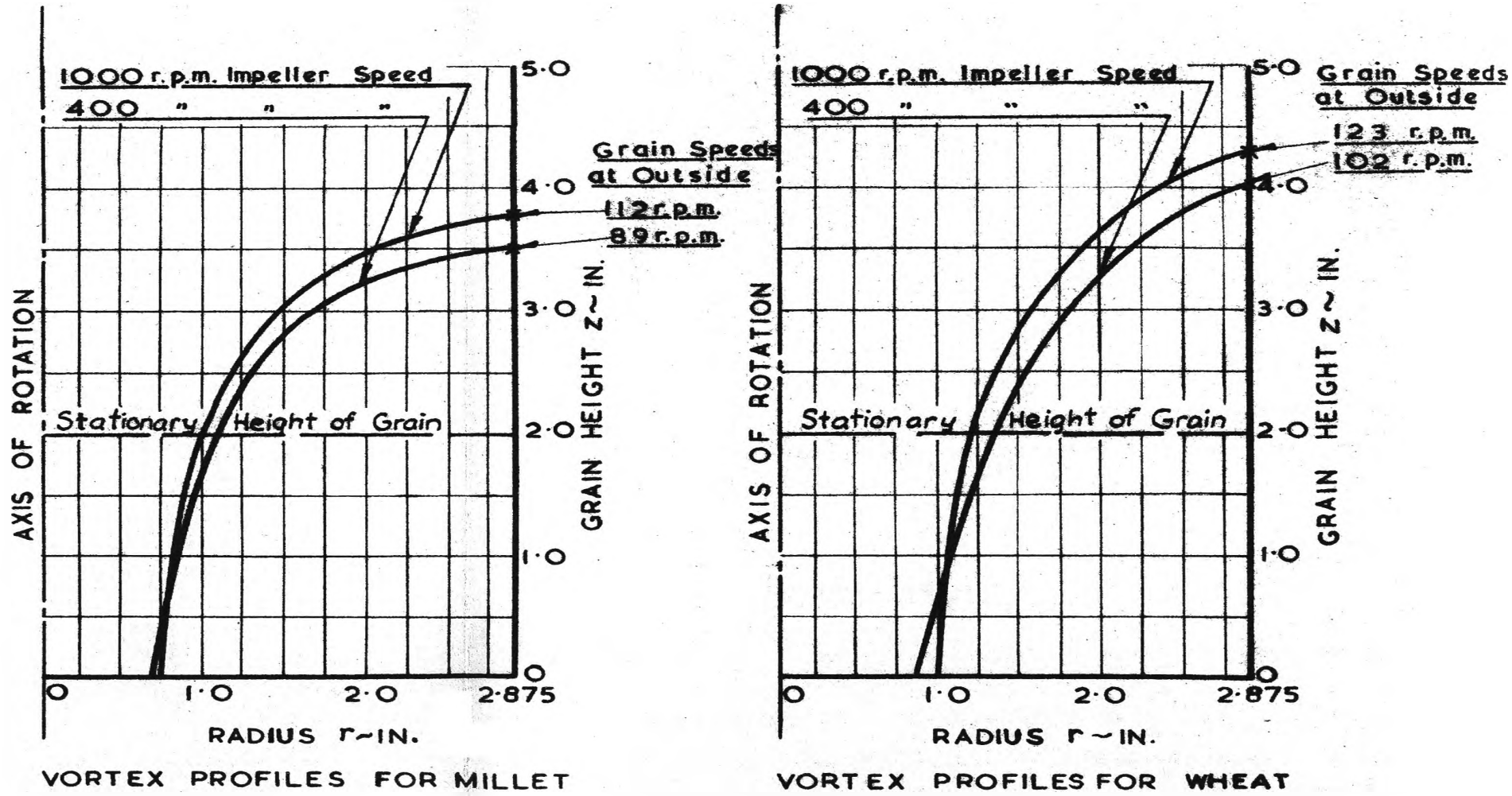

FIG. 41. VORTEX PROFILES FOR MILLET AND WHEAT FOR THE 400 AND 1000 R.P.M. IMPELLER SPEEDS

(Vortex profiles were obtained, also, for the 600 and 800 r.p.m. impeller speeds, but have been omitted from this diagram to avoid confusion. Co-ordinates of these profiles are tabulated in Appendix V.)

FIG. 42.

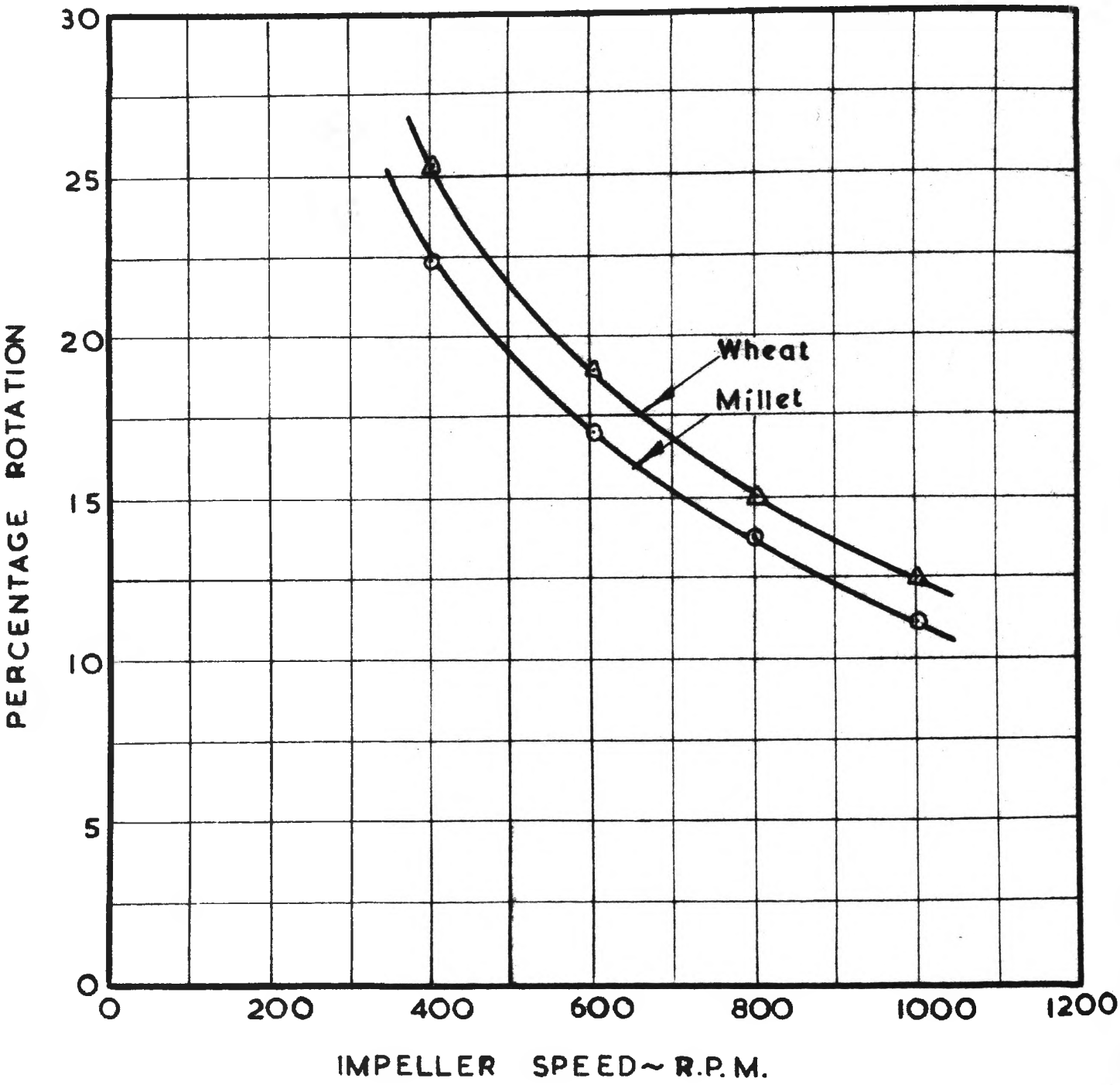

FIG. 42. PERCENTAGE ROTATION OF GRAIN

(c) Discussion of Experimental Results and Development of Vortex Equations

The results obtained from the tests using the vortex apparatus are given in Appendix V and the vortex profiles for millet and wheat are shown in Fig. 41. Measurements of the grain speed at the outer periphery showed that the wheat had a slightly higher rotational speed than the millet and this accounts for the wheat having a steeper vortex profile. For the range of impeller speeds used, the vortex profile for each grain is shown to retain the same general shape although the grain surface actually rose slightly with increase in speed owing to a slight reduction in the bulk density of the grain.

It is interesting to note that the rotational speed of the grain measured at the outer periphery increased at a much lesser rate than the increase in impeller speed. For this reason the percentage rotation decreases with increase in speed as shown in Fig. 42. The curves for the millet and wheat are shown to have the same characteristic shape, although the rotational motion of the wheat is slightly higher than that of the millet. These findings endorse the findings of Section 3.2 where the various grain velocity components of a vertical auger were studied; the V_T'/V_S' graph plotted in Fig. 24 page 23 has the same characteristic shape as the graphs of Fig. 42. Observation showed that the rotational speed of the grain increased towards the axis of rotation, but attempts to measure the speeds at the inner radii were unsuccessful.

The vortex velocity distribution equations for the millet and wheat respectively may be established by comparing the experimentally

FIG. 43.

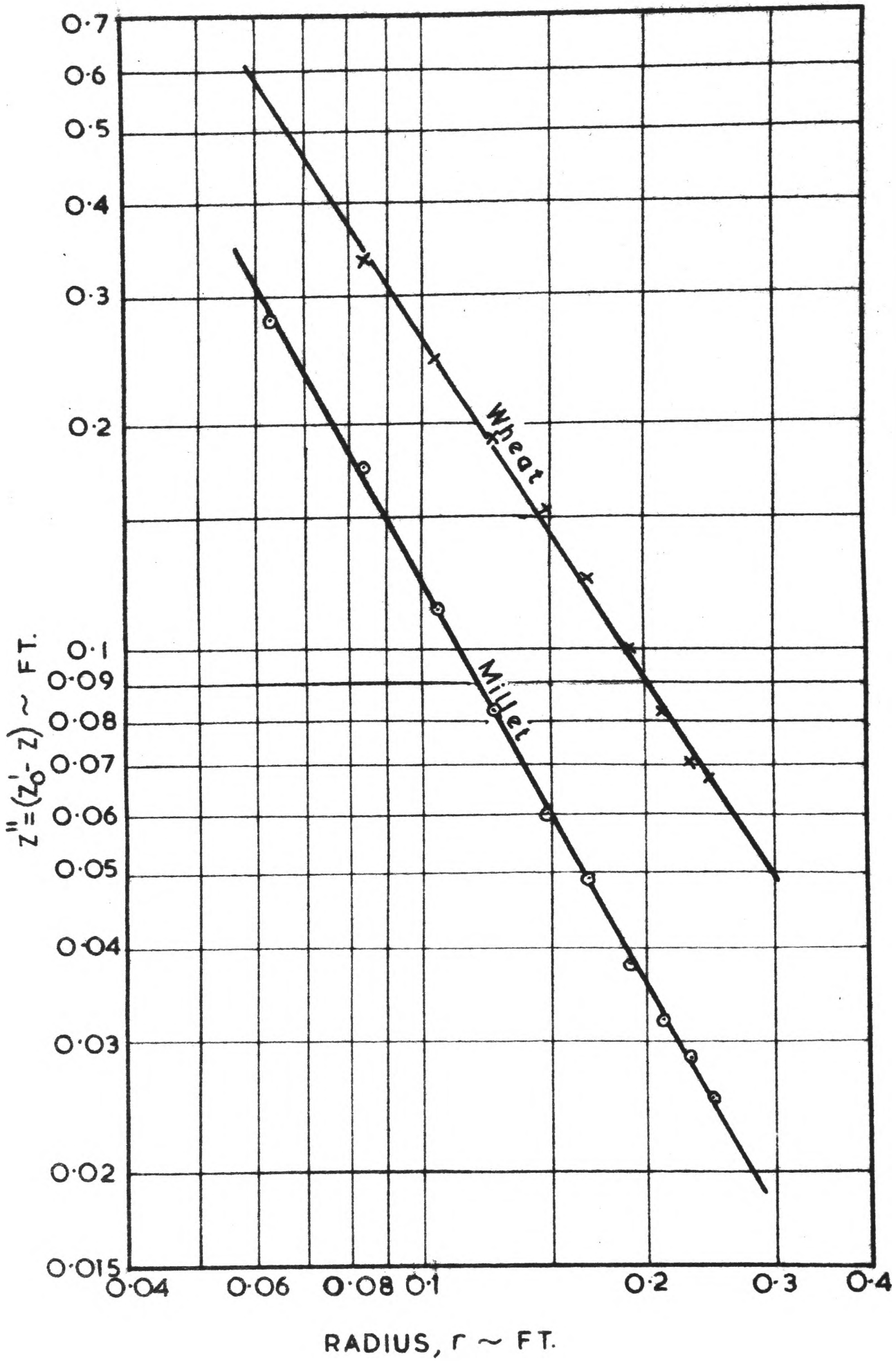

FIG. 43. VORTEX PROFILES ~ z'' VERSUS r

obtained equations with the theoretical equation. The actual vortex profile equations can be approximated by plotting the profiles on logarithmic axes and obtaining the equations for "best fit". The profile graphs for the millet and the wheat corresponding to the 400 r.p.m. rotational speed of the impeller are shown in Fig. 43. In this case $z'' = (z_o' - z)$ is plotted against r to give a straight line. The general form of the equation is

$$z'' = z_1'' \left(\frac{r}{r_1}\right)^x \qquad \text{----------(5 - 15)}$$

where x is the slope of the logarithmic graph and z_1'' and r_1 are co-ordinates of a point on the graph. z_o represents the height of the zero z'' axis above the z axis (Found by trial and error).

The various values obtained from Fig. 43 are:-

(i) For millet $x = -1.8$

$z_1'' = 0.122$ ft.

$r_1 = 0.1$ ft.

$z_o' = 0.317$ ft.

(ii) For wheat $x = -1.56$

$z_1'' = 0.26$ ft.

$r_1 = 0.1$ ft.

$z_o' = 0.400$ ft.

The final equations for the vortices corresponding to the impeller speed of 400 r.p.m. are

(i) For millet $$z = -\frac{1}{515\, r^{1.8}} + 0.317 \qquad \text{-----(5 - 16)}$$

(ii) For wheat $$z = -\frac{1}{140\, r^{1.56}} + 0.400 \qquad \text{-----(5 - 17)}$$

Because equations (5 - 16) and (5 - 17) are of the same form as equation (5 - 14), the various terms may be compared.

(i) Vortex Motion of Millet:-

By comparison,

$$-\frac{k\, C_1^2}{2\, n\, g\, r^{2n}} = \frac{1}{515\, r^{1.8}}$$

$$\therefore \quad n = \frac{1.8}{2} = 0.90$$

The angle of repose of the millet was measured to be 31°. Therefore using equation (5 - 13)

$$k = 0.32$$

$$\therefore \quad \frac{k\, C_1^2}{2 \times g} = \frac{1}{515}$$

$$C_1 = \frac{2\, n\, g}{515\, k} = \frac{1.8 \times 32.2}{515 \times 0.32}$$

$$= 0.593$$

In accordance with equations (5 - 2) and (5 - 3) the velocity distribution in this vortex will be given by

$$V_T = \frac{0.593}{r^{0.9}} \qquad \text{----------(5 - 18)}$$

or $$N_T = \frac{5.66}{r^{1.9}} \qquad \text{----------(5 - 19)}$$

(ii) Vortex Motion of Wheat:-

In a similar way the following velocity distribution equation

for the wheat vortex is found:

$$V_T = \frac{0.98}{r^{0.78}} \qquad \text{----------(5 - 20)}$$

or

$$N_T = \frac{9.36}{r^{1.78}} \qquad \text{----------(5 - 21)}$$

(The value of k = 0.375 calculated from equation (5 - 13) and used in the development of equations (5 - 20) and (5 - 21) is based on an angle of repose for the wheat of 27°).

Equations (5 - 18) and (5 - 20) show that the actual velocity distributions obtained are very close to the velocity distribution for a free vortex, particularly in the case of the millet. For a free vortex, the index n of equation (5 - 2) equals one making the tangential velocity inversely proportional to the radius.

$$\text{i.e.} \quad V_T = \frac{C_1}{r} \qquad \text{----------(5 - 22)}$$

It is interesting to note that the tangent of the helix angle is also inversely proportional to the radius and this may be of some significance.

The corresponding equation for the rotational speed in the free vortex is

$$N_T = \frac{C_2}{r^2} \qquad \text{----------(5 - 23)}$$

The validity of equations (5 - 18) to (5 - 21) depends largely on whether the assumptions made in the theoretical analysis are approximately correct. However, it is possible to make one check by

using these equations to calculate the rotational speed of the grain at the outer periphery and compare these computed speeds with the actual grain speeds as measured during the test for the 400 r.p.m. speed of the impeller. The rotational speed of the grain at the outer periphery will be denoted by N_T' and the corresponding radius denoted by r'

For the outer periphery, $r' = 2.875$ ins. $= 0.24$ ft.

Using equation (5 - 19), the value of N_T' for the millet is

$$N_T' = 86 \text{ r.p.m.}$$

This compares quite well with the 89 r.p.m. as measured (Appendix V).

Using equation (5 - 21), the value of N_T' for the wheat is

$$N_T' = 119 \text{ r.p.m.}$$

This is slightly higher than the 105 r.p.m. as measured, although inaccuracies in measuring the vortex profile could account for this variation.

It is interesting to compare the velocity distributions given by equations (5 - 19) and (5 - 21) with those for a free vortex. Since the actual rotational velocities at the outer periphery are known, then the constant in the free vortex equation of (5 - 23) may be found.

$$C_2 = N_T' \quad (r')^2 \qquad \text{----------(5 - 24)}$$

For millet $C_2 = 89 \times 0.24^2 = 5.12$

For wheat $C_2 = 105 \times 0.24^2 = 6.05$

The free vortex equations can be now written.

For millet $$N_T = \frac{5.12}{r^2} \qquad \text{----------(5 - 25)}$$

FIG. 44.

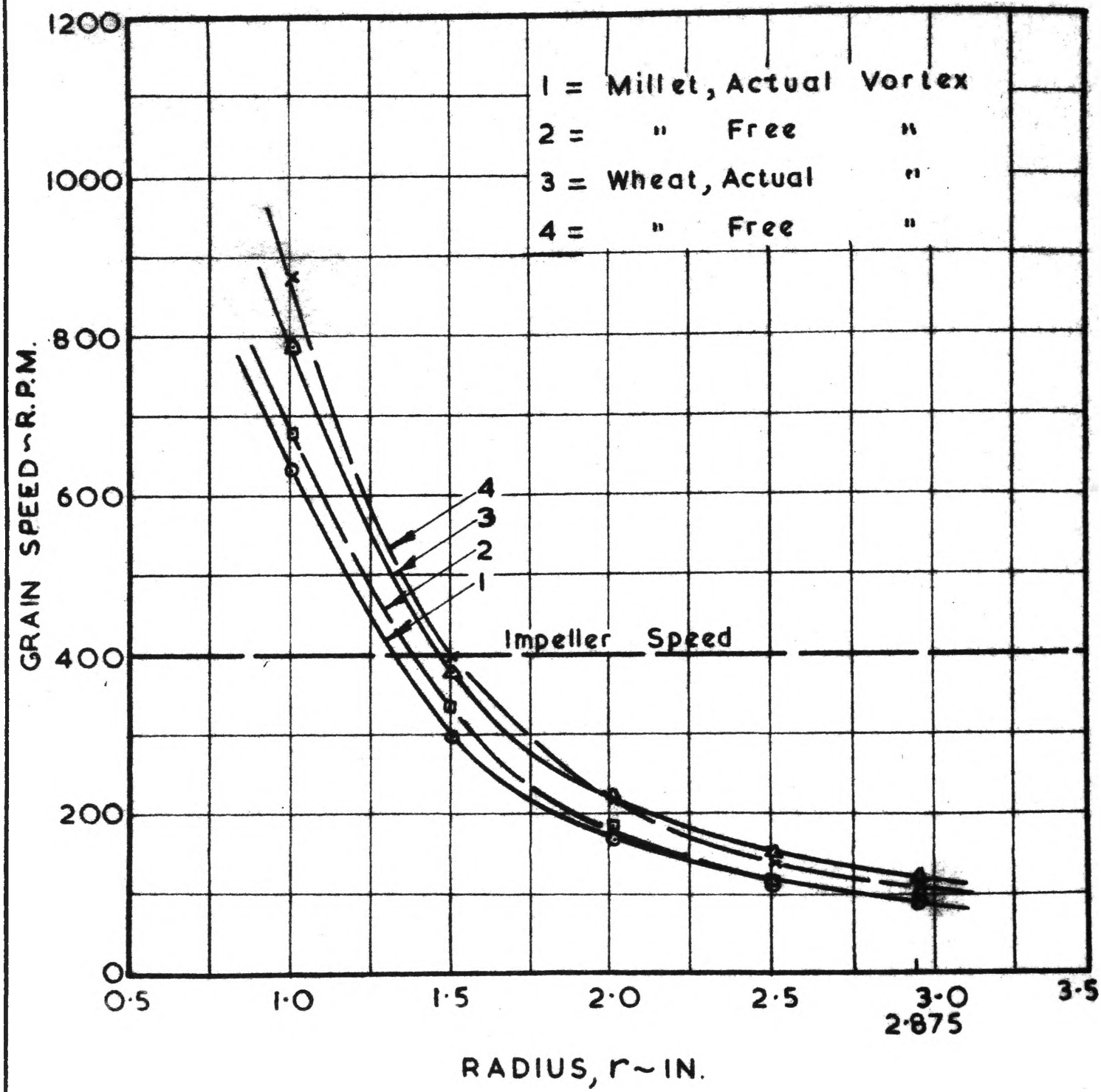

FIG. 44. VARIATION OF GRAIN SPEED WITH RADIUS

For wheat $N_T = \frac{6.05}{r^2}$ ----------(5 - 26)

Fig. 44 shows a comparison between the actual rotational velocity distributions (shown as full lines) as given by equations (5 - 19) and (5 - 21) with those for a free vortex (shown as dotted lines) as given by equations (5 - 25) and (5 - 26). The close agreement between graphs (1) and (2) for the millet and between graphs (3) and (4) for the wheat indicates that, for most practical purposes, a free vortex distribution can be assumed.* The graphs also reveal the rapid increase in the grain speed at the lower radii.

Also shown in Fig. 44 is the 400 r.p.m. auger speed line; this intersects graph (2) at $r = 1.38$ in. for millet and graph (4) at $r = 1.5$ in. for wheat. These radii may be regarded as being critical, since at radii below these respective values, the grain rotates faster than the screw. For this to happen, the grain must move relative to the screw in the same direction as the direction of rotation. Thus the spiral motion of the grain causes reverse flow or slipping back in the central region; this action in an actual auger results in a reduction in output and a wastage of power. The reverse flow of the grain is illustrated in the velocity diagram of Fig. 45 which depicts this condition; the lifting velocity is negative in this case. At the critical radius, the relative velocity V_R is zero and the absolute velocity V_A and screw velocity V_S coincide.

---

* While the analysis has been based on the 400 r.p.m. impeller speed, it is expected that similar results would be obtained for the other impeller speeds since the shape of the vortex profiles remained substantially constant. (Fig. 41).

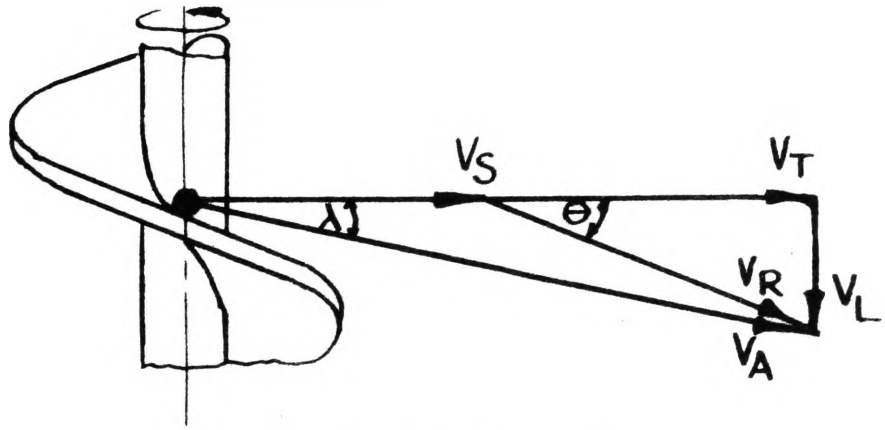

FIG.45.

(d) General Discussion.

This investigation has shown that the approximate theoretical analysis of the vortex motion of grain based on the vortex equations for fluids gives good agreement with the experimentally obtained results. While the findings of the investigation have indicated that the grain velocity increases toward the axis of rotation and the rotational motion approximates that of a free vortex, it is not known whether this is an accurate account of the vortex motion in an actual auger over a wide range of loadings. The nature of the tests conducted suggests that these findings may only apply to an auger running partially full when the vortex is unrestricted.

The vertical auger volumetric efficiency graphs shown in Fig. 19 page 20 show a falling off in volumetric efficiency in the low speed range at high percentage "fullness" values. In this case there is no grain leakage in the clearance space owing to the small radial clearance, and the leakage, therefore, is confined to the central region of the screw; this indicates that the spiral motion is prevalent under

all conditions of loading. In explanation it can be said that, when an auger runs nearly full of grain, the vortex profile cannot form completely owing to the limited screw space. However, in this case, it is possible that the vertical pressure required to support the vortex motion is provided by the grain pressing against the underside of the auger flight. Further investigation is necessary to establish the vortex velocity distributions for such conditions of loading.

Another factor to be considered in the examination of grain vortex motion in augers is the effect of full immersion of the choke. The model auger tests have revealed that, under static conditions, a mass of grain may be held on the auger flight without slip when the exposed portion of the screw forming the choke is fully immersed in the grain pile. However, under dynamic conditions, it is apparent that the feeding action of grain into the screw space of the choke will permit slip to take place in the central region of the screw owing to the spiral motion. This suggests that the characteristics of the vortex motion will change somewhat over the low speed range. While the index $n = 1$ for a free vortex, it is probable that n will be less than this value in an actual auger.

There is a further factor which must not be overlooked; while the present analysis is based on the assumption of n being constant, this may not always be so; it is possible for n to be a function of the radius. The assumption of a constant n, however, has allowed a simpler analysis with sufficient accuracy for most practical purposes as vortex tests have indicated.

5.2 EXAMINATION OF AUGER SPEED IN RELATION TO CORE DIAMETER OF A VERTICAL AUGER.

The study of grain vortex motion in augers provides a useful means for examining the ratio of the core diameter to the screw diameter, D_c/D, in relation to auger performance. For an auger of given geometrical proportions there is a certain speed of operation at which the reverse flow or slipping back of grain in the central region ceases. This will be referred to as the critical speed and denoted by N_c. It is possible to develop an expression for the critical speed in terms of the auger diameter and the D_c/D ratio for a given vortex velocity distribution.

(a) Extension of Vortex Theory with the Aid of Experimental Data.

If the grain speed at the outer periphery of an auger is known, then in accordance with equation (5 - 3), the speed at any radius will be given by

$$N_T = N_T' \left(\frac{r'}{r}\right)^{n+1} \qquad \text{----------(5 - 27)}$$

In particular, the rotational speed of the grain at the core, denoted by N_T'', will be given by

$$N_T'' = N_T' \left[\frac{D}{D_c}\right]^{n+1} \qquad \text{----------(5 - 28)}$$

The usefulness of equation (5 - 28) in determining the grain speed at the core for a given vortex velocity distribution depends on knowing the rotational speed of the grain at the outer periphery. A general expression for the rotational speed N_T'' for vertical augers of the same geometrical proportions as those of the model can be found from

FIG. 46.

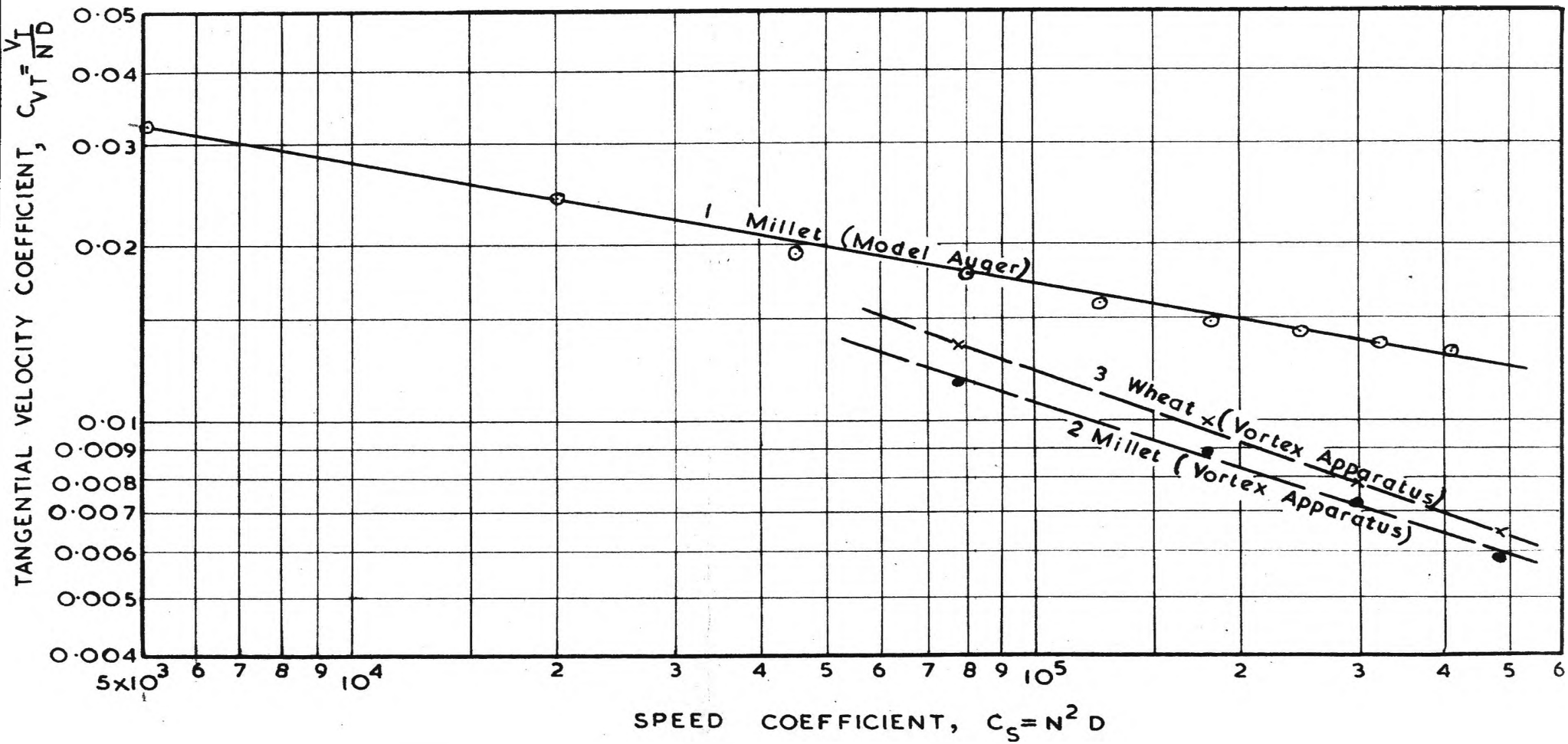

FIG. 46. TANGENTIAL VELOCITY COEFFICIENT VERSUS SPEED COEFFICIENT

the experimental data of Section 3.2; in this section the various grain velocities at the outer periphery were found with the aid of velocity diagrams. The tangential velocity of the grain V_T' is of particular importance, but in order that the experimental data can be applied to geometrically similar augers, it is necessary to introduce another dimensionless parameter.

In accordance with Section 4.1, the tangential velocity parameter will be given by $\frac{V_T'}{N\ D}$. It will be referred to as the tangential velocity coefficient and denoted by C_{VT}.

$$\text{i.e.} \quad C_{VT} = \frac{V_T'}{N\ D} \qquad \text{----------(5 - 29)}$$

A plot of C_{VT} versus the speed coefficient C_S is shown in Fig. 46; in this case a logarithmic plot is used since the graphs may be approximated by straight lines. Graph (1) (shown as full line) is based on the model auger test data while graphs (2) and (3) (shown as dotted lines) are based on the rotational speeds of the millet and wheat determined in the tests on the special vortex apparatus. There is shown to be an appreciable difference between graph (1) and graphs (2) and (3), particularly at the higher C_S values; the difference is less marked at the lower C_S values. The reason for this is not known, although it is suspected that the vortex apparatus not being exactly equivalent to an actual auger may have had some influence.

An equation for the grain speed can be obtained, the form of the equation being

$$\frac{C_{VT}}{C_{VT1}} = \left[\frac{C_S}{C_{S1}}\right]^{-b}$$

This may be written as

$$C_{VT} = \left(\frac{C_S}{a}\right)^{-b} \qquad \text{----------(5 - 30)}$$

where b is the slope of the graph

and $a = \left[C_{VT1} \ (C_{S1})^b\right]^{-1}$ is a constant,

C_{VT1} and C_{S1} being co-ordinates of a point on the graph.

Substituting for C_{VT} and C_S in (5 - 30)

$$\frac{V_T'}{N \ D} = \left(\frac{N^2 \ D}{a}\right)^{-b}$$

which reduces to

$$V_T' = \frac{N^{1-2b} \ D^{1-b}}{a} \qquad \text{----------(5 - 31)}$$

The rotational speed at the outer periphery will be given by

$$N_T' = \frac{60}{\pi \ a} \left[\frac{N^{1-2b}}{D^b}\right] \qquad \text{----------(5 - 32)}$$

The experimentally obtained constants which suit the data of Graph (1) Fig. 46 are:

$$b = 0.2$$

$$a = 6$$

(Although these constants are based on a choke length to screw pitch ratio $^1c/p = 2.0$ and a clearance ratio $C/D = 0.0104$, they may be applied to other ratios without

serious error. The constants are restricted, however, to one-to-one screw pitch to screw diameter ratio).

Substituting for N_T' from equation (5 - 32) into equation (5 - 28), the following general expression for the grain speed at the core is obtained:-

$$N_T'' = \frac{60}{\pi a} \left[\frac{N^{1-2b}}{D^b} \right] \left[\frac{D}{D_c} \right]^{n+1} \qquad \text{----------(5 - 33)}$$

Reverse flow or leakage back of grain at the core will take place when N_T'' is greater than the auger speed N. Slipping will cease when N_T'' equals the critical auger speed N_C. This condition is illustrated in Fig. 47 where the grain speed graph intersects the auger speed line at the core radius.

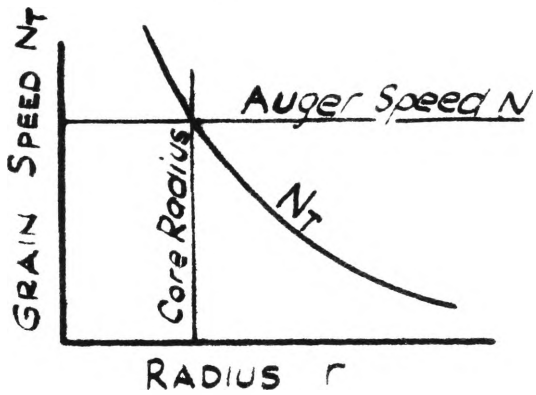

FIG. 47.

An expression for the critical speed of a vertical auger can be found by substituting $N_T'' = N_C$ and $N = N_C$ in equation (5 - 33)

$$N_C = \left[\frac{60}{\pi a} \frac{1}{D^b} \left(\frac{D}{D_c} \right)^{n+1} \right]^{\frac{1}{2b}} \qquad \text{----------(5 - 34)}$$

FIG. 48.

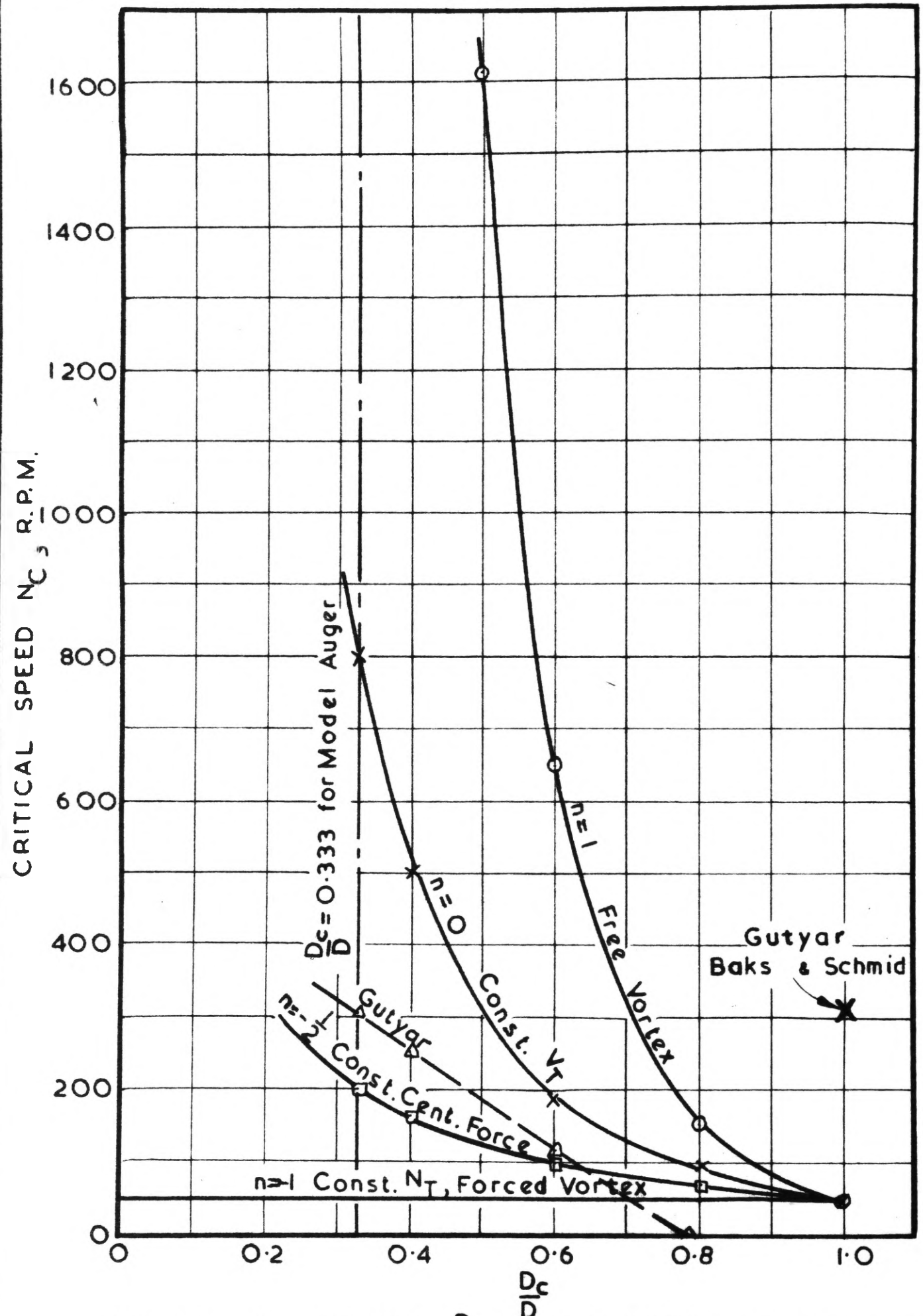

FIG. 48. N_C VERSUS $\frac{D_c}{D}$ FOR VARIOUS VALUES OF n
$D = \frac{1}{8}$ FT; $\alpha = 90°$; $p = D$.

(b) General Discussion.

Equation (5 - 34), which is based on the combination of experimental and theoretical data, enables the critical speed of an auger of given diameter D and D_c/D ratio to be determined for a particular vortex velocity distribution. Although the experimental work on the model auger has been confined to the ratio $D_c/D = 1/3$, it may be assumed that this equation will apply also to other D_c/D ratios; this is a reasonable assumption considering the method by which the equation was developed. However, the experimentally obtained constants will restrict the use of the equation to the one-to-one screw pitch to screw diameter ratio.

The application of equation (5 - 34) depends on a knowledge of the vortex velocity distribution, that is, on the index n. While the vortex motion of the grain tested in the special vortex apparatus was shown to approximate that of a free vortex for which $n = 1$, as previously discussed, it is suspected that this particular motion may be only approximated in an actual auger running partially full; it is probable that, for most cases, n will be less than one. Fig. 48 illustrates the variation of the critical speed N_c with D_c/D ratio for various values of n; the rapid increase of N_c at the lower D_c/D ratios for the larger values of n is clearly shown. The critical speeds plotted in Fig. 48 are for the model auger for which $D = 0.125$ ft; the application of equation (4 - 6) will permit the corresponding critical speeds for various size augers to be determined.

The slipping of grain at the outer screw periphery has been examined in the theoretical analyses given by Gutyar (29) and Baks and

Schmid (31). These workers considered the equilibrium of the forces acting on a single grain particle on the surface of the screw at the outer periphery in contact with the casing as shown in Fig. 49

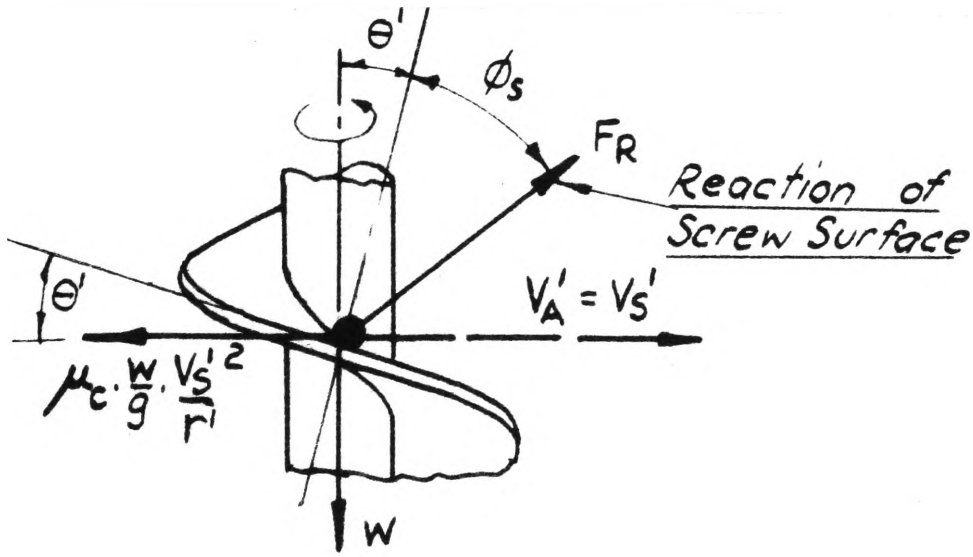

FIG. 49.

The following equation for the critical auger speed at which slip just ceases was derived:-

$$N_C' = \frac{30}{\pi}\sqrt{\frac{2\,g\,\tan(\theta' + \phi_s)}{\mu_c\,D}} \qquad \text{----------(5 - 35)}$$

(In this case the absolute velocity V_A' is horizontal and equals the screw velocity V_S'. The frictional resistive force of the casing equals $\mu_c \frac{w}{g} \frac{V_S'^2}{r'}$ and is horizontal in a direction opposing V_A' as shown).

Assuming $\mu_s = \mu_c = 0.4$, then the critical speed at the outer periphery for the model auger calculated from equation (5 - 35) is $N_C' = 314$ r.p.m. For model auger, $\theta' = 17^\circ 39'$. This speed, indicated by the point X in Fig. 48, is much higher than the speed of

approximately 50 r.p.m. determined in the present investigation. While equation (5 - 35) may hold for a single grain particle, it does not hold for a mass of grain passing through an auger; for a mass of grain, slipping is reduced by the full immersion of the choke in the grain pile, as previously discussed.

Gutyar also examined the slipping back of grain in the central region of the screw near the core. He considered the equilibrium of the forces acting on a single grain particle on the surface of the screw and rotating with it, the particle being held by centrifugal force against a rim attached to the screw as shown in Fig. 50.

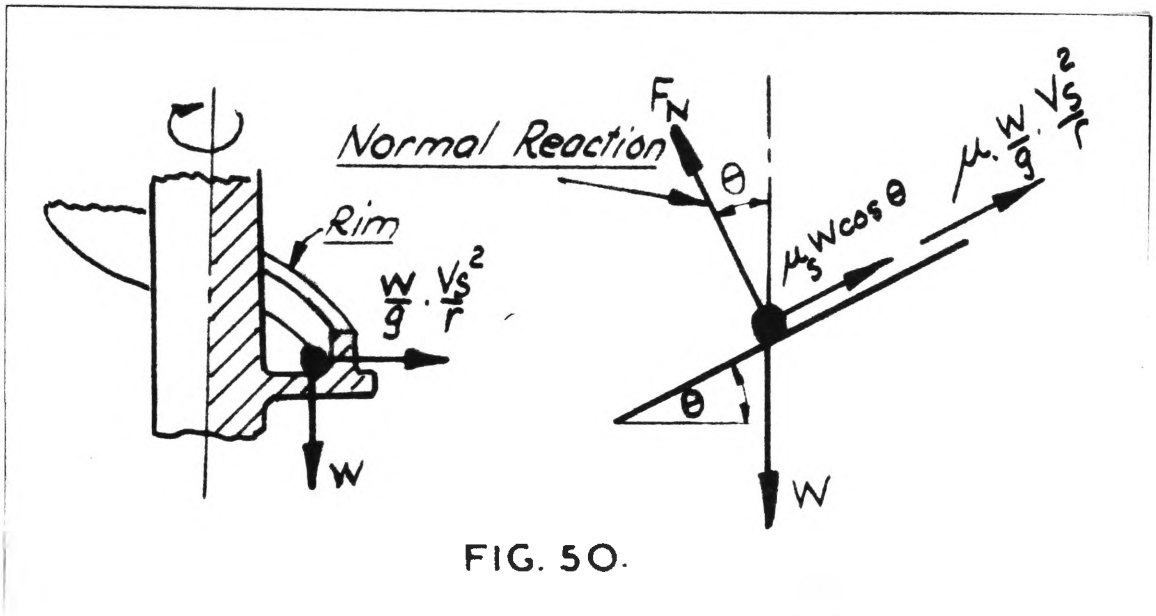

FIG. 50.

Gutyar postulated that the critical speed of an auger would correspond to the equilibrium of a grain particle pressed against a rim of inside diameter approximately equal to the core diameter of the screw. The following equation for this condition was derived:-

$$N_c = \frac{30}{\pi} \sqrt{\frac{2g}{\mu D_c} \left[\sin\theta'' - \mu_s \cos\theta'' \right]} \qquad \text{------(5 - 36)}$$

Here μ is the coefficient of friction between the grain and the rim. In applying equation (5 - 36) to actual augers, μ will be equal to the grain-on-grain friction.

Values of N_c for the model auger have been determined from equation (5 - 36) and are shown plotted as a dotted line in Fig. 48. For the computations, it has been assumed that $\mu_s = 0.4$ and $\mu = \tan^{-1} 31^\circ = 0.6$ ($\phi = 31^\circ$ for millet).

Equation (5 - 36) does not give a true indication of the critical auger speed, since it neglects the effects of the velocity gradient from the outside of the screw to the core. According to this equation, the critical speed will equal zero when $\tan \theta'' = \mu_s$, that is when $\theta'' = \phi_s$; for the one-to-one screw pitch to screw diameter ratio, this corresponds to a D_c/D ratio of 0.795. While this suggests that slipping back is not possible for D_c/D ratios higher than 0.795, this fact is contradicted by equation (5 - 35) which gives a finite critical speed corresponding to the outer screw periphery ($D_c/D = 1.0$). This accounts for the discontinuity between the dotted graph of Fig. 48 and the point X.

It would appear, therefore, that equation (5 - 36), in neglecting the velocity gradient of the grain, gives critical speed values lower than the true values. Although the dotted graph of Fig.48 indicates that the index n in the vortex equation lies between $n = -1/2$ and $n = 0$, it is probable that the actual value of n will be closer to the value of $n = 0$, or even higher than this value.

Even though the actual velocity distribution for the grain vortex is not known, the graphs of Fig. 48 clearly emphasise that, from

a performance point of view, particularly in regard to power consumption, low $D_{c/D}$ ratios should be avoided. The graphs indicate that $D_{c/D}$ ratios less than about 0.4 are undesirable; the ratio $D_{c/D} = 0.333$ as adopted in the model auger is certainly the limiting value. Further experimental evidence is necessary to support these findings.

Because the performance of augers is largely influenced by the amount of grain trapped in the choke, it is probable that the adoption of high $D_{c/D}$ ratios would also yield a gain in output by increasing the "fullness" of running owing to more efficient feeding of grain in the choke. Practical and manufacturing considerations will have a bearing on the final $D_{c/D}$ ratio adopted.

SECTION 6

RELATED EXPERIMENTS

FIG. 51.

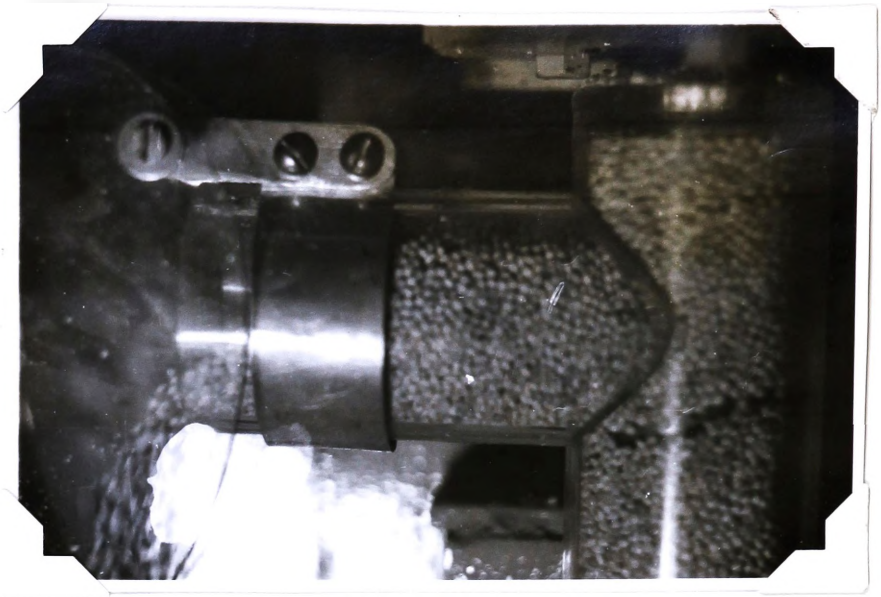

(a) $\alpha = 90°$, N = 200 R.P.M.

(b) $\alpha = 75°$, N = 200 R.P.M.

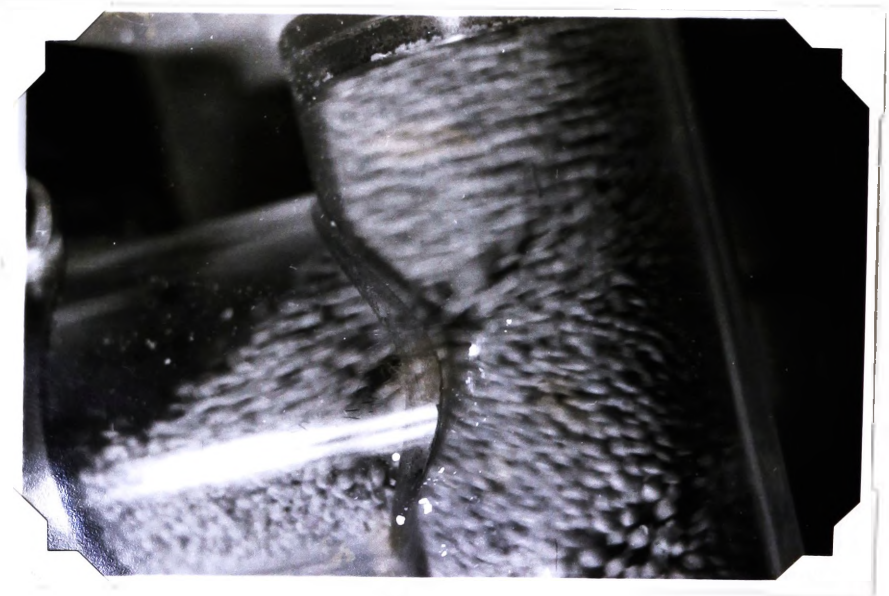

(c) $\alpha = 75°$, N = 700 R.P.M.

FIG. 51. CONVENTIONAL DISCHARGE CHUTE.

6.1 COMPARISON OF POWER CONSUMPTIONS FOR TWO TYPES OF DISCHARGE CHUTE AND TWO TYPES OF GRAIN.

In the preliminary experiments conducted on the model auger apparatus (33), a casing was used having a conventional type discharge chute leading off perpendicularly to the casing axis. It was found that the power consumptions at the higher angles of elevation were rather excessive owing to grain compaction occurring in the top of the casing. This is illustrated in Figs. 51(a),(b) and (c); the compaction occurred at all speeds for the auger at 90° and at the higher speeds for the auger at 75°.

With a view to reducing this compaction, a special type of discharge chute was constructed. This chute, shown diagrammatically in Fig. 52 allows the grain to be discharged radially from the casing without restriction. (A photograph of the actual radial discharge chute was given in Fig. 3, page 9 .)

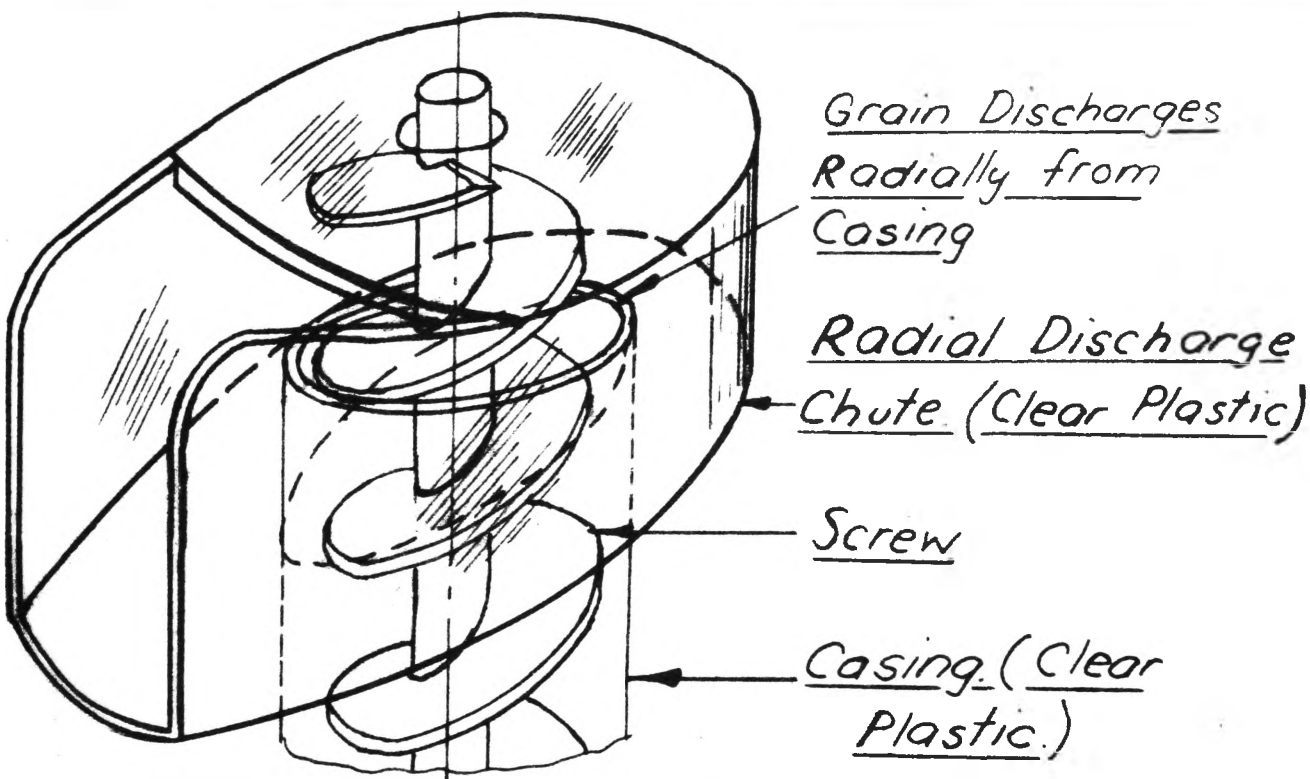

FIG. 52. RADIAL DISCHARGE CHUTE

FIG. 53.

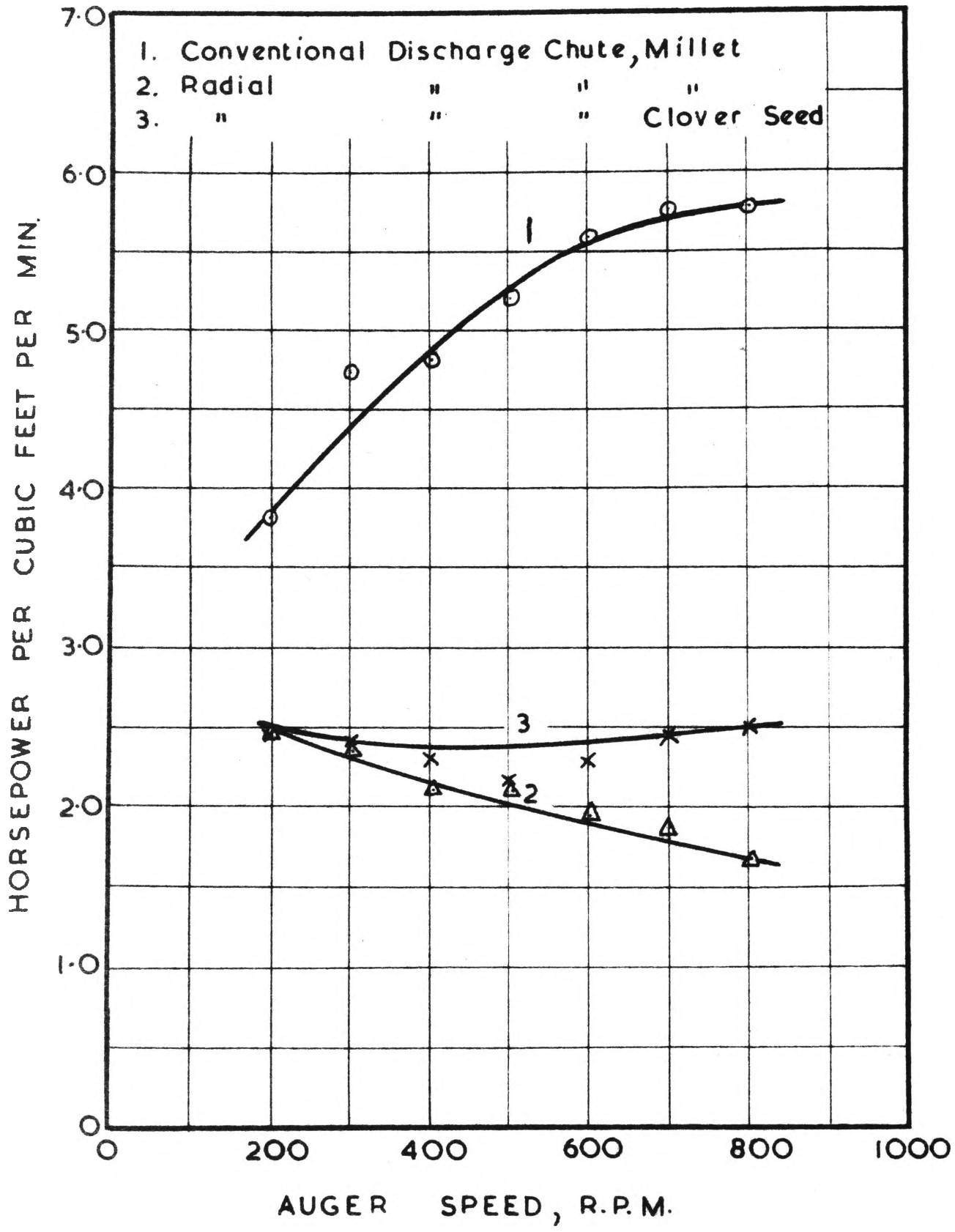

FIG. 53. COMPARISON OF HORSEPOWERS PER UNIT OUTPUT.

Tests were conducted on the auger in the vertical position to show the reduction in power achieved by using the radial discharge chute. The comparative results, given in Table 1, page 76, are shown plotted in Fig. 53. In these tests the main comparison is between graphs 1 and 2 which are for polished millet seed. (This particular millet seed was slightly larger than the Japanese millet used in the main work on the model auger). Graph 3 is for clover seed which is approximately one third the size of the millet.

Referring to Table 1 it can be seen that the output results for the conventional discharge chute (column 1) are slightly in excess of those for the radial discharge chute (column 2). The reason for this is not known; it may be a spurious effect although it is possible that the grain compaction may have had some influence on the higher output. The lower output results for the clover seed (column 3) compared with those for the millet (column 2) are mainly due to leakage in the clearance space. Because of these differing results, the comparisons made in Fig. 53 are based on the horsepower per unit output.

The rising characteristic of graph 1 shows how the compaction effect becomes worse as the speed increases. However, this effect is somewhat exaggerated here since the auger flight extended above the discharge chute opening (Fig.5(b)); in many augers the helical flight terminates at the centre line of the discharge chute which would make the compaction effect less marked. The reduction in power by using the radial discharge chute is quite appreciable, ranging from approximately 35 per cent at 200 r.p.m. to approximately 66 per cent at 800 r.p.m.

Comparing graphs 2 and 3 for the two grain sizes it can be seen that the power requirements are not greatly different. The slightly higher power consumption for the smaller grain is to be expected because of greater leakage in the clearance space.

TABLE 1. COMPARATIVE RESULTS FROM TESTS CONDUCTED ON AUGER IN VERTICAL POSITION.

Speed R.P.M.	Output Cubic Feet/Min.			Horsepower x 10^{-3}			Horsepower per unit Output H.P./Cub.Ft/Min. x 10^{-2}		
	(1)	(2)	(3)	(1)	(2)	(3)	(1)	(2)	(3)
200	0.107	0.073	0.063	4.07	1.79	1.52	3.80	2.45	2.41
300	0.169	0.130	0.103	7.98	3.03	2.48	4.72	2.33	2.40
400	0.234	0.200	0.152	11.22	4.19	3.46	4.80	2.09	2.28
500	0.306	0.257	0.205	15.85	5.38	4.40	5.18	2.09	2.15
600	0.369	0.319	0.248	20.5	6.22	5.66	5.56	1.95	2.28
700	0.438	0.374	0.292	25.20	6.96	7.14	5.74	1.86	2.45
800	0.502	0.432	0.335	28.90	8.38	8.38	5.76	1.67	2.50

(1) Conventional Discharge Chute, Polished Millet Seed

(2) Radial Discharge Chute, Polished Millet Seed

(3) Radial Discharge Chute, Clover seed.

Note: For all cases the radial casing clearance is 1/8 in. and the choke length is 3 in.

FIG. 55.

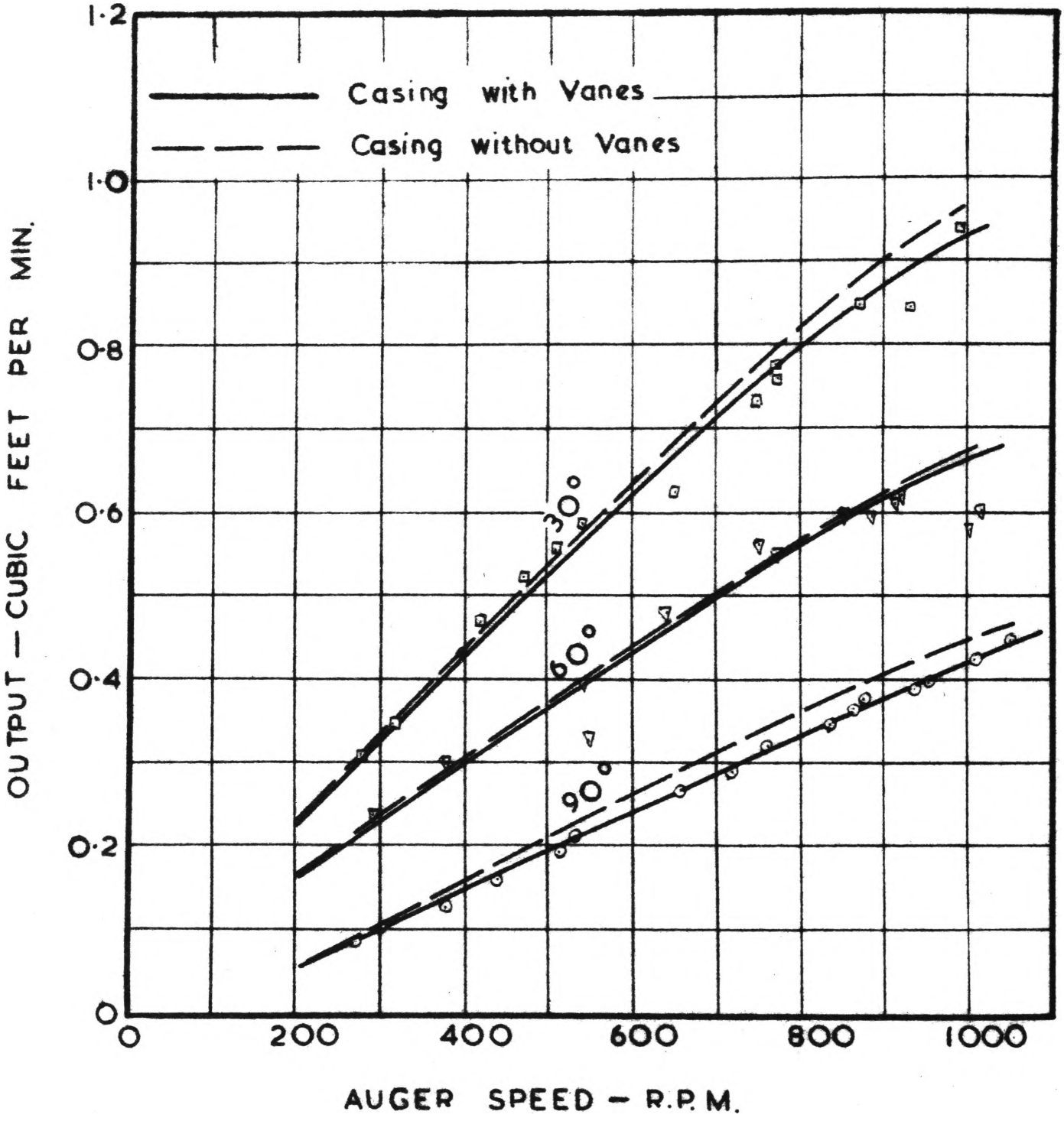

FIG. 55. COMPARISON OF OUTPUTS FOR AUGER CASINGS WITH AND WITHOUT VANES.

Choke Length: 3 inches Radial Clearance: $\frac{1}{8}$ inch

6.2 TEST CONDUCTED ON MODEL AUGER FITTED WITH CASING HAVING LONGITUDINAL VANES.

With a view to improving the output of an auger, a test was conducted using a special casing fitted with four longitudinal vanes. The vanes were equally spaced as shown in Fig. 54 and projected into the clearance space between the screw and the casing. The casing was of clear plastic and had a radial clearance of 1/8 in. (C/D = 0.0833); the clearance between the screw and the vanes was just sufficient to permit the screw to rotate freely.

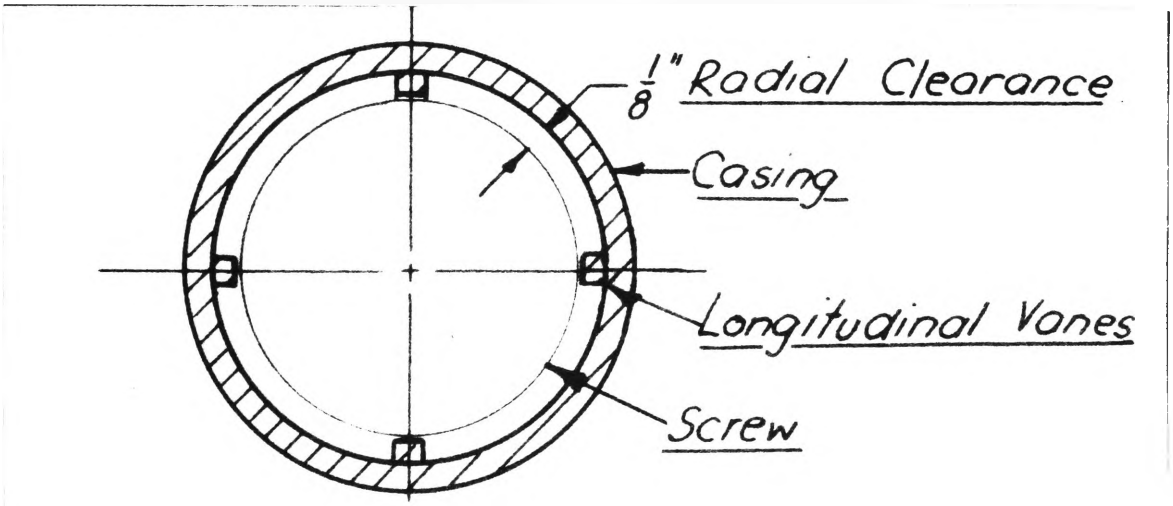

FIG. 54. SPECIAL CASING.

Output measurements conveying millet seed were obtained for the 30°, 60° and 90° angles of elevation for the speed range 200 to 1000 r.p.m. The results (tabulated in Appendix VII) are shown plotted as full lines in Fig. 55. For comparison purposes, the output results for the auger casing having the same radial clearance but without vanes are shown plotted as dotted lines in Fig. 55; this was one of the two casings used in the main work of the investigation.

It can be seen that the casing with vanes yielded a slightly

lower output than the plain casing. Observation showed that the vanes arrested the rotation of the outer grain particles, but this was offset by a greater leakage back in the clearance space. Since the vanes slightly reduced the potential carrying capacity, this also contributed to the lower output obtained with this casing.

SECTION 7

CONCLUSIONS, BIBLIOGRAPHY AND EQUATIONS

7.1 SUMMARY OF CONCLUSIONS.

(1) The output of an auger is governed by speed, angle of elevation, choke length and radial casing clearance. Output is shown to increase at a diminishing rate with speed, reaching a maximum and then remaining constant or falling off slightly. Since the motion of the grain is largely influenced by its centrifugal inertia, augers of large diameters attain their maximum output at lower speeds than augers of small diameters. Output also increases with decrease in angle of elevation.

Choke length has a marked effect on output. While a choke length of one pitch is sufficient to give the maximum output at very low speeds, much greater choke lengths are necessary at high speeds. Although practical considerations may be the limiting factor, it is desirable that choke lengths less than two pitches should be avoided.

Only two radial casing clearances were investigated in this present work, namely clearances of 1/96th and 1/12th of the auger diameter, but the results have shown the advantage of the larger clearance. While little improvement was achieved at the higher angle of elevation, a considerable increase in output was gained at the lower angles of elevation. Further investigation is required to establish the optimum casing clearance.

(2) The volumetric efficiency of steeply inclined augers is generally quite low, this being attributed to the auger running only partially full and the high rotational motion of the grain. Although the one-to-one screw pitch to screw diameter ratio as used in this investigation has been shown by other workers to produce the maximum

outputs of augers at low angles of elevation, further work is necessary to establish whether or not this ratio yields the highest volumetric efficiency for the higher angles of elevation.

(3) For an auger of given length, the power for conveying grain increases almost uniformly with speed, the maximum powers occurring in the range 30° to 45°. The low overall efficiencies indicate that this type of conveyor requires quite large power consumptions to elevate grain. The highest overall efficiencies obtained are in the range 18 to 24 per cent occurring at the steeper angles of elevation.

(4) Based on dimensional analysis and dynamic similarity, equations have been obtained and design charts prepared for predicting the performance of augers of the same geometrical proportions as the model. These data apply mainly to granular materials of similar shape and properties to wheat. While the predicted performance data have been compared with performance data of actual augers showing good agreement, further verification of the performance data, particularly with large size augers is necessary. However, it is expected that the predicted performance data will be satisfactory for estimation purposes.

Further work is necessary to extend the design equations with correction factors to allow their application to widely differing granular materials.

(5) The predicted performance data presented in this work shows that there are many combinations of auger size, speed and angle of elevation that may be adopted for a particular conveying application. For high rates of output, large diameters and/or low angles of elevation

are necessary. Where economical operation is desired and rate of output is unimportant, augers operating at steep angles of elevation may be preferred; in such cases the auger length is kept to a minimum and the power requirements are moderate. In all cases the maximum economical speed of the auger should not be exceeded.

(6) A study of the vortex motion of grain in vertical augers has been conducted with the aid of a special apparatus designed to simulate the rotary motion of grain on an auger flight. An approximate theoretical analysis based on the vortex motion of fluids was given, and this was shown to give good agreement with the experimentally obtained results. The findings of this investigation showed that the vortex profile for the given quantity of grain tested approximated that of a free vortex. For this motion the tangential velocity is inversely proportional to the radius. However, the nature of the tests conducted suggests that these findings may only apply to an auger running partially full when the vortex is not restricted by the limited space between each successive screw pitch.

(7) As a result of the vortex motion in vertical or steeply inclined augers, reverse flow or slipping back of the grain in the central region of the screw can occur at the lower auger speeds. Because of this, the ratio of the core diameter to the screw diameter, D_c/D, is shown to have an important bearing on auger output and power consumption. A general equation has been developed for the critical auger speed at which slipping at the core ceases; for a given vortex velocity distribution, the critical speed decreases both with increase in auger diameter, D, and increase in the D_c/D ratio. Although the actual velocity

distribution for the grain vortex is not known, the results emphasise that low D_c/D ratios should be avoided. While further experimental examination of various D_c/D ratios is necessary, the present findings indicate that D_c/D ratios less than about 0.4 are undesirable. Practical and manufacturing considerations will have a bearing on the final ratio adopted.

(8) It was found that in using a conventional type discharge chute leading off perpendicularly to the casing, grain compaction occurred in the top of the casing at the steeper angles of elevation, particularly at high speed. By using a special radial discharge chute which allowed unrestricted discharge of the grain, the compaction was eliminated and the power substantially reduced; the reduction ranged from approximately 35 per cent at 2000 r.p.m. to approximately 66 per cent at 800 r.p.m.

(9) Tests have been conducted with a special casing fitted with four longitudinal vanes which projected into the clearance space between the screw and the casing. The aim of these tests was to reduce the grain rotational motion with a view to increasing the output. No improvement was achieved; the vanes arrested the rotation of the outer grain particles but this was offset by a greater leakage back in the clearance space.

7.2 BIBLIOGRAPHY

(1) Donaldson, A.C. "Discharge Tests on an Archimedean Screw" Proceedings - Institution of Mechanical Engineers, 1947, V157 page 93-99.

(2) Addison, H. "Experiments on an Archimedean Screw." The Institution of Civil Engineers. Selected Engineering Papers. No. 75, 1929.

(3) Owen, J.H. "Power Absorption in Screw Conveyors." Engineering, Lond. V142, No. 3687, 11th Sept., 1936. page 291-2.

(4) Bergmann, R.F. "Rational Method of Selecting Screw Conveyors." Chem. and Met. Engr. V41, No. 9. Sept. 1934, page 470-2.

(5) "Easy Way to Estimate Screw Conveyor Power Needs." Mill and Factory V51, No. 4. Oct. 1952, page 132.

(6) Hudson, W.G. "Conveyors and Related Equipment." John Wiley and Sons, New York. 2nd Ed.

(7) Atherton, W.H. "Conveyor Comparisons, Spiral, Screw or Worm Conveyor." Mechanical Handling. Aug. 1941. V28 page 189-93.

(8) McGuire, W.B. "Modern Materials Handling." April, 1954, V9, N4 page 79.

(9) "Screw Conveyors and Screw Feeders." Book 2289. Link Belt Company.

(10) Carley, J.F. and Strub, R.A. "Basic Concepts of Extrusion" Ind. Eng. Chem. Vol. 45, No. 5. May, 1953 page 970.

(11) Carley, J.F. Mallouk, R.S. and McKelvey, J.M. "Simplified Flow Theory for Screw Extruders." Ind. Eng. Chem. Vol.45 No. 5. May 1953 page 975

(12) Carley J.F. and Strub R.A. "Application of Theory to Design of Screw Extruders." Ind. Eng. Chem. Vol.45 No. 5. May 1953. page 975.

(13) McKelvey, J.M. "Experimental Studies of Melt Extrusion." Ind. Eng. Chem. Vol.45 No. 5. May 1953. page 982.

(14) Mallouk, R.S. and McKelvey, J.M. "Power Requirements of Melt Extruders." Ind. Eng. Chem. Vol. 45. No. 5. May 1953. page 987.

(15) Carley, J.F. and McKelvey, J.M. "Extruder Scale-Up Theory and Experiments." Ind. Eng. Chem. Vol.45. No. 5. May 1953. page 989.

(16) Jepson, C.H. "Future Extrusion Studies." Ind. Eng. Chem. Vol. 45 No. 5. May 1953. page 992

(17) Mohr, W.D. Saxton, R.L. and Jepson, C.H. "Theory of Mixing in the Single-Screw Extruder." Ind. Eng. Chem. Vol. 49. No. 11 November 1957. page 1857

(18) Mohr, W.D. and Mallouk R.S. "Flow, Power Requirements and Pressure Distribution of Fluid in a Screw Extruder." Ind. Eng. Chem. Vol. 51 No. 6. June 1959. page 765.

(19) Peart, M. "Vertical Augers for a Silo Unloader." Bulletin No. 631, June 1958. University of Illinois.

(20) Millier, W.F. "Bucket Elevators - Auger Conveyors." Agricultural Engineering, Sept. 1958. page 552.

(21) Regan, W.M. and Henderson, S.M. "Performance Characteristics of Inclined Screw Conveyors." Agricultural Engineering, Aug. 1959. page 450.

(22) Rehkugler, G.E. "Performance of Auger Conveyors for Handling Grains and Ground Feeds." Agric. Eng. Extension Bulletin 325. Dept. of Agric. Eng. New York State College of Agriculture. Cornell University, Ithaca, New York.

(23) Rehkugler, G.E. "Performance Characteristics of Farm Type Auger Elevators." Paper presented to the meeting of the North Atlantic Section A.S.A.E. Sept. 1-3. 1959.

(24) Morin, I.V. "O proizvoditelnosti shneka." Selkhozmashina. 1956 (11) 19-24.

(25) Morin, I.V. "O konstruktsii vinta shneka dlya kombaiov." Selkhozmashina. 1954, No. 9.

(26) Drozdov, N.I. "Issledovanie elevatorov i shnekov kombainov." Selkhozmashina. 1948, No. 4.

(27) Anakin, I.A. "Analiz rabochego protsessa shnekov kombaina." Selkhozmashina. 1953. No. 5.

(28) Zaika, P.M. "O vybore parametrov vintovykh transporterov zernovykh kombainov." Trakt i Selkn Mash, 1958 (1) 22.

(29) Gutyar, E.M. Elementarnaya teoriya vertikalnovo vintovovo transportera." Trudy Mosk. Inst. Mekh. i Elekt. Selsk. Khoz. im. V.M. Molotov, 1956, (2) 102-122.

(30) Thüsing, H. "Die Förerschnecke als stetiger Senkrechtförderer für Schütt - und Stückgut." Fördern und Heben 1958, Vol. 5. 302-303.

(31) Baks, A. and Schmid, W.L. "Verticaal transport met schroeftransporteurs." Orgaan van Het Nederlands Instituut Van Register-Ingenieurs en Afgestudeerden van Hogere Technische Scholen. 4 - 15e Jaarg. Feb. 1960. 169-174.

(32) Cady, J. "Investigation of Model Grain Auger." Unpublished undergraduate thesis, School of Mechanical Engineering, The New South Wales University of Technology.

(33) Roberts, A.W. "An Investigation into the Performance of an Experimental Grain Auger". Unpublished undergraduate thesis, School of Mechanical Engineering, The New South Wales University of Technology.

(34) Cumming, G.H. "Test Bench for Grain Augers" unpublished undergraduate thesis, School of Mechanical Engineering, The University of New South Wales.

(35) Tong, K.S. "Performance of a Commercial Grain Auger". Unpublished undergraduate thesis, School of Mechanical Engineering, The University of New South Wales.

7.3 SUMMARY OF EQUATIONS

The main equations obtained in the investigation are summarised in this section. Where appropriate, the experimentally obtained constants which apply to augers geometrically similar to the model auger are given.

Section 3

$$Q_t = \frac{\pi}{4}\left[(D + 2C)^2 - D_c^2\right]\left[p - t\right] N \qquad \text{------(3 - 1)}$$

or $$Q_t = \gamma N D^3 \qquad \text{----------(3 - 2)}$$

where $\gamma = 0.67$ for $\frac{C}{D} = 0.0104$

$\gamma = 0.90$ for $\frac{C}{D} = 0.0833$

$$V_L = V_S \frac{\sin\theta \cos(\theta + \beta)}{\cos\beta} \qquad \text{----------(3 - 3)}$$

$$V_T = V_S \frac{\sin\theta \sin(\theta + \beta)}{\cos\beta} \qquad \text{----------(3 - 4)}$$

for max V_L, $\theta = 45^\circ - \frac{\phi_s}{2}$ ----------(3 - 5)

for max V_T, $\theta = 90^\circ - \frac{\phi_s}{2}$ ----------(3 - 6)

$$P_t = \frac{Q\,w\,H}{33000} \qquad \text{----------(3 - 7)}$$

Section 4

$$C_Q = \frac{Q}{N D^3} \qquad \text{----------(4 - 3)}$$

$$C_P = \frac{P}{\rho D^5 N^3} \qquad \text{----------(4 - 4)}$$

$$C_S = N^2 D \qquad \text{----------(4 - 5)}$$

$$N_p = N_m \sqrt{\frac{D_m}{D_p}} \qquad \text{----------(4 - 6)}$$

For $\frac{l_c}{p} = 2.0$

$$Q = N D^3 \left[E + G \cos (\alpha + \psi) \right] \left[B - N^2 D \right] \qquad \text{----(4 - 10)}$$

or $$Q = \gamma N D^3 \eta_V \qquad \text{----------(4 - 11)}$$

where $$\eta_V = \frac{\left[E + G \cos (\alpha + \psi) \right] \left[B - N^2 D \right]}{\gamma} \qquad \text{----------(4 - 12)}$$

For equations (4 - 10), (4 - 11) and (4 - 12),

$B = 1.18 \times 10^6$

$E = 3.9 \times 10^{-7}$

$G = 2.57 \times 10^{-7}$

$\psi = 45^\circ$

$\gamma = 0.90 \quad (\frac{C}{D} = 0.0833)$

$$K_c = \left[\frac{N^2 D}{Z} \right]^{\frac{J - (M - \frac{l_c}{p})^3}{R}} \qquad \text{----------(4 - 16)}$$

where $Z = 1300$

$J = 0.042$

$M = 3.67$

$R = 112$

For all $\frac{l_c}{p}$ ratios

$$Q = N D^3 \left[E + G \cos (\alpha + \psi) \right] \left[B - N^2 D \right] K_c \qquad \text{------(4 - 18)}$$

and $$\eta_V = \frac{\left[E + G \cos (\alpha + \psi) \right] \left[B - N^2 D \right] K_c}{\gamma} \qquad \text{------(4 - 19)}$$

$$P = \left[X + Y \sin (2\alpha + \epsilon)\right] w N D^3 L F \qquad \text{-------(4 - 24)}$$

where $X = 3.3 \times 10^{-5}$

$Y = 2.0 \times 10^{-5}$

$\epsilon = 15^{\circ}$

$$\eta_o = \frac{\left[E + G \cos (\alpha + \psi)\right]\left[B - N^2 D\right] \sin\alpha}{\left[X + Y \sin (2\alpha + \epsilon)\right] 33000} \qquad \text{-------(4 - 26)}$$

$$N_{max} = \frac{700}{\sqrt{D}} \qquad \text{--------(4 - 27)}$$

Section 5

$$V_T \; r^n = C_1 \qquad \text{----------(5 - 2)}$$

or $$N_T \; r^{n+1} = C_2 \qquad \text{----------(5 - 3)}$$

$$p_r = \frac{-w C_1^2}{2 n g r^{2n}} + p_o \qquad \text{----------(5 - 5)}$$

$$p_r = \frac{w z}{k} \qquad \text{----------(5 - 12)}$$

where $$k = \frac{1 - \sin \phi}{1 + \sin \phi} \qquad \text{----------(5 - 13)}$$

$$z = -\frac{k C_1^2}{2 n g r^{2n}} + z_o' \qquad \text{----------(5 - 14)}$$

Actual Vortex for millet (for vortex apparatus)

$$z = - \frac{1}{515\, r^{1.8}} + 0.317 \qquad \text{----------(5 - 16)}$$

and $$V_T = \frac{0.593}{r^{0.9}} \qquad \text{----------(5 - 18)}$$

or $$N_T = \frac{5.66}{r^{1.9}} \qquad \text{----------(5 - 19)}$$

Actual vortex for wheat (for vortex apparatus)

$$z = - \frac{1}{140 r^{1.56}} + 0.400 \qquad \text{----------(5 - 17)}$$

and $$V_T = \frac{0.98}{r^{0.78}} \qquad \text{----------(5 - 20)}$$

or $$N_T = \frac{9.36}{r^{1.78}} \qquad \text{----------(5 - 21)}$$

Free vortex equations:-

for millet $$N_T = \frac{5.12}{r^2} \qquad \text{----------(5 - 25)}$$

for wheat $$N_T = \frac{6.05}{r^2} \qquad \text{----------(5 - 26)}$$

$$N_T'' = N_T' \left[\frac{D}{D_c} \right]^{n+1} \qquad \text{----------(5 - 28)}$$

$$C_{VT} = \frac{V_T'}{ND} \qquad \text{----------(5 - 29)}$$

$$N_T' = \frac{60}{\pi a} \left[\frac{N^{1-2b}}{D^b} \right] \qquad \text{----------(5 - 32)}$$

where $b = 0.2$

$a = 6$

$$N_T'' = \frac{60}{\pi a}\left[\frac{N^{1-2b}}{D^b}\right]\left[\frac{D}{D_c}\right]^{n+1} \qquad \text{----------(5 - 33)}$$

$$N_C = \left[\frac{60}{\pi a}\ \frac{1}{D^b}\ \left(\frac{D}{D_c}\right)^{n+1}\right]^{\frac{1}{2}b} \qquad \text{----------(5 - 34)}$$

SECTION 8

APPENDICES

FIGS. 56 &57

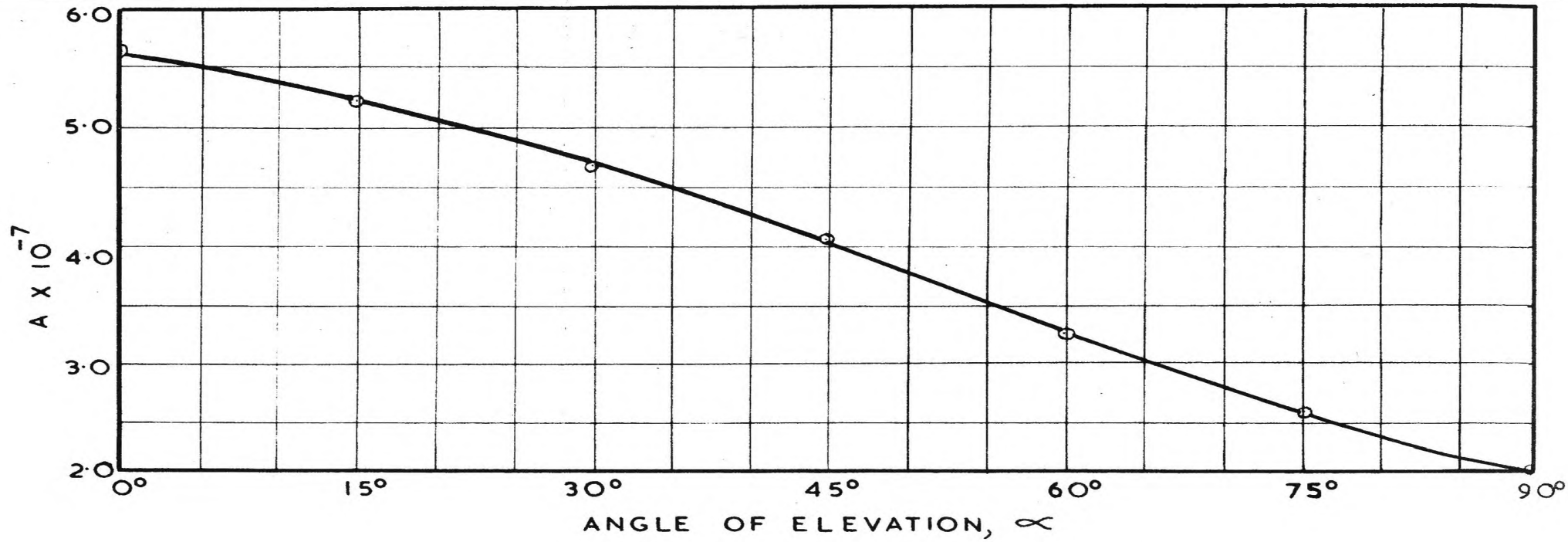

FIG. 56. A VERSUS ∝

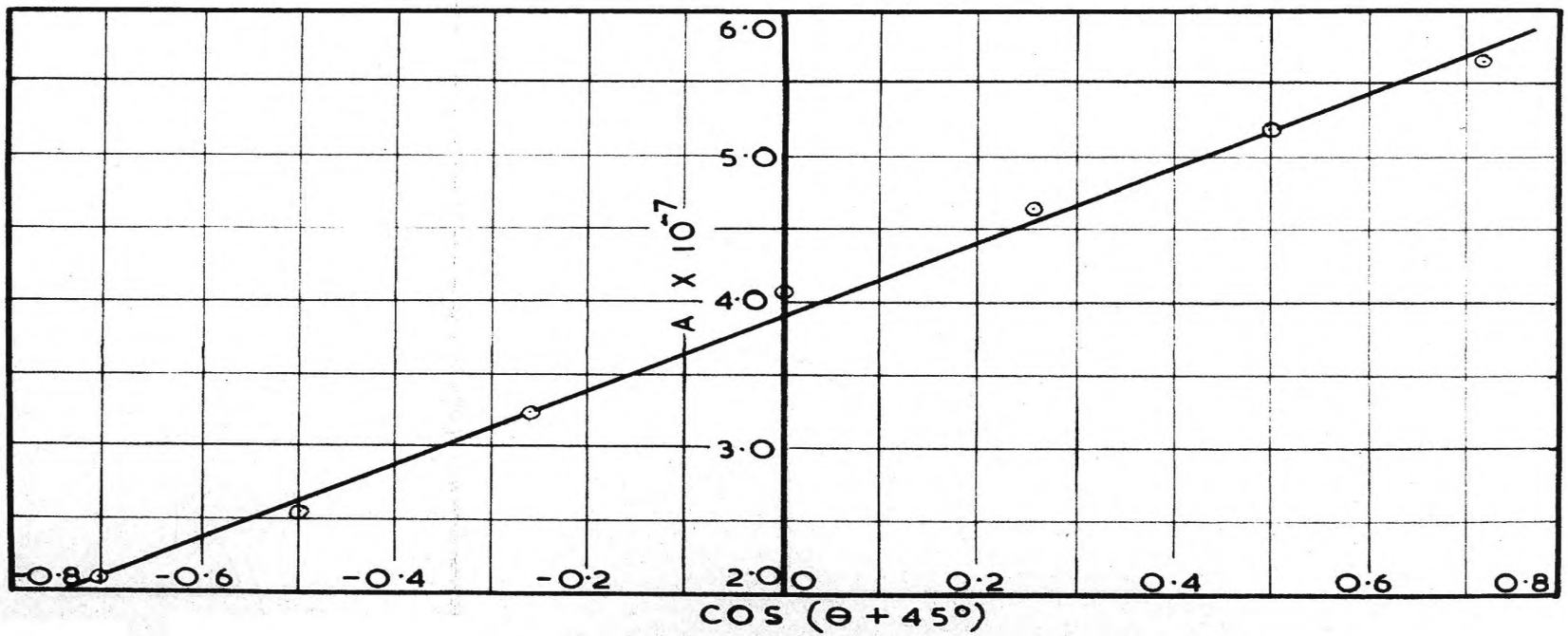

FIG. 57. A VERSUS COS(θ+45°)

APPENDIX I

DEVELOPMENT OF EQUATION (4 - 9)

In the development of the output equation (4 - 10) from the data of the C_Q versus C_S graph of Fig. 28 page 35 , it was necessary to obtain an equation expressing the slope A of each line in terms of the angle of elevation α . The various values of A are summarised in Table 2 and are shown plotted against α in Fig. 56. This graph has the characteristic shape of a cosine curve. An approximate straight line graph is obtained when A is plotted against cos (α + 45°) as shown in Fig. 57. The general equation for A can be now written:-

$$A = E + G \cos (\alpha + \psi) \qquad \text{----------(4 - 9)}$$

where E = intercept on A axis = 3.9×10^{-7}

G = slope of line = 2.57×10^{-7}

and $\psi = 45^\circ$

TABLE 2. DATA FOR DEVELOPMENT OF EQUATION (4 - 9)

Angle of Elevation	Slope A ✻ $\times 10^{-7}$	$(\alpha + 45^\circ)$	$\cos(\alpha + 45^\circ)$
0°	5.66	45°	0.7071
15°	5.20	60°	0.5000
30°	4.67	75°	0.2588
45°	4.07	90°	0.0000
60°	3.22	105°	- 0.2588
75°	2.57	120°	- 0.5000
90°	2.08	135°	- 0.7071

✻ Although the actual slopes of lines in Fig. 28 are negative, this has been accounted for in equation (4 - 7)

FIGS. 58 & 59

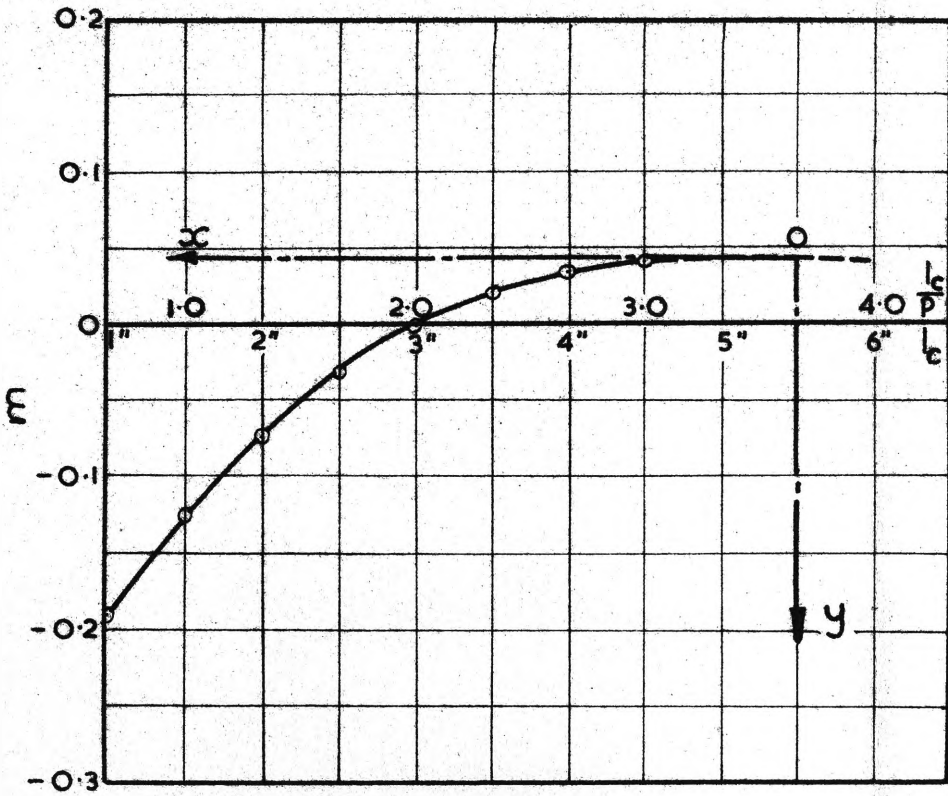

FIG. 58. m VERSUS $\frac{l_c}{p}$

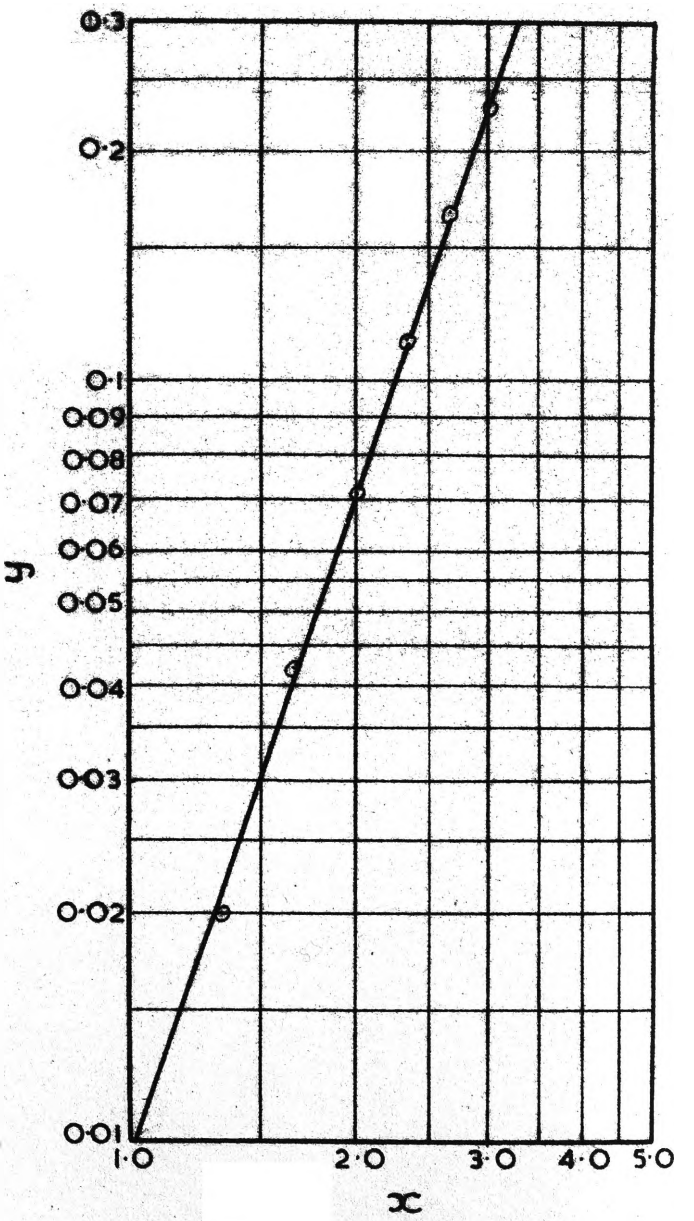

FIG. 59. y VERSUS x

APPENDIX II

DEVELOPMENT OF EQUATION (4 - 15)

In the development of the choke length correction factor equation (4 - 16) from the data of the K_c versus C_S graph of Fig. 30 page 38, it was necessary to obtain an equation expressing the index m in terms of the choke length to screw pitch ratio $\frac{l_c}{p}$.

The various values of m are summarised in Table 3 and are shown plotted against $\frac{l_c}{p}$ in Fig. 58.

To establish an equation for the m versus $\frac{l_c}{p}$ curve, a new set of co-ordinates x and y are assigned with the origin at O as shown; the relationships between x and y and the original co-ordinates m and $\frac{l_c}{p}$ are

$$x = M - \frac{l_c}{p} \qquad \text{-------(i)}$$

$$\text{and } y = J - m \qquad \text{--------(ii)}$$

where M = 3.67

and J = 0.042.

Values of x and y are given in Table 3. When plotted on logarithmic axes, a straight line graph is obtained as shown in Fig. 59. This graph has a slope of 3 indicating a cubic relationship between x and y, and hence, between $\frac{l_c}{p}$ and m. The equation relating x and y is of the form

$$y = \frac{x^3}{R} \qquad \text{----------(iii)}$$

where $R = \frac{y'}{(x')^3}$ x' and y' being co-ordinates of a point on the graph.

Choosing the point for which $x' = 1.67$ and $y' = 0.042$ gives

$$R = 112$$

substituting for x and y from equations (i) and (ii), then

$$m = J - \frac{(M - \frac{l_c}{p})^3}{R} \qquad \text{----------(4 - 15)}$$

TABLE 3. DATA FOR DEVELOPMENT OF EQUATION (4 - 15)

Choke Length l_c ins.	$\frac{l_c}{p}$	Index m	$x = 3.67 - \frac{l_c}{p}$	$y = 0.042 - m$
1.0	0.67	- 0.19	3.0	0.232
1.5	1.0	- 0.126	2.67	0.168
2.0	1.33	- 0.072	2.33	0.114
2.5	1.67	- 0.030	2.0	0.072
3.0	2.0	0.000	1.67	0.042
3.5	2.33	+ 0.022	1.33	0.020
4.0	2.67	+ 0.035	1.0	0.007
4.5	3.0	+ 0.042	0.67	0.000

FIG. 60.

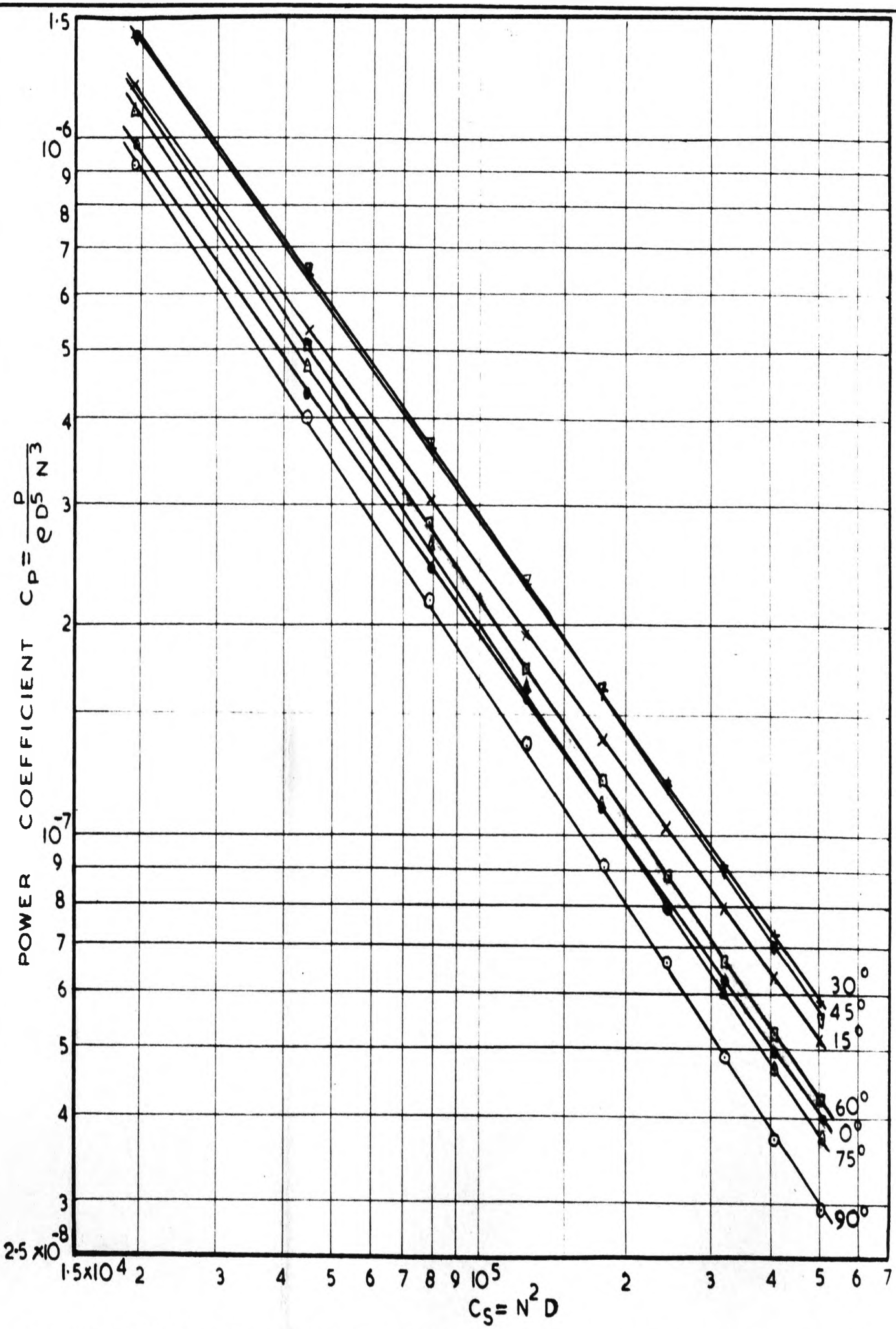

FIG.60 POWER COEFFICIENT VERSUS SPEED COEFFICIENT FOR VARIOUS ANGLES OF ELEVATION

FIGS. 61 &62

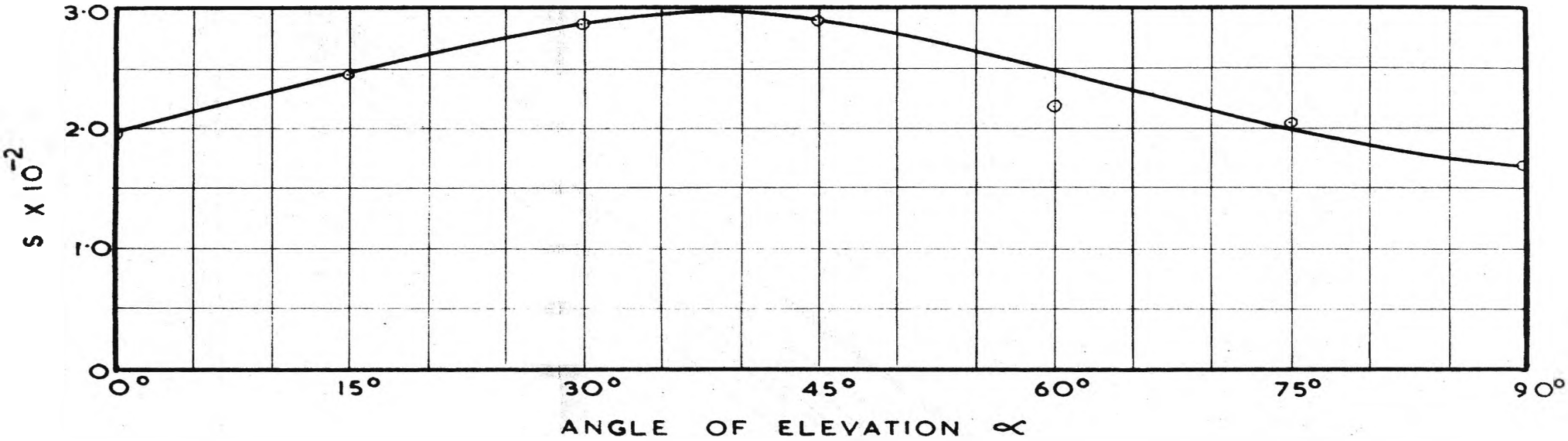

FIG. 61. S VERSUS ∝

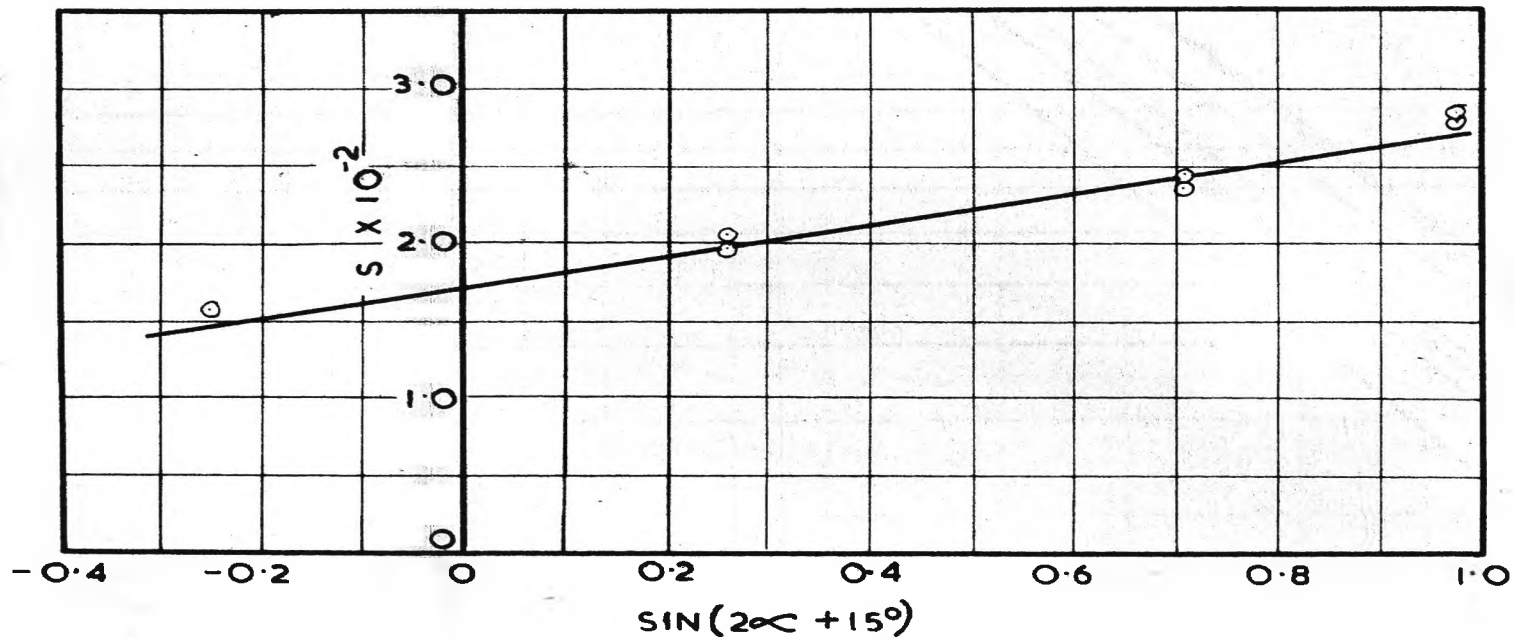

FIG. 62. S VERSUS SIN(2∝ +15°)

APPENDIX III

DEVELOPMENT OF EQUATION (4 - 22)

The graphs of C_P versus C_S on logarithmic axes are shown in Fig. 60; each line has a negative slope of magnitude approximately equal to unity. This indicates that C_P is proportional to $\frac{1}{C_S}$ as is also verified by the straight line C_P versus $\frac{1}{C_S}$ graphs of Fig. 33 page 41.

In the development of the horsepower equation (4 - 23) from the data of the C_P versus $\frac{1}{C_S}$ graphs, it was necessary to obtain an equation expressing the slope S of each line in terms of the angle of elevation α The various values of S are summarised in Table 4 and are shown plotted against α in Fig. 61. This graph has the characteristic shape of a sine curve. An approximate straight line graph is obtained when S is plotted against $\sin (2\alpha + 15^\circ)$ as shown in Fig. 62. The general equation for S can be now written :-

$$S = T + U \sin (2\alpha + \epsilon) \quad \text{----------(4 - 22)}$$

where T = intercept on S axis = 1.7×10^{-2}

U = slope of line = 1.03×10^{-2}

and $\epsilon = 15^\circ$

TABLE 4. DATA FOR DEVELOPMENT OF EQUATION (4 - 22)

Angle of Elevation	Slope S x 10^{-2}	$(2\alpha + 15^{\circ})$	$\sin (2\alpha + 15^{\circ})$
0°	1.96	15°	0.2588
15°	2.40	45°	0.7071
30°	2.80	75°	0.9659
45°	2.85	105°	0.9659
60°	2.32	135°	0.7071
75°	2.04	165°	0.2588
90°	1.60	195°	- 0.2588

APPENDIX IV

GRAIN VELOCITIES FOR OUTER SCREW PERIPHERY FOR 90° ANGLE OF ELEVATION

The various velocities corresponding to the outer periphery of the model auger are summarised in Table 5. These results are associated with the work of Sections 3.2 and 5.2.

Explanation of Derived Results.

(i) Helix Angle of Grain Path (column 4)

Corrected results were read from Fig. 22

(ii) Screw Speed V_S' (column (5))

$$V_S' = \frac{\pi (D + 2C) N}{60} = \frac{N}{149.5} \quad (\frac{C}{D} = 0.0104)\ D = 1/8 \text{ ft.})$$

(iii) Grain Velocities V_T', V_L' and V_{Lt}' (columns (6), (8) and (9))

Obtained from velocity diagrams Fig. 23

(iv) Speed Coefficient C_S (column (11))

Obtained from equation (4 - 5)

$$C_S = N^2 D = \frac{N^2}{8}$$

(v) Tangential Velocity Coefficient C_{VT} (column (12))

Obtained from equation (5 - 29)

$$C_{VT} = \frac{V_T'}{ND} = \frac{8\ V_T'}{N}$$

TABLE 5. VELOCITIES FOR OUTER SCREW PERIPHERY

Angle of Elevation = 90° ($\frac{l_c}{D}$ = 2.0) Material Conveyed: Millet

Experimental Results		Corrected and Derived Results									
Speed R.P.M.	λ Degrees	Speed R.P.M.	λ Degrees	V_S' Ft/Sec.	V_T' Ft/Sec.	$\frac{V_T'}{V_S'}$	V_L' Ft/Sec.	V_{Lt}' Ft/Sec.	$\frac{V_L'}{V_{Lt}'}$	C_S x 10^4	C_{VT} x 10^{-2}
(1)	(2)	(3)	(4)	(5)	(6)	(7)	(8)	(9)	(10)	(11)	(12)
210	13	200	12	1.34	0.80	0.597	0.20	0.44	0.455	0.5	3.20
400	22	400	22	2.68	1.22	0.456	0.50	0.88	0.568	2.0	2.43
500	29	600	29	4.02	1.43	0.356	0.83	1.30	0.615	4.5	1.91
600	31	800	34	5.35	1.70	0.318	1.18	1.73	0.682	8.0	1.70
800	33	1000	37.5	6.68	1.98	0.296	1.52	2.18	0.697	12.5	1.58
900	36	1200	39.5	8.03	2.24	0.279	1.86	2.60	0.715	18.0	1.49
1000	38	1400	42	9.38	2.47	0.263	2.22	3.03	0.733	24.8	1.41
1200	39	1600	43	10.72	2.72	0.253	2.57	3.46	0.743	32.0	1.36
1300	39	1800	44	12.03	3.00	0.249	2.90	3.90	0.750	40.5	1.33
1400	42										
1600	46.5										

APPENDIX V

TEST RESULTS FOR GRAIN VORTEX MOTION INVESTIGATION

The various experimental and derived results for the grain vortex motion investigation described in Section 5 are summarised in Tables 6, 6A, 7 and 7A.

(a) Explanation of Table 6.

This gives the grain velocities measured at the outer periphery and the measured co-ordinates of the vortex profile.

(i) Grain Speed V_T' (column (7))

$$V_T' = \frac{\pi D N_T'}{60}$$

For vortex apparatus $D = 5.75$ in. $= 0.479$ ft.

hence $$V_T' = \frac{N_T'}{39.8}$$

(ii) Speed coefficient C_S (column (8))

Obtained from equation (4 - 5)

$$C_S = N^2 D = 0.479 N^2$$

(iii) Tangential Velocity Coefficient C_{VT} (column (9))

Obtained from equation (5 - 29)

$$C_{VT} = \frac{V_T'}{ND} = \frac{2.09}{N} V_T'$$

(b) Explanation of Table 6A.

This gives the corrected ordinates for the vortex profiles and the rotational speeds of the grain at different radii. These results correspond to the 400 r.p.m. speed of the impeller.

(i) Height z (columns (3) and (8))

Obtained from Fig. 41.

(ii) z" for millet (column (5))

Obtained from z" = 0.317 - z ft.

(iii) z" for wheat (column (10)

Obtained from z" = 0.400 - z ft.

(iv) Rotational speed of millet

Column (6) gives speeds for actual vortex calculated from equation (5 - 19)

$$N_T = \frac{5.66}{r^{1.9}}$$

Column (7) gives speeds for free vortex calculated from equation (5 - 25)

$$N_T = \frac{5.12}{r^2}$$

(v) Rotational speed of wheat

Column (11) gives speeds for actual vortex calculated from equation (5 - 21)

$$N_T = \frac{9.36}{r^{1.78}}$$

Column (12) gives speeds for free vortex calculated from equation (5 - 26)

$$N_T = \frac{6.05}{r^2}$$

(c) Explanation of Table 7.

This gives the critical speeds for the model auger for various $\frac{D_c}{D}$ ratios calculated from equation (5 - 34) and used in

plotting Fig. 48.

Substituting the constants and the model auger diameter in equation (5 - 34) yields

$$N_C = \left[4.82 \left(\frac{D}{D_c} \right)^{n+1} \right]^{2.5}$$

(d) Explanation of Table 7A.

This gives the critical speeds for the model auger for various $\frac{D_c}{D}$ ratios calculated from Gutyar's equation (5 - 36)

$$N_C = \frac{30}{\pi} \sqrt{\frac{2g}{\mu D_c} \left[\sin \theta'' - \mu_s \cos \theta'' \right]}$$

$$\theta'' = \tan^{-1} \frac{D}{\pi D_c} \qquad (p = D = 1/8 \text{ ft.})$$

$$\mu = \tan^{-1} 31^\circ = 0.6$$

$$\mu_s = 0.4$$

TABLE 6. VORTEX MOTION TEST RESULTS - GRAIN VELOCITIES AT OUTER PERIPHERY AND VORTEX PROFILE MEASUREMENTS.

Grain Type	Impeller Speed N R.P.M.	Speed of Grain N_T' at Outer Periphery			$\frac{N_T'}{N}$ %	V_T' Ft/Sec	C_S x 10^4	C_{VT} x 10^{-2}	Vortex Profile ≠ Grain Height Ordinates ϕ/ in inches at the following Radii expressed in inches:-								
		Revs	Secs	R.P.M.					0.75	0.92	1.15	1.42	1.68	1.95	2.20	2.52	2.875
(1)	(2)	(3)	(4)	(5)	(6)	(7)	(8)	(9)	(10)	(11)	(12)	(13)	(14)	(15)	(16)	(17)	(18)
Millet	400	20	13.2	89.3	22.3	2.25	7.7	1.17	0	1.35	2.25	2.73	2.98	3.18	3.38	3.45	3.50
		20	13.7														
	600	20	11.6	103	17.2	2.59	17.3	0.90	0	1.40	2.40	2.78	3.17	3.33	3.50	3.60	3.70
		20	11.7														
	800	20	10.7	112.2	14.0	2.82	30.7	0.734	0	1.40	2.20	2.90	3.28	3.32	3.59	3.70	3.75
		20	10.7														
	1000	20	10.7	112.2	11.2	2.82	48.0	0.586	0	0	1.85	2.90	3.25	3.50	3.62	3.77	3.80
		20	10.7														
Wheat	400	20	11.7	102	25.5	2.57	7.7	1.34	0	-	1.60	2.52	2.80	3.30	3.57	3.93	4.00
		20	11.8														
	600	20	10.5	114.2	19.02	2.87	17.3	1.00	0	-	1.60	2.45	3.18	3.48	3.78	4.08	4.20
		20	10.5														
	800	20	10.0	120	15.0	3.02	30.7	0.785	0	-	1.38	2.70	3.20	3.56	3.86	4.10	4.25
		20	10.0														
	1000	20	9.8	122.5	12.25	3.08	48.0	0.644	0	-	1.38	2.80	3.30	3.58	3.85	4.20	4.30
		20	9.8														

≠ The vortex profiles corresponding to the 400 and 1000 r.p.m. impeller speeds have been plotted in Fig. 41.

ϕ/ In stationary position, level height of grain = 2 inches.

TABLE 6A. DERIVED RESULTS FOR GRAIN VORTEX MOTION CORRESPONDING TO 400 R.P.M. SPEED OF IMPELLER

Radius r		MILLET SEED					WHEAT				
		Height z		z''	Grain Speed		Height z		z''	Grain Speed	
in.	ft.	in.	ft.	ft.	N_T ≠ R.P.M.	N_T ∅ R.P.M.	in.	ft.	ft.	N_T ≠ R.P.M.	N_T ∅ R.P.M.
(1)	(2)	(3)	(4)	(5)	(6)	(7)	(8)	(9)	(10)	(11)	(12)
0.75	0.0625	0.47	.039	0.278			–	–	–		
1.0	0.0833	1.70	0.142	0.175	637	667	0.80	0.067	0.333	788	875
1.25	0.1042	2.45	0.204	0.113			1.80	0.150	0.250		
1.5	0.125	2.81	0.234	0.083	295	330	2.47	0.206	0.194	375	390
1.75	0.146	3.08	0.257	0.060			2.93	0.244	0.156		
2.0	0.167	3.21	0.268	0.049	171	186	3.30	0.275	0.125	226	218
2.25	0.188	3.35	0.279	0.038			3.60	0.300	0.100		
2.5	0.209	3.42	0.285	0.032	111	118	3.82	0.318	0.082	152	139
2.75	0.229	3.46	0.289	0.028			3.96	0.330	0.070		
2.875	0.240	3.50	0.292	0.025	86	89	4.0	0.333	0.067	119	105

≠ For actual Vortex ∅ For free Vortex

TABLE 7. VALUES CALCULATED FROM EQUATION (5 - 34)

$\frac{D_c}{D}$	$\frac{D}{D_c}$	$\left(\frac{D}{D_c}\right)^{n+1}$				N_C			
		n = 1	n = 0	n = $-\frac{1}{2}$	n = -1	n = 1	n = 0	n = $-\frac{1}{2}$	n = -1
0.33	3	9	3	1.732	1	12200	800	200	51
0.4	2.5	6.25	2.5	1.585	1	5000	500	162	51
0.6	1.667	2.77	1.667	1.292	1	650	183	98	51
0.8	1.25	1.563	1.25	1.12	1	155	89	68	51
1.0	1.0	1.0	1.0	1.0	1	51	51	51	51

TABLE 7A VALUES CALCULATED FROM EQUATION (5 - 36)

$\frac{D_c}{D}$	D_c ft.	Tan θ''	θ''	Sin θ''	$\mu_s \cos \theta''$	N_C
0.33	0.0417	0.956	43° 43'	0.6911	0.289	308
0.4	0.05	0.797	38° 33'	0.6232	0.313	247
0.6	0.0752	0.236	27° 57'	0.4687	0.353	123

$\frac{D_c}{D}$ Ratio for $N_C = 0$:-

For this case

$$\sin \theta'' = \mu_s \cos \theta''$$

$$\tan \theta'' = \mu_s = 0.4$$

but $\tan \theta'' = \frac{D}{\pi D_c}$ (for p = D)

$$\therefore \quad \frac{D_c}{D} = \frac{1}{0.4 \times \pi} = 0.795$$

FIG.63.

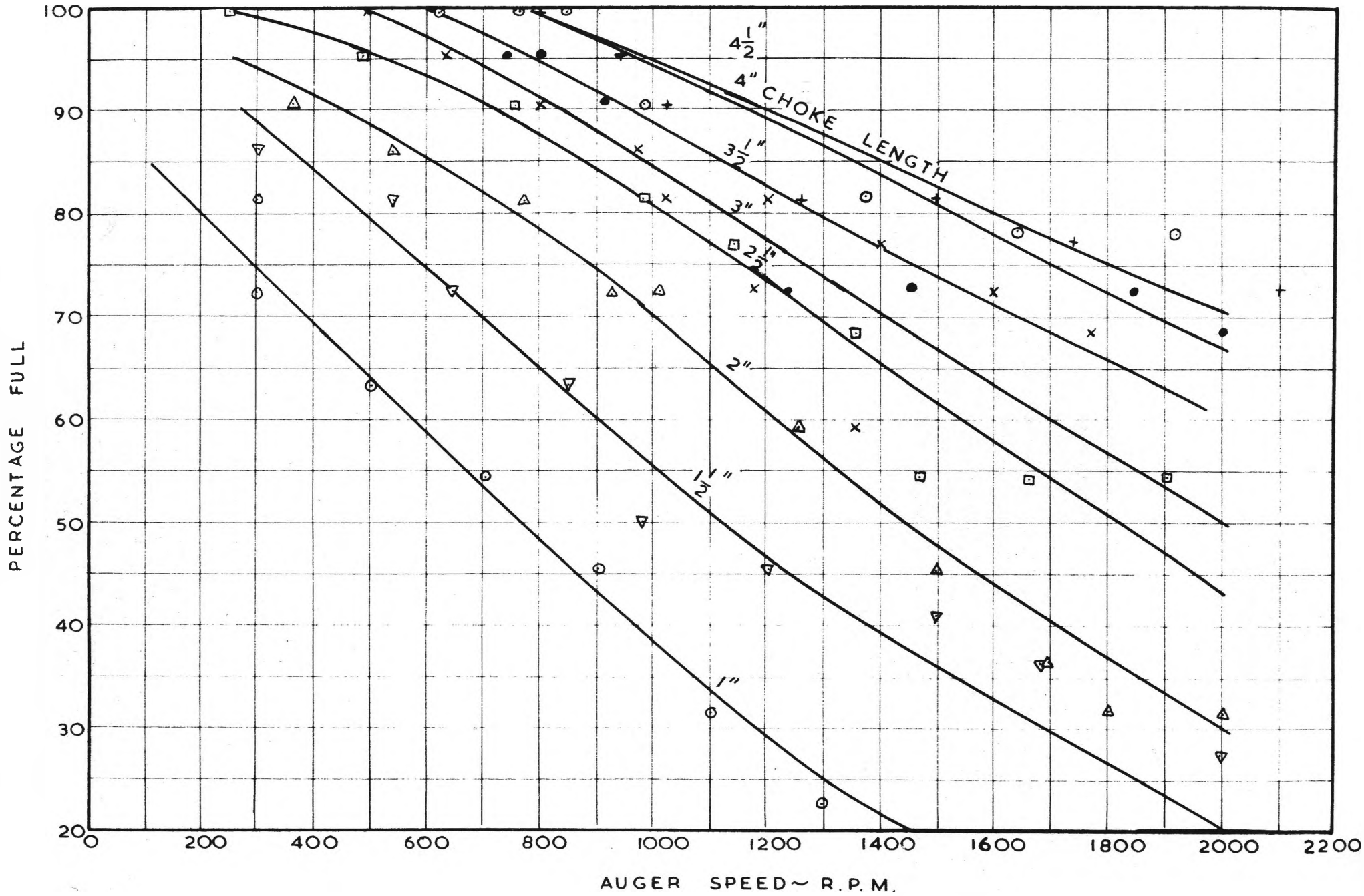

FIG.63. ESTIMATED PERCENTAGE FULL — 30° ANGLE OF ELEVATION.

FIG. 64

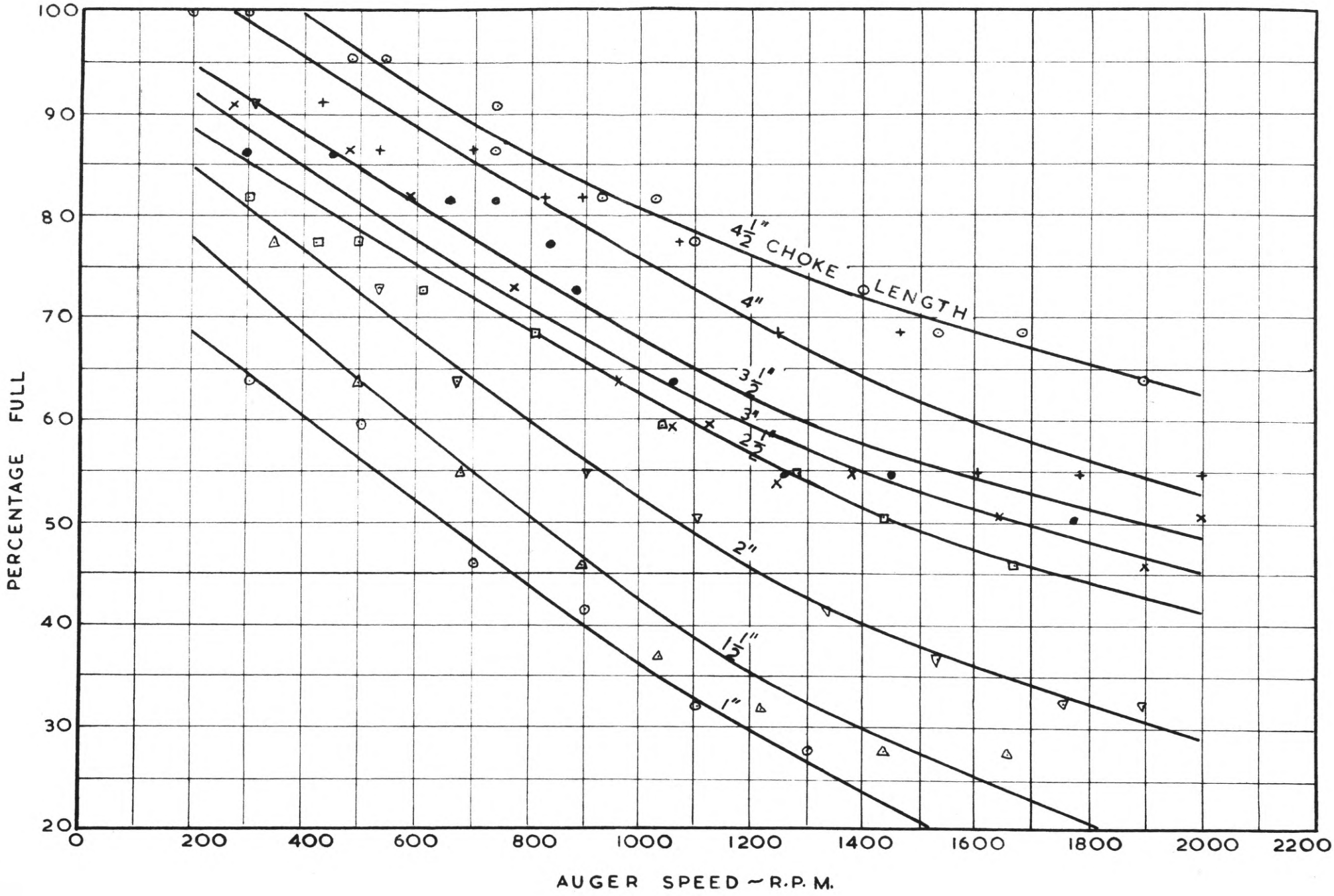

FIG. 64. ESTIMATED PERCENTAGE FULL — 60° ANGLE OF ELEVATION

FIG. 65.

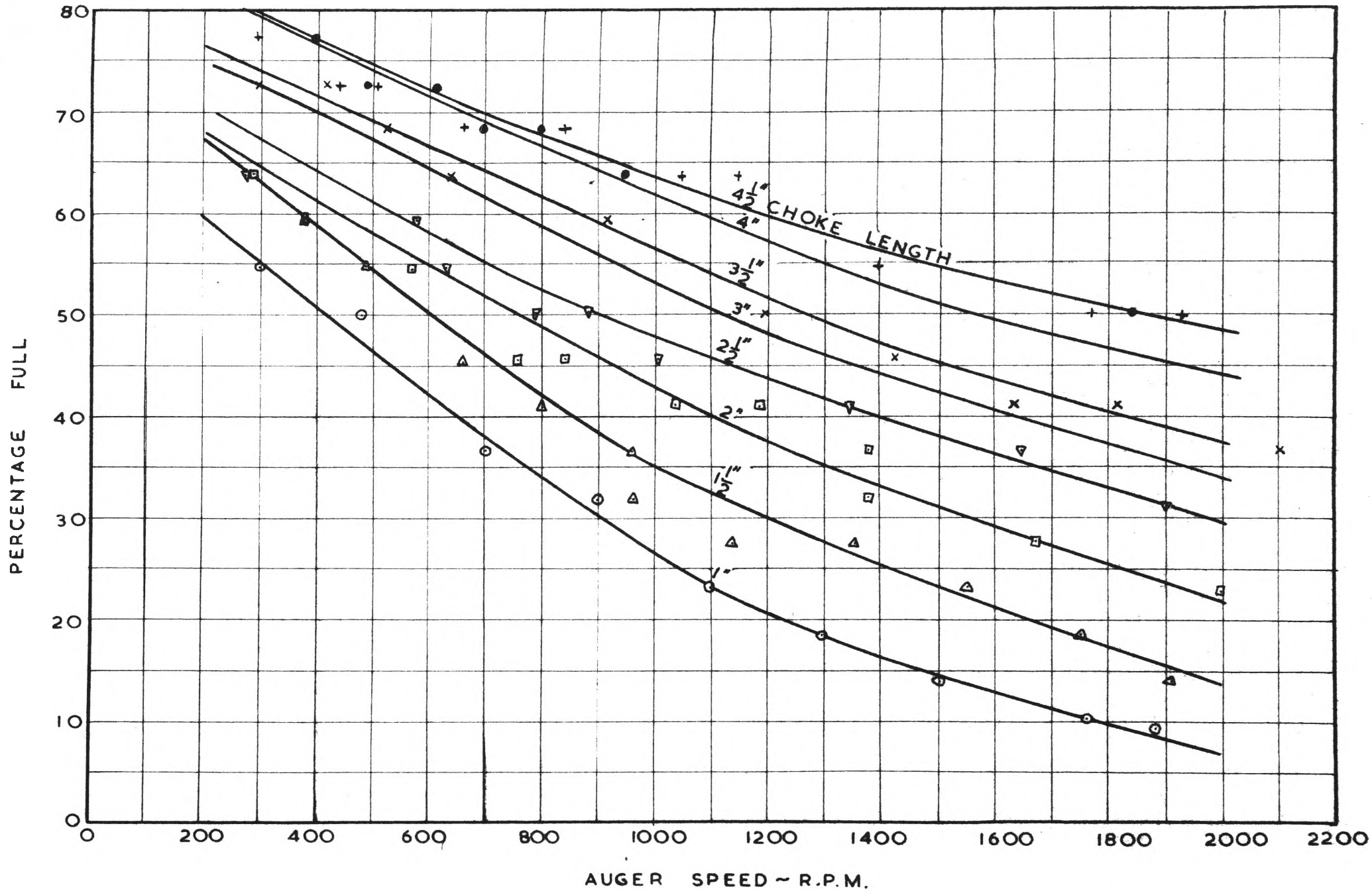

FIG. 65. ESTIMATED PERCENTAGE FULL — 90° ANGLE OF ELEVATION

FIG. 66.

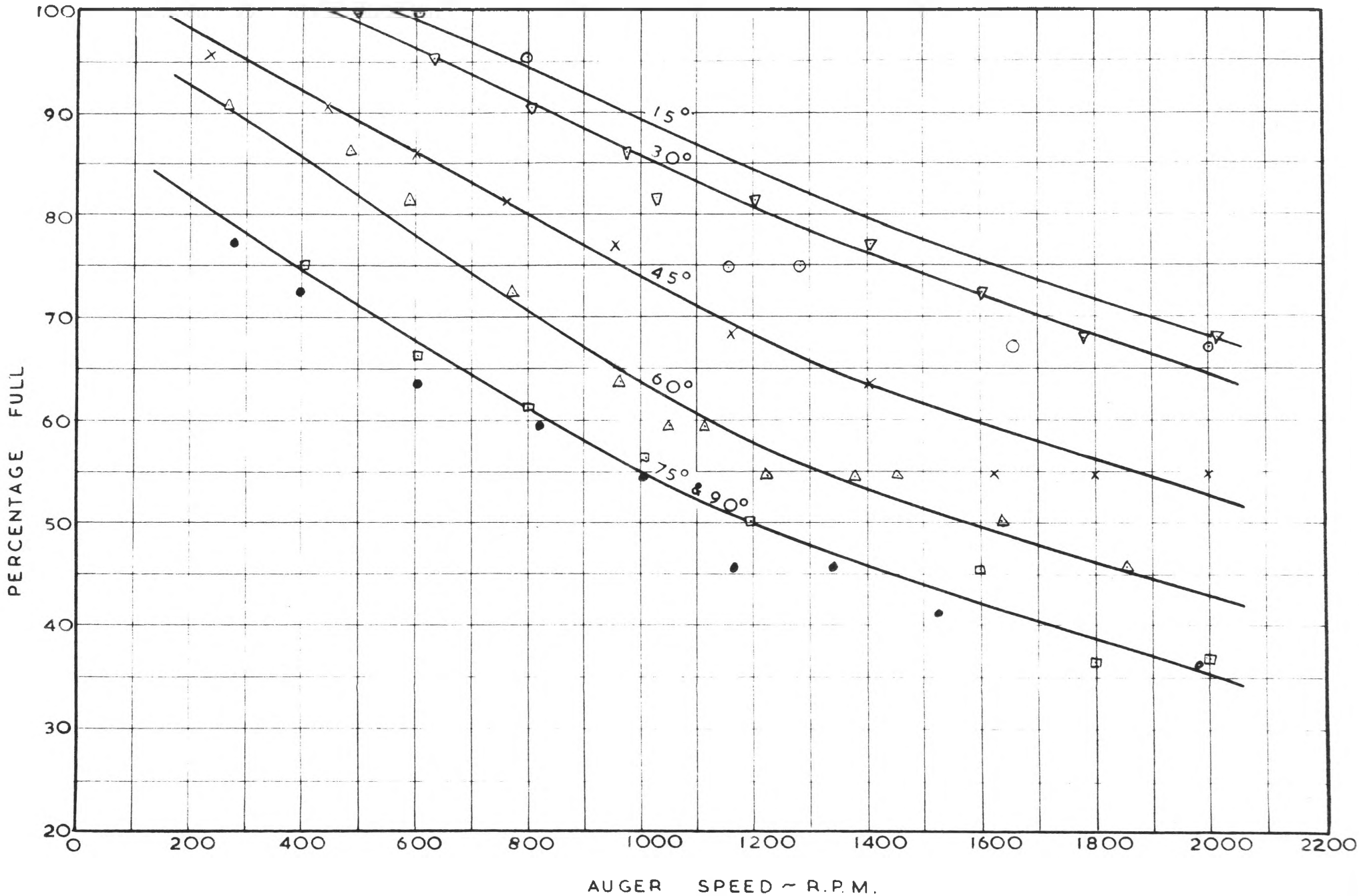

FIG. 66. ESTIMATED PERCENTAGE FULL — 3" CHOKE LENGTH

APPENDIX VI

PERFORMANCE RESULTS MODEL AUGER FITTED WITH CASING OF RADIAL CLEARANCE OF 1/64 INCH (C/D = 0.0104)

The output, percentage full and volumetric efficiency results obtained from the tests on the model auger fitted with the casing of 1/64 inch radial clearance are given in Tables 8 to 35 inclusive, and refer to the work described in Section 3. These results are for choke lengths ranging from 1 inch $(\frac{l_c}{p} = 0.67)$ to 4 inch $(\frac{l_c}{p} = 3.0)$ in 1/2 inch steps and for the angles of elevation 30°, 60°, 90°; for the 3 inch choke length, results have been also obtained for the angles of elevation 0°, 15°, 45° and 75°. In all cases the material conveyed was Japanese millet seed.

Explanation of Derived Results:

(i) Corrected Output, Q (Column (8))

Values obtained from Figs. 9 to 12 inclusive.

(ii) Theoretical Output Q_t (Column (9))

Obtained from equation (3 - 2)

$$Q_t = \gamma N D^3 = \frac{N}{764}$$

(γ = 0.67 in this case and D = 1/8 ft.)

(iii) Volumetric Efficiency (Column (10))

Ratio of values in column (8) to corresponding values in column (9).

(iv) Corrected Percentage Full Values.

The estimated % full values of column (6) are shown plotted against speed in Figs. 63 to 66. Corrected values obtained from these

graphs were used for plotting the percentage full lines on the volumetric efficiency graphs of Figs. 17 to 20.

RESULTS EXPERIMENTALLY OBTAINED						CORRECTED & DERIVED RESULTS			
	Output			% Full					
Speed R.P.M.	Vol. C. Ft.	Time Sec.	Q C.Ft/Min.	Height in.	%	Nom. Speed R.P.M.	Q C.Ft/Min.	Q_t C.Ft/Min.	η_v %
(1)	(2)	(3)	(4)	(5)	(6)	(7)	(8)	(9)	10
TABLE 8. 1" Choke Length, 30° Angle of Elevation									
300	0.133	45.8	0.174	1⅛	81.6	200	0.114	0.262	43.6
500	0.105	24.0	0.263	⅞	63.7	400	0.220	0.524	42.5
700	0.106	20.0	0.318	¾	54.6	600	0.293	0.785	37.3
900	0.119	20.0	0.360	⅝	45.5	800	0.342	1.05	32.7
1100	0.130	20.0	0.390	7/16	31.8	1000	0.378	1.31	28.9
1300	0.131	20.6	0.382	5/16	22.8	1200	0.387	1.57	24.6
1550	0.125	19.8	0.379	¼	18.2	1400	0.384	1.83	20.9
1900	0.117	20.0	0.351	3/16	13.6	1600	0.372	2.09	17.8
						1800	0.363	2.35	15.4
						2000	0.348	2.62	13.3
TABLE 9. 1" Choke Length, 60° Angle of Elevation									
300	0.090	45.0	0.120	⅞	63.7	200	0.090	0.262	344
500	0.084	29.1	0.173	13/16	59.2	400	0.147	0.524	28.1
700	0.070	20.2	0.208	⅝	45.5	600	0.192	0.785	24.5
900	0.086	21.9	0.236	9/16	41.0	800	0.222	1.05	21.2
1100	0.081	20.0	0.243	7/16	31.8	1000	0.240	1.31	18.35
1300	0.082	20.0	0.246	⅜	27.3	1200	0.249	1.57	15.84
1500	0.080	20.0	0.240	¼	18.2	1400	0.244	1.83	13.33
1900	0.072	20.0	0.216	⅛	9.1	1600	0.236	2.09	11.25
						1800	0.222	2.35	9.44
						2000	0.210	2.62	8.03

RESULTS EXPERIMENTALLY OBTAINED						CORRECTED & DERIVED RESULTS			
	Output			% Full					
Speed R.P.M.	Vol. C. Ft.	Time Sec.	Q C.Ft/Min.	Height in.	%	Nom. Speed R.P.M.	Q C.Ft/Min.	Q_t C.Ft/Min.	η_v %
(1)	(2)	(3)	(4)	(5)	(6)	(7)	(8)	(9)	(10)
TABLE 10. 1" Choke Length, 90° Angle of Elevation									
300	0.075	45.0	0.100	3/4	54.6	200	0.066	0.262	25.20
480	0.079	36.4	0.130	11/16	50.0	400	0.123	0.524	23.60
700	0.084	31.8	0.158	1/2	36.4	600	0.147	0.785	18.73
900	0.069	24.0	0.172	7/16	31.8	800	0.165	1.05	15.75
1100	0.069	24.0	0.172	5/16	22.8	1000	0.174	1.31	13.30
1300	0.067	24.0	0.167	1/4	18.2	1200	0.174	1.57	11.05
1500	0.065	24.0	0.163	3/16	13.6	1400	0.165	1.83	9.02
1880	0.059	24.0	0.147	1/8	9.1	1600	0.162	2.09	7.73
						1800	0.150	2.35	6.38
						2000	0.138	2.62	5.28
TABLE 11. 1-1/2" Choke Length, 30° Angle of Elevation									
300	0.113	30.0	0.226	1-3/16	86.2	200	0.156	0.262	59.7
540	0.139	22.6	0.369	1-1/8	81.6	400	0.288	0.524	55.1
640	0.153	21.6	0.425	1	72.6	600	0.402	0.785	51.2
850	0.116	14.2	0.490	7/8	63.7	800	0.474	1.05	45.3
980	0.121	14.3	0.508	11/16	50.0	1000	0.513	1.31	39.2
1200	0.131	14.8	0.531	5/8	45.5	1200	0.534	1.57	34.0
1380	0.127	13.7	0.556			1400	0.552	1.83	30.1
1500	0.103	11.2	0.552	9/16	41.0	1600	0.556	2.09	26.5
1680	0.143	15.2	0.565	1/2	36.4	1800	0.553	2.35	23.5
2000	0.108	11.9	0.545	3/8	27.3	2000	0.547	2.62	20.9

RESULTS EXPERIMENTALLY OBTAINED						CORRECTED & DERIVED RESULTS			
	Output			% Full					
Speed R.P.M.	Vol. C. Ft.	Time Sec.	Q C.Ft/Min.	Height in.	%	Nom. Speed R.P.M.	Q C.Ft/Min.	Q_t C.Ft/Min.	η_v %
(1)	(2)	(3)	(4)	(5)	(6)	(7)	(8)	(9)	(10)
TABLE 12. 1-1/2" Choke Length, 60° Angle of Elevation									
340	0.088	30.6	0.173	1-1/16	77.2	200	0.108	0.262	41.3
490	0.094	27.2	0.207	7/8	63.7	400	0.183	0.524	35.0
680	0.092	21.7	0.254	3/4	54.6	600	0.234	0.785	29.8
890	0.102	20.2	0.303	5/8	45.5	800	0.282	1.05	26.9
1030	0.128	23.2	0.331	1/2	36.4	1000	0.324	1.31	24.8
1210	0.111	19.3	0.345	7/16	31.8	1200	0.345	1.57	21.9
1450	0.115	19.4	0.356	3/8	27.3	1400	0.357	1.83	19.5
1650	0.088	14.7	0.359	3/8	27.3	1600	0.356	2.09	17.0
2000	0.091	15.9	0.342	1/4	18.2	1800	0.352	2.35	15.0
						2000	0.345	2.62	13.2
TABLE 13. 1-1/2" Choke Length, 90° Angle of Elevation									
290	0.07	38.5	0.109	7/8	63.7	200	0.066	0.262	25.2
490	0.099	33.7	0.176	13/16	59.2	400	0.147	0.524	28.1
660	0.097	26.6	0.219	5/8	45.5	600	0.207	0.785	26.4
800	0.108	27.0	0.240	9/16	41.0	800	0.243	1.05	23.2
960	0.109	25.0	0.262	1/2	36.4	1000	0.264	1.31	20.2
1140	0.107	23.8	0.270	3/8	27.3	1200	0.270	1.57	17.15
1350	0.107	23.9	0.269	3/8	27.3	1400	0.267	1.83	14.60
1550	0.101	23.8	0.254	5/16	22.8	1600	0.258	2.09	12.30
1750	0.099	24.0	0.248	1/4	18.2	1800	0.252	2.35	10.72
1900	0.099	24.0	0.248	3/16	13.6	2000	0.240	2.62	9.18

RESULTS EXPERIMENTALLY OBTAINED						CORRECTED & DERIVED RESULTS			
	Output			% Full					
Speed R.P.M.	Vol. C. Ft.	Time Sec.	Q C.Ft/Min.	Height in.	%	Nom. Speed R.P.M.	Q C.Ft/Min.	Q_t C.Ft/Min	η_v %
(1)	(2)	(3)	(4)	(5)	(6)	(7)	(8)	(9)	(10)
TABLE 14. 2" Choke Length, 30° Angle of Elevation									
250	0.176	49.5	0.0212						
360	0.157	30.7	0.307	1-1/4	90.8	200	0.168	0.262	64.3
540	0.159	21.7	0.439	1-3/16	86.2	400	0.336	0.524	64.2
770	0.144	15.7	0.550	1-1/8	81.6	600	0.468	0.785	59.6
1010	0.020	18.8	0.638	1	72.6	800	0.567	1.05	54.2
920	0.140	13.8	0.609	1	72.6	1000	0.627	1.31	48.0
1260	0.137	12.0	0.684	13/16	59.2	1200	0.669	1.57	42.6
1500	0.140	11.7	0.718	5/8	45.5	1400	0.696	1.83	38.0
1690	0.157	13.1	0.720	1/2	36.4	1600	0.717	2.09	34.3
1800	0.133	10.7	0.745	7/16	31.8	1800	0.729	2.35	31.0
1870	0.200	16.3	0.735	7/16	31.8	2000	0.741	2.62	28.4
TABLE 15. 2" Choke Length, 60° Angle of Elevation									
310	0.126	41.4	0.182	1-1/4	90.8	200	0.123	0.262	47.1
530	0.138	27.9	0.296	1	72.6	400	0.231	0.524	44.2
670	0.130	22.0	0.355	7/8	63.7	600	0.327	0.785	41.7
900	0.130	18.3	0.427	3/4	54.6	800	0.396	1.05	37.8
1100	0.137	17.8	0.462	11/16	50.0	1000	0.444	1.31	33.9
1330	0.140	17.5	0.480	9/16	41.0	1200	0.471	1.57	30.0
1530	0.131	15.7	0.501	1/2	36.4	1400	0.489	1.83	26.7
1750	0.134	15.9	0.506	7/16	31.8	1600	0.496	2.09	23.7
1890	0.131	15.7	0.501	7/16	31.8	1800	0.504	2.35	21.4
						2000	0.507	2.62	19.4

RESULTS EXPERIMENTALLY OBTAINED						CORRECTED & DERIVED RESULTS			
Speed R.P.M.	Output Vol. C. Ft.	Output Time Sec.	Output Q C.Ft/Min.	% Full Height in.	% Full %	Nom. Speed R.P.M.	Q C.Ft/Min.	Q_t C.Ft/Min.	η_v %
(1)	(2)	(3)	(4)	(5)	(6)	(7)	(8)	(9)	(10)
TABLE 16. 2" Choke Length. 90° Angle of Elevation									
290	0.086	50.2	0.103	7/8	63.7	200	0.06	0.262	23.0
570	0.117	31.7	0.221	3/4	54.6	400	0.154	0.524	29.5
760	0.125	26.5	0.283	5/8	45.5	600	0.234	0.785	29.8
1040	0.135	24.5	0.331	9/16	41.0	800	0.294	1.05	28.1
840	0.097	19.4	0.300	5/8	45.0	1000	0.327	1.31	25.0
1200	0.125	21.6	0.347	9/16	41.0	1200	0.339	1.57	21.6
1380	0.100	17.5	0.343	1/2	36.4	1400	0.348	1.83	19.0
1670	0.100	16.5	0.364	3/8	27.3	1600	0.348	2.09	16.6
2000	0.132	23.5	0.337	5/16	22.8	1800	0.347	2.35	14.8
						2000	0.342	2.62	13.1
TABLE 17. 2-1/2" Choke Length, 30° Angle of Elevation									
250	0.105	28.0	0.225	Full	100.0	200	0.171	0.262	65.3
480	0.115	15.7	0.439	1-5/16	95.4	400	0.363	0.524	69.3
750	0.176	17.5	0.603	1-1/4	90.8	600	0.519	0.785	66.1
980	0.171	13.6	0.756	1-1/8	81.6	800	0.636	1.05	60.8
1140	0.156	11.7	0.799	1-1/16	77.2	1000	0.741	1.31	56.7
1350	0.143	9.8	0.876	15/16	68.3	1200	0.819	1.57	52.1
1470	0.144	9.5	0.909	3/4	54.6	1400	0.882	1.83	48.3
1660	0.144	9.2	0.939	3/4	54.6	1600	0.927	2.09	44.3
1900	0.153	9.3	0.987	3/4	54.6	1800	0.957	2.35	40.7
						2000	0.984	2.62	37.7

RESULTS EXPERIMENTALLY OBTAINED						CORRECTED & DERIVED RESULTS			
Speed R.P.M.	Output Vol. C. Ft.	Output Time Sec.	Output Q C.Ft/Min.	% Full Height in.	% Full %	Nom. Speed R.P.M.	Q C.Ft/Min.	Q_t C.Ft/Min.	η_v %
(1)	(2)	(3)	(4)	(5)	(6)	(7)	(8)	(9)	(10)
TABLE 18.	2-1/2" Choke Length, 60° Angle of Elevation								
420	0.098	20.8	0.283	1-1/16	77.2	200	0.147	0.262	56.3
610	0.108	16.5	0.393	1	72.6	400	0.279	0.524	53.3
850	0.141	16.8	0.504	15/16	68.3	600	0.387	0.785	49.3
1020	0.142	15.5	0.550	13/16	59.2	800	0.474	1.05	45.3
300	0.105	26.4	0.239	1-1/8	81.6	1000	0.543	1.31	41.5
490	0.149	27.0	0.331	1-1/16	77.2	1200	0.597	1.57	38.0
810	0.118	14.7	0.482	15/16	68.3	1400	0.637	1.83	34.9
1280	0.138	13.4	0.618	3/4	54.6	1600	0.663	2.09	31.7
1430	0.153	14.3	0.642	11/16	50.0	1800	0.687	2.35	29.2
1660	0.113	10.1	0.672	5/8	45.5	2000	0.708	2.62	27.1
1910	0.113	9.7	0.699	5/8	45.5				
TABLE 19.	2-1/2" Choke Length, 90° Angle of Elevation								
375	0.078	33.0	0.142	13/16	59.2	200	0.060	0.262	23.0
630	0.123	29.1	0.254	3/4	54.6	400	0.150	0.524	28.7
880	0.118	20.7	0.342	11/16	50.0	600	0.240	0.785	30.6
1010	0.131	20.5	0.383	5/8	45.5	800	0.318	1.05	30.4
275	0.083	53.8	0.092	7/8	63.7	1000	0.384	1.31	29.4
575	0.116	32.8	0.212	13/16	59.2	1200	0.420	1.57	26.7
790	0.123	23.3	0.317	11/16	50.0	1400	0.435	1.83	23.7
1190	0.132	19.0	0.417	9/16	41.0	1600	0.441	2.09	21.0
1350	0.137	18.9	0.435	9/16	41.0	1800	0.444	2.35	18.9
1650	0.120	16.6	0.434	1/2	36.4	2000	0.444	2.62	17.0
1900	0.137	18.4	0.447	7/16	31.8				

RESULTS EXPERIMENTALLY OBTAINED						CORRECTED & DERIVED RESULTS			
	Output			% Full					
Speed R.P.M.	Vol. C. Ft.	Time Sec.	Q C.Ft/Min.	Height in.	%	Nom. Speed R.P.M.	Q C.Ft/Min.	Q_r C.Ft/Min.	η_v %
(1)	(2)	(3)	(4)	(5)	(6)	(7)	(8)	(9)	(10)
TABLE 20. 3" Choke Length 0° (Horizontal)									
300	0.122	23.5	0.311	Full	100	200	0.210	0.262	80.2
400	0.135	19.6	0.413	Full	100	400	0.410	0.524	78.2
550	0.177	18.8	0.565	Full	100	600	0.605	0.785	77.0
750	0.178	15.0	0.711	1-1/4	90.8	800	0.785	1.05	75.2
950	0.159	10.4	0.918	1-3/16	81	1000	0.950	1.31	72.5
1300	0.194	10.8	1.08	1	72.6	1200	1.06	1.57	67.5
1120	0.172	10.2	1.02	1	72.6	1400	1.14	1.83	62.3
1470	0.184	9.6	1.15	9/16	56	1600	1.21	2.09	57.8
1650	0.157	7.7	1.22	9/16	56	1800	1.25	2.35	53.2
1850	0.161	7.8	1.24	1/2	50	2000	1.26	2.62	48.2
TABLE 21. 3" Choke Length. 15° Angle of Elevation									
330	0.121	22.5	0.323	Full	100	200	0.198	0.262	75.8
370	0.146	21.8	0.402	Full	100	400	0.390	0.524	74.7
600	0.149	15.2	0.588	Full	100	600	0.582	0.785	74.2
510	0.121	14.5	0.501	Full	100	800	0.774	1.05	73.8
790	0.164	13.0	0.757		95	1000	0.906	1.31	69.3
1000	0.157	10.4	0.906			1200	1.011	1.57	64.3
1150	0.152	9.2	0.991		75	1400	1.092	1.83	59.7
1280	0.185	10.8	1.028		75	1600	1.152	2.09	55.0
1550	0.181	9.5	1.143			1800	1.182	2.35	50.3
1650	0.160	8.2	1.170		67	2000	1.206	2.62	46.2
2000	0.174	8.3	1.206		67				

RESULTS EXPERIMENTALLY OBTAINED						CORRECTED & DERIVED RESULTS			
	Output			% Full					
Speed R.P.M.	Vol. C. Ft.	Time Sec.	Q C.Ft/Min.	Height in.	%	Nom. Speed R.P.M.	Q C.Ft/Min.	Q_t C.Ft/Min.	η_v %
(1)	(2)	(3)	(4)	(5)	(6)	(7)	(8)	(9)	(10)
TABLE 22. 3" Choke Length, 30° Angle of Elevation									
270	0.108	25.4	0.255	Full	100	200	0.172	0.262	65.9
490	0.145	18.8	0.463	Full	100	400	0.366	0.524	70.0
630	0.135	14.2	0.570	1-5/16	95.4	600	0.546	0.785	69.6
800	0.149	13.4	0.667	1-1/4	90.8	800	0.699	1.05	66.8
1020	0.157	11.3	0.834	1-1/8	81.6	1000	0.822	1.31	62.9
1180	0.168	11.1	0.908	1	72.6	1200	0.918	1.57	58.4
1350	0.173	10.8	0.961			1400	0.990	1.83	54.1
970	0.163	12.0	0.815	1-3/16	86.2	1600	1.056	2.09	50.4
1400	0.167	10.1	0.992	1-1/16	77.2	1800	1.095	2.35	46.6
1600	0.161	9.0	1.073	1	72.6	2000	1.122	2.62	43.0
1770	0.162	9.0	1.080	15/16	68.3				
2200	0.135	7.2	1.125	15/16	68.3				
TABLE 23. 3" Choke Length, 45° Angle of Elevation									
230	0.101	29.3	0.207	1-5/16	95.4	200	0.162	0.262	61.9
440	0.155	24.8	0.375	1-1/4	90.8	400	0.324	0.524	61.9
600	0.146	18.2	0.481	1-3/16	86.2	600	0.486	0.785	61.9
760	0.139	14.2	0.587	1-1/8	81.6	800	0.606	1.05	57.8
950	0.146	12.8	0.684	1-1/16	77.2	1000	0.705	1.31	53.9
1160	0.140	10.7	0.785	15/16	68.3	1200	0.792	1.57	50.4
1400	0.203	14.5	0.840	7/8	63.7	1400	0.855	1.83	46.8
1620	0.139	9.2	0.906	3/4	54.6	1600	0.906	2.09	43.3
1830	0.128	8.0	0.960	3/4	54.6	1800	0.945	2.35	40.2
1920	0.127	7.9	0.965	3/4	54.6	2000	0.960	2.62	36.7

RESULTS EXPERIMENTALLY OBTAINED						CORRECTED & DERIVED RESULTS			
	Output			% Full					
Speed R.P.M.	Vol. C. Ft.	Time Sec.	Q C.Ft/Min.	Height in.	%	Nom. Speed R.P.M.	Q C.Ft/Min.	Q_t C.Ft/Min.	η_v %
(1)	(2)	(3)	(4)	(5)	(6)	(7)	(8)	(9)	(10)
TABLE 24. 3" Choke Length, 60° Angle of Elevation									
270	0.113	34.7	0.196	1-1/4	90.8	200	0.147	0.262	56.3
480	0.127	21.9	0.348	1-3/16	86.2	400	0.291	0.524	55.7
590	0.140	20.3	0.414	1-1/8	81.6	600	0.417	0.785	53.2
770	0.138	16.4	0.505	1	72.6	800	0.516	1.05	49.3
960	0.130	13.3	0.587	7/8	63.7	1000	0.597	1.31	45.6
1380	0.161	13.8	0.701	3/4	54.6	1200	0.660	1.57	42.0
1120	0.146	13.7	0.639	13/16	59.2	1400	0.710	1.83	38.8
1050	0.148	14.1	0.630	13/16	59.2	1600	0.744	2.09	35.5
1220	0.145	12.9	0.674	3/4	54.6	1800	0.770	2.35	32.8
1450	0.134	11.3	0.711	3/4	54.6	2000	0.795	2.62	30.4
1640	0.133	10.2	0.782	11/16	50.0				
1850	0.137	10.6	0.775	5/8	45.5				
2150	0.119	9.0	0.793	5/8	45.5				
TABLE 25. 3" Choke Length, 75° Angle of Elevation									
280	0.740	29.7	0.149	1-1/16	77.2	200	0.105	0.262	40.2
390	0.104	30.0	0.208	1	72.6	400	0.210	0.524	40.2
600	0.109	21.0	0.311	7/8	63.7	600	0.315	0.785	40.2
820	0.139	20.0	0.417	13/16	59.2	800	0.405	1.05	38.7
1000	0.126	15.9	0.476	3/4	54.6	1000	0.480	1.31	36.7
1160	0.115	13.0	0.531	5/8	45.5	1200	0.534	1.57	34.0
1340	0.117	12.4	0.566	5/8	45.5	1400	0.582	1.83	31.8
1520	0.119	12.0	0.595	9/16	41.0	1600	0.606	2.09	28.9
1770	0.144	14.0	0.617	9/16	41.0	1800	0.618	2.35	26.3
1980	0.131	12.6	0.624	1/2	36.4	2000	0.624	2.62	23.9

RESULTS EXPERIMENTALLY OBTAINED						CORRECTED & DERIVED RESULTS			
	Output			% Full					
Speed R.P.M.	Vol. C. Ft.	Time Sec.	Q C.Ft/Min.	Height in.	%	Nom. Speed R.P.M.	Q C.Ft/Min.	Q_t C.Ft/Min.	η_v %
(1)	(2)	(3)	(4)	(5)	(6)	(7)	(8)	(9)	(10)
TABLE 26. 3" Choke Length 90° Angle of Elevation									
230	0.153	99.2	0.093	1-1/8	81.6	200	0.069	0.262	26.4
300	0.153	75.0	0.122	1-1/16	77.2	400	0.168	0.524	32.1
405	0.156	55.4	0.169	1	72.6	600	0.264	0.785	33.6
510	0.158	43.0	0.220	1	72.6	800	0.354	1.05	33.8
595	0.156	36.6	0.256	1	72.6	1000	0.426	1.31	32.6
690	0.192	37.2	0.310	15/16	68.3	1200	0.472	1.57	30.0
805	0.192	31.6	0.365	15/16	68.3	1400	0.501	1.83	27.4
890	0.190	29.6	0.385	7/8	63.7	1600	0.519	2.09	24.7
1070	0.149	20.1	0.445			1800	0.536	2.35	22.8
1190	0.119	15.4	0.464	11/16	50.0	2000	0.552	2.62	21.1
1430	0.135	15.9	0.509						
1600	0.120	14.0	0.515	5/8	45.5				
1800	0.125	14.0	0.536	1/2	36.4				
2000	0.110	12.0	0.550	1/2	36.4				

RESULTS EXPERIMENTALLY OBTAINED						CORRECTED & DERIVED RESULTS			
	Output			% Full					
Speed R.P.M.	Vol. C. Ft.	Time Sec.	Q C.Ft/Min.	Height in.	%	Nom. Speed R.P.M.	Q C.Ft/Min.	Q_t C.Ft/Min	η_v %
(1)	(2)	(3)	(4)	(5)	(6)	(7)	(8)	(9)	(10)
TABLE 27. 3-1/2" Choke Length 30° Angle of Elevation									
320	0.150	30.6	0.294	Full	100	200	0.172	0.262	66.0
430	0.125	18.7	0.401	Full	100	400	0.370	0.524	71.1
550	0.153	17.3	0.531	Full	100	600	0.552	0.785	70.3
620	0.127	12.7	0.600	Full	100	800	0.732	1.05	69.8
740	0.158	13.7	0.692	1-5/16	95.4	1000	0.873	1.31	66.7
800	0.138	11.3	0.732	1-5/16	95.4	1200	0.996	1.57	63.4
910	0.148	10.7	0.892	1-1/4	90.8	1400	1.110	1.83	60.7
1070	0.197	13.0	0.909			1600	1.185	2.09	56.5
1240	0.174	10.3	1.014	1	72.6	1800	1.242	2.35	52.6
1460	0.153	8.0	1.147	1	72.6	2000	1.293	2.62	49.5
1600	0.187	9.5	1.181						
1850	0.181	9.0	1.206						
2200	0.159	7.3	1.308	15/16	68.3				

RESULTS EXPERIMENTALLY OBTAINED						CORRECTED & DERIVED RESULTS			
	Output			% Full					
Speed R.P.M.	Vol. C. Ft.	Time Sec.	Q C.Ft/Min.	Height in.	%	Nom. Speed R.P.M.	Q C.Ft/Min.	Q_t C.Ft/Min.	η_v %
(1)	(2)	(3)	(4)	(5)	(6)	(7)	(8)	(9)	(10)
TABLE 28.	3-1/2" Choke Length, 60° Angle of Elevation								
300	0.112	28.2	0.238	1-3/16	86.2	200	0.162	0.262	62.0
450	0.113	19.6	0.346	1-3/16	86.2	400	0.312	0.524	59.7
500	0.128	20.7	0.371	1-1/8	81.6	600	0.444	0.785	56.6
660	0.118	15.0	0.472	1-1/8	81.6	800	0.564	1.05	53.8
740	0.148	16.7	0.512	1-1/8	81.6	1000	0.663	1.31	50.7
840	0.135	13.9	0.583	1-1/16	77.2	1200	0.750	1.57	47.7
880	0.161	16.2	0.596	1	72.6	1400	0.822	1.83	44.9
1060	0.143	12.6	0.681	7/8	63.7	1600	0.870	2.09	41.6
1260	0.145	11.2	0.777	3/4	54.6	1800	0.897	2.35	38.1
1450	0.137	10.0	0.822	3/4	54.6	2000	0.918	2.62	35.2
1600	0.160	11.4	0.842	3/4	54.6				
1750	0.143	9.5	0.903	11/16	50.0				
2150	0.137	8.8	0.934						

RESULTS EXPERIMENTALLY OBTAINED						CORRECTED & DERIVED RESULTS			
	Output			% Full					
Speed R.P.M.	Vol. C. Ft.	Time Sec.	Q C.Ft/Min.	Height in.	%	Nom. Speed R.P.M.	Q C.Ft/Min.	Q_t C.Ft/Min.	η_v %
(1)	(2)	(3)	(4)	(5)	(6)	(7)	(8)	(9)	(10)
TABLE 29.	3-1/2" Choke Length, 90° Angle of Elevation								
300	0.087	42.0	0.124	1	72.6	200	0.069	0.262	26.4
420	0.090	30.8	0.175	1	72.6	400	0.174	0.524	33.3
490	0.115	30.0	0.230	15/16	68.3	600	0.273	0.785	34.8
640	0.121	24.7	0.294	7/8	63.7	800	0.372	1.05	35.5
820	0.110	18.0	0.367	7/8	63.7	1000	0.456	1.31	34.9
920	0.126	18.0	0.420	13/16	59.2	1200	0.519	1.57	33.0
970	0.133	18.0	0.443	13/16	59.2	1400	0.558	1.83	30.5
1110	0.124	15.0	0.496	3/4	54.6	1600	0.588	2.09	28.1
1200	0.143	16.8	0.511	11/16	50.0	1800	0.612	2.35	26.0
1430	0.120	12.8	0.563	5/8	45.5	2000	0.636	2.62	24.3
1630	0.126	12.8	0.590	9/16	41.0				
1820	0.109	10.6	0.617	9/16	41.0				
2100	0.114	10.6	0.645	1/2	36.4				

RESULTS EXPERIMENTALLY OBTAINED						CORRECTED & DERIVED RESULTS			
	Output			% Full					
Speed R.P.M.	Vol. C. Ft.	Time Sec.	Q C.Ft/Min.	Height in.	%	Nom. Speed R.P.M.	Q C.Ft/Min.	Q_t C.Ft/Min.	η_v %
(1)	(2)	(3)	(4)	(5)	(6)	(7)	(8)	(9)	(10)
TABLE 30.	4" Choke Length,		30° Angle of Elevation						
220	0.110	34.6	0.191	Full	100	200	0.174	0.262	66.6
390	0.147	25.1	0.352	Full	100	400	0.360	0.524	68.8
530	0.139	17.0	0.491	Full	100	600	0.552	0.785	70.3
640	0.134	13.2	0.609	Full	100	800	0.738	1.05	70.3
600	0.145	15.6	0.558	Full	100	1000	0.912	1.31	69.7
800	0.164	13.0	0.757	Full	100	1200	1.05	1.57	66.8
940	0.165	11.5	0.861	1-5/16	95.4	1400	1.16	1.83	63.6
1020	0.165	10.7	0.924	1-1/4	90.8	1600	1.26	2.09	60.2
1260	0.182	10.1	1.083	1-1/8	81.6	1800	1.35	2.35	57.4
1490	0.170	8.6	1.185	1-1/8	81.6	2000	1.43	2.62	54.6
1740	0.195	8.8	1.332	1-1/16	77.2				
2100	0.196	8.2	1.434	1	72.6				
TABLE 31.	4" Choke Length,		60° Angle of Elevation						
300	0.128	29.8	0.257	Full	100	200	0.165	0.262	63.2
400	0.114	23.0	0.298	Full	100	400	0.318	0.524	60.8
480	0.159	25.4	0.376	1-5/16	95.4	600	0.462	0.785	58.9
540	0.150	21.4	0.421	1-5/16	95.4	800	0.594	1.05	56.8
740	0.177	19.2	0.553	1-1/4	90.8	1000	0.711	1.31	54.4
930	0.191	17.0	0.674	1-1/8	81.6	1200	0.810	1.57	51.5
1030	0.201	17.2	0.702	1-1/8	81.6	1400	0.888	1.83	48.5
1100	0.166	13.1	0.761	1-1/16	77.2	1600	0.936	2.09	44.7
1400	0.185	12.5	0.888	1	72.6	1800	0.972	2.35	41.3
1530	0.168	11.1	0.909	15/16	68.3	2000	0.996	2.62	38.1
1680	0.204	13.0	0.942	15/16	68.3				
1900	0.173	10.5	0.989	7/8	63.7				

RESULTS EXPERIMENTALLY OBTAINED						CORRECTED & DERIVED RESULTS			
	Output			% Full					
Speed R.P.M.	Vol. C. Ft.	Time Sec.	Q C.Ft/Min.	Height in.	%	Nom. Speed R.P.M.	Q C.Ft/Min.	Q_t C.Ft/Min.	η_v %
(1)	(2)	(3)	(4)	(5)	(6)	(7)	(8)	(9)	(10)
TABLE 32. 4" Choke Length, 90° Angle of Elevation									
250	0.102	60.0	0.102	1-1/8	81.6	200	0.069	0.262	27.4
400	0.132	43.6	0.181	1-1/16	77.2	400	0.186	0.524	35.6
490	0.123	31.1	0.237	1	72.6	600	0.294	0.785	37.5
620	0.142	27.5	0.310	1	72.6	800	0.402	1.05	38.4
700	0.152	26.0	0.351	15/16	68.3	1000	0.498	1.31	38.1
830	0.165	23.8	0.416	7/8	63.7	1200	0.564	1.57	35.9
950	0.155	19.6	0.474	7/8	63.7	1400	0.612	1.83	33.5
970	0.132	16.3	0.486	13/16	59.2	1600	0.654	2.09	31.3
1170	0.167	18.1	0.554	13/16	59.2	1800	0.687	2.35	29.2
1350	0.168	16.7	0.603	3/4	54.6	2000	0.717	2.62	27.4
1490	0.156	14.8	0.632	3/4	54.6				
1850	0.150	12.8	0.702	11/16	50.0				
2000	0.158	12.4	0.765	5/8	45.5				

RESULTS EXPERIMENTALLY OBTAINED						CORRECTED & DERIVED RESULTS			
	Output			% Full					
Speed R.P.M.	Vol. C. Ft.	Time Sec.	Q C.Ft/Min.	Height in.	%	Nom. Speed R.P.M.	Q C.Ft/Min.	Q_t C.Ft/Min.	η_V %
(1)	(2)	(3)	(4)	(5)	(6)	(7)	(8)	(9)	(10)
TABLE 33. 4-1/2" Choke Length, 30° Angle of Elevation									
275	0.126	30.0	0.252	Full	100	200	0.180	0.262	68.9
375	0.150	24.5	0.367	Full	100	400	0.381	0.524	72.8
490	0.196	24.2	0.486	Full	100	600	0.582	0.785	74.2
660	0.157	14.6	0.645	Full	100	800	0.783	1.05	74.8
680	0.177	15.4	0.690	Full	100	1000	0.972	1.31	74.3
870	0.195	13.7	0.855			1200	1.120	1.57	71.4
760	0.162	13.2	0.737	Full	100	1400	1.25	1.83	68.2
980	0.157	9.7	0.970	1-1/4	90.8	1600	1.35	2.09	64.2
1050	0.170	9.2	1.11	1-3/16	86.2	1800	1.43	2.35	60.8
980	0.156	9.6	0.975	1-1/4	90.8	2000	1.50	2.62	57.4
610	0.159	16.4	0.582	Full	100				
820	0.155	11.3	0.822	Full	100				
1260	0.173	9.0	1.15	1-3/16	86.2				
1370	0.163	8.4	1.16	1-1/8	81.6				
1640	0.169	7.4	1.37	1-1/16	77.2				
1920	0.188	7.7	1.46	1-1/16	77.2				
2180	0.194	7.5	1.55	1	72.6				

RESULTS EXPERIMENTALLY OBTAINED						CORRECTED & DERIVED RESULTS			
	Output			% Full					
Speed R.P.M.	Vol. C. Ft.	Time Sec.	Q C.Ft/Min.	Height in.	%	Nom. Speed R.P.M.	Q C.Ft/Min.	Q_t C.Ft/Min.	η_V %
(1)	(2)	(3)	(4)	(5)	(6)	(7)	(8)	(9)	(10)
TABLE 34. 4-1/2" Choke Length, 60° Angle of Elevation									
280	0.132	32.4	0.244	Full	100	200	0.171	0.262	64.2
430	0.128	20.2	0.380	1-1/4	90.8	400	0.339	0.524	64.8
530	0.116	15.7	0.443	1-3/16	86.2	600	0.486	0.785	61.8
620	0.148	17.5	0.508			800	0.618	1.05	59.1
700	0.155	16.9	0.551	1-3/16	86.2	1000	0.738	1.31	56.4
830	0.155	14.2	0.654	1-1/8	81.6	1200	0.837	1.57	53.3
890	0.171	15.4	0.666	1-1/8	81.6	1400	0.906	1.83	49.4
1070	0.160	12.4	0.774	1-1/16	77.2	1600	0.966	2.09	46.2
1250	0.159	11.5	0.829	15/16	68.3	1800	1.014	2.35	43.1
1460	0.157	10.3	0.915	15/16	68.3	2000	1.062	2.62	40.7
1600	0.190	12.0	0.910	3/4	54.6				
1780	0.168	9.9	1.018	3/4	54.6				
2000	0.167	9.2	1.089	3/4	54.6				

RESULTS EXPERIMENTALLY OBTAINED						CORRECTED & DERIVED RESULTS			
	Output			% Full					
Speed R.P.M.	Vol. C. Ft.	Time Sec.	Q C.Ft/Min.	Height in.	%	Nom. Speed R.P.M.	Q C.Ft/Min.	Q_t C.Ft/Min.	η_v %
(1)	(2)	(3)	(4)	(5)	(6)	(7)	(8)	(9)	(10)
TABLE 35. 4-1/2" Choke Length. 90° Angle of Elevation									
300	0.082	37.0	0.133	1-1/16	77.2	200	0.072	0.262	27.5
440	0.108	30.0	0.216	1	72.6	400	0.186	0.524	35.6
510	0.131	30.2	0.260	1	72.6	600	0.300	0.785	38.2
665	0.138	23.1	0.359	15/16	68.3	800	0.414	1.05	39.5
700	0.136	23.8	0.343	15/16	68.3	1000	0.516	1.31	39.4
850	0.144	19.2	0.450	15/16	68.3	1200	0.594	1.57	37.8
890	0.165	21.4	0.463	15/16	68.3	1400	0.651	1.83	35.6
1050	0.151	16.6	0.546	7/8	63.7	1600	0.702	2.09	33.5
1150	0.114	12.2	0.561	7/8	63.7	1800	0.738	2.35	31.4
1530	0.174	15.2	0.687	11/16	50.0	2000	0.768	2.62	29.4
1400	0.132	12.0	0.660	11/16	50.0				
1930	0.153	12.0	0.765	11/16	50.0				
1770	0.119	9.4	0.759	11/16	50.0				

APPENDIX VII

OUTPUT RESULTS FOR MODEL AUGER FITTED WITH CASING HAVING LONGITUDINAL VANES.

The output results for the tests on the model auger fitted with the casing having four longitudinal vanes are given in Table 36; these tests are described in Section 6.2. The results were obtained for the angles of elevation 30°, 60° and 90°, the material conveyed being millet seed. The radial casing clearance was 1/8 inch ($C/D = 0.0833$) and the choke length 3 inches ($\frac{l_c}{p} = 2.0$).

TABLE 86 OUTPUT RESULTS FOR AUGER FITTED WITH CASING HAVING LONGITUDINAL VANES

Radial Clearance = 1/8 in. Material Conveyed Japanese Millet Seed

90° Angle of Elevation				60° Angle of Elevation				30° Angle of Elevation			
Speed R.P.M.	Vol. C.Ft.	Time Sec.	Q C.Ft/Min	Speed R.P.M.	Vol. C.Ft.	Time Sec.	Q C.Ft/Min	Speed R.P.M.	Vol. C.Ft.	Time Sec.	Q C.Ft/Min.
305	0.15	86.0	0.105	290	0.100	25.0	0.240	320	0.120	20.6	0.349
270	0.055	36.4	0.091	300	0.099	25.3	0.240	280	0.145	28.0	0.311
380	0.132	60.7	0.131	375	0.089	17.7	0.302	470	0.131	15.0	0.524
440	0.073	26.6	0.165	380	0.091	18.8	0.296	420	0.139	17.5	0.477
515	0.145	44.7	0.195	550	0.143	20.7	0.330	510	0.142	15.2	0.560
530	0.144	40.2	0.215	540	0.153	23.0	0.399	540	0.098	10.0	0.588
660	0.091	20.2	0.271	640	0.130	16.1	0.484	650	0.117	10.2	0.628
660	0.014	22.6	0.372	640	0.152	19.0	0.480	660	0.170	15.0	0.621
720	0.134	27.6	0.291	750	0.112	12.0	0.561	770	0.126	9.7	0.780
760	0.140	26.2	0.321	770	0.133	14.4	0.553	775	0.123	9.7	0.762
835	0.113	19.3	0.351	850	0.110	11.0	0.600	750	0.177	14.5	0.732
865	0.081	13.4	0.363	880	0.133	13.4	0.595	870	0.071	5.0	0.852
875	0.148	23.5	0.378	920	0.091	8.8	0.621	950	0.131	9.6	0.823
1050	0.143	19.2	0.448	915	0.114	11.2	0.612	930	0.107	7.6	0.846
935	0.105	16.2	0.390	1000	0.115	12.0	0.576	990	0.058	3.7	0.943
950	0.085	12.8	0.400	1010	0.110	11.1	0.594	1020	0.067	4.4	0.812
1010	0.114	16.1	0.423					1100	0.087	5.6	0.930

FIG. 67.

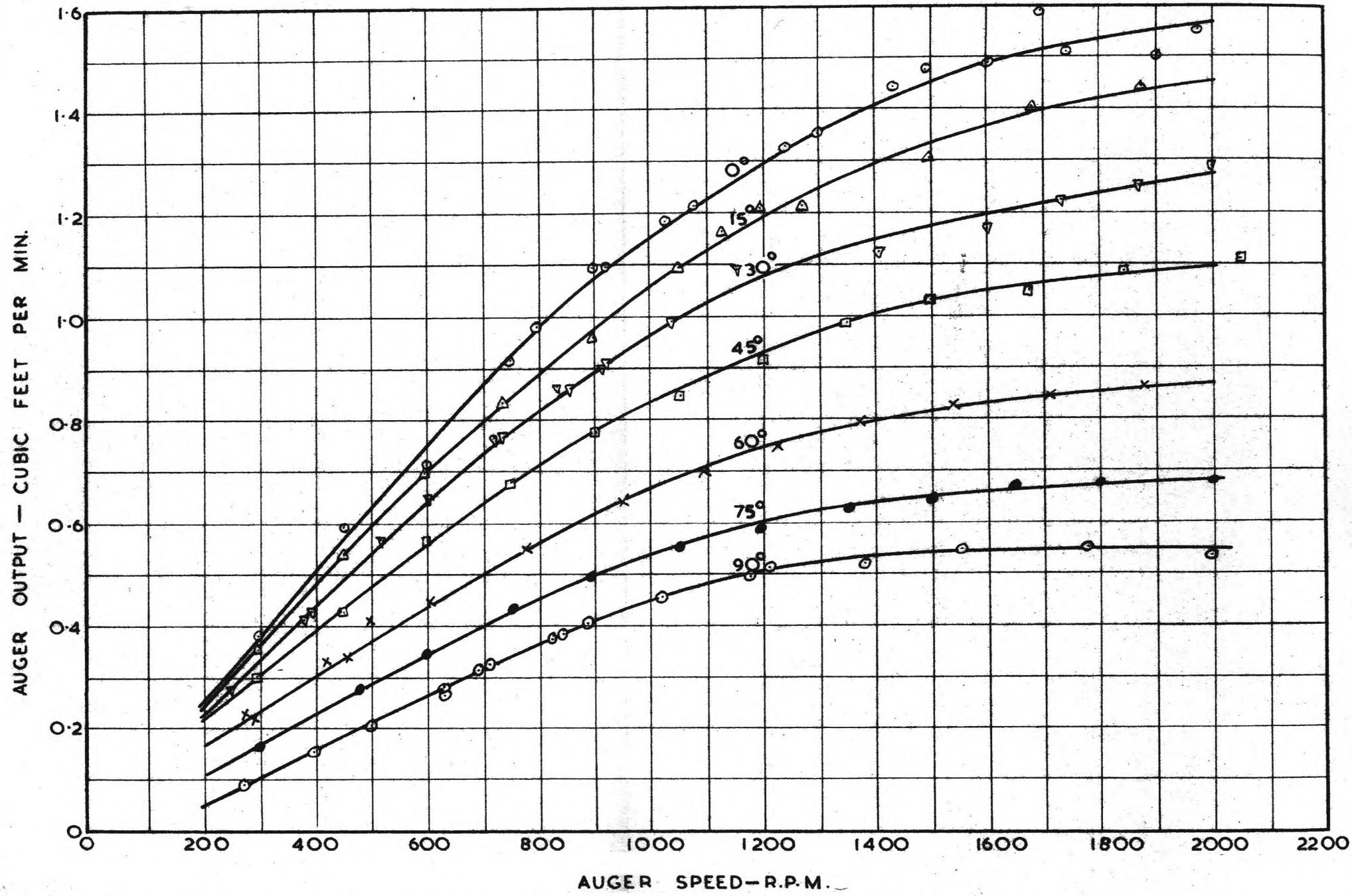

FIG.67. OUTPUT VERSUS SPEED FOR VARIOUS ANGLES OF ELEVATION

Choke Length: 3 inches Radial Clearance: $\frac{1}{8}$ inch Material Conveyed: Millet

APPENDIX VIII

OUTPUT RESULTS FOR MODEL AUGER FITTED WITH CASING OF RADIAL CLEARANCE OF 1/8 INCH (C/D = 0.0833)

The output results from the tests conducted on the model auger fitted with the casing of 1/8 inch radial clearance are given in Tables 37 to 45 inclusive. These results refer to the work of Sections 3.3 and 4.2. The tests were conducted for the 3 inch choke length ($\frac{l_c}{p}$ = 2.0).

Tables 37 to 43 give the results obtained for millet seed ($^{d}/_{D}$ = 0.05) for the angles of elevation ranging from 0° to 90° in 15° steps. Tables 44 and 45 give the results obtained for wheat ($^{d}/_{D}$ = 0.12) for the angles of elevation 60° and 90°. The various output values are shown plotted against speed in Fig. 67, corrected output values have been read from these graphs and used in calculating the results given in Appendix X.

PERFORMANCE RESULTS FOR MILLET ($^{d}/_{D}$ = 0.05)

TABLE 37. 0° Angle of Elevation

Speed R.P.M.	Output		
	Vol. C.Ft.	Time Secs	Q C.Ft/Min.
300	0.146	22.7	0.386
450	0.179	18.0	0.597
600	0.151	12.0	0.715
750	0.186	12.2	0.915
900	0.183	10.0	1.100
1030	0.198	10.0	1.190
1320	0.210	9.3	1.360
1490	0.198	8.0	1.482
1690	0.189	7.1	1.595
1970	0.207	8.0	1.555
800	0.213	13.1	0.984
920	0.183	10.0	1.100
1080	0.207	10.2	1.218
1240	0.191	8.6	1.332
1435	0.189	7.8	1.452
1600	0.208	8.4	1.490
1740	0.199	7.9	1.510
1910	0.188	7.5	1.505

TABLE 38. 15° Angle of Elevation

Speed R.P.M.	Output		
	Vol. C.Ft.	Time Secs	Q C.Ft/Min.
300	0.179	30.0	0.359
450	0.137	15.1	0.545
600	0.177	15.0	0.708
740	0.167	12.0	0.835
900	0.193	12.0	0.966
1050	0.183	10.0	1.098
1200	0.202	10.0	1.212
1130	0.195	10.0	1.170
1275	0.179	8.8	1.218
1500	0.177	8.1	1.308
1680	0.187	8.0	1.404
1880	0.194	8.0	1.452

PERFORMANCE RESULTS FOR MILLET ($^{d}/_{D}$ = 0.05)

TABLE 39. 30° Angle of Elevation

Speed R.P.M.	Output		
	Vol. C.Ft.	Time Secs	Q C.Ft/Min.
250	0.113	24.9	0.272
380	0.143	20.5	0.418
390	0.129	18.0	0.430
515	0.154	16.2	0.571
515	0.150	15.7	0.574
600	0.155	14.2	0.655
600	0.165	15.2	0.651
720	0.143	11.2	0.767
735	0.151	11.8	0.768
835	0.175	12.1	0.870
850	0.151	10.5	0.864
915	0.166	11.0	0.906
920	0.167	11.0	0.911
1040	0.170	10.3	0.990
1250	0.183	10.0	1.098
1410	0.187	10.0	1.122
1600	0.193	9.9	1.170
1730	0.193	9.5	1.218
1870	0.200	9.6	1.251
2000	0.192	8.9	1.296

TABLE 40. 45° Angle of Elevation

Speed R.P.M.	Output		
	Vol. C.Ft.	Time Secs	Q C.Ft/Min.
300	0.150	30.0	0.300
450	0.128	18.0	0.427
600	0.172	18.0	0.573
750	0.136	12.0	0.680
900	0.156	12.0	0.780
1050	0.170	12.0	0.850
1200	0.152	10.0	0.912
1350	0.164	10.0	0.984
1500	0.172	10.0	1.032
1670	0.174	10.0	1.045
1840	0.181	10.0	1.085
2050	0.185	10.0	1.110

PERFORMANCE RESULTS FOR MILLET ($^{d}/_{D}$ = 0.05)

TABLE 41. 60° Angle of Elevation

Speed R.P.M.	Output		
	Vol. C.Ft.	Time Secs	Q C.Ft/Min.
275	0.093	24.2	0.231
275	0.090	24.2	0.214
410	0.120	22.0	0.327
420	0.108	19.1	0.339
500	0.122	17.7	0.414
500	0.133	19.3	0.414
290	0.111	30.0	0.222
460	0.156	27.0	0.347
610	0.150	20.0	0.450
780	0.139	15.1	0.553
950	0.160	15.0	0.640
1100	0.139	12.0	0.695
1230	0.149	12.0	0.745
1370	0.136	10.3	0.793
1540	0.140	10.1	0.832
1710	0.155	11.0	0.846
1880	0.142	9.9	0.862
2300	0.156	10.8	0.867

TABLE 42. 75° Angle of Elevation

Speed R.P.M.	Output		
	Vol. C.Ft.	Time Secs	Q C.Ft/Min.
300	0.123	45.0	0.164
480	0.112	24.0	0.280
600	0.120	21.0	0.343
750	0.129	18.0	0.430
900	0.149	18.0	0.497
1050	0.140	15.3	0.549
1200	0.147	15.0	0.588
1350	0.158	15.2	0.624
1500	0.129	12.0	0.645
1650	0.134	12.0	0.671
1800	0.135	12.0	0.675
2000	0.136	12.0	0.680

PERFORMANCE RESULTS FOR MILLET ($^{d}/_{D}$ = 0.05)

TABLE 43. 90° Angle of Elevation

Speed R.P.M.	Output		
	Vol. C. Ft.	Time Secs	Q C.Ft/Min.
270	0.072	49.5	0.087
270	0.080	53.7	0.089
400	0.077	30.2	0.153
405	0.084	32.4	0.155
500	0.101	29.7	0.204
500	0.105	29.7	0.212
615	0.102	23.1	0.265
615	0.107	23.2	0.277
690	0.105	20.7	0.304
715	0.113	20.7	0.327
840	0.103	16.0	0.387
825	0.095	15.1	0.378
895	0.107	15.9	0.404
895	0.109	15.9	0.412
1020	0.113	15.1	0.448
1200	0.174	20.5	0.509
1180	0.148	18.0	0.494
1380	0.138	16.1	0.514
1550	0.139	15.4	0.542
1770	0.141	15.3	0.553
2000	0.133	15.0	0.533

PERFORMANCE RESULTS FOR WHEAT ($^{d}/_{D}$ = 0.05)

TABLE 44. 60° Angle of Elevation

Speed R.P.M.	Output		
	Vol. C.Ft.	Time Secs	Q C.Ft/Min.
265	0.154	46.5	0.199
430	0.170	31.0	0.329
490	0.196	32.4	0.363
660	0.200	25.8	0.465
790	0.166	17.8	0.560
900	0.161	15.7	0.616
1040	0.177	15.9	0.668
1175	0.192	16.4	0.703
1370	0.220	16.4	0.805
1560	0.180	13.7	0.790
1860	0.200	15.0	0.800
2000	0.193	14.3	0.810

TABLE 45. 90° Angle of Elevation

Speed R.P.M.	Output		
	Vol. C.Ft.	Time Secs	Q C.Ft/Min.
300	0.148	83.0	0.107
450	0.162	52.4	0.186
510	0.169	47.5	0.214
640	0.168	36.6	0.275
745	0.151	29.2	0.310
860	0.156	26.5	0.353
945	0.158	25.4	0.373
1050	0.158	23.4	0.405
1110	0.162	22.5	0.432
1275	0.170	22.9	0.445
1440	0.161	20.5	0.472
1630	0.166	20.5	0.486
1870	0.175	21.2	0.496

FIGS. 68, 69 & 70.

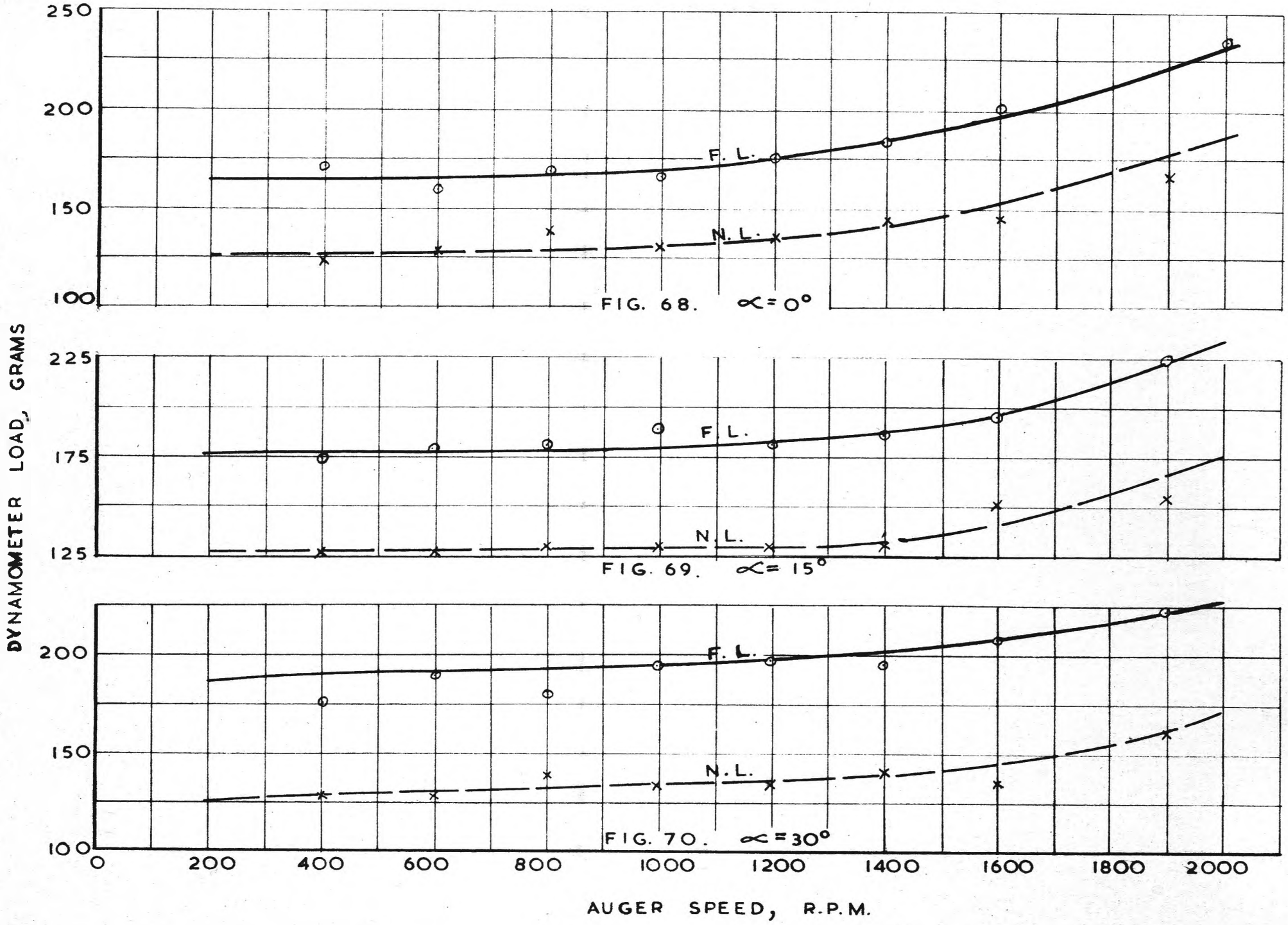

FIG. 68. $\alpha = 0°$

FIG. 69. $\alpha = 15°$

FIG. 70. $\alpha = 30°$

FIGS. 71 & 72

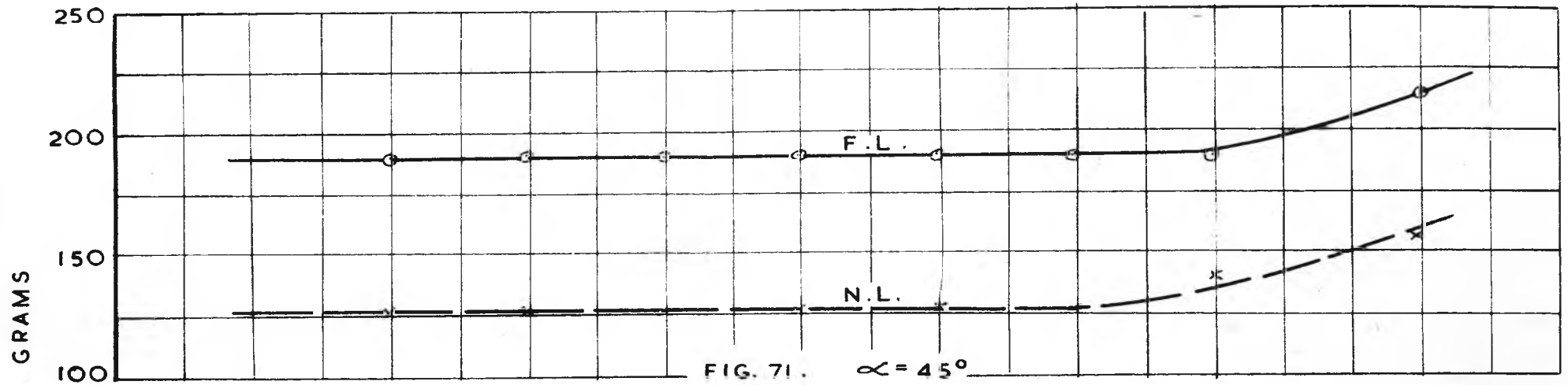

FIG. 71. $\alpha = 45°$

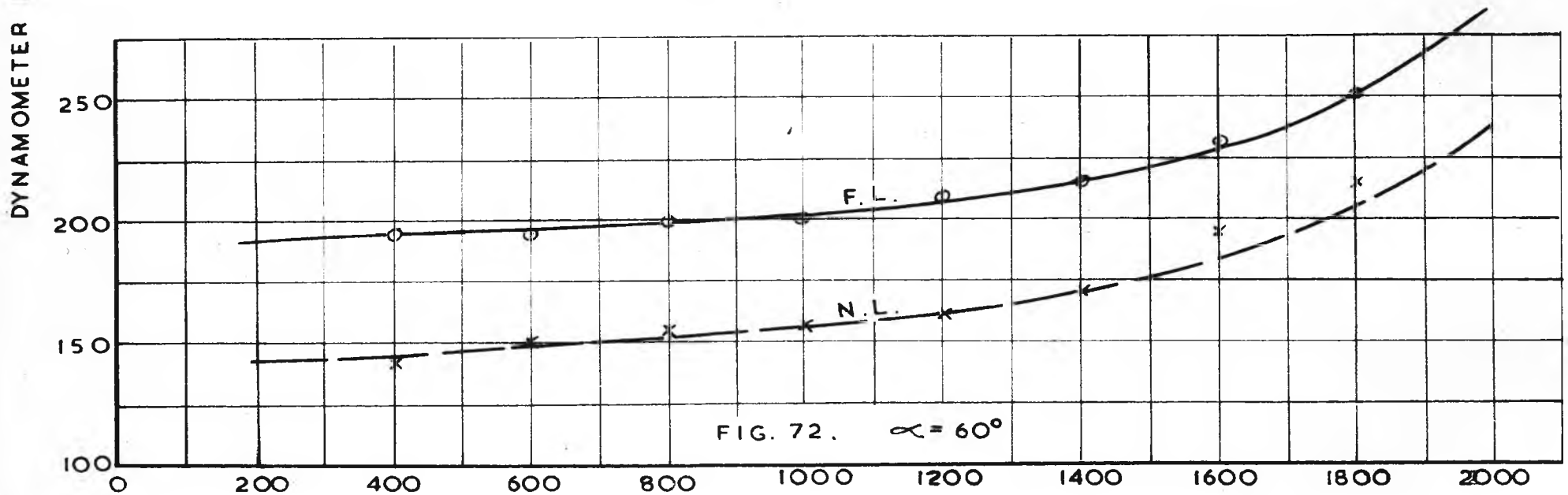

FIG. 72. $\alpha = 60°$

DYNAMOMETER LOAD, GRAMS

0 200 400 600 800 1000 1200 1400 1600 1800 2000

AUGER SPEED, R.P.M.

FIGS. 73 & 74

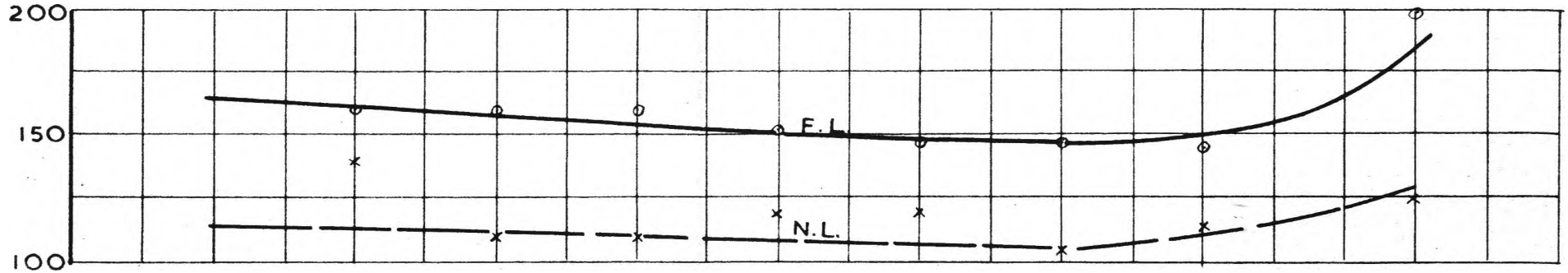

FIG. 73. $\alpha = 75°$

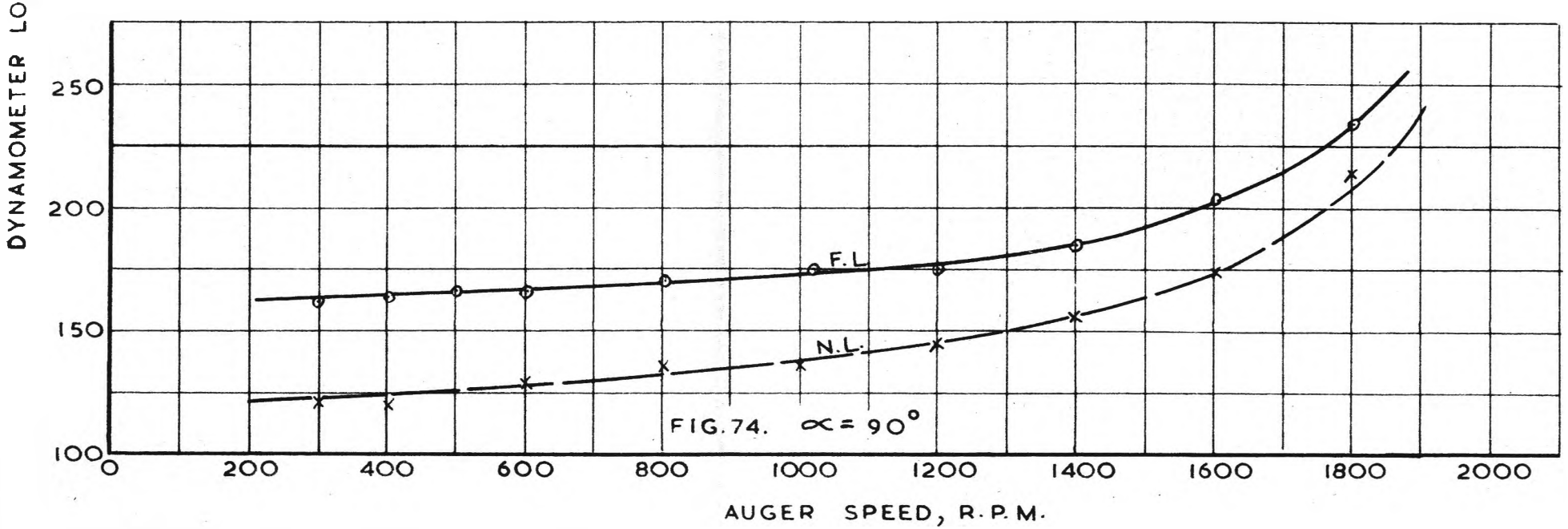

FIG. 74. $\alpha = 90°$

FIGS. 75, 76 & 77.

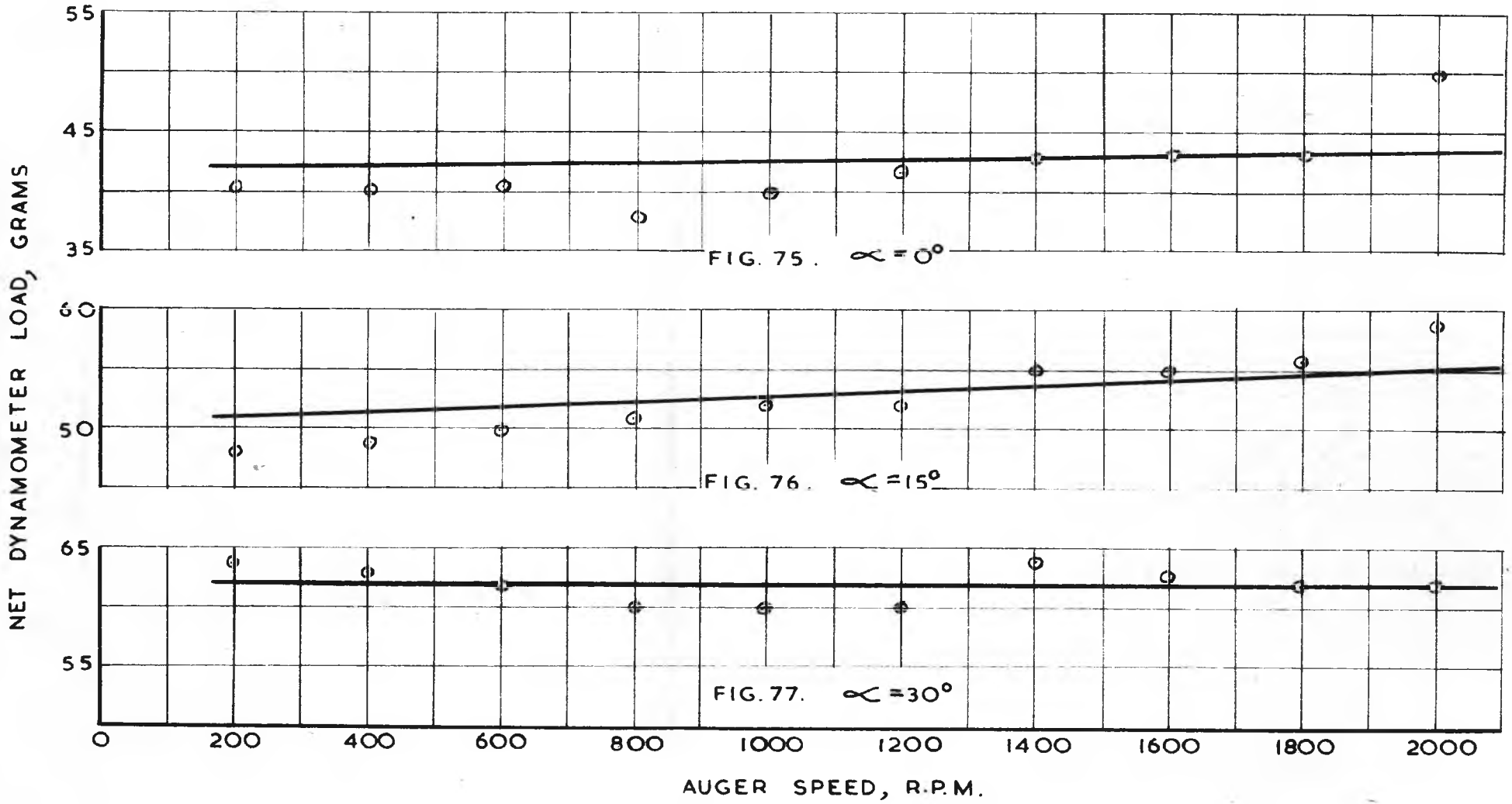

FIG. 75. $\alpha = 0°$

FIG. 76. $\alpha = 15°$

FIG. 77. $\alpha = 30°$

FIGS. 78, 79, 80 & 81.

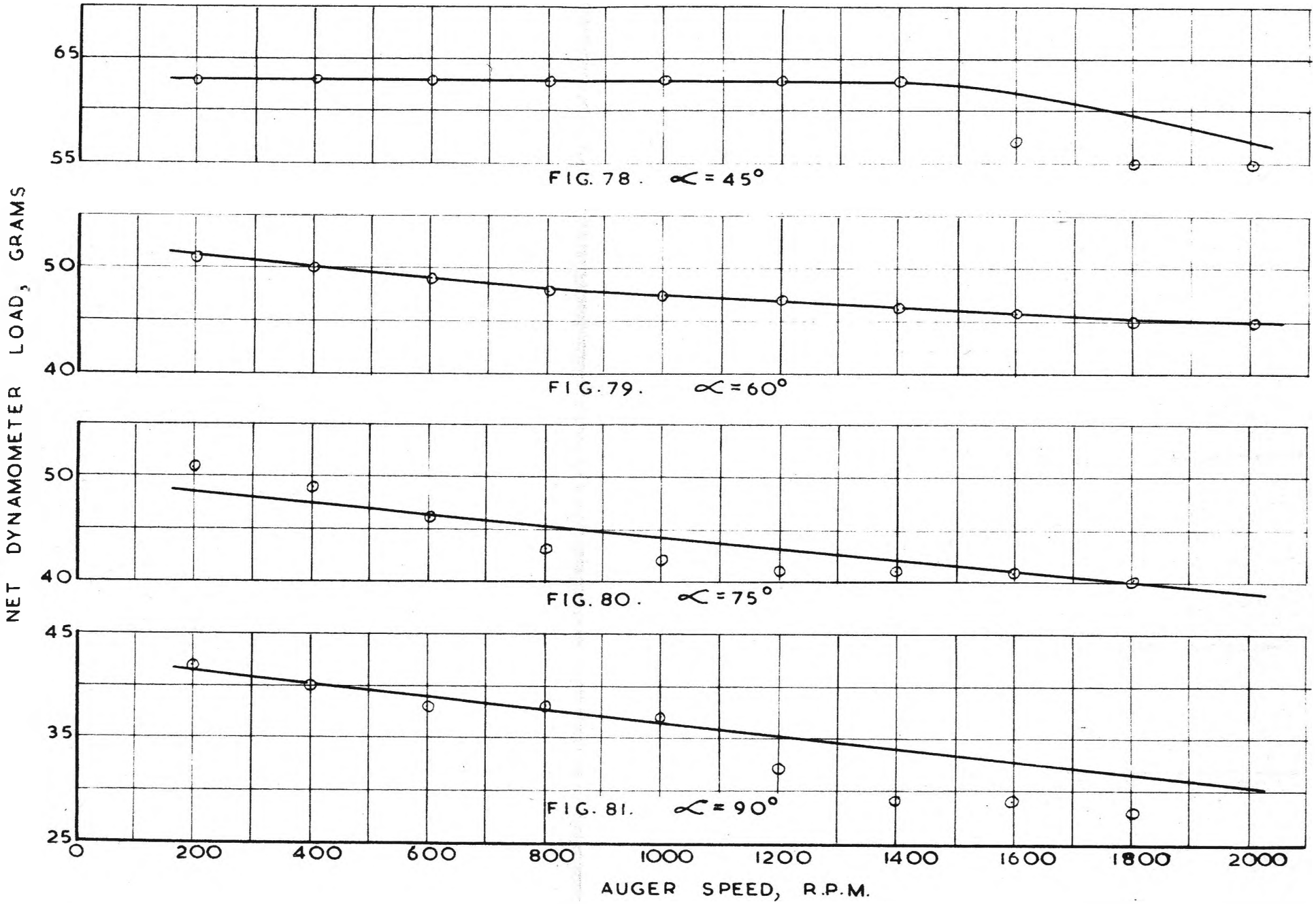
65
55
FIG. 78. ∝ = 45°
50
40
FIG. 79. ∝ = 60°
50
40
FIG. 80. ∝ = 75°
45
35
25
FIG. 81. ∝ = 90°
NET DYNAMOMETER LOAD, GRAMS
0
200
400
600
800
1000
1200
1400
1600
1800
2000
AUGER SPEED, R.P.M.

APPENDIX IX

POWER RESULTS FOR MODEL AUGER FITTED WITH CASING OF RADIAL CLEARANCE OF 1/8 INCH (C/D = 0.0833)

The power results from the tests conducted on the model auger fitted with the casing of 1/8 inch radial clearance are given in Tables 46 to 52 inclusive. These results refer to the work of Sections 3-4 and 4-3. The tests were conducted for the 3 inch choke length ($\frac{l_c}{p}$ = 2-0), the material conveyed being millet seed.

Explanation of Derived Results.

The method of obtaining the final power results is as follows:-

The mean full-load and no-load spring balance readings from columns (3) and (5) have been plotted as full lines and dotted lines respectively in Figs. 68 to 74. (It is to be noted that the actual spring balance readings are not the true dynamometer reaction loads owing to the zero error introduced by the dynamometer counterweight. However, the differences between the full-load and no-load graphs will be the true net loads).

The net dynamometer loads were obtained from the full-load and no-load graphs and are shown plotted in Figs. 75 to 81. The corrected net loads were obtained from these graphs and are tabulated in column (7) of the results. The horsepowers of column (8) were computed from these figures using following equation:-

$$H.P. = \frac{W\,N}{16800}$$

W = net load

(Torque arm = 3.75 in.)

TABLE 46. 0° Angle of Elevation

RESULTS EXPERIMENTALLY OBTAINED					Derived Results		
Speed R.P.M.	Spring Balance Reading, Gms.				Nom. Speed R.P.M.	Net Load Grams	H.P. x 10^{-3}
	Full - Load		No - Load				
		Mean		Mean			
(1)	(2)	(3)	(4)	(5)	(6)	(7)	(8)
200			110	125	200	42.0	1.10
			140				
400	200	172	110	125	400	42.1	2.20
	145		140				
600	205	162	110	130	600	42.2	3.31
	120		150				
800	205	170	130	140	800	42.4	4.43
	135		150				
1000	190	167	110	132	1000	42.5	5.56
	145		155				
1200	185	177	120	137	1200	42.8	6.74
	170		155				
1400	195	185	135	145	1400	43.0	7.87
	175		155				
1600	210	202	135	145	1600	43.1	9.02
	195		155				
1800					1800	43.2	10.15
2000	240	235	170	167	2000	43.3	11.32
	230		165				

TABLE 47. 15° Angle of Elevation

RESULTS EXPERIMENTALLY OBTAINED					DERIVED RESULTS		
Speed R.P.M.	Spring Balance Reading, Gms.				Nom. Speed R.P.M.	Net Load Grams	H.P. x 10^{-3}
	Full - Load		No - Load				
		Mean		Mean			
(1)	(2)	(3)	(4)	(5)	(6)	(7)	(8)
200					200	51.1	1.34
400	160	175	100	127	400	51.5	2.70
	190		155				
600	160	180	100	127	600	52.0	4.08
	200		155				
800	165	182	105	130	800	52.3	5.48
	200		155				
1000	170	190	105	130	1000	52.8	6.90
	210		155				
1200	165	182	105	130	1200	53.2	8.35
	200		155				
1400	165	187	105	130	1400	53.8	9.86
	210		155				
1600	185	197	145	152	1600	54.2	11.33
	210		160				
1900	220	225	140	152	1800	54.8	12.92
	230		170				
					2000	55.2	14.45

TABLE 48. 30° Angle of Elevation

RESULTS EXPERIMENTALLY OBTAINED					DERIVED RESULTS		
Speed R.P.M.	Spring Balance Reading, Gms.				Nom. Speed R.P.M.	Net Load Grams	H.P. x 10^{-3}
	Full - Load		No - Load				
		Mean		Mean			
(1)	(2)	(3)	(4)	(5)	(6)	(7)	(8)
200					200	62.0	1.62
400	150	177	160	130	400	62.0	3.25
	205		100				
600	170	190	160	130	600	62.0	4.87
	210		100				
800	170	182	130	140	800	62.0	6.50
	195		150				
1000	175	195	120	135	1000	62.0	8.12
	215		150				
1200	175	197	120	135	1200	62.0	9.73
	220		150				
1400	210	195	140	140	1400	62.0	11.37
	180		140				
1600	225	207	135	135	1600	62.0	12.98
	190		135				
1900	210	222	155	160	1800	62.0	14.61
	235		165				
					2000	62.0	16.23

TABLE 49. 45° Angle of Elevation

RESULTS EXPERIMENTALLY OBTAINED					DERIVED RESULTS		
Speed R.P.M.	Spring Balance Reading, Gms.				Nom. Speed R.P.M.	Net Load Grams	H.P. x 10^{-3}
	Full - Load		No - Load				
		Mean		Mean			
(1)	(2)	(3)	(4)	(5)	(6)	(7)	(8)
200					200	63.0	1.65
400	205	190	110	127	400	63.0	3.30
	175		145				
600	205	190	110	127	600	63.0	4.95
	175		145				
800	205	190	110	127	800	63.0	6.60
	175		145				
1000	205	190	110	127	1000	63.0	8.25
	175		145				
1200	205	190	110	127	1200	63.0	9.90
	175		145				
1400	205	190	110	127	1400	63.0	11.55
	175		145				
1600	205	190	115	140	1600	61.5	12.88
	175		165				
1900	230	217	170	157	1800	60.0	14.15
	205		145				
					2000	58.0	15.18

TABLE 50. 60° Angle of Elevation

RESULTS EXPERIMENTALLY OBTAINED					DERIVED RESULTS		
Speed R.P.M.	Spring Balance Reading, Gms.				Nom. Speed R.P.M.	Net Load Grams	H.P. $\times 10^{-3}$
	Full - Load		No - Load				
		Mean		Mean			
(1)	(2)	(3)	(4)	(5)	(6)	(7)	(8)
200					200	51.2	1.34
400	200	195	150	142	400	50.0	2.62
	190		135				
600	185	195	155	152	600	49.0	3.85
	205		140				
800	210	200	150	155	800	47.9	5.03
	190		160				
1000	210	202	150	157	1000	47.4	6.21
	195		165				
1200	225	210	150	162	1200	47.1	7.40
	195		175				
1400	225	215	160	172	1400	46.3	8.50
	205		185				
1600	235	232	200	195	1600	45.5	9.55
	230		190				
1800	252	252	220	217	1800	45.4	10.60
	252		215				
					2000	45.4	11.80

TABLE 51. 75° Angle of Elevation

RESULTS EXPERIMENTALLY OBTAINED					DERIVED RESULTS		
Speed R.P.M.	Spring Balance Reading, Gms.				Nom. Speed R.P.M.	Net Load Grams	H.P. x 10^{-3}
	Full - Load		No - Load				
		Mean		Mean			
(1)	(2)	(3)	(4)	(5)	(6)	(7)	(8)
200					200	48.6	1.27
400	145	160	110	140	400	47.5	2.49
	175		170				
600	145	160	160	110	600	46.5	3.65
	175		60				
800	145	160	160	110	800	45.3	4.74
	175		60				
1000	130	152	100	120	1000	44.2	5.79
	175		140				
1200	120	147	135	120	1200	43.1	6.78
	175		105				
1400	120	147	100	105	1400	42.1	7.71
	175		110				
1600	115	145	110	115	1600	41.0	8.60
	175		120				
1900	225	200	130	125	1800	40.0	9.42
	175		120				
					2000	39.0	10.20

TABLE 52. 90° Angle of Elevation

RESULTS EXPERIMENTALLY OBTAINED					DERIVED RESULTS		
Speed R.P.M.	Spring Balance Reading, Gms.				Nom. Speed R.P.M.	Net Load Grams	H.P. x 10^{-3}
	Full - Load		No - Load				
		Mean		Mean			
(1)	(2)	(3)	(4)	(5)	(6)	(7)	(8)
300	155	162	130	120	200	41.4	1.08
	170		110				
400	155	165	110	120	400	40.1	2.09
	175		130				
600	180	167	140	130	600	39.0	3.06
	155		120				
800	160	172	145	137	800	37.7	3.95
	183		130				
1000	185	177	145	137	1000	36.5	4.78
	170		130				
1200	185	177	155	147	1200	35.2	5.53
	170		140				
1400	180	187	165	157	1400	34.0	6.24
	195		150				
1600	200	205	175	173	1600	33.0	6.92
	210		170				
1800	235	235	* 220	220	1800	31.8	7.50
					2000	30.4	8.16

* Auger Hitting Casing

APPENDIX X

DERIVED RESULTS FOR MODEL AUGER FITTED WITH CASING OF RADIAL CLEARANCE OF 1/8 INCH (C/D = 0.0833)

The derived results corresponding to the experimental results of Appendices VIII and IX are summarised in Tables 53 to 60 inclusive. Tables 53 to 59 give the results for millet ($^{d}/_{D} = 0.05$) for the angles of elevation 0° to 90° in 15° steps, while Table 60° gives the results for wheat ($^{d}/_{D} = 0.12$) for the angles of elevation 60° and 90°. The results are based on a choke length of 3 inches ($\frac{l_c}{p} = 2.0$) and refer to the work of Sections 3 and 4.

Explanation of Results (Tables 53 to 59)

(i) Output, Q (column (2))

Values obtained from Fig. 67 of Appendix VIII

(ii) Theoretical Output, Q_t (column (3))

Obtained from equation (3 - 2)

$$Q_t = \gamma N D^3 = \frac{N}{569}$$

($\gamma = 0.90$ in this case and D = 1/8 ft.)

(iii) Power, P (column (4))

Values obtained in Appendix IX

(iv) Theoretical Power, P_t (column (5))

Obtained from equation (3 - 7)

$$P_t = \frac{Q w L \sin\alpha}{33000} = \frac{Q \sin\alpha}{460}$$

(Average weight of millet seed = 35.74 lbs/cub.ft.)

$$L = 2 \text{ ft.}$$

(v) Speed Coefficient, C_S (column (6))

Obtained from equation (4 - 5)

$$C_S = N^2 D = \frac{N^2}{8}$$

(vi) Discharge Coefficient C_Q (column (7))

Obtained from equation (4 - 3)

$$C_Q = \frac{Q}{ND^3} = \frac{Q}{512N}$$

(vii) Power Coefficient, C_P (column (8))

Obtained from equation (4 - 4)

$$C_P = \frac{P}{\rho D^5 N^3} = \frac{2.85\ P}{N^3} \times 10^4$$

(viii) Volumetric Efficiency, η_V

Ratio of values in column (2) to corresponding values in column (3)

(ix) Overall Efficiency, η_O

Ratio of values in column (5) to corresponding values in column (4).

PERFORMANCE RESULTS FOR MILLET ($^{d}/_{D}$ = 0.05)

Nom. Speed R.P.M.	Q C.Ft/Min.	Q_t C.Ft/Min.	P H.P. x 10^{-3}	P_t H.P. x 10^{-3}	C_S x 10^{4}	C_Q	C_P x 10^{-7}	η_V %	η_O %
(1)	(2)	(3)	(4)	(5)	(6)	(7)	(8)	(9)	(10)
TABLE 53. 0° Angle of Elevation									
200	0.252	0.35	1.10	0	0.5	0.645	39.0	72.0	0
400	0.502	0.702	2.20	0	2.0	0.640	9.75	71.5	0
600	0.753	1.05	3.31	0	4.5	0.642	4.35	71.8	0
800	0.990	1.40	4.43	0	8.0	0.633	2.45	70.8	0
1000	1.158	1.75	5.56	0	12.5	0.593	1.575	65.8	0
1200	1.295	2.10	6.74	0	18.0	0.553	1.104	61.7	0
1400	1.410	2.45	7.87	0	24.5	0.516	0.813	57.6	0
1600	1.490	2.80	9.02	0	32.0	0.476	0.623	53.3	0
1800	1.533	3.16	10.15	0	40.5	0.436	0.493	48.5	0
2000	1.568	3.50	11.32	0	50.0	0.402	0.401	44.8	0
TABLE 54. 15° Angle of Elevation									
200	0.240	0.35	1.34	0.135	0.5	0.615	47.5	68.7	10.1
400	0.483	0.702	2.70	0.271	2.0	0.618	11.95	68.7	10.05
600	0.694	1.05	4.08	0.390	4.5	0.592	5.36	66.0	9.55
800	0.882	1.40	5.48	0.495	8.0	0.564	3.03	63.0	9.02
1000	1.055	1.75	6.90	0.593	12.5	0.540	1.954	60.3	8.60
1200	1.192	2.10	8.35	0.670	18.0	0.508	1.37	56.8	8.03
1400	1.288	2.45	9.86	0.724	24.5	0.471	1.02	52.5	7.35
1600	1.370	2.80	11.33	0.770	32.0	0.439	0.784	49.0	6.80
1800	1.428	3.16	12.92	0.802	40.5	0.407	0.627	45.3	6.20
2000	1.460	3.50	14.45	0.820	50.0	0.374	0.512	41.7	5.68

PERFORMANCE RESULTS FOR MILLET ($^{d}/_{D}$ = 0.05)

Nom. Speed R.P.M.	Q C.Ft/Min.	Q_t C.Ft/Min.	P H.P. x 10^{-3}	P_t H.P. x 10^{-3}	C_S x 10^{4}	C_Q	C_P x 10^{-7}	η_v %	η_g %
(1)	(2)	(3)	(4)	(5)	(6)	(7)	(8)	(9)	(10)
TABLE 55. 30° Angle of Elevation									
200	0.228	0.35	1.623	0.247	0.5	0.584	57.4	65.2	15.1
400	0.432	0.702	3.25	0.468	2.0	0.554	14.4	61.5	14.4
600	0.642	1.05	4.87	0.696	4.5	0.548	6.38	61.2	14.3
800	0.822	1.40	6.50	0.890	8.0	0.526	3.60	58.7	13.7
1000	0.972	1.75	8.12	1.050	12.5	0.498	2.30	55.5	12.95
1200	1.075	2.10	9.73	1.165	18.0	0.458	1.60	51.2	12.0
1400	1.152	2.45	11.37	1.250	24.5	0.421	1.175	47.1	11.0
1600	1.20	2.80	12.98	1.300	32.0	0.384	0.897	42.8	10.0
1800	1.24	3.16	14.61	1.345	40.5	0.354	0.708	38.2	9.2
2000	1.278	3.50	16.23	1.385	50.0	0.327	0.574	36.5	8.52
TABLE 56. 45° Angle of Elevation									
200	0.204	0.35	1.65	0.312	0.5	0.522	58.4	58.3	18.9
400	0.387	0.702	3.30	0.592	2.0	0.494	14.6	55.2	17.9
600	0.561	1.05	4.95	0.860	4.5	0.479	6.49	53.4	17.4
800	0.711	1.40	6.60	1.09	8.0	0.455	3.65	50.7	16.5
1000	0.834	1.75	8.25	1.28	12.5	0.428	2.33	47.7	15.5
1200	0.924	2.10	9.90	1.42	18.0	0.394	1.62	44.0	14.4
1400	1.002	2.45	11.50	1.53	24.5	0.366	1.17	40.8	13.2
1600	1.05	2.80	12.88	1.61	32.0	0.336	8.90	37.5	12.5
1800	1.07	3.16	14.15	1.65	40.5	0.306	6.86	33.9	11.7
2000	1.102	3.50	15.18	1.69	50.0	0.282	5.37	31.5	11.1

PERFORMANCE RESULTS FOR MILLET ($^{d}/_{D}$ = 0.05)

Nom. Speed R.P.M.	Q C.Ft/Min.	Q_t C.Ft/Min.	P H.P. x 10^{-3}	P_t H.P. x 10^{-3}	C_S x 10^{4}	C_Q	C_P x 10^{-7}	η_V %	η_O %
(1)	(2)	(3)	(4)	(5)	(6)	(7)	(8)	(9)	(10)
TABLE 57. 60° Angle of Elevation									
200	0.162	0.35	1.34	0.304	0.5	0.415	47.5	45.3	22.6
400	0.300	0.702	2.62	0.562	2.0	0.384	11.6	42.8	21.4
600	0.438	1.05	3.85	0.821	4.5	0.374	5.04	41.7	21.3
800	0.562	1.40	5.03	1.050	8.0	0.359	2.79	40.2	20.8
1000	0.662	1.75	6.21	1.242	12.5	0.340	1.76	37.8	20.0
1200	0.744	2.10	7.40	1.395	18.0	0.317	1.215	35.4	18.9
1400	0.798	2.45	8.50	1.495	24.5	0.292	0.878	32.6	17.6
1600	0.830	2.80	9.55	1.560	32.0	0.266	0.660	29.6	16.3
1800	0.855	3.16	10.60	1.600	40.5	0.243	0.513	27.0	15.1
2000	0.876	3.50	11.80	1.640	50.0	0.218	0.417	25.0	13.9
TABLE 58. 75° Angle of Elevation									
200	0.102	0.35	1.27	0.214	0.5	0.261	44.8	29.2	16.8
400	0.228	0.702	2.49	0.477	2.0	0.292	11.0	32.5	19.1
600	0.345	1.05	3.65	0.722	4.5	0.294	4.78	32.9	19.8
800	0.454	1.40	4.74	0.948	8.0	0.290	2.62	32.4	20.0
1000	0.528	1.75	5.79	1.120	12.5	0.274	1.64	30.1	19.3
1200	0.594	2.10	6.78	1.242	18.0	0.254	1.11	28.2	18.3
1400	0.631	2.45	7.71	1.320	24.5	0.230	0.797	25.7	17.1
1600	0.663	2.80	8.60	1.390	32.0	0.212	0.594	23.7	16.1
1800	0.676	3.16	9.42	1.412	40.5	0.193	0.456	21.4	15.0
2000	0.684	3.50	10.20	1.430	50.0	0.169	0.361	19.5	14.6

PERFORMANCE RESULTS FOR MILLET ($^{d}/_{D}$ = 0.05)

Nom. Speed R.P.M.	Q C.Ft/Min.	Q_t C.Ft/Min.	P H.P. x 10^{-3}	P_t H.P. x 10^{-3}	C_S x 10^{4}	C_Q	C_P x 10^{-7}	η_V %	η_O %
(1)	(2)	(3)	(4)	(5)	(6)	(7)	(8)	(9)	(10)
TABLE 59. 90° Angle of Elevation									
200	0.048	0.35	1.08	0.104	0.5	0.123	38.3	13.7	9.63
400	0.156	0.702	2.09	0.338	2.0	0.200	9.25	22.2	16.2
600	0.264	1.05	3.06	0.572	4.5	0.225	4.02	25.1	18.7
800	0.367	1.40	3.95	0.795	8.0	0.235	2.18	26.3	20.1
1000	0.447	1.75	4.78	0.970	12.5	0.229	1.352	25.5	20.3
1200	0.498	2.10	5.53	1.08	18.0	0.212	0.907	23.7	19.5
1400	0.531	2.45	6.24	1.15	24.5	0.195	0.645	21.6	18.4
1600	0.540	2.80	6.92	1.17	32.0	0.173	0.478	19.3	16.9
1800	0.547	3.16	7.50	1.19	40.5	0.155	0.363	17.3	15.8
2000	0.547	3.50	8.16	1.19	50.0	0.140	0.289	15.6	14.6

TABLE 60. Performance Results for Wheat ($\frac{d}{D}$ = 0.12)

Nom Speed R.P.M.	C_S x 10^4	α = 60°		α = 90°	
		Q C.Ft/Min.	C_Q	Q C.Ft/Min.	C_Q
200	0.5	0.156	0.399	0.048	0.123
400	2.0	0.297	0.380	0.162	0.207
600	4.5	0.432	0.368	0.255	0.217
800	8.0	0.562	0.359	0.330	0.211
1000	12.5	0.660	0.338	0.390	0.200
1200	18.0	0.735	0.314	0.438	0.187
1400	24.8	0.768	0.281	0.468	0.171
1600	32.0	0.786	0.252	0.483	0.155
1800	40.5	0.796	0.226	0.493	0.140
2000	50.0	0.804	0.205	0.497	0.127

APPENDIX XI

DATA FOR PLOTTING PREDICTED OUTPUT GRAPH OF FIG. 29

The data used for plotting the predicted output graph of Fig. 29 is given in Tables 61 to 64 inclusive. The various C_Q values were read from the C_Q versus C_S graph of Fig. 28 and the output values calculated using equation (4 - 3).

Fig. 29 was drawn by plotting the speed lines corresponding to the outputs and diameters for the 45° angle of elevation; the diameter scales for the other angles of elevation were then found by reverse plotting.

PREDICTED OUTPUT FIGURES FOR VARIOUS SIZE AUGERS

Speed R.P.M.	C_s x 10^4	0°		15°		30°		45°		60°		75°		90°	
		C_Q	Q	C_Q	Q	C_Q	Q	C_Q	Q	C_Q	Q	C_Q	Q	C_Q	Q
TABLE 61.		D = 3"													
200	1.0	0.650	2.03	0.620	1.94	0.567	1.77	0.502	1.57	0.393	1.23	0.268	0.840	0.166	0.519
300	2.25	0.650	3.05	0.613	2.87	0.560	2.63	0.492	2.30	0.383	1.80	0.291	1.36	0.203	0.951
400	4.0	0.646	4.04	0.600	3.75	0.550	3.44	0.482	3.01	0.376	2.35	0.296	1.85	0.224	1.40
500	6.25	0.636	4.97	0.581	4.54	0.539	4.21	0.469	3.67	0.363	2.84	0.293	2.29	0.235	1.84
600	9.0	0.620	5.82	0.563	5.28	0.521	4.89	0.450	4.22	0.352	3.30	0.286	2.68	0.237	2.22
700	12.25	0.596	6.53	0.543	5.94	0.497	5.44	0.427	4.67	0.340	3.72	0.273	2.99	0.230	2.52
800	16.0	0.567	7.09	0.520	6.50	0.471	5.89	0.405	5.06	0.323	4.04	0.261	3.26	0.219	2.74
900	20.25	0.535	7.52	0.493	6.94	0.443	6.24	0.373	5.25	0.307	4.32	0.247	3.50	0.205	2.89
1000	25.0	0.505	7.89	0.469	7.34	0.416	6.50	0.360	5.62	0.288	4.50	0.230	3.59	0.192	3.00
1200	36.0	0.453	8.50	0.420	7.88	0.370	6.94	0.319	5.98	0.252	4.72	0.200	3.75	0.165	3.09
1400	49.0	0.410	8.97	0.380	8.31	0.331	7.25	0.285	6.24	0.221	4.84	0.173	3.78	0.142	3.11
TABLE 62.		D = 6"													
200	2.0	0.650	16.25	0.613	15.35	0.561	14.02	0.494	12.35	0.384	9.60	0.292	7.3	0.200	5.0
300	4.5	0.642	24.1	0.592	22.2	0.548	20.5	0.479	18.0	0.374	14.0	0.294	11.0	0.225	8.44
400	8.0	0.633	31.7	0.564	28.2	0.526	26.3	0.455	22.7	0.359	17.95	0.290	14.5	0.235	11.75
500	12.5	0.593	37.1	0.540	33.7	0.498	31.2	0.428	26.8	0.340	21.2	0.274	17.1	0.229	14.3
600	18.0	0.553	41.5	0.508	38.1	0.458	34.4	0.394	29.5	0.317	23.8	0.254	19.1	0.212	15.9
700	24.5	0.516	45.2	0.471	41.2	0.421	36.8	0.366	32.0	0.292	25.5	0.230	20.1	0.195	17.0
800	32.0	0.476	47.6	0.439	43.9	0.384	38.4	0.336	33.6	0.266	26.6	0.212	21.2	0.173	17.3
900	40.5	0.436	49.0	0.407	45.8	0.354	39.8	0.306	34.4	0.243	27.3	0.193	21.7	0.155	17.4
1000	50.0	0.402	50.2	0.374	46.8	0.327	40.9	0.282	35.2	0.218	27.3	0.169	21.1	0.140	17.5

PREDICTED OUTPUT FIGURES FOR VARIOUS SIZE AUGERS

Speed R.P.M.	C_s x 10^4	0°		15°		30°		45°		60°		75°		90°	
		C_Q	Q	C_Q	Q	C_Q	Q	C_Q	Q	C_Q	Q	C_Q	Q	C_Q	Q
TABLE 63. D = 9"															
200	3.0	0.648	54.8	0.607	51.2	0.555	46.8	0.487	41.1	0.380	52.1	0.294	24.8	0.214	18.1
300	6.75	0.633	80.1	0.578	73.3	0.535	67.7	0.465	58.9	0.361	45.7	0.292	37.0	0.236	29.1
400	12.0	0.598	101.0	0.545	91.8	0.500	84.3	0.429	72.5	0.340	57.4	0.275	46.4	0.230	38.8
500	18.75	0.542	114.2	0.500	105.4	0.450	94.8	0.390	82.2	0.312	65.8	0.250	52.7	0.210	44.3
600	27.0	0.495	125.3	0.460	116.5	0.407	103.0	0.352	89.1	0.280	70.8	0.225	57.0	0.186	47.1
700	36.75	0.450	133.0	0.418	123.5	0.368	108.8	0.317	93.7	0.250	73.8	0.200	59.1	0.164	48.4
TABLE 64. D = 12"															
200	4.0	0.646	129.2	0.600	120.0	0.550	110.0	0.482	96.4	0.376	75.2	0.297	59.4	0.223	44.6
300	9.0	0.620	186.0	0.563	169.0	0.521	156.3	0.450	135.0	0.342	102.6	0.286	85.8	0.236	70.8
400	16.0	0.565	226.0	0.519	208.0	0.470	188.0	0.405	162.0	0.325	130.0	0.260	104.0	0.219	87.6
500	25.0	0.505	252.5	0.469	233.5	0.417	208.5	0.360	180.0	0.288	144.0	0.230	115.0	0.192	96.0
600	36.0	0.455	273.0	0.421	252.6	0.371	222.6	0.320	192.0	0.253	151.8	0.200	120.0	0.165	99.0
700	49.0	0.410	287.0	0.380	266	0.331	231.7	0.285	199.5	0.221	154.7	0.173	121.1	0.142	99.4

APPENDIX XII

COMPARISON OF PREDICTED OUTPUT RESULTS

The predicted outputs as calculated from equation (4 - 10) have been compared with the corresponding values read from Fig. 29. (Fig. 29 was drawn up using the actual C_Q values of the C_Q versus C_S graphs of Fig. 28, while equation (4 - 10) is based on the approximated C_Q versus C_S graphs). The various values are given in Table 65; series (1) results are those calculated from equation (4 - 10), while series (2) results are those read from Fig. 29.

TABLE 65. Comparison of Predicted Outputs

Auger Diam. Ins.	Speed R.P.M.	Output					
		0°		45°		90°	
		(1)	(2)	(1)	(2)	(1)	(2)
3"	200	2.09	2.03	1.43	1.57	.762	.519
	600	5.84	5.90	3.98	4.15	2.12	2.12
	1000	8.3	7.89	5.67	6.24	3.03	3.0
6"	200	16.6	16.25	11.3	12.35	6.04	5.0
	600	42.9	41.5	29.3	29.5	15.6	15.9
	1000	48.7	50.2	33.2	35.2	17.7	17.5
12"	200	131	129.2	88.8	94.0	47.5	44.6
	600	281	287	192	192	102.5	99.0

APPENDIX XIII

CHOKE LENGTH CORRECTION FACTORS

The choke length correction factors for various speeds and $\frac{l_c}{p}$ ratios are given in Tables 66 to 72 inclusive. The final correction factors adopted are the mean values for the 30°, 60° and 90° angles of elevation. The correction factors were obtained by finding the ratio of the outputs for the $\frac{l_c}{p}$ ratio considered to the corresponding outputs for $\frac{l_c}{p}$ = 2-0; for $\frac{l_c}{p}$ = 2-0, the correction factor K_c = 1-0.

Tables 73 and 74 summarise the values calculated from equation (4 - 16); these values were used in the plotting of the choke length correction factor graph of Fig. 31.

CHOKE LENGTH CORRECTION FACTORS FOR VARIOUS SPEEDS AND $^{l}c/_{p}$ RATIOS

Speed R.P.M.	200	400	600	800	1000	1200	1400	1600	1800	2000
$C_s \times 10^4$	0.5	2.0	4.5	8.0	12.5	18.0	24.5	32.0	40.5	50.0
TABLE 66. $^{l}c/_{p}$ = 0.67										
90°	0.956	0.732	0.557	0.466	0.408	0.367	0.330	0.312	0.280	0.250
60°	0.613	0.505	0.461	0.430	0.403	0.379	0.330	0.317	0.288	0.264
30°	0.663	0.607	0.536	0.489	0.460	0.422	0.388	0.352	0.332	0.311
Mean	0.744	0.615	0.518	0.462	0.424	0.389	0.349	0.327	0.300	0.275
TABLE 67. $^{l}c/_{p}$ = 1.0										
90°	0.956	0.875	0.785	0.686	0.620	0.570	0.534	0.497	0.471	0.435
60°	0.735	0.629	0.562	0.546	0.543	0.523	0.494	0.478	0.457	0.434
30°	0.906	0.787	0.732	0.678	0.625	0.581	0.558	0.526	0.502	0.490
Mean	0.865	0.764	0.694	0.637	0.596	0.558	0.529	0.500	0.477	0.453
TABLE 68. $^{l}c/_{p}$ = 1.33										
90°	0.870	0.918	0.887	0.830	0.768	0.715	0.696	0.670	0.649	0.620
60°	0.837	0.794	0.785	0.767	0.735	0.715	0.689	0.668	0.655	0.637
30°	0.977	0.918	0.860	0.814	0.765	0.728	0.704	0.680	0.666	0.663
Mean	0.895	0.877	0.844	0.804	0.756	0.719	0.696	0.673	0.657	0.640

CHOKE LENGTH CORRECTION FACTORS FOR VARIOUS SPEEDS AND $^{l}c/_{p}$ RATIOS

Speed R.P.M.	200	400	600	800	1000	1200	1400	1600	1800	2000
$C_s \times 10^4$	0.5	2.0	4.5	8.0	12.5	18.0	24.5	32.0	40.5	50.0
TABLE 69. $^{l}c/_{p}$ = 1.67										
90°	0.870	0.893	0.908	0.898	0.902	0.887	0.869	0.850	0.830	0.805
60°	1.000	0.958	0.928	0.918	0.910	0.904	0.900	0.893	0.892	0.891
30°	0.994	0.992	0.951	0.908	0.902	0.891	0.891	0.878	0.873	0.878
Mean	0.955	0.948	0.929	0.908	0.905	0.894	0.887	0.874	0.865	0.858
TABLE 70. $^{l}c/_{p}$ = 2.33										
90°	1.00	1.036	1.035	1.052	1.072	1.095	1.117	1.134	1.142	1.155
60°	1.103	1.072	1.065	1.091	1.111	1.138	1.160	1.168	1.168	1.155
30°	1.002	1.017	1.012	1.047	1.063	1.085	1.120	1.120	1.136	1.145
Mean	1.035	1.042	1.037	1.063	1.082	1.106	1.132	1.141	1.149	1.152
TABLE 71. $^{l}c/_{p}$ = 2.67										
90°		1.108	1.115	1.136	1.172	1.190	1.221	1.260	1.282	1.302
60°	1.123	1.112	1.108	1.148	1.191	1.228	1.252	1.256	1.262	1.252
30°	1.012	1.015	1.012	1.057	1.110	1.143	1.178	1.190	1.235	1.274
Mean	1.068	1.078	1.078	1.114	1.158	1.187	1.217	1.235	1.260	1.276

CHOKE LENGTH CORRECTION FACTORS FOR VARIOUS SPEEDS AND $^{l_c}/_{p}$ RATIOS

Speed R.P.M.	200	400	600	800	1000	1200	1400	1600	1800	2000
$C_s \times 10^4$	0.5	2.0	4.5	8.0	12.5	18.0	24.5	32.0	40.5	50.0
TABLE 72. $^{l_c}/_{p}$ = 3.0										
90°	1.043	1.108	1.138	1.170	1.213	1.255	1.302	1.351	1.380	1.395
60°	1.163	1.165	1.167	1.198	1.238	1.269	1.280	1.298	1.318	1.338
30°	1.046	1.041	1.068	1.120	1.183	1.221	1.260	1.270	1.310	1.338
Mean	1.084	1.105	1.124	1.163	1.211	1.248	1.281	1.306	1.336	1.354

VALUES CALCULATED IN ACCORDANCE WITH EQUATION (4-16) FOR USE IN PLOTTING FIG. 31

TABLE 73. C_S Values (All Values x 10^4)

Speed R.P.M.	D = 3" $C_S = N^2/4$	D = 6" $C_S = N^2/2$	D = 9" $C_S = 3N^2/4$	D = 12" $C_S = N^2$	D = 15" $C_S = 5N^2/4$
200	1.0	2.0	3.0	4.0	5.0
300	2.25	4.5	6.75	9.0	11.25
400	4.0	8.0	12.0	16.0	20.0
500	6.25	12.5	18.75	25.0	31.25
600	9.0	18.0	27.0	36.0	45.0
700	12.25	24.5	36.75	49.0	61.25
800	16.0	32.0	48.0	64.0	
900	20.25	40.5	60.75		
1000	25.0	50.0			
1200	36.0				
1400	49.0				

TABLE 74. Values of Index "m"

$$m = \frac{(3.67 - \frac{l_c}{p})}{112}$$

$\frac{l_c}{p}$	m
1	-0.1275
1.25	-0.855
1.5	-0.050
1.75	-0.214
2.0	0
2.25	+ 0.0163
2.5	+ 0.0277
2.75	+ 0.0360
3.0	+ 0.0393

APPENDIX XIV

DATA FOR PLOTTING PREDICTED HORSEPOWER GRAPH OF FIG. 34

Fig. 34, which gives the predicted horsepowers per length for conveying wheat, was drawn up using values calculated from equation (4 - 24).

$$\text{H.P. per foot} = 3.3 + 2 \sin (2\alpha + 15)\omega D^3 N \times 10^{-5}$$

For wheat, $\omega = 48$ lb/ft.^{3}

The computed values are given in Tables 75 to 78 inclusive.

Fig. 34 was drawn by plotting the speed lines corresponding to the outputs and diameters for the 45° angle of elevation; the diameter scales for the other angles of elevation were then found by reverse plotting.

TABLE 75. 30° and 45° Angles of Elevation

Speed R.P.M.	H.P. per Foot Length			
	D = 3"	D = 6"	D = 9"	D = 12"
200	0.00762	0.063	0.211	0.502
300	0.0118	0.094	0.318	0.753
400	0.0157	0.125	0.423	1.000
500	0.0196	0.157	0.530	1.253
600	0.0236	0.188	0.636	1.505
700	0.0275	0.220	0.742	1.755
800	0.0314	0.251	0.848	2.01
900	0.0353	0.283	0.955	2.26
1000	0.0393	0.314	1.058	2.51
1200	0.0472	0.377	1.270	3.01
1400	0.0550	0.440	1.481	3.51

Speed R.P.M.	H.P. per Foot Length			
	D = 3"	D = 6"	D = 9"	D = 12"
TABLE 76. 0° and 75° Angles of Elevation				
200	0.00573	0.046	0.106	0.364
600	0.0172	0.137	0.319	1.10
1000	0.0286	0.229	0.531	1.83
TABLE 77. 15° and 60° Angles of Elevation				
200	0.0071	0.057	0.131	0.462
600	0.0212	0.169	0.393	1.355
1000	0.0353	0.283	0.655	2.26
TABLE 78. 90° Angle of Elevation				
200	0.0042	0.034	0.114	0.268
600	0.0126	0.101	0.339	0.804
1000	0.0209	0.168	0.566	1.34

APPENDIX XV

TABLE 79. PERFORMANCE RESULTS * FOR 6 in. AUGER

These values are compared with the predicted performance data from the model tests in Fig. 35

(* Reference (35) of Bibliography)

Speed R.P.M.	30°		60°		90°	
	Q c.ft/Min	P H.P.	Q C.ft/Min	P H.P.	Q C.ft/Min	P H.P.
300	21.9	0.875	15.6	0.60	10.5	0.52
400	27.0	1.103	18.0	0.76	12.9	0.64
500	30.3	1.23	20.1	0.89	15.0	0.78
600	33.0	1.445	21.9	1.04	16.3	0.88
700	34.7	1.58	23.2	1.21	16.5	0.96
800	35.4	1.87	24.6	1.38	16.2	1.08
900	34.7	2.31	23.7	1.55	15.75	1.18
1000	34.5	2.48	22.3	1.76	15.30	1.35

Details of 6" Auger

$D = 6"$

$P = 6"$

$D_c = 2"$

$l_c = 12"$

$L = 8' - 0"$

$C = 3/8"$